Vol. 13● No. 2● October 2019

ISSN: 0976 - 1330

Journal of GEOMATICS

INDIAN SOCIETY OF GEOMATICS

Journal of Geomatics

(A publication of the Indian Society of Geomatics)

Editorial Board

Advisory Board

Indian Society of Geomatics
Executive Council 2017 – 2020

Secretary: (address for correspondence)
6202, SAC Bopal Campus, Ahmedabad – 380058, India
Email: secretary@isgindia.org; sasharma@sac.isro.gov.in

Journal of Geomatics
(A Publication of the Indian Society of Geomatics)
Vol. 13. No. 2 Research articles October 2019

Special Section: Selected papers of National Symposium on Advancements in Geospatial Technology for Societal Benefits, Dec 03-07, 2018, Ahmedabad (Part-2)

Journal of Geomatics Vol. 13, No. 2, October 2019

A decision based approach to develop action plans for land degradation neutrality using geospatial techniques in a semi arid region of India

Sujatha G., Tarik Mitran*, Kimeera Tummala, Janaki Rama Suresh K. G., Fyzee M. A., Sreenivas K. and Ravisankar, T.
National Remote Sensing Centre, ISRO, Balanagar, Hyderabad, 500037
*Email: tarikmitran@nrsc.gov.in

(Received: Sep 13, 2018; in final form: July 04, 2019)

Abstract: Land Degradation (LD) is one of the most serious environmental problem leading to temporary or permanent decline in the productive capacity of the land and hence affects the food security. There is a need to rehabilitate degraded lands to support sustainable food production. In the present study, an attempt has been made to develop decision based approach for action plan development aimed towards achieving regional level LD neutrality in the state of Telengana using existing Land Use/Land Cover (LU/LC), LD and slope maps prepared at 1:50,000 scale using Resourcesat-1 LISS-III and Cartosat DEM. Results of the study revealed that water erosion, salt affected soils and forest degradation were the major category of LD accounting to 87.7%, 5.3% and 3.6% respectively of the total LD area. A number of rule sets were generated for each LD class based on various land conservation practices advocated by regional and international organizations. Afforestation/ gulley plugging, contour graded bunds, grass cover establishment are the major action plans recommended to reduce the loss of land due to water erosion and forest degradation. Adoption of such activities may help restoring 76.4% of the area under LD in the study region.

Keywords: Land Degradation, Neutrality, Remote Sensing and GIS

1. Introduction

India is endowed with vast natural resources specifically land which is a vital source growing food, fibre and firewood to meet the human needs, preserving forests and biodiversity, facilitating the natural management of water system and acting as a Carbon store. India homes over 16% of world's population in an area, which is 2.42% of global spread. Per Capita arable land in India, which is around 0.15 ha at present, is expected to decrease to a meagre 0.09 ha by 2075 (Navalgund, 2006).The degradation of dry land is one of the most serious environmental problem and major reason for such projected changes in India. LD is reducing the natural resources available, making us all less resilient and more vulnerable to the impacts of climate change on food security (Gomiero, 2016). Lack of adequate information on soil resources coupled with improper land use planning have resulted in many of the present day LD problems in our country such as salinity/ alkalinity and water logging in command areas, severe erosion in catchments leading to siltation of reservoirs, decrease in productivity of crops etc. LD tends to be an irreversible process, therefore in order to establish sustainable land use system, it is important to make attempts to discover the area prone to LD as well as to monitor the progress of degradation (Uchida, 1994).

The traditional soil surveys are providing information on degraded lands which are subjective, time consuming and laborious. Geo spatial techniques have reduced field work to a considerable extent. It is due to advantages with satellite data like availability of data in multi-spectral channels, repetitive coverage of same area at regular intervals and compatibility for data analysis at faster rates on computers. Currently, remote sensing data is being regularly employed in the survey of degraded soils, because of development of operational methodologies. Synoptic coverage in narrow and discrete spectral bands provided by space borne sensors at regular interval enabled inventorying degraded land and monitoring their temporal behaviour at operational level (Dwivedi, 2001). The quantification of spatial behaviour at the specific moment is an initial step to monitor the progress of LD. The capability of wide spatial coverage of remote sensing data is its advantageous characteristic. Systematic research and development efforts in the application of satellite data in soil studies has now resulted in the development of operational methodology to map degraded lands and monitor them on routine basis at 1:50,000 or larger scale (Manchanda et al., 2002).

Several researchers in India have used remote sensing data for LD assessment to delineate the state of soil erosion, soil salinization, water logging, foliage deterioration, etc (Venkataratnam and Ravisankar, 1992; Dwivedi and Sreenivas, 1998; Dwivedi et al., 2006). Beside that efforts were also made by various agencies across the India to identify various types of degraded lands, their spatial extent and severity levels (DAC, 1994; http://www.nbsslup.in; http://bhuvan.nrsc.gov.in). Bhattacharyya et al. (2015) reported that soil degradation in India is estimated to be occurring on 147 Mha of land, including 94 Mha from water erosion, 16 Mha from acidification, 14 Mha from flooding, 9 Mha from wind erosion, 6 Mha from salinity, and 7 Mha from a combination of factors. Therefore, in recent years increasing emphasis is laid on the information on the nature, extent, spatial distribution and magnitude of LD which plays a vital role in planning the strategies for reclamation /conservation of degraded lands. Assessment of LD status in terms of water and wind erosion, salt affected and water logging is an important pre-requisite for land resources conservation planning and reclamation programmes. The water erosion in the erosion map depicts areas having soil loss greater than 10 tons/ha/year (http://bhuvan.nrsc.gov.in).Salt affected areas are one of

the most important degraded areas where soil productivity is reduced due to either salinization (EC > 4 dS/m) or sodicity (ESP > 15) or both(http://bhuvan.nrsc.gov.in). Water logging is considered as physical deterioration of land. It is affected by excessive ponding / logging of water for quite some period and affects the productivity of land or reduces the choice of taking crops.

The degraded lands need to be rehabilitated to support sustainable food production or, where appropriate, be restored to its natural or semi-natural state. Hence action plans are to be generated for achieving LD neutrality of our country based on existing data bases like LULC, LD, slope etc. The United Nations Convention to Combat Desertification (UNCCD) defines land degradation neutrality as "a state whereby the amount and quality of land resources necessary to support ecosystem functions and services and enhance food security remain stable or increase within specified temporal and spatial scales and ecosystems" (UNCCD, 2015).

Actions to achieve Land Degradation Neutrality (LDN) include land management approaches that avoid or reduce degradation, coupled with efforts to reverse degradation through restoration or rehabilitation of land that has lost productivity. Sustainable Land Management (SLM) practices provided in the action plans, such as agro forestry and conservation agriculture, can boost yields and prevent future LD. Analysis of time series database, space based indices along with ecological and economic variables can help in identification of LD vulnerability. This information along with existing LD information will help in developing action plans in more holistic way to achieve land degradation neutrality.

Hence the current study has been conducted in the state of Telengana as a representative of semi arid region of India with the objectives, viz., 1) To develop methodology for assessing LD vulnerability 2) To develop action plan towards LD Neutrality (LDN). Achieving LDN may contribute to sustainable development efforts; it may improve food, energy and water security and build the resilience to the impacts of drought and other climate-related disasters.

2. Materials and methods

2.1 Study sites

The study was carried out in the state of Telangana which located between 17.36° and 12.97°N latitude (Figure 1). The geographical area of Telangana is 112,077 square kilometers. Telangana is situated on the Deccan Plateau in the central stretch of the eastern seaboard of the Indian peninsula.

Major soil types of Telangana include red sandy, dubbas chalkas, deep red loamy, and very deep black cotton soils (Biswas et al., 2015). Telangana lies in a semi-arid region and has a predominantly hot and dry climate. The annual rainfall is between 900 and 1500 mm in northern Telangana and 700 to 900 mm in southern Telangana. The average temperatures during summer and winter are 40-42 & 22-23 °C respectively.

Figure 1: Location of the study site

2.2 Data and software used

The existing LD and LU/LC maps at 1:50,000 scale generated by National Remote Sensing Centre (NRSC) for the year 2005-06 have been used in the present study (http://bhuvan.nrsc.gov.in). The LD mapping was carried out using Resourcesat-1 multi-temporal LISS-III data of 2005-06 on 1:50,000 using visual interpretation using the multi-temporal LISS-III data. Classification system along with visual interpretation cues were developed for LD mapping (NRSC, 2007). This was supported by adequate field checks, soil chemical analysis and internal as well as external quality checks at various stages. The land degradation processes addressed were water erosion, wind erosion, water logging, salinisation / alkalization, acidification, glacial, anthropogenic and others. Similarly, LU/LC mapping was carried out using Resourcesat-1 multi-temporal LISS-III data of 2005-06 on 1:50,000 scale using visual interpretation of the multi-temporal LISS-III data. Around 900 LISS-III images acquired during kharif, rabi and summer seasons were used. Visual interpretation of multi-season data was supported with knowledge from historic thematic bases like waste lands and LU/LC as well as Cartosat DEM. Slope map at 1:50,000 was generated from the existing 1:10,000 slope maps using resampling techniques. All the analysis has been carried out using ArcGIS version 10.2.1 and Erdas Imagine-2016 software.

2.3 Methodology

The existing databases on LD, LULC and slope maps were brought into a common projection system and rasterized with a cell size of 24 m resolution. The rule sets were generated for each LD classes based on the various land conservation practices advocated by regional and international organizations for action plan generation. These rules were applied on the integrated dataset in GIS environment to generate an action plans for LD neutrality. The overall methodology of the research is presented in figure 2.

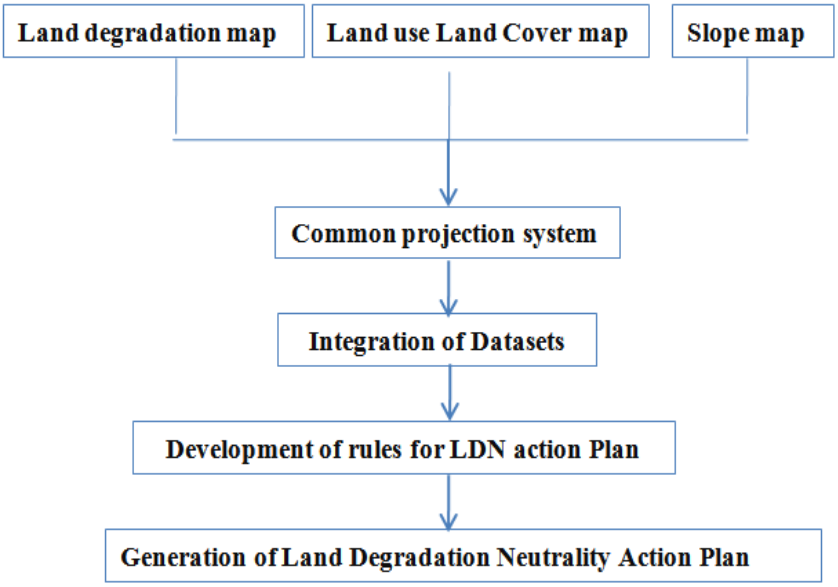

Figure 2: Flowchart of the methedology

3. Results and discussion

3.1 Variability in land use and slope

The distribution of LU/LC in Telengana state is shown in figure 3. It is observed that agricultural land is the dominant land use in the study area followed by forest and grassland. About 7.09 Mha of land is under crop cultivation, 2.63 Mha of land is under forest and grass. Wikramanayake et al., (2002) reported that over 80% of the original forest cover has been cleared for agriculture, timber harvesting, or cattle grazing. The Eastern Highlands are moist deciduous forests in the state. The slope mostly varies from very gentle to gentle (1-3%) and covers major portion of the study area. These areas comprise of pediplain with shallow weathering, sheet rock flat topped portion of hills etc. The moderately sloping area (8-15%) occur as isolated small patches at the foot hill zones. Moderately steep (15-30%) to very steep sloping zones (30-50%) are mostly observed in the hilly slopes of residual hills, denudational hills, and in the peripheral zones of the hilly terrain in the study region (Figure 3). The steeply sloping areas are also observed along isolated hills and covers very small extent.

3.2 Spatial distribution of LD processes

The overall status of LD in Telengana as per 2005-06 assessment is given in table 1. It is clear from this table that about 3322.5 thousand ha of land is under various processes of LD in the state of Telangana. The LD map of Telangana state is presented in figure 4. The water erosion is the major category of LD (2889 thousand ha) in the study area accounting to 87.7% of total LD of the state. It is mostly observed in the eastern region of the study site. It is followed by salt affected soils accounting to 5.3% of total LD in the state. The Salinization / alkalization (comprising various categories like saline, sodic and saline-sodic with varying severity) is distributed over 176 thousand ha of land. The barren rocky, mass movement and riverine sands (others category) are distributed over 120 thousand ha of land and accounts for 3.6% of total LD in the study area. The severe forest degradation (forest to non-forest) mostly occurs as isolated patches contributing 3.6% (113 thousnad ha) of total LD in the study region.

3.3. Rule-sets for generating LD neutrality action plan

The rule sets were generated (Table 2) for each LD classes based on the various land conservation practices advocated by regional and international organizations. The specific rule set has been formulated by referring the slope and type of land use to generate LD neutrality action plan for a particular LD process. There are number of practices, which can reduce the loss due to water erosion from agricultural land at different slope levels namely at 0-1 % slope: levelling & field bund; 1-3 % slope: contour farming (http://nass.usda.gov) & avoiding ploughing along slopes; 3-8 % slope: contour bunding/contour trenching; 8-15 % slope: contour terracing/bench terracing; 15-30 % slope: bench terracing with stone retaining walls etc. Similar combinations are also followed for forest and grassland to protect loss from water erosion. Whereas shelter belt is found to be more suitable measure to protect loss of top soil due to wind erosion stabilized-unstabilized dunes from agricultural, forest and waste land.

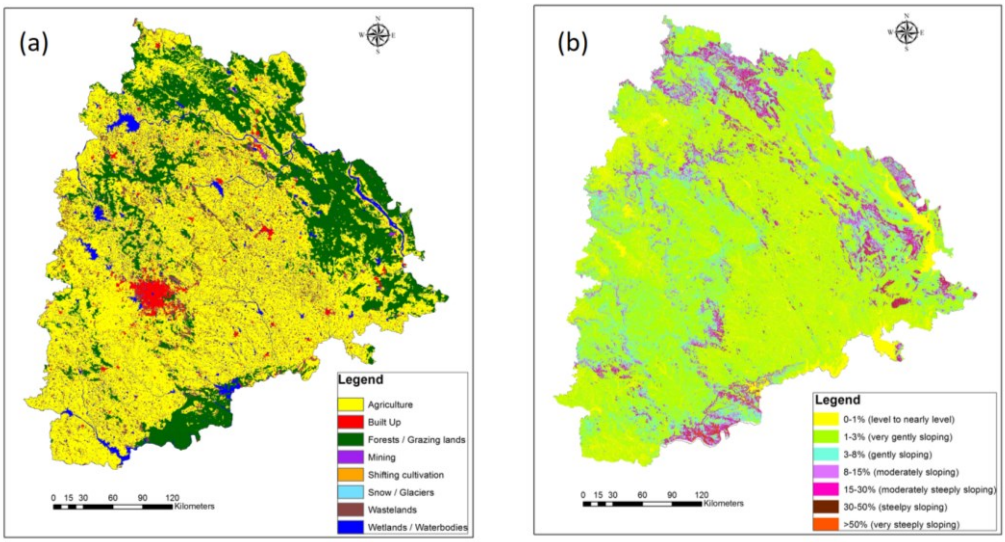

Figure 3: Land Use/Land Cover (a) and Slope map of the study area (b)

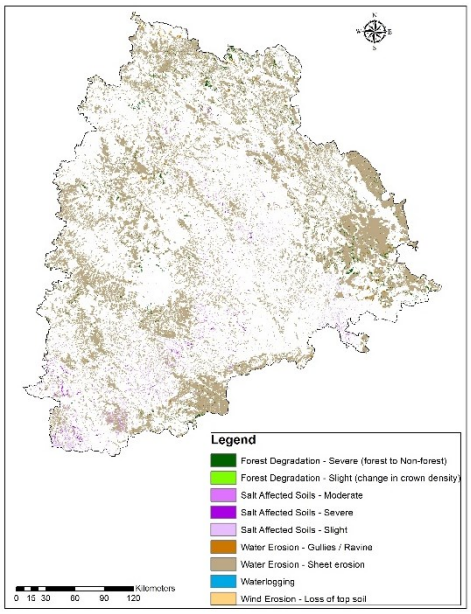

Figure 4: Spatial distribution of the Land degradation processes in the study area

Table 1: Area statistics of various LD processes in Telangana State

LD_Processess	Area ('000 ha)	% of Total LD of the study area
Water Erosion - Sheet erosion	2889	87.12
Water Erosion - Gullies / Ravine	19.0	0.56
Forest Degradation - Slight (change in crown density)	1.00	0.03
Forest Degradation - Severe (forest to Non-forest)	113.0	3.40
Salt Affected Soils - Slight	120.0	3.60
Salt Affected Soils - Moderate	38.0	1.139
Salt Affected Soils - Severe	18.0	0.55
Water logging	0.2	0.008
Barren Rocky Areas	76.0	2.29
Anthropogenic	42.0	1.26
Others (Riverine Sand)	3.00	0.005
Total	3322.5	100.0

Afforestation is considered as one of the most beneficial process of natural regeneration of a forest, where the area is under forest and suffering from the loss of topsoil (Veldman et al., 2015). The suitable reclamation practices; adoption of salt tolerant crops /varities and proper drainage are the criteria (www.fao.org) has been considered to reduce various intensity of salt affected soils in the current study. Subsurface drainage is an effective tool to combat the problem of water logging has also incorporated in the rulsets (Ritzema et al., 2008).

3.4 LD neutrality action plan

The regional level LD neutrality action plans were developed based on the above mentioned rule sets for Telangana state which is shown in the figure 5. The area under different action plans is presented in table 3. Afforestation/ gulley plugging, contour graded bunds, grass cover establishment,and other vegetative measures are the major options to reduce water erosion, forest degradation/desertification in the study region. These action plans could be employed over 2520 thousand ha of land under water erosion and forest degradation. Adoption of such activities may help restore 76.4% of the area under total LD of the study region. The various intensity of salt affected soil can be reclaimed with different management practices, growing of salt and tolerant crops and with proper drainage. An area of 130 thousand ha may be brought to normal condition with adaption of such measures. In addition, well defined land use policies or strict legislation policies are also required to rehabilitate the degraded land.

Table 2: Rule sets for generating LD neutrality action plan

Sl No	LD process	LULC	Slope (%)	Measures
1.	Water erosion-Sheet Erosion	Agriculture	1-3	Levelling & field bund , Contour farming & avoiding ploughing along slopes
			3-8	Contour bunding/Contour Trenching
			8-15	Contour terracing/Bench terracing
			15-30	Bench terracing with stone retaining walls
2	Water erosion-Sheet Erosion	Forest	3-8	Contour Trenching
			8-15	Contour terracing
			15-30	Stone retaining walls
			30-50	Retaining walls and grass seeding
			50	Grass seeding
3	Water erosion-Sheet Erosion	Wasteland	<8	Agro-forestry; Silviculture
4	Water erosion Gullies/ravines	Agriculture		Contour graded bunds/ Gulley plugging/Soil moisture conservation measures/ Ravine side slope stabilisation with grasses
5.	Water erosion Gullies/ravines	Forest and Grassland		Afforestation/Gulley plugging
6	Water erosion Gullies/ravines	Wasteland		Gulley plugging; soil moisture conservation measures;
7	Wind erosion- Loss of Top soil/ Stabilised/Unstabilized dunes	Agriculture		Shelter belts; wind barriers; trap crops
8	Wind erosion- Loss of Top soil	Forest and Grassland/Wasteland		Shelter belts
9	Forest Degradation	Forest		Afforestation
10	Forest Degradation	Wasteland		Protected Afforestation; landscape restoration
11	Forest Degradation	Wetlands		Land rehabilitation and ecosystem restoration
12	Forest Degradation- Land Transformations	Forest		Protected Afforestation; landscape restoration
13	Forest Degradation- Land Transformations	Wasteland		Agro-forestry; Silvipasture
14	Salt affected soils	Agriculture		Reclamation; salt tolerant crops; proper drainage
15	Salt affected soils	Wasteland		Reclamation and Agroforestry, Salt tolerant trees and grasses
16.	Water logging	Agriculture		Surface and Sub surface drainage
17	Water logging	Wetlands		Land rehabilitation and ecosystem restoration

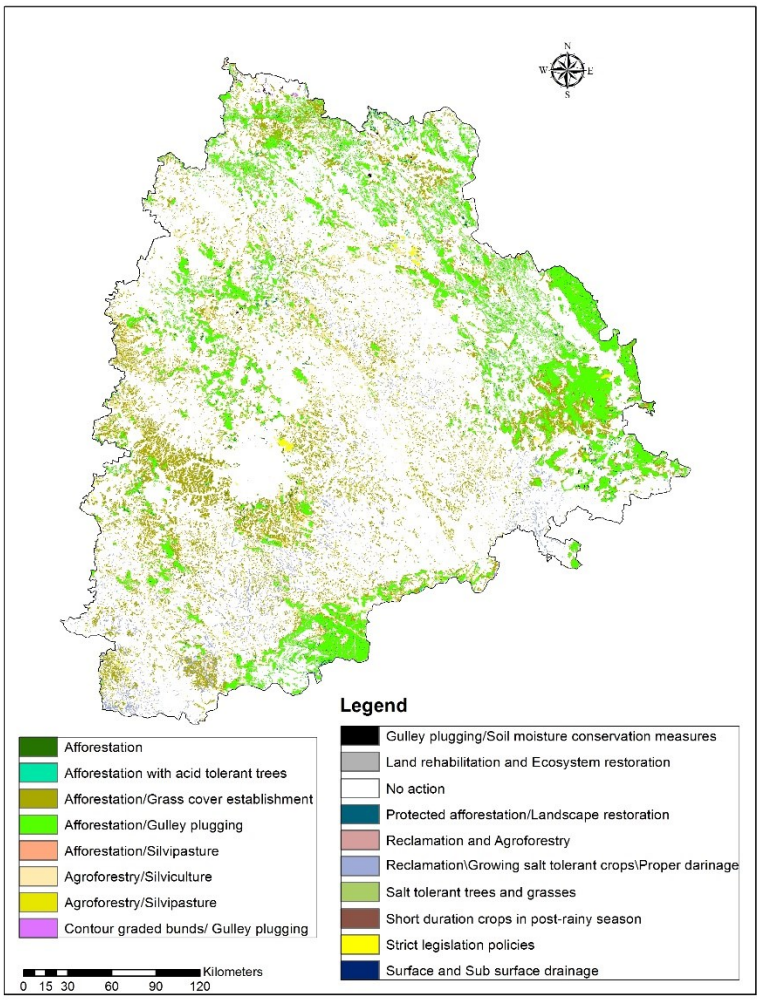

Figure 5: Land degradadtion neutrality action plan of Telangana State, India

Table 3: Area under various LD neutrality action plan in Telangana State

Action Plan	**Area (000 ha)**
Afforestation/Silvipasture	0.004
Land rehabilitation and ecosystem restoration	0.02
Short duration crops in post-rainy season	0.10
Surface and sub surface drainage	0.20
Reclamation and agroforestry	4.0
Salt tolerant trees and grasses	5.0
Gulley plugging/soil moisture conservation measures	5.0
Contour graded bunds/ Gulley plugging/soil moisture conservation measures/ ravine side slope stability	6.0
Afforestation with acid tolerant trees	10.0
Afforestation	20.0
Strict legislation policies	40.0
Agroforestry/silvipasture	50.0
Protected afforestation/landscape restoration	50.0
Reclamation/growing salt tolerant crops\providing proper drainage	130.0
No action	140.0
Agroforestry/silviculture	280.0
Afforestation/grass cover establishment &other vegetative measures	1090.0
Afforestation/gulley plugging	1420

4. Conclusions

In the present study, a decision based approach was developed to generate regional level LD neutrality action plan using geo-spatial techniques. Around 3322.5 thousand ha of land is under various processes of LD in the state of Telangana. Water erosion, salt affected soils and forest degradation were the major category of LD accounting to 87.7%, 5.3% and 3.6% respectively of the total LD area. Afforestation/ gulley plugging, contour graded bunds, grass cover establishment are the major action plans recommended to reduce the loss of land due to water erosion and forest degradation. Adoption of such activities may help restoring 76.4% of the area under LD in the study region. The future scope of work requires generation of action plans at 1:10, 000 scale or larger for effective utilisation by the users.

References

Bhattacharyya, R., N. G. Birendra, K. M. Prasanta, M. Biswapati, S. R. Cherukumalli, S. Dibyendu and D. Krishnendu et al (2015). Soil degradation in India: Challenges and potential solutions, Sustainability, 7(4), 3528-3570.

Biswas, H., A. Raizada, D. Mandal, S. Kumar, S. Srinivas and P. K. Mishra (2015). Identification of areas vulnerable to soil erosion risk in India using GIS methods. Solid Earth, 6(4),1247-2015.

DAC (1994). Draft Report on Status of Land Degradation in India, Department of Agriculture and Co-operation, Ministry of Agriculture and Co-operation, Govt. of India, New Delhi.

Dwivedi, R. S. (2001). Soil resources mapping: A remote sensing perspective. Remote Sensing Reviews, 20(2), 89-122.

Dwivedi, R. S., and K. Sreenivas (1998). Delineation of salt-affected soils and waterlogged areas in the Indo-Gangetic plains using IRS-1C LISS-III data, International Journal of Remote Sensing, 19(14), 2739-2751.

Dwivedi, R. S., K. Sreenivas, K. V. Ramana, P. R. Reddy and G. Ravi Sankar (2006). Sustainable development of land and water resources using geographic information system and remote sensing, Journal of the Indian Society of Remote Sensing, 34(4), 351-367.

Gomiero, T. (2016). Soil degradation, land scarcity and food security: Reviewing a complex challenge. Sustainability, 8(3), 281.

http://bhuvan.nrsc.gov.in

http://nbsslup.in

http://nass.usda.gov

Manchanda, M. L., M. Kudrat and A. K. Tiwari (2002). Soil survey and mapping using remote sensing, Tropical ecology, 43(1), 61-74.

Navalgund, Ranganath R. (2006). Indian Earth Observation Programme toward societal benefits: a GEOSS perspective, In Proceedings of SPIE – The International Society for Optical Engineering, 6407, 1-.10.1117/12.697269.

NRSC (2007). Nationwide mapping of Land degradation using multi-temporal satellite data. Project Manual. Soil and Land Resources Assessment Division, Earth Resources Group, RS &GIS application area, Department of Space, Govt. of India, Balanagar, Hyderabad, India.

Ritzema, H. P., T. V. Satyanarayana, S. Raman and J. Boonstra (2008). Subsurface drainage to combat waterlogging and salinity in irrigated lands in India: Lessons learned in farmers' fields. Agricultural Water Management, 95(3), 179-189.

Uchida, S. (1994). Land degradation analysis of rainfed agricultural area in Pakistan using remote sensing data. In Proc. 15th Asian Conf. Remote Sensing, 1-5.

UNCCD (2015). Report of the Conference ofthe Parties on its twelfth session, held inAnkara from 12 to 23 October 2015. Parttwo: Actions taken by the Conference ofthe Parties at its twelfth session. ICCD/COP(12)/20/Add. Bonn: United NationsConvention to Combat Desertification.

Veldman, Joseph W., E. Gerhard Overbeck, D. Negreiros, G. Mahy, S.L. Stradic, G. Wilson Fernandes, G. Durigan, E. Buisson, Francis E. Putz and W. J. Bond (2015). Tyranny of trees in grassy biomes. Science, 347(6221), 484-485.

Venkataratnam, L. and T. Ravisankar (1992). Digital analysis of Landsat TM data for assessing degraded lands, In: Remote Sensing Applications and Geographical Information Systems–Recent Trends, 87-190.

Wikramanayake, Eric D., E. Dinerstein and Colby J. Loucks (2002). Terrestrial ecoregions of the Indo-Pacific: a conservation assessment, Vol. 3. Island Press.

Journal of Geomatics Vol. 13, No. 2, October 2019

Route alignment planning in hilly terrain using geospatial technology: A case study in parts of Arunachal Pradesh, India

M. Somorjit Singh*,1, Victor Saikhom[1], P.L.N. Raju[1] and Siva Shankar Prasad[2]
[1] North Eastern Space Applications Centre, Meghalaya
[2] Border Roads Organization (BRO), 761 BRTF (GREF), Arunachal Pradesh
*Email: msomorjit69@gmail.com

(Received: Dec 31 2018; in final form: Oct 10, 2019)

Abstract: Several studies show the use of geospatial technology in various aspects of planning and development activities as well as in the monitoring of implementation stages. This present paper highlights the advantages and effective utilization of geospatial technology for alignment of new route where the accessibility is the main cause of concerned. Since the study area is in rugged hilly terrain, the generation of landslide susceptibility map and the vertical alignment with defined criteria were adopted to find out the best possible route to connect two locations or points. Landslide susceptibility map that provides the information on spatial likelihood of occurrences of landslide was generated using heuristic or knowledge based approach. Using the contour map derived from Cartosat-1 Digital Elevation Model (DEM) and susceptibility map as a background with the incorporation of gradient criteria, the final route was prepared / generated connecting Dumro and Same Basti, Arunachal Pradesh, India.

Keywords: Geospatial technology, landslide susceptibility, vertical alignment, spatial likelihood, DEM

1. Introduction

Planning and construction of a new road or highway requires proper understanding of different aspects related to environment. It also requires a detail analysis of the site characteristics pertaining to the area such as existing dry and perennial streams, river configuration, surface soil conditions, geology, physiographic conditions, groundwater, land use/ land cover and particularly the slope condition. In absence of thorough investigation and proper scientific approaches, it may lead to more time consumption and expensive than expectations. Moreover, the degree of complexities may rise to double fold if the issues related to environment, social and or cultural are not properly addressed in public domain. However, in the last few decades with the advent of space technology and GIS, alignment/realignment planning of new route and/or old road in any area becomes easier and viable in resolving these issues extensively.

Since the study area is falling in hilly terrain, it was realized the need and the importance of landslide susceptibility map as an essential component for alignment of new route to avoid landslide prone areas. Landslide or slope failure is one of the major recurring natural hazards which cause loss of lives, property in hilly terrain (Champati et al., 2004). North Eastern Region (NER) falls in the high and medium to high category of the Global Landslide Susceptibility Map with few hotspot areas along Arunachal Himalaya (Hong and Adler, 2008). In global view of landslide susceptibility, the study area is falling in severe category (Dalia and Stanley, 2017).

The present study has been carried at the request of Boarder Road Organization (BRO) under the Project Brahmank, Arunachal Pradesh. The study aims to find out a best suitable route to connect two villages - Dumro and Same Basti of Upper Siang and Lower Dibang Districts, Arunachal Pradesh.

1.1 Objectives

- To generate landslide susceptibility map on 1:50,000 scale using various geo-environmental parameters with the help of remote sensing and GIS techniques in conjunction with existing data such as Survey of India Topographical Maps, published maps and literatures with limited field check.
- To generate and suggest a new route alignment using Cartosat-1 DEM and the landslide susceptibility map to avoid landslide prone areas with maximum possibility

2. Materials and methods

2.1 Study area

The study area covers part of Upper Siang and Lower Dibang Districts and a very small northern portion of East Siang district of Arunachal Pradesh and falling under the Yamme and Sessari River Catchment of Lesser Himalaya (Figure 1). It is located between 95˚11'E to 95˚13' longitudes and 28˚13' N to 28˚29' N latitudes with an area of 537 sq. km. The highest and lowest elevation is 3251.54 m and 234.21 m with reference to ellipsoidal datum (WGS 84) respectively. Apart from the various means of communication facilities, the study area is connected only with one road which is in a very poor condition with frequent landslides and subsidence. It has a relatively long rainy and winter season but a short and pleasant summer. During winter the mercury drops below 0˚C and during summer the maximum temperature is about 25˚C. Dumro village, located at the height of 1126 m, is relatively a larger settlement area compared to Muri Basti, Lema Basti etc. The nearest town is Yinkiong and Pashigahat.

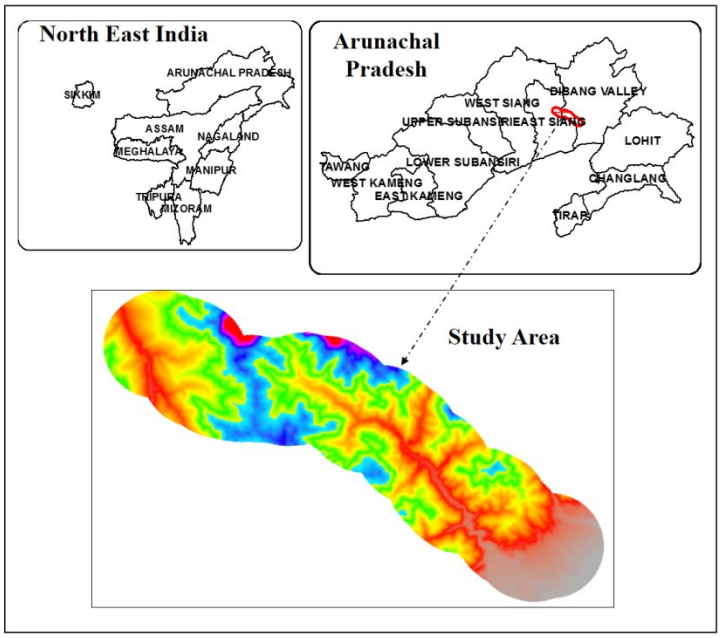

Figure 1: Location map of the study area

2.2 Data used

Cartosat-1 (2.5 m resolution) of year 2007&2008, Cartosat-1 Digital Elevation Model (DEM-30m resolution), Multispectral LISS-IV-MX (5.8m resolution) of year 2013 & 2014 of Indian Remote Sensing Satellite were used. Survey of India topographical map (1:50,000 scale) was also used as a reference to identify the location information for preparation of base map as well as other details. Details of satellite imagery and other collateral data used in the study are as follows:

- Cartosat-1 data of year 2007 and 2008 (2.5 m spatial resolution)
- IRS (Indian Remote Sensing Satellite) Resourcesat 2, LISS-IV MX, 113-051c data acquired on 15 Nov, 2013
- IRS (Indian Remote Sensing Satellite) Resourcesat 2, LISS-IV MX, 113-051d data acquired on 26 Jan, 2014 (3 Band, 6 m spatial resolution)
- Cartosat-1 stereo pair derived Digital Elevation Model (DEM-30m spatial resolution) prepared by NESAC
- Survey of India (SOI) Topographical Map No.82P/3, 82P/7, 82P/11and 82P/12 (1: 50, 000 scale)
- Collateral data with limited field survey

2.3 Methodology

In order to meet the objectives, the methodology has been divided broadly into two parts. Preparation of various thematic layers and generation of landslide susceptibility map. Flow chart of the methodology implemented is shown in figure 2.

Base Map: Base map was prepared from IRS LISS-IV data aided by information from the topographical maps (1: 50,000 scale). These include major road, other road, village or settlement locations etc. The locations of villages were interpreted from IRS Resourcesat-2 LISS-IV MX satellite image and names were taken from topographical maps.

Lithology: Lithology map was prepared by compiling all existing information from literature and published maps and maps prepared for groundwater prospect mapping under Rajiv Gandhi National Drinking Water Mission (ARSAC, 2010).

Necessary modification in delineating the boundaries of the litho units and further details were carried out based on the interpretation of satellite data and finalized with selective field verifications (Figure 3). The major portion of the study area falls in Tenga formation composed of green phyllite, meta-volcanics, sericite, quartzite and phyllite and Ziro biotite granite gneiss of Bomdila Group. Miri formation which is mainly composed of feldspathic quartzite, purple shale, and conglomerate of Gondwana Group is exposed in the south eastern part of the study area. Abor volcanic composed of mainly basalt of the same Group was exposed in North western part of the study area. Older Alluvium of Quaternary sediments composed of boulders, cobbles, pebble, sand and sandy clay beds are found deposited in the south eastern corner of the study area where the rivers inters in the piedmont zone (GSI, 2010).

Geomorphology: It was prepared from remotely sensed data and accordingly various units were delineated using the manual/ guidelines framed under National Geomorphology and Lineament Mapping (NRSC, ISRO, GSI, 2012) with minor modification as per the requirement (Figure 4). It is the study of classification, description, nature, origin, and development of present landform and their relationship to underlying structures and geologic changes as recorded by these surface features (Bates & Jackson, 1980). The major portion of the study area falls under Lesser Himalaya and portion of extreme south eastern part under Brahmaputra Plain (GSI, 2010).

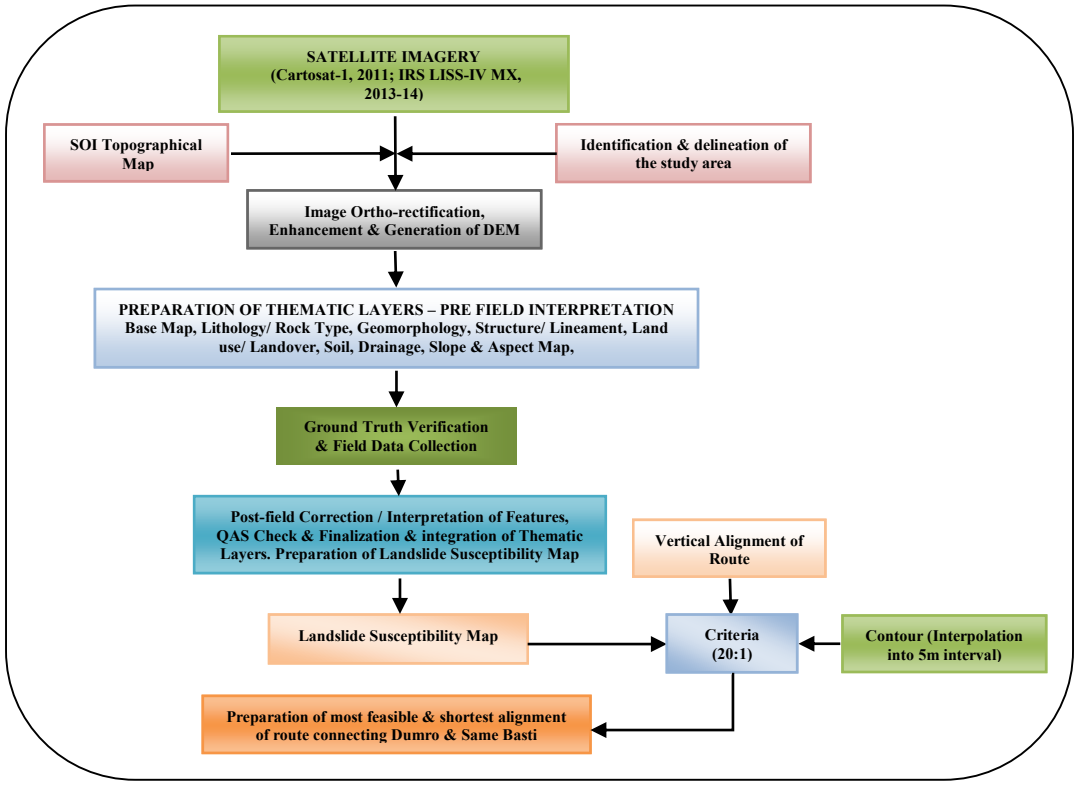

Figure 2: Methodology flow chart

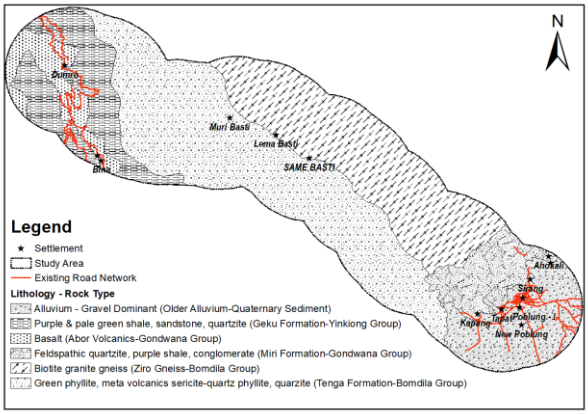

Figure 3: Lithology of the study area

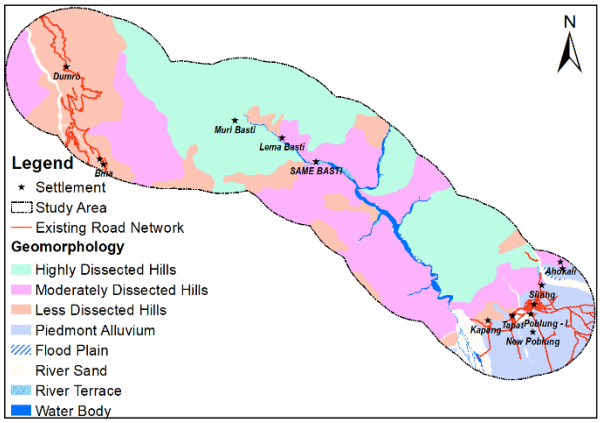

Figure 4: Geomorphology of the study area

Dissected hills of structural and older alluvium of fluvial origin are major geomorphic units found in the area with larger area coverage and other features like flood plain, river terrace, and river sand occupy small portion. Dissected hills of structural origin are further divided into- highly dissected, moderately dissected and low dissected hills according to their degree of dissection pattern on land surface.

Structure/ lineament: The lineament map was prepared from satellite data in conjunction with other diagnostic criteria such as channel offset, bank erosion and down-cutting of channel along lineament, branching of river course, abrupt change of river course, presence of dry channel in an active river course, linear ridges, scarp surface, linear alignment of water bodies, straight channel segments etc.

It may be defined as 'A linear topographic feature of regional extent that is believed to reflect crustal structure' (Bates & Jackson, 1980) or in simplest term 'A linear feature of geologic interest' that reflects the discontinuity of the underlying bedrock. Lineaments occur as straight, curvilinear, and parallel or en-echelon features which are generally related to fracture systems, discontinuity planes, fault planes, shear zones in rocks (Gupta, 2003). They are also considered very important parameter as they influence slope stability of a region. The lineament map thus prepared from satellite data was used in calculation of lineament density (Figure 5). The density map was slices into three classes of intervals using natural breaks - low (11.13% of total area), moderate (44% of total area) and high (44.6% of total area) to understand a particular area falls into which area of bedrock conditions having highest discontinuity as well as to establish the relationship with

the occurrences or likelihood of occurrences of landslides. Major portion of the study area falls under moderate and high category.

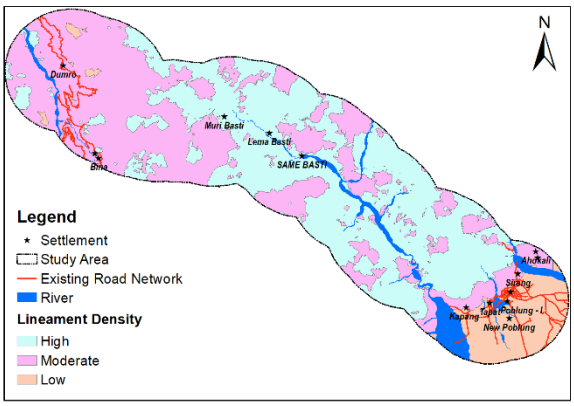

Figure 5: Lineament density of the study area

Drainage: Drainage in an area is governed by bedrocks, soils and rock structures and one of the important geotechnical or terrain element used as a clue to identify the same in an area (Pandey, 1984). Drainage map was prepared mainly from the remotely senses data aided by information from topographical maps (Figure 6).

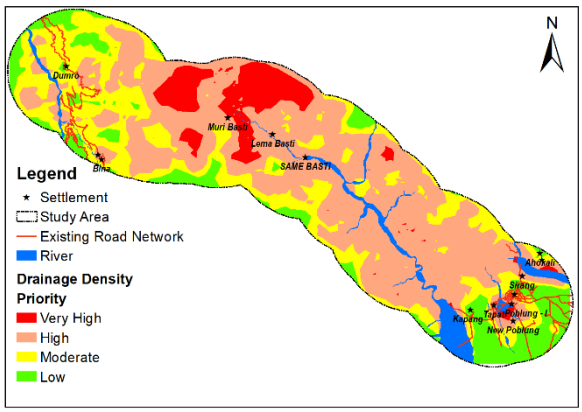

Figure 6: Drainage map of the study area

Major rivers having sufficient width are represented as polygon features and the remaining are represented as line features. The study area falls under the catchment of Yamme and Sesseri or Sissar River which shows overall dendritic drainage pattern. However, in the upper reaches of Sissar River, minor anomalies in pattern are observed which generally inferred that the major controlling factors may be fractures/ joints. Using the drainage, drainage density was generated. The density map was further slices into four classes of intervals using natural breaks low (12.32% of total area) moderate (26.18% of total area), high (52.38% of total area) and very high (9.13% of area). This map helps in understanding the landscape dissection and runoff potential in the area. From this map, it is well observed that the major portion of the study area falls under moderate and high drainage density where the actual alignment of route is being carried out.

Land use/ land cover: Land use/land cover map was prepared from remotely sensed dada with existing information and limited field investigation (Figure 7). Different classes of land use/ land cover were interpreted using NRC-LULC50K Mapping Project (NRSA, 2006) manual with minor modification as per the requirement.

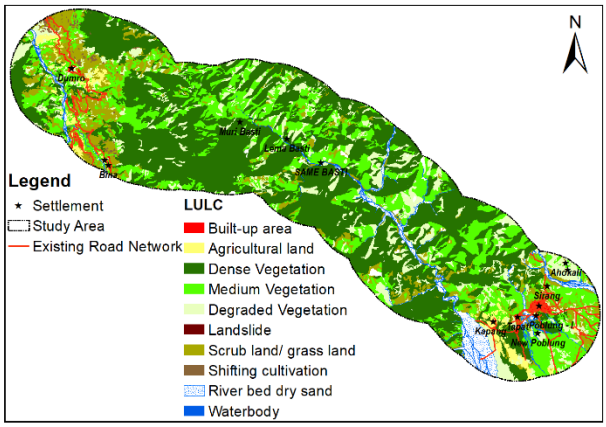

Figure 7: Land use/land cover map of the study area

In the study area, major portion was occupied by dense vegetation (more than 40% canopy cover/density), medium vegetation (10 to 40% canopy cover/density) and degraded vegetation (less than 10% canopy cover/ density) and the built-up area occupied the least. Area-wise percentage is given in table 1.

Table 1: Land use/ Land cover Class (area %)

Sl. No	Land Use /Land Cover Type	Area %
1	Built-up area	0.41
2	Agricultural land	1.90
3	Dense Vegetation	46.54
4	Medium Vegetation	23.53
5	Degraded Vegetation	12.05
6	Scrub land/ grass land	10.39
7	Barren/ Rocky area	0.53
8	Shifting cultivation	0.44
9	River bed dry sand	3.61
10	Water body	0.58

Soil texture: The soil texture map was prepared with the help of available small scale map (NBSS & LUP, 1997) since 1: 50,000 scale map or larger is not available of the study area. Three broad textural classes such as clayey, loamy and loamy skeleton were considered (Figure 8). It may be noted that, at the time of data integration it has been given lower rank since it is highly generalized and arbitrary in nature.

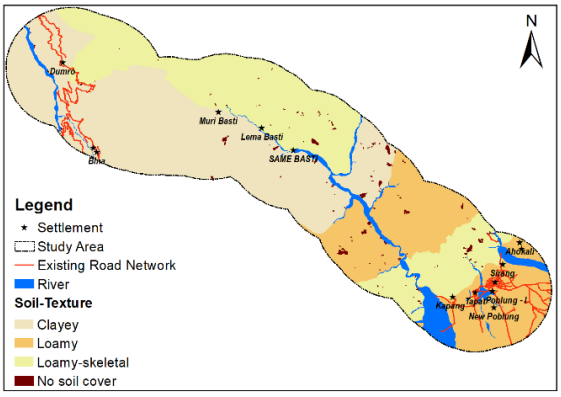

Figure 8: Soil texture map of the study area

Slope & aspect map: The various slope components are considered as important inputs for evaluation of slope stability of the area. Slope steepness or amount of slope is a factor which associates the effectiveness of gravity acting on a slope to landslide susceptibility (NESAC, 2014). The topographic slope / slope gradient map and slope aspect or orientation maps was prepared from Cartosat-I DEM with 30m spatial resolution and 8m height accuracy. The slope map was classified into eight classes (Figure 9). Slope aspect is the compass direction that a slope faces and it can have a strong influence on temperature. Direction/ orientation of maximum slope aspect was calculated for each pixel in 3×3 pixels' window and classified into nine classes (Figure 10).

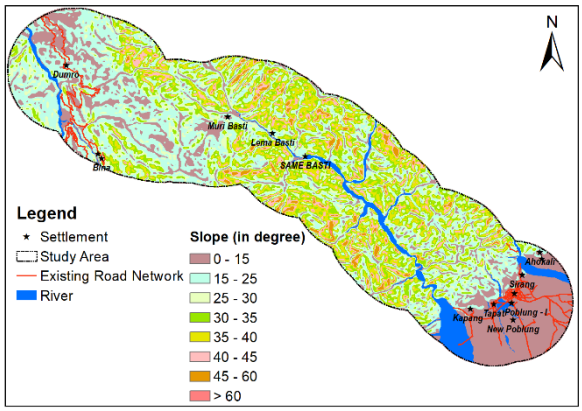

Figure 9: Slope map of the study area

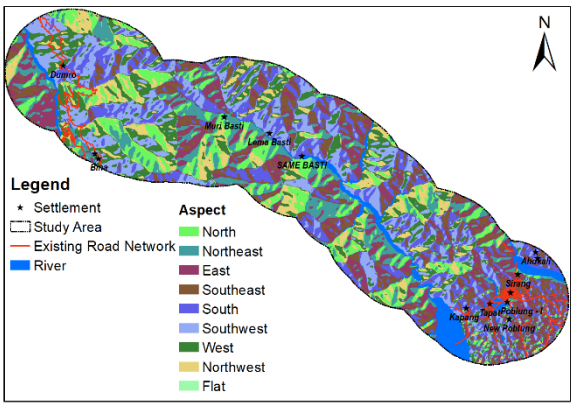

Figure 10: Slope aspect map of the study area

Data integration & susceptibility zonation: There are various approaches for the preparation of landslide susceptibility zonation adopted by many experts. Susceptibility is defined as 'a quantitative or qualitative assessment of the classification, volume (or area) and spatial distribution of landslide which exist or potentially may occur in an area (Australian Geomechanics Society, 2007). It may also include a description of the velocity and intensity of the existing or potential land sliding. Zonation refers to the division of a land surface into homogeneous areas or domains and their ranking according to the different degrees of actual/ potential hazard caused by mass movement (Varnes, 1984). Landslide Susceptibility map can be prepared using pure statistical techniques as well as pure knowledge-based approach (Westen, 1993; Carrara et al., 1995; NRSA, 2001). In the present study, knowledge-driven heuristic approach (Guzzetti et al., 1999) was adopted. Each geo-environmental factors/ parameters class influencing landslides, such as lithology / rock type, geomorphology / landform, structure/ lineament (density), drainage (density), land use/ land cover, soil texture, slope and aspect were assigned weights for each class and integrated in GIS with knowledge based rank and thus generated the cumulative susceptibility map. These weights and ranks are based on their assumed or expected importance in causing mass movements/ landslide and 'a-priori' knowledge available to the experts in the particular area of study (IIRS, 2008). Finally, the susceptibility pixels are classified into one of the following five classes – very low, low, moderate, high and very high using natural cut-off ranges (Figure 11).

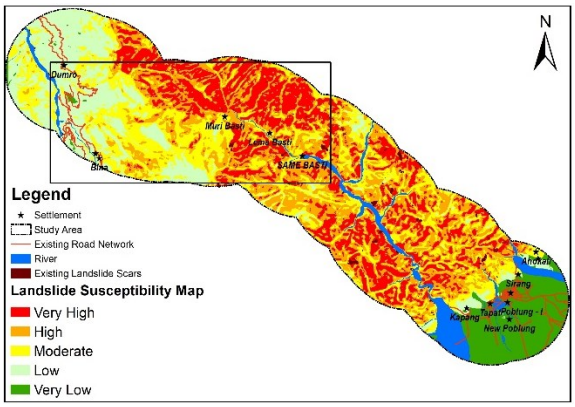

Figure 11: Landslide susceptibility map

The validation of the susceptibility map thus generated was carried out based on the distribution existing landslide in the area. It was observed that 80% of the slides are falling in high and very high category which occupies 53.25% and 31.01 % of the total area respectively and 20% are falling in moderate and low category which occupies 11.01% and 4.45% of the total area. Very low category occupies 0.28% of the total area where no slide has been detected.

Route alignment (vertical alignment)

Route alignment / location aims at evaluating the ground condition of a very large area between two end points. Planning for development of a new route to connect between two end points or places is based on the various factors such as the socio-economic, administrative as well as strategic importance of the area, region or the country. 'The position or the layout of the centre line of the highway on the ground is called alignment'. In general, alignment is of two type – horizontal alignment and vertical alignment (Subramani and Kumar, 2012). Route alignments in hilly areas are more winding/ curving in nature up to certain extent in comparison to horizontal alignment and it is mostly controlled by the topography. During the analysis the identified criteria i.e. for every 20 m horizontal length, the permissible vertical raise or fall of 1 m (20:1) was incorporated wherever applicable. The aligned route superimposed on susceptible map is shown in figure 12.

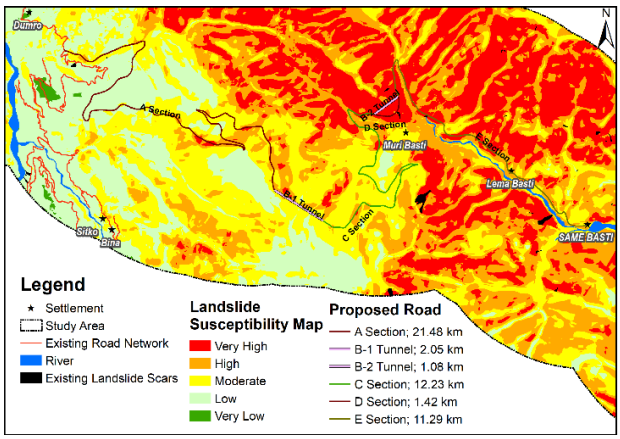

Figure 12: Aligned route superimposed on susceptibility map

3. Results and discussion

The proposed aligned route has been carried out to connect between Dumro Village of Upper Siang and Same Basti Village of Lower Debang Valley Districts of Arunachal Pradesh. It may be highlighted that the aligned road is about 48.47 km in length. The starting point of the aligned route is from the existing road at the height of 850 m, on the right bank of Sipung Korong stream and about 1.5 km before reaching Dumro Village. For easy understanding and clear viewing, the entire length of the route is divided into A, B1 & B2 tunnels, C, D and E sections respectively.

The first section denoted as 'A Section' is 21.48 km in length. In this section it is observed that 31% falls in low, 39% in moderate, 25% in high and 5% in very high category in the susceptibility map. Figure 13a &13b shows the 3D-view and longitudinal profile of 'A-Section'. The second section denoted as 'B-1 Tunnel' is the suggested tunnel site having 2.05 km in length. It started at an elevation 1870 m and ends at 1850 m with 0.0098 percent raise or 0.5615˚ gradients. The thickness of the overburden is 230m at the highest point. Figure 14a &14b shows the 3D-view, longitudinal and overburden profile of 'B-1 Tunnel' Section. The third section denoted as 'C Section' is 12.66 km in length. Out of which 65% falling in moderate, 22% and 13% are falling in high and very high category in the susceptibility map. 3D-view and longitudinal profile of 'C Section' is shown in figures 15a & b.

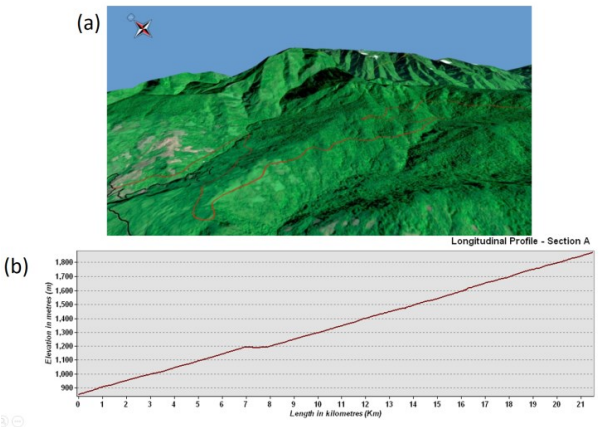

Figure 13: (a) 3D-view and (b) longitudinal profile of A-section

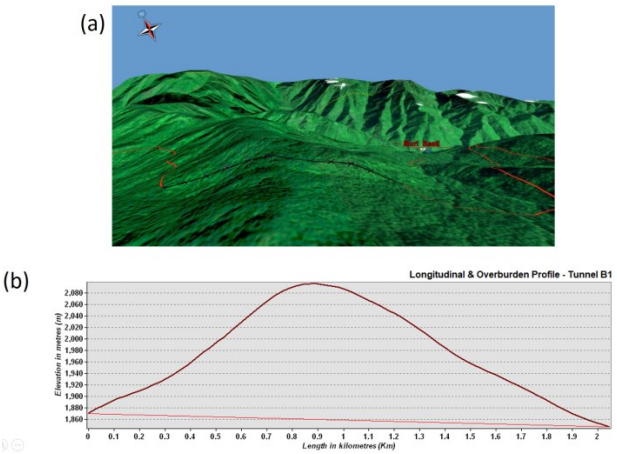

Figure 14: (a) 3D-view and (b) longitudinal profile of B-1 tunnel section

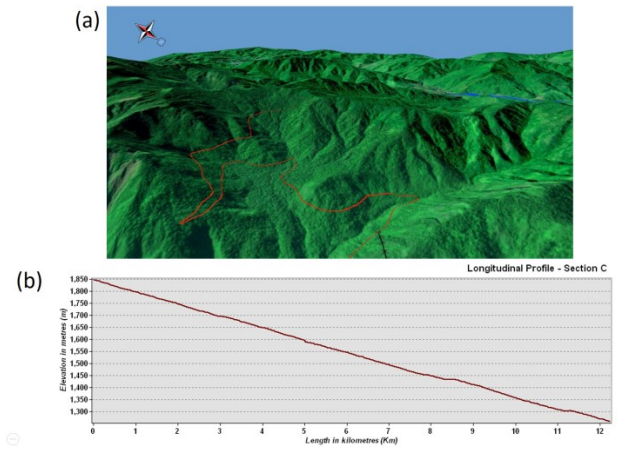

Figure 15: (a) 3D-view and (b) longitudinal profile of C section

The fourth section denoted as 'D Section' is having a length of 12.42 km. It may be noted that 95% of the length of the section is falling under very high and 5% in high category in the susceptibility map.

Figure 16 a & b shows the 3D-view and the longitudinal profile of the 'D Section'. It is observed that this section is passing just above the crown of an active landslide area that may reactivate at any time. With this observation, a tunnel denoted as 'B-2 Tunnel' is suggested in the same section having a length of 1.08 km that reduces the 0.34 km of the total length. The suggested tunnel is having 2.3 percent raise or 1.33˚ gradient. The thickness of the overburden is 90 m at the highest point. The last section denoted as 'E Section' is 11.29 km in length and follows a small section on the right bank and major section on the left bank of Sessari River. In this section, maximum length of the suggested route is falling under very high category (44%) in the susceptible map in comparison to high (38%) and moderate (18%) category.

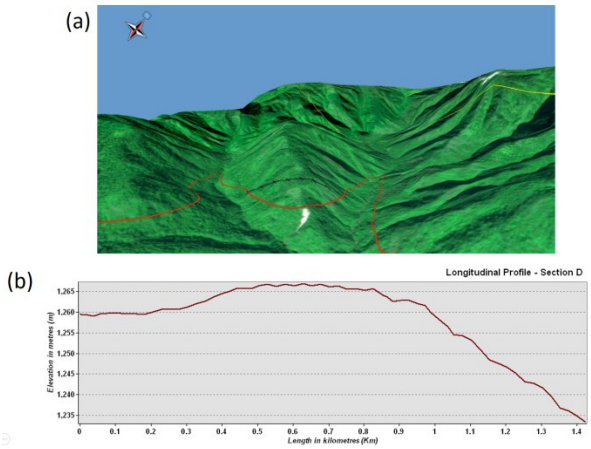

Figure 16: (a) 3D-view and (b) longitudinal profile of D tunnel section

Figure 17 a &17 b shows the 3D-view and longitudinal profile of 'E Section'.

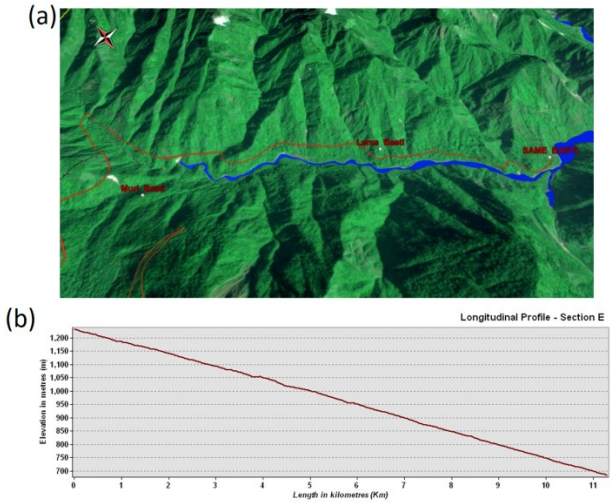

Figure 17: (a) 3D-view and (b) longitudinal profile of E section

In the suggested 'A section' of the route, it is well observed that there are two hairpin bend curves (Hairpin Bend Curve 1 & 2) and one major curve over the Sipung Korong stream is indicated as Major Bridge Location–1 in satellite data with suggested length of 100 m approximately. Three major curves are observed in the suggested 'C Section' out of which one is hairpin bend (Hairpin Bend Curve–3) one is major curve (Major Curve – 2) which is indicated as major bridge location-2 with approximate length of 45 m over the Sipinala. In the 'E Section' of the route, three major bridges are suggested over the Sikhu Nala (Major Bridge Location-3), Namsi Nala (Major Bridge Location-4), Same Nala (Major Bridge Location-5) with approximate length of 122 m, 99 m and 100 m respectively. Locations of major bridges and curves on Satellite data are shown in figure 18.

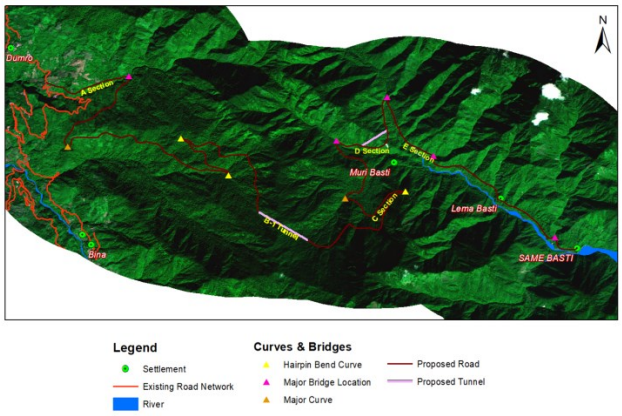

Figure 18: Locations of major bridges and curves on satellite data

4. Conclusion and recommendations

From the results and discussion, it is clearly indicated that remote sensing techniques aided with limited field investigation are very useful in various stages of preliminary study of the area especially where the accessibility is very poor. On the other hand, GIS played a significant role in providing the most feasible and shortest alignment of new route/road since it has the capability of handling large spatial data and integration. In the entire process of alignment, an attempt has been made to follow the criteria strictly and maximum effort has been given to avoid the existing active landslide areas as well as high and very high categories as indicated in the susceptibility map. However, it may be noted that during and/ or after the construction of the road, different category of different category of susceptibility zone may change into another due to the disturbance on the stability of slope. The environment of the area may be affected in micro or meso scale due to felling of trees as well as wildlife habitats.

The following points are put forward as recommendations

- Proper channelization of seepage zones.
- Adoption of slope and landslide protection measures wherever possible such as afforestation and other conservation measures (engineering & bio-engineering), terrace cultivation on steep slopes, etc.
- Protection of river bank erosion or toe cutting.

Limitations

More than 90% of the study area is inaccessible so that limited field investigation was concentrated along the road for some of the parameter used in the study. It may also be noted that, soil texture map was derived from available small scale soil map so that it is highly generalized and arbitrary in nature. Geo-technical properties of rocks such as dip-slope relationship, fracture/ joint patterns, their orientation and tectonic relationship are not included in the study. Hence, the landslide susceptibility map generated is qualitative in nature and provide only broad idea about the spatial likelihood of occurrence of landslide in future. Moreover, since the alignment of the route is mandatory with strict gradient criteria and predefined approximate length, complete avoidance of very high and high landslide susceptible zone is hardly possible. In addition, due to

resolution of the satellite data used and working scale factor, detection/ identification of number of culverts, minor bridges etc. which require extensive ground information are not included in this scope of the work.

Acknowledgements

The authors extend their sincere thanks to Border Roads Organization (BRO), 761 BRTF, (GREF), Project Brahmank, Arunachal Pradesh, for providing the opportunity to carry out the work.

References

ARSAC, (2010). Groundwater Prospect Mapping-Phase - III (A). Under Rajiv Gandhi National Drinking Water Mission, Arunachal Pradesh

Australian Geomechanics Society (2007). Landslide Risk Management, Journal and News of the Australian Geomechanics Society, Vol. 42 No. 1. ISSN 0818-9110.

Bates R. L and J. A. Jackson (1980). Glossary of Geology, 2nd Edition, American Geological Institute, Fall Church, Virginia, ISBN 0-913312-15-0.

Carrara, A., M. Cardinali, F. Guzzetti and P. Reichenbach (1995). GIS technology in mapping landslide hazard. In: Carrara, A. and Guzzetti, F. (eds.), Geographical Information Systems in assessing natural hazards, Dordrecht: Kluwer, 135– 175.

Champati R, P.K., and R. C. Lakhera (2004). Landslide Hazards in India, Proceedings of the Asian Workshop on Regional Capacity Enhancement for Landslide Mitigation (RECLAIM), organised by Asian Disaster Preparedness Centre (ADPC), Bangkok and Norwegian Geotechnical Institute, Oslo, Bangkok, 13-15 Sept. 2004

Dalia, K and T. Stanley (2017). A Global View of Landslide Susceptibility. Available: https://earthobservatory.nasa.gov/images/89937/a-global-view-of-landslide-susceptibility

GSI, (2010). Geology and mineral resources of Arunachal Pradesh, Miscellaneous publication, No. 30 Part IV Vol.1 (i), Arunachal Pradesh.

Gupta. R. P (2003). Remote Sensing Geology. (2nd Ed.). Springer. ISBN 978-3-662-05283-9.

Guzzetti, F., A. Carrara, M. Cardinali and P. Reichenbach, (1999) Landslide hazard evaluation: a review of current techniques and their application in a multi-scale study, Central Italy, Geomorphology, 31, 181–216.

Hong, Y. and Adler, R.F(2008). Predicting global landslide spatiotemporal distribution: Integrating landslide susceptibility zoning techniques and real-time satellite rainfall estimates, Int. J. of Sediment Research, Vol.23, pp 249-257.

IIRS, (2008). Landslide Hazard Zonation Mapping Along Shillong-Silchar-Aizawl Highway Corridor In Northeastern Region of India, Technical Report and Atlas, 1st Issue: Dec., 2008

NBSS & LUP, (1997). Soils Arunachal Pradesh for Optimizing Land Use, NBSS, Publ.55b, ISBN: 81085460-42-6.

NESAC, (2014). Remote Sensing and GIS Based Landslide Hazard Zonation Map and Reservoir Rim Stability Studies for Subansiri Lower Project (SLP) (NESAC-SR-96-2013).

NRSA, (2001). Technical Report and Atlas: Landslide Hazard Zonation Mapping in the Himalayas of Uttaranchal and Himachal Pradesh using Remote Sensing and GIS techniques, National Remote Sensing Agency, Department of Space, Hyderabad.

NRSA, (2006). Manual. National Land Use Land Cover Mapping using Multi-Temporal Satellite Data, National Remote Sensing Agency, Dept. of Space, Govt. of India, Hyderabad.

NRSC ISRO, GSI (2012). National Resource Census (NRC)-National Geomorphology and Lineament Mapping, User Manual.

Pandey, S. N (1984). Principle and Applications of Photogeology, Wiley Eastern Limited.

Subramani, T and S.N. Kumar (2012). National Highway Alignment Using GIS, Int. J. of Engineering Research and Applications (IJERA), 2(4),427-436.

Varnes, D. J (1984). Landslide Hazard Zonation: A Review of Principles and Practice. UNESCO, Paris, ISBN 92-3-101895-7.

Westen, C. J. van, (1993). GISSIZ Training Package for Geographic Information Systems in Slope Instability Zonation, UNESCO-ITC Project. ITC Publication No. 15, Enschede, The Netherlands.

Journal of Geomatics Vol. 13, No. 2, October 2019

Development of a Web-GIS based system for safer ship navigation in Antarctic region using open source technologies

Ujjwal K. Gupta*, Purvee Joshi, Pankaj Bodani, Sandip R. Oza, D. Ram Rajak and Markand Oza
Space Applications Centre, ISRO, Ahmedabad – 380 015
*Email: ujjwal_gupta@sac.isro.gov.in

(Received: June 13, 2019; in final form: Nov 11, 2019)

Abstract: Polar ecosystem plays a crucial role in global climate change processes. Antarctica is an ideal natural laboratory for advanced research related to climate change and polar ecosystem studies. Concerned global scientific community carries out various scientific experiments by organising expeditions to various research stations located in Antarctica. These stations are heavily dependent on outer world for their maintenance, logistic requirements as well as scientific needs. The number of vessels travelling to and from Antarctica; and between research stations are increasing every year. These vessels face adverse climatic conditions viz. high wind conditions, sea ice resistance, changing polar currents, sea ice deformations etc. Remote sensing data available through various satellites can provide relevant and needed information such as Sea Ice Thickness (SIT), Sea Ice Concentration (SIC) and Sea Ice Extent (SIE) which, when utilized rationally can provide a suitability map for safer ship navigation. Web-GIS acts as a low-cost modus operandi that brings GIS based system in public reach across the globe. Therefore, a need of Web-GIS enabled Earth Observation (EO) satellite data based safer ship navigation system is felt. This paper discusses development and dissemination of a rich Graphical User Interface (GUI) based Web-GIS application which inherits power of open source technologies for generation as well as geo-visualization of ship navigation suitability map in the Antarctic region. In backend, relevant data is automatically downloaded, ingested and processed using Python. VueJS framework is deployed for in-browser visualization experience at client's end. Users can pan, scale, get feature information at a given pixel by clicking on image and perform temporal pixel drilling. User can also download temporal profile in .csv format. The developed system has been used for Indian Scientific Expedition to Antarctica during 2018-19 and available at https://vedas.sac.gov.in/vstatic/ship_nav/.

Keywords: Ship navigation suitability map, Sea-ice, Antarctica, Remote Sensing, Web-GIS, VEDAS

1. Introduction

A polar ecosystem is unique and differs significantly from other ecosystems. It consists of atmosphere, ocean, sea ice, polynyas, ice shelf, ice sheet etc. In recent years, there has been increasing interest in polar studies to understand impact of climate change. Several studies suggest that ice cover, having growth and melting order of one year, captures climate signal and acts as an indicator, if integrated over short period (Rees, 2006).

These studies provided further curiosity and momentum to research related to polar ecosystem. Global scientific community carries out various scientific experiments by organising expeditions to various research stations located in Antarctica. However, frequent variability of atmospheric and oceanic conditions, such as high wind conditions, rapidly changing ocean waves, varying sea ice conditions etc. causes challenges for safer ship navigation. Therefore, accurate knowledge of sea ice conditions is crucial for ship navigation in polar region during various expeditions. In recent years, there have been news of vessels stranding in sea ice in Antarctic Ocean, e.g., stranding of a Russian vessel MV Akademik Shokalskiy in December 2013 (Pearlman, 2013). There are several vessels engaged in scientific expeditions from different countries in the Antarctic region. Some may have limited ice breaking capability. In such conditions, there is a need for an automated satellite data based web GIS integrated system to provide near real time navigation suitability map.

Safer navigation through Antarctic Ocean requires information on major sea ice parameters, viz., Sea Ice Thickness (SIT), Sea Ice Concentration (SIC), Sea Ice Extent (SIE) etc, which is primarily derived using Earth Observation (EO) satellite data. This information when combined with Web based Geographic Information System (WebGIS) results into a near real time information system for safer ship navigation. The Arctic Ice Regime Shipping System (AIRSS) provides a flexible framework for decision making along with minimum risk of pollution in the Arctic waters due to damage to vessels by sea ice (Anonymous, 2018). Space Applications Centre (SAC) has been providing regular sea ice advisories to the Indian Scientific Expeditions to Antarctica since 2012-13 using various sea ice products derived from EO data (Rajak et al., 2014 and 2015). Several attempts have been made to develop expedition specific navigation system (Hui et al. 2017). However, a more user friendly near real time Web-based GIS information system is lacking for Antarctica.

Web-based GIS is open source, distributed, standardized by OGC (Open Geospatial Consortium) system that brings GIS technology to the public at little or no cost (Caldeweyher et al., 2006). A web-GIS based system increases visibility of system and enhances effectiveness of system for decision making process as all related data is available at a single place. Today, only a reliable internet connection and compatible browser makes it possible for users to access such system.

In the study presented in this paper, a Web-GIS enabled satellite data based system for safer ship navigation is developed for Antarctic region. This system utilizes available sea ice related information viz. SIE, SIC, SIT derived using EO data to generate near real time navigation suitability map.

Table 1: EO satellite data products used in the study

Sr. No.	Input	Data type	Spatial Resolution	Temporal interval	Data Sensor / Source
1	Sea Ice Thickness (SIT)	Image	10 km	Daily moving 15-day composite	SARAL/AltiKa
2	Sea Ice Extent (SIE)	Image	~2.2 km	Daily composite	SCATSAT-1
3	Sea Ice Concentration (SIC)	Image	25 km	Daily composite	SSMIS

2. Study area

Study area covers entire oceanic region surrounding the Antarctica. It includes the ocean portion nearby Amery ice shelf (Prydz Bay), Brunt ice shelf & Larsen ice shelf (Weddell sea), Bellingshausen sea, Amundsen sea, Ross ice shelf (Ross sea) and Shackleton ice shelf as well ocean portions neighbouring Indian research stations viz., Maitri (70º 45' S, 11º 43' E) and Bharati (69º 24'S, 76º 11' E).

3. Data used

Table 1 summarizes information regarding input data used in this study.

3.1 Sea Ice Thickness (SIT)

The developed system uses a daily product of Sea Ice Thickness derived from SARAL/AltiKa. The SARAL/AltiKa program is a collaborative programme between ISRO, India and CNES, France. SARAL (acronym for "Satellite for ARgos and ALtiKa". SARAL/AltiKa), launched on 23 February 2013, is the world's first satellite equipped with a Ka-band (35.75 GHz) altimeter for measuring ocean sea-surface height (https://altika-saral.cnes.fr/en/home-20). Sea ice thickness is retrieved using SARAL/AltiKa radar waveforms (Joshi and Oza, 2018). Sea ice thickness retrieved as point data from satellite is later interpolated at grid size of 10 km.

3.2 Sea Ice Concentration (SIC)

The SIC information is obtained from Near-Real-Time NOAA/NSIDC Climate Data Record of Passive Microwave Sea Ice Concentration, Version 1 dataset (Meier et al. 2017). This dataset is a near real time version of final NOAA/NSIDC Climate Data Record of Passive Microwave Sea Ice Concentration which provides daily sea ice concentration estimates from two well established algorithms: the NASA Team algorithm (Cavalieri et al. 1984) and NASA Bootstrap (BT) algorithm (Comiso, 1986) on a 25 km x 25 km grid. This dataset is available in netCDF4 format and has been used in present study.

3.3 Sea Ice Extent (SIE)

The system utilizes data from Ku-band scatterometer on-board SCATSAT-1 instrument to extract information of sea ice extent (SAC, 2016). A multiple thresholds based classification algorithm comprising four parameters, namely Gamma naught (γ^0) and Brightness temperature (T_b) of H-pol and V-pol i.e. $\gamma_H^0, \gamma_V^0, T_{b_H}, T_{b_V}$ along with the polarization ratio of H-pol and V-pol data which are Normalized Difference Gamma Naught Index (NDGI) and Normalized Difference Brightness Temperature Index (NDBI), are used to discriminate sea ice from water and other classes. This product is available at 2.25 km spatial resolution on daily basis at VEDAS (Web portal of Space Applications Centre, ISRO, Ahmedabad).

4. Methodology

The development of Web-GIS based system can be divided into three subsystem or modules: (1) Data generation / download module, (2) Ship navigation suitability classification map generation, (3) Publishing and visualization of ship navigation suitability map.

4.1 Data download and generator module

The main functionality of this module is to download data automatically from data storage server and process it to bring it in common projection and spatial resolution. In order to develop a sustainable and operationalized system, automated scripts are used to download respective SIT, SIC and SIE data on daily basis. This module read incoming SIC and SIE data from given file format, georeference it from given metadata details, resample it to a common spatial resolution of 10 km. The unprocessed daily SIT data is available in ESRI shapefile format where sea ice thickness is given with its coordinates along with date of its retrieval from AltiKa daily data.

4.2 Ship navigation suitability classification map

Generator module

This module is back bone of the system which generates ship navigation suitability class map at a spatial resolution of 10 km. SIT values are spatially interpolated based on 17-day SIT composite data on one day temporal resolution. In order to eliminate daily processing of past 16-days thickness values from AltiKa, an incremental algorithm that processes same-day thickness values with last 16 days thickness values iteratively, designed and implemented. In this implementation, only daily incoming data is processed, and past 16-days processed thickness values are fetched from central database. Once incoming data is processed then it is stored in central database. This way duplication of processing AltiKa data for generating SIT values is avoided, resulting in faster processing.

Interpolated SIT image, along with SIC, is then processed to their weighted version with an indigenously developed individual weighting schemes. Weights are given in such a way that higher the weights, high suitability for ship navigation. The details of respective scheme are as shown in tables 2 and 3.

Table 2: Weighting scheme for Sea Ice Thickness (SIT) and Sea Ice Concentration (SIC)

SIT (in m)			SIC (in %)		
> SIT	**<=SIT**	**Weighted SIT**	**> SIC**	**<= SIC**	**Weighted SIC**
0	0.25	50	0	50	50
0.25	0.5	30	50	70	30
0.5	1	10	70	80	10
1	1.5	7	80	90	7
1.5	2	2	90	95	2
2	Any	1	95	100	1

Table 3: Criteria for ship navigation suitability classification (With enough ice floes points)

Suitability Class	**< TW**	**>= TW**
Low	0	50
Medium	50	100
High	100	2500

Table 4: Threshold range of SIC for ship navigation suitability classes in case of unavailability of SIT

Suitability Class	**SIC (in %) in case of "Ice" in SIE**
Low	80-100
Medium	60-80
High	<60

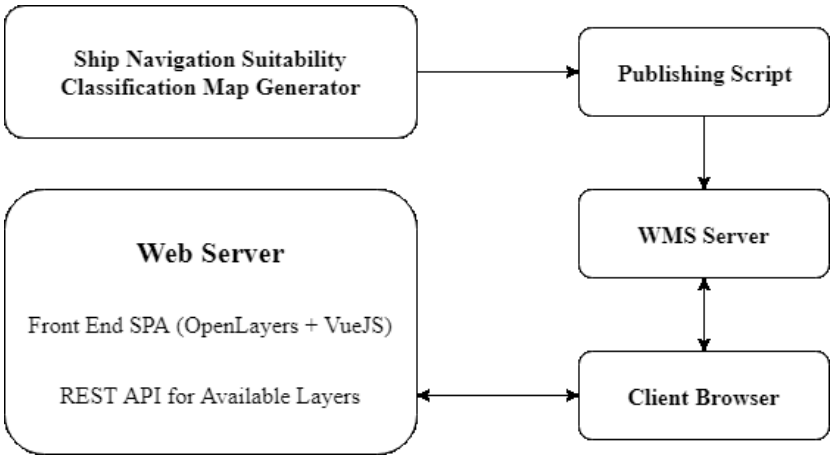

Figure 1: Web-GIS system architecture of ship navigation suitability

From Weighted SIC and SIT values, Total Weights (TW) are computed as:

$$TW = Weighted\ SIT * Weighted\ SIC$$

Once TW is calculated, Sea Ice Extent (SIE) data is finally used to mask out "No-Ice" pixels. In case of "No-Ice" pixels, highest value, 2500, is given as TW. After weights computation, ship navigation suitability classified image is generated based on conditions given in table 3. However, in cases when there will not be enough ice floes points such as during winter season, sea ice thickness at floes points cannot be computed. Therefore, in such case, sea ice concentration and sea ice extent are used in decision making related to ship navigation suitability. This modified criterion for suitability is tabulated in table 4.

4.3 Publishing and visualization module

The overall architecture of the system is illustrated in figure 1. All processes of the system from downloading of data to layer publishing is handled by automated scripts without any manual intervention. Each component of the system is described below.

4.3.1 Ship navigation suitability classification map generator

This component is responsible for generating ship navigation suitability map based on sea ice parameters. Output is then stored in a shared data storage location, which is accessed by the publishing script. This generator

uses Python with GDAL library for generating map.

4.3.2 Publishing Script

This component reads the generated products from the shared data store and publishes the same on a WMS server. The publishing process comprises extraction of timestamp from the filename of the generated product file and loading the product file to the WMS server data store.

4.3.3 WMS server

The WMS server is responsible for serving images generated from the SIT product for client-side visualization. The client-side mapping scripts can consume OGC standard WMS services exposed by the WMS server for visualization of data in browser.

4.3.4 Frontend Single Page Application (SPA)

Frontend application is a Single-Page-Application (SPA) for in-browser visualization is developed using VueJS framework with OpenLayers as a mapping library. The SPA consists of static JavaScript and HTML files, which are served by a static web server. These are loaded and executed on the client browser.

4.3.5 REST API for available layers

The client SPA queries a REST API which returns a list of available published layers. This service relies on the shared data store to list the available datasets for visualization.

5. Results and discussion

A Web-GIS enabled system increases the scope and reach of developed system from a local to global scale. In this endeavour, the role of open source software/tools cannot be ignored to provide cost effective and interoperable system. The developed system uses open source technologies that assist system in geo-visualization on both web and mobile platform. Figure 2 shows ship navigation suitability map generated as per discussed methodology. This map classifies study area in three suitability classes, namely Low, Medium and High. In figure 2, different colours red and green, yellow and blue are given to low, medium or intermediate and high suitability classes respectively.

This developed system facilitates user by providing a web-based interactive satellite data based ship navigation suitability classification map, along with other overlaying layers viz. countries and continental boundary, Antarctica boundary, Average Antarctica Winter OSCAT backscatter mask etc. These layers give clarity on classification by giving geographic details as well as sea ice related details. The system overlays SCATSAT-1 daily False Colour Composite (FCC) providing visual appearance of sea ice variations. The SCATSAT-1 gamma0 HH (horizontal), vertical (VV) and polarization ratio were used to generate FCC. It also shows input parameters as layer which can be selected for a date at a click as shown in figures 3 and 4.

The developed system performs pixel drilling operation to extract temporal information which can be accessed by clicking at “Tools and Chart”. This shows temporal charts related to SIT and SIC at one click by fetching data on-the-fly. Users can download charts through developed application in .png, .jpg and .pdf format. Users can also download temporal data in .csv format.

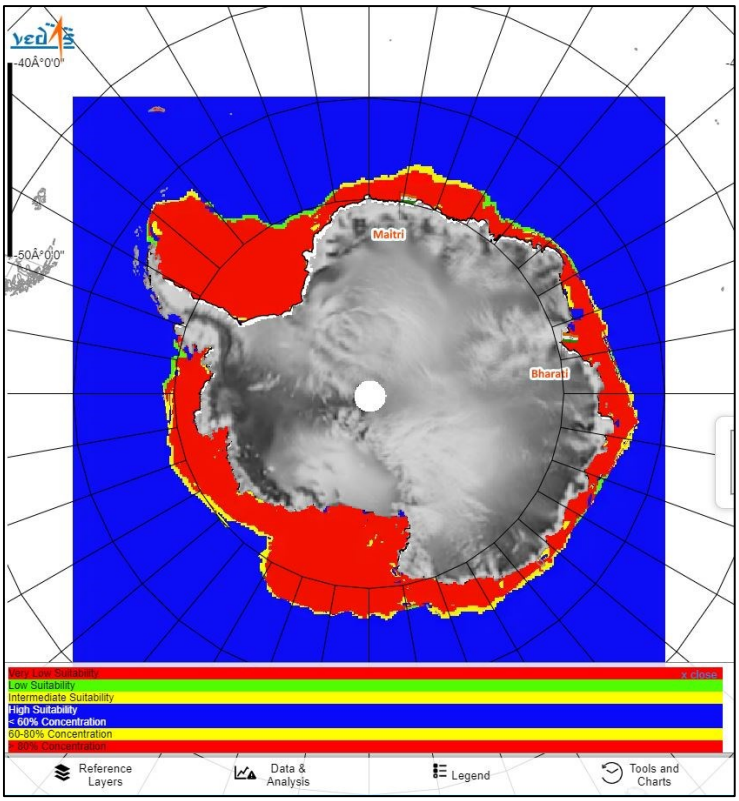

Figure 2: Safer ship navigation suitability map as per discussed methodology (Date: 05/05/2019)

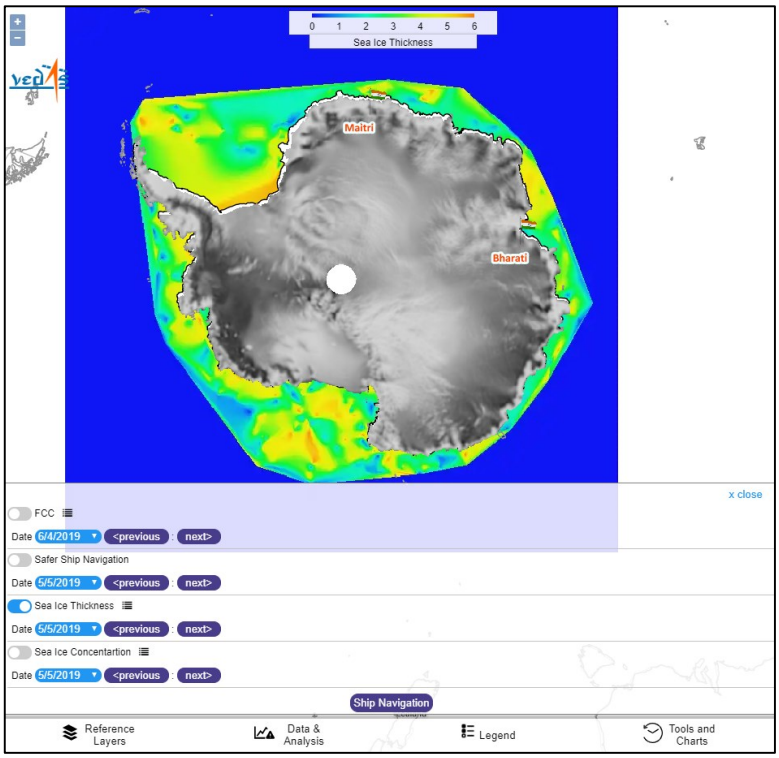

Figure 3: Sea ice thickness visualized through Web-GIS system (Date: 05/05/2019)

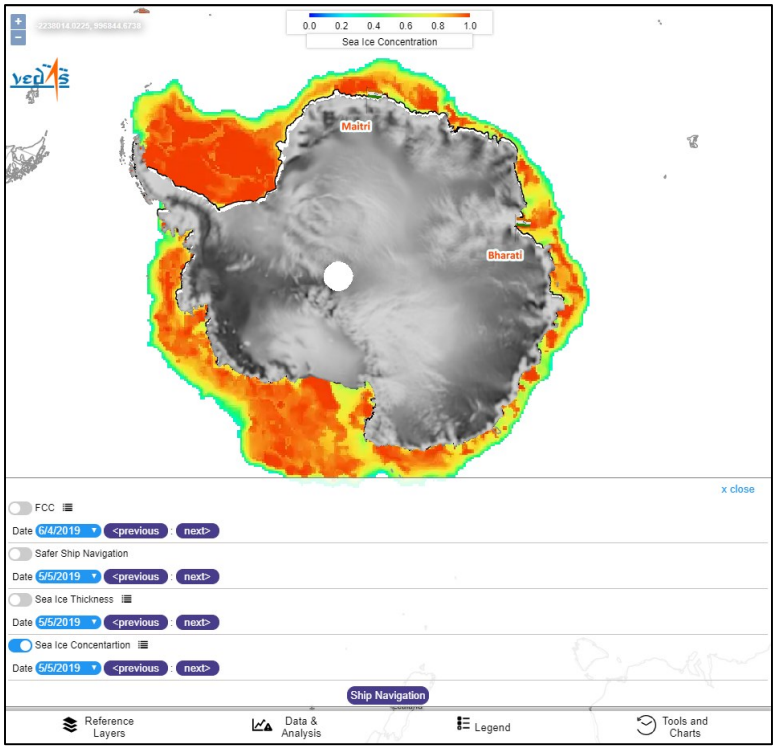

Figure 4: Sea ice concentration visualized through Web-GIS system (Date: 05/05/2019)

6. Conclusions

This paper presents details of a Web-GIS based system for safer ship navigation, based on satellite derived remote sensing data for the Antarctic. The proposed methodology uses important aspects of sea ice such as Sea Ice Thickness (SIT), Sea Ice Concentration (SIC), Sea Ice Extent (SIE) as inputs to generate ship navigation suitability classes. The developed Web-GIS based system can be accessed by user community, globally. However, current system lacks use of information related to vessel characteristics and route optimisation techniques, which are planned to be taken up in near future.

Acknowledgements

Authors would like to thank Shri D. K. Das, Director, Space Applications Centre, Ahmedabad and Dr. M. Ravichandran, Director, NCPOR-ESSO for providing Institutional support and encouragement to carry out this

work. Authors are also grateful to Dr. Raj Kumar, Deputy Director, EPSA and Dr. A. S. Rajawat, Group Director, GHCAG, Space Applications Centre, Ahmedabad for their guidance and support to bring out this paper in the present form. Authors would also like to acknowledge Shri Shashikant A. Sharma, Group Head, VRG and Dr. I. M. Bahuguna, Head, CSD, Space Applications Centre, Ahmedabad for providing their valuable suggestions and necessary facilities.

References

Anonymous (2018). Arctic Ice Regime Shipping System (AIRSS) Standard. TP 12259E. ISBN: 978-0-660-24937-7.

Caldeweyher D., J. Zhang and B. Pham (2006). OpenCIS—Open Source GIS- based web community information system. International Journal of Geographical Information Science, 20(8), 885-898.

Cavalieri, D. J., P. Gloersen, and W. J. Campbell (1984). Determination of sea ice parameters with the NIMBUS-7 SMMR. J. Geophys. Res., 89(D4), 5355-5369.

Comiso, J. C. (1986). Characteristics of Arctic winter sea ice from satellite multispectral microwave observations. J. Geophys. Res., 91(C1), 975-994.

Hui, F., T. Zhao, X. Li, M. Shokr, P. Heil, J. Zhao, L. Zhang and X. Cheng (2017). Satellite-based sea ice navigation for Prydz Bay, East Antarctica. Remote Sensing, 9(6), 518.

Joshi P. and S. R. Oza (2018). Sea ice thickness distribution from AltiKa: A case study of the Indian Ocean Sector in the Antarctic. SAC Scientific Report, SAC/EPSA/GHCAG/CSD/SR/128/2018.

Meier, W. N., F. Fetterer, and A. K. Windnagel (2017). Near-Real-Time NOAA/NSIDC Climate Data Record of Passive Microwave Sea Ice Concentration, Version 1. DOI: https://doi.org/10.7265/N5FF3QJ6. Retrieved 31.03.2019.

Pearlman J. (2013). Antarctica ship passengers prepare ice helipad after latest rescue bid fails. The Telegraph. London. Retrieved 04.06.2019.

Rajak D. R., R. K. Kamaljit Singh, P. Jayaprasad, S. R. Oza, and M. Javed Beg (2015). Sea ice advisories for Indian research & supply vessels operating in East Antarctica. Presented at COMNAP 2015: Sea Ice Challenges (Hobart, Tasmania, Australia on 12-13 May 2015).

Rajak, D. R., R. K. Kamaljit Singh, M. Maheshwari, P. Jayaprasad, S. R.Oza, J. M. Beg, R. Sharma and R. Kumar (2014). Sea ice advisory using Earth Observation data for ship routing during Antarctic Expedition. Scientific Report No. SAC/EPSA/AOSG/SR/22/2014, Space Applications Centre (ISRO), Ahmedabad – 380015, India. DOI: 10.13140/RG.2.1.5073.8725. https://www.mosdac.gov.in/data/doc/seaice/SIA_Rajak-et-al-2014.pdf

Rees, W. G. (2006). Remote Sensing of Snow and Ice. Taylor & Francis Group, Boca Raton, FL 33487-2742, p. 16.

SAC (2016). Algorithm and Theoretical Basis Document for SCATSAT1 Data Products. 2016. ISRO/SAC/SCATSAT1/DP/ATBD/V1.0. Data available at ftp://ftp.mosdac.gov.in. Data last accessed on 5.5.2019

Journal of Geomatics Vol. 13, No. 2, October 2019

Spatio-temporal analysis of land use and land cover changes in the Little Andaman Island, Andaman, India using geospatial techniques

Manik Mahapatra*, Sridhar R. and Badarees K. O.
National Centre for Sustainable Coastal Management, Ministry of Environment, Forest & Climate Change, Government of India, Anna University Campus, Chennai – 600 025, Tamil Nadu
*Email: mahapatra.sac@gmail.com

(Received: Apr 05, 2019; in final form: Nov 15, 2019)

Abstract: Land Use and Land Cover (LULC) changes play an important role while planning for sustainable development of an area. Present study examines the spatial and temporal dynamics of LULC changes in the Little Andaman Island, Andaman, India, using remote sensing and Geographical Information System (GIS) techniques for a period of past 41 years. Landsat satellite data of 1976, 1989, 2005 and 2017 were used to investigate the changes. LULC classes mapped are forest, built up, mangrove, coral reefs, creek/river, sandy area/beach/sand dune and mining area. Little Andaman is mostly covered by forest (83.29 %) in 2017 and remaining 16.71% area is under other different classes. Results show that forest area has gradually decreased from 87.59% (623.65 km^2) in 1976 to 83.29% (593 km^2) in 2017 whereas the built up area which occupied about 16.54 km^2 (2.32%) in 1976 has gradually increased to 42.58 km^2 (5.98%) in 2017. Built up area is observed on the eastern side of the island and has increased due to increasing population and associated infrastructural development, agriculture development, establishment of permanent tsunami shelter and tourism development. The findings of this study are intended to contribute to effective and appropriate decision-making with respect to resource management and in preparing holistic island development plan.

Keywords: Land Use and Land Cover change, Little Andaman, Island Coastal Regulation Zone (ICRZ), GIS

1. Introduction

Land Use and Land Cover (LULC) changes have attracted wide attention due to its importance in global and regional environmental change (Turner et al., 1990; Liu et al., 2003). The LULC changes of an area reflects the assimilated product of the relation between natural environment and human activity (Mahapatra et al., 2013). The land cover is defined by the attributes of the earth's land surface and immediate subsurface, including biota, soil, topography, surface and groundwater and human structures, whereas land use is defined by the purposes for which humans exploit the land cover (Lambin et al., 2003). Anthropogenic activities such as destruction of forest, infrastructure development etc. are continuously altering the environment at alarming rates, magnitudes, and spatial scales (Turner et al., 1994). A better understanding of LULC change is of crucial importance to the study of global environmental change (Foley et al., 2005). Information on land use and land cover in the form of maps and statistical data is crucial for planning, management, and utilization of land for various purposes (Roy and Giriraj, 2008; Mahapatra et al., 2013).

Remote sensing and Geographic Information Systems (GIS) are powerful tools to derive accurate and timely information on the spatial distribution of LULC changes (Rawat and Kumar, 2015; Reis, 2008). Orbital remote sensing technique are used to study coastal zone due to it's synoptic, multi-spectral and repetitive coverage (Nayak and Bahuguna, 2001). On the other hand, GIS techniques are utilized to store, retrieve, and handle large datasets of heterogeneous origin and to represent these in visual format (Burrough and McDonnell, 1998; Fabbri, 1998). Satellite remote sensing data and GIS techniques have been utilized in numerous studies for coastal land use and land cover mapping and monitoring in Andaman island, India (Mageswaran et al., 2015; Yuvaraj et al., 2014; Prasad et al., 2010).

In this study, the LULC changes in Little Andaman were investigated using remote sensing and GIS techniques. This assessment would assist the Andaman Administration in policy formulation for land use planning and preparing island management plan.

2. Study area

The Andaman and Nicobar Islands are the largest archipelago system in the Bay of Bengal. The northern group of islands is called the Andaman group which has an area of 6408 km^2, whereas southern group of island is called Nicobar group covering 1841 km^2 area (Jayaraj and Andrews, 2005). The study area, i.e., Little Andaman is the southernmost island of the Andaman group of islands and is the fourth largest island of that group. Little Andaman is located between 10°30' to 10° 54' N and 92° 29' to 92° 31'E and at a distance of 120 km away from Port Blair, the capital of Andaman and Nicobar Islands (Figure 1).

The total geographical area of the Little Andaman is 73,799 ha, out of which 70,365 ha (95% of geographical area) is reserved forest area, including 50,323 ha (68 % of geographical area) as a tribal reserve area (Department of Environment & Forests, Andaman and Nicobar Islands, 2011). According to Census of India (2011), Little Andaman Tehsil consists of 16 inhabited and 3 uninhabited villages which cover an area of 34.34 km^2 area with total population of 18,823 (9964 males and 8859 females). Apart from the settlers, tribal people such as Onges and Nicobarese live within this island.

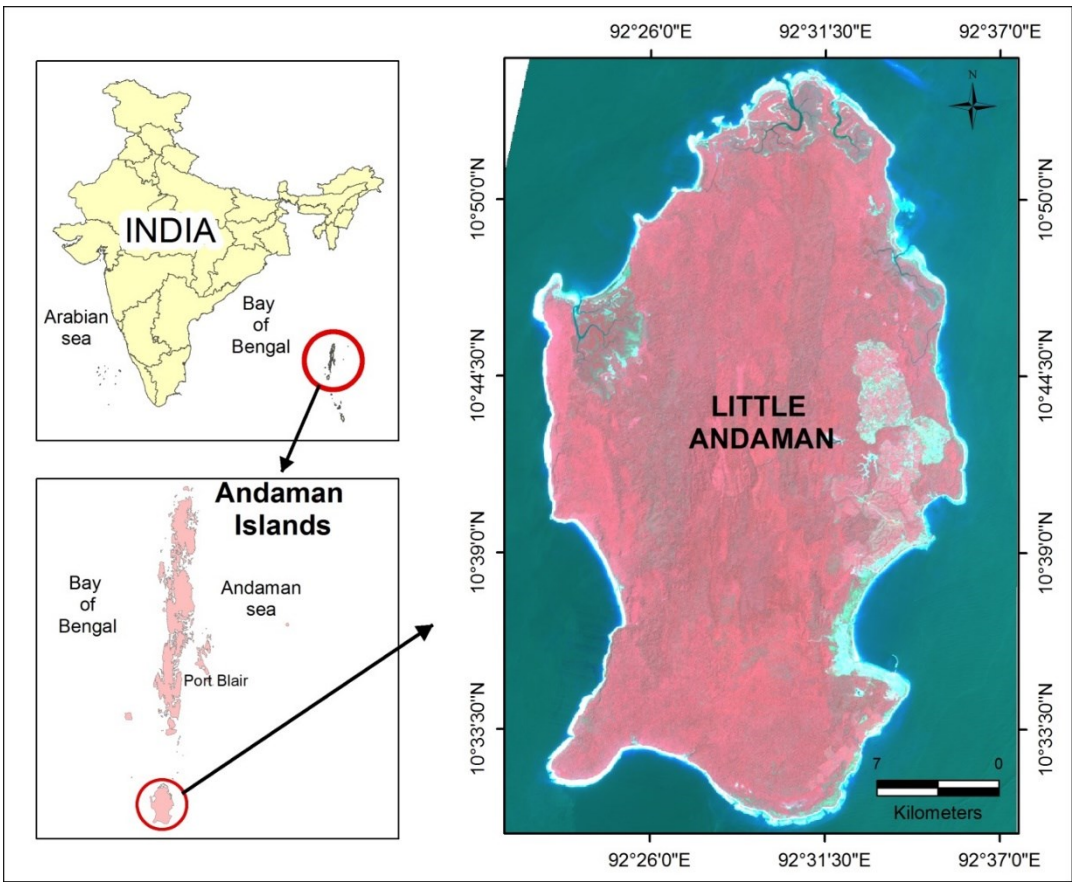

Figure 1: Study area

The island has tropical climate with very little variation in temperature. The mean maximum temperature is 30°C and the mean minimum is 23°C. Rainfall is received from both southwest (May to October) and northeast monsoons (November to December). Average annual rainfall is 3000 mm. The general topography of the island is undulating. The central and southern portions of the island are hilly with the highest point rising to 210 m above sea level, whereas the north and northwestern portions show low elevation. Hut Bay and Dugong Creek in Little Andaman island are two Ports notified under the Indian Ports Act, 1908. This island has a waterfall, dam, beautiful beaches, coral reef, palm oil plantation, coconut plantation etc. which attract tourists.

3. Materials and methods

Multi-temporal satellite data of Landsat-2 MSS of 1976 with a spatial resolution of 60 m, Landsat-5 TM of 1989 with a spatial resolution of 30 m, Landsat-5 TM of 2005 with a spatial resolution of 30 m and Landsat-8 OLI of 2017 with a spatial resolution of 30 m were acquired and used to evaluate LULC changes in Little Andaman Island (Table 1). In addition, Survey of India toposheets on 1: 50,000 scale were also used to prepare base map and used for nomenclature. Topographic maps were geo-referenced/ geo-coded based on grid coordinates in the toposheet and were later re-projected into a cartographic projection of UTM Zone 46 N, WGS 84. In pre-processing phase, the individual band with GeoTIFF (Geographic Tagged Image File Format) of Landsat-8 OLI of 2017 was stacked and converted into image format using ERDAS Imagine 10 software and a similar work was carried out with other Landsat satellite images i.e. Landsat-2 MSS of 1989 and Landsat-5 TM of 2005. Since MSS satellite images does not have geographical coordinates, they were geometrically corrected using images of Landsat-8 OLI of 2017.

All the satellite images were re-projected into a cartographic projection of UTM Zone 46 N, WGS 84. The geo-coded images were subjected to enhancements to improve the interpretability of the image. The enhancement techniques adopted in the present study included contrast stretching. The satellite data products after due processing as described above were interpreted using visual interpretation techniques for preparation of LULC map using the Arc Map 10 software. The visual interpretation keys prepared by Space Applications Centre (SAC, 1991) were used to identify various LULC features. Field visits were conducted to confirm the presence of classes shown in the prepared LULC map and additional ancillary information were collected. The broad methodology is shown in figure 2.

Table 1: Details of satellite images used

Sl. No	Satellite/Sensor	Date of Acquisition	Path/Row	Spatial Resolution (m)	Data Source
1	Landsat-8 / OLI	23/08/2017	134/53	30	http://earthexplorer.usgs.gov/
2	Landsat-5 / TM	20/02/2005	134/53	30	
3	Landsat- 5 / TM	21/11/1989	134/53	30	
4	Landsat- 2 / MSS	18/03/1976	144/53	60	

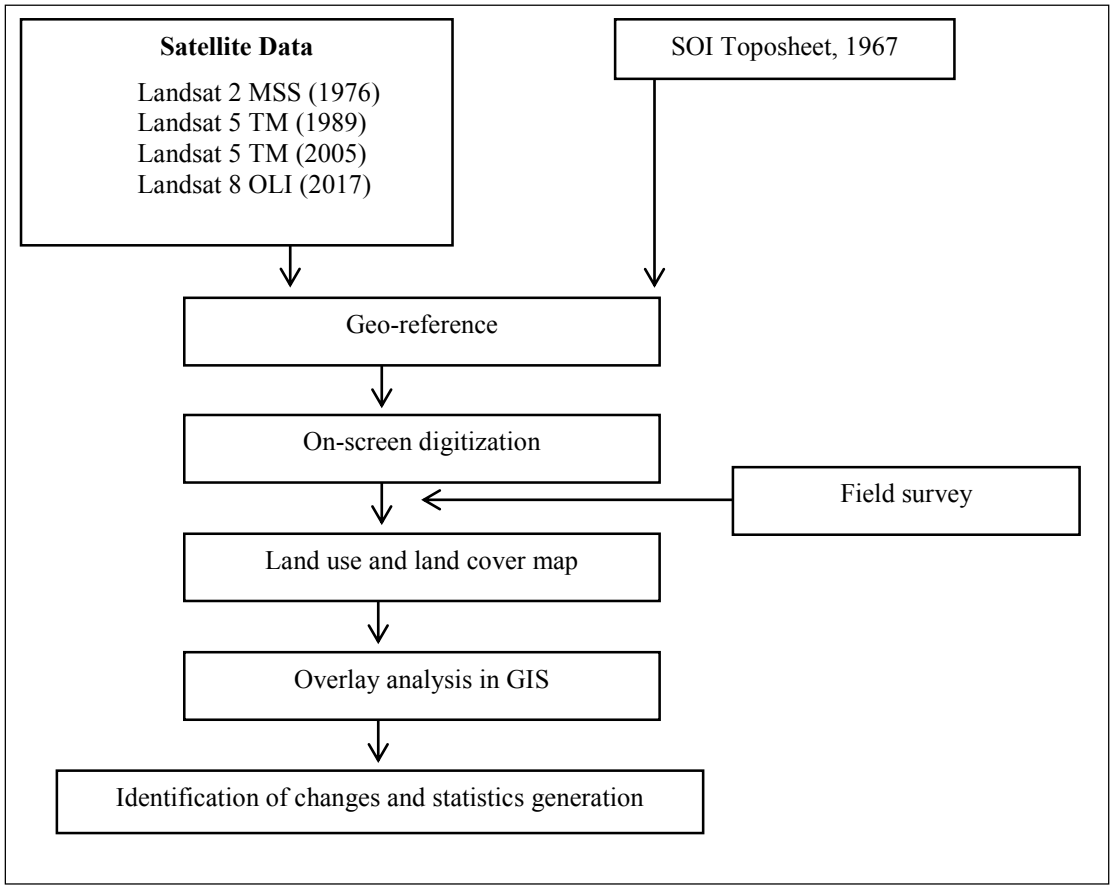

Figure 2: Methodology flow chart for LULC change mapping

4. Results and discussion

LULC changes of Little Andaman were analyzed using Landsat satellite imagery over a period of 41 years. The LULC maps for 1976, 1989, 2005 and 2017 are shown in figure 3. Land cover features mapped are forest, mangrove, coral reefs, sandy area/beach/sand dune, creek/river. These are listed in table 2. Land use classes include mining area and built up area. The results of the change detection studies and the trends identified with reference to particular classes are discussed here in detail.

4.1 Built up area

Built up area comprises of settlement area, industries, road, jetty, and ponds/tanks and is observed on the eastern side of the island. The study reveals that the built up area which occupied about 16.64 km^2 (2.32%) in 1976 gradually increased to 20.97 km^2 (2.95%) in 1989, 36.95 km^2 (5.19%) in 2005 and presently is 42.58 km^2 (5.98%) in 2017. The built up area has increased due to increasing population and associated infrastructural development, establishment of permanent tsunami shelter and tourism development. The total population of Little Andaman Island was 12,247 (6703 males and 5544 females) in 1991 and it has increased to 17528 (males: 9540 and females 7988) in 2001 and 18,823 (males 9964 and 8859 females) in 2011 (Census of India, 2011). The population primarily comprises of people from West Bengal and Tamil Nadu. December 2004 Indian Ocean tsunami had huge impacts on Little Andaman Island. About 56 people were dead, 14 missing and 6569 people stayed at camp (ICMAM 2005). After the tsunami, a large number of permanent shelters were constructed at Little Andaman including community hall, sub center and primary schools by Andaman Public Works Department (APWD).

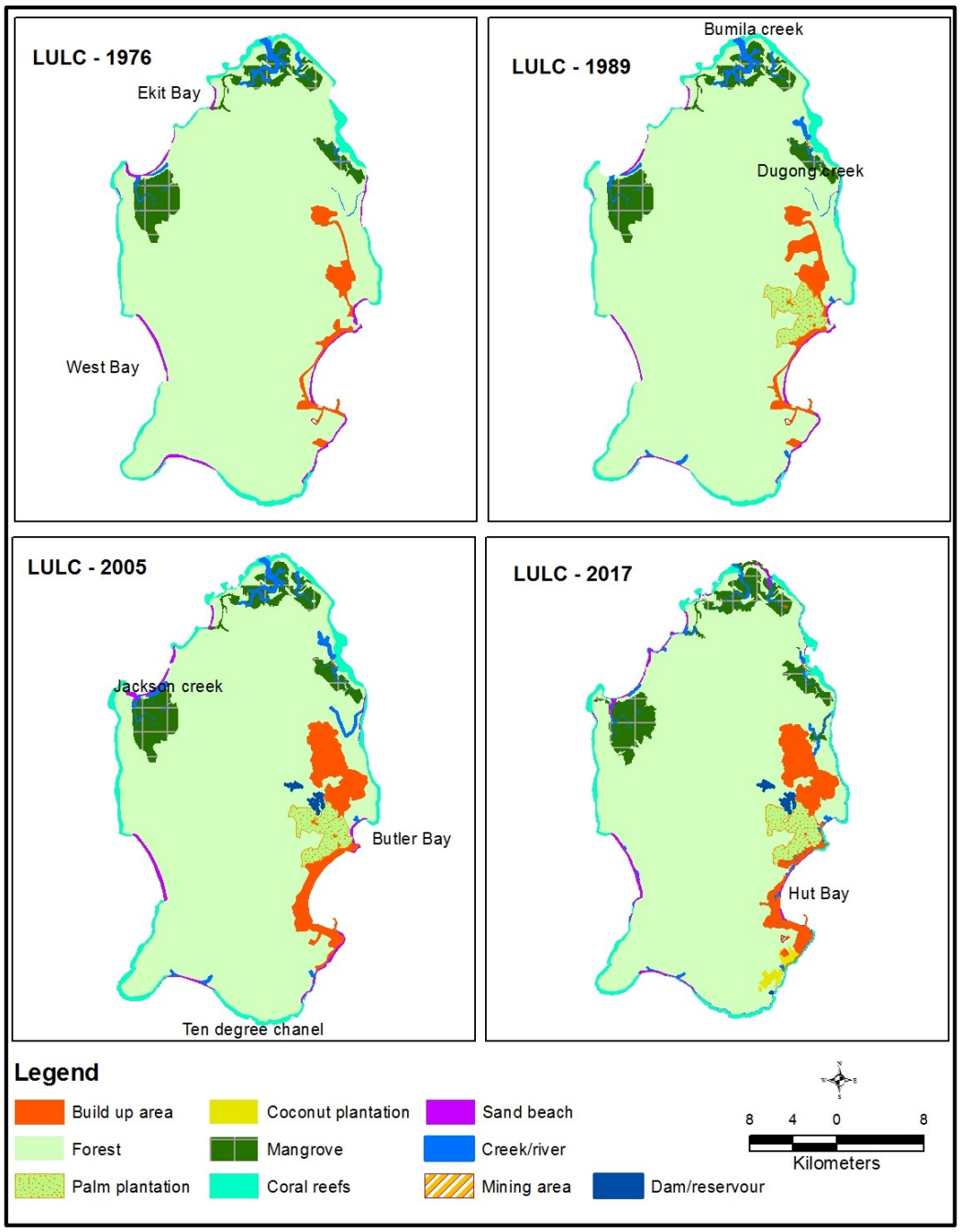

Figure 3: Spatial patterns of LULC changes in the Little Andaman Island for 1976 to 2017

Table 2: Landsat derived LULC change statistics of four different time period for the study area

LULC classes	Area in 1976 (Km^2)	Area in 1989 (Km^2)	Area in 2005 (Km^2)	Area in 2017 (Km^2)
Forest	623.65 (87.59%)	617.48 (86.72%)	600.13 (84.29%)	593.00 (83.29%)
Built up area	16.54 (2.32%)	20.97 (2.95%)	36.95 (5.19%)	42.58 (5.98%)
Mangrove	38.36 (5.39 %)	39.58 (5.56%)	39.44 (5.54%)	42.36 (5.95%)
Coral reef	21.37 (3.00%)	22.76 (3.20%)	23.42 (3.29%)	22.54 (3.17%)
Creek/River	5.00 (0.70%)	5.84 (0.82%)	5.70 (0.80%)	5.75 (0.81%)
Sandy area / Beach / sand dune	6.89 (0.97%)	5.13 (0.72%)	6.11 (0.86%)	5.51 (0.77%)
Mining area	0.19 (0.03%)	0.23 (0.03%)	0.25 (0.04%)	0.26 (0.04)
Total area (km^2)	**712.00**			

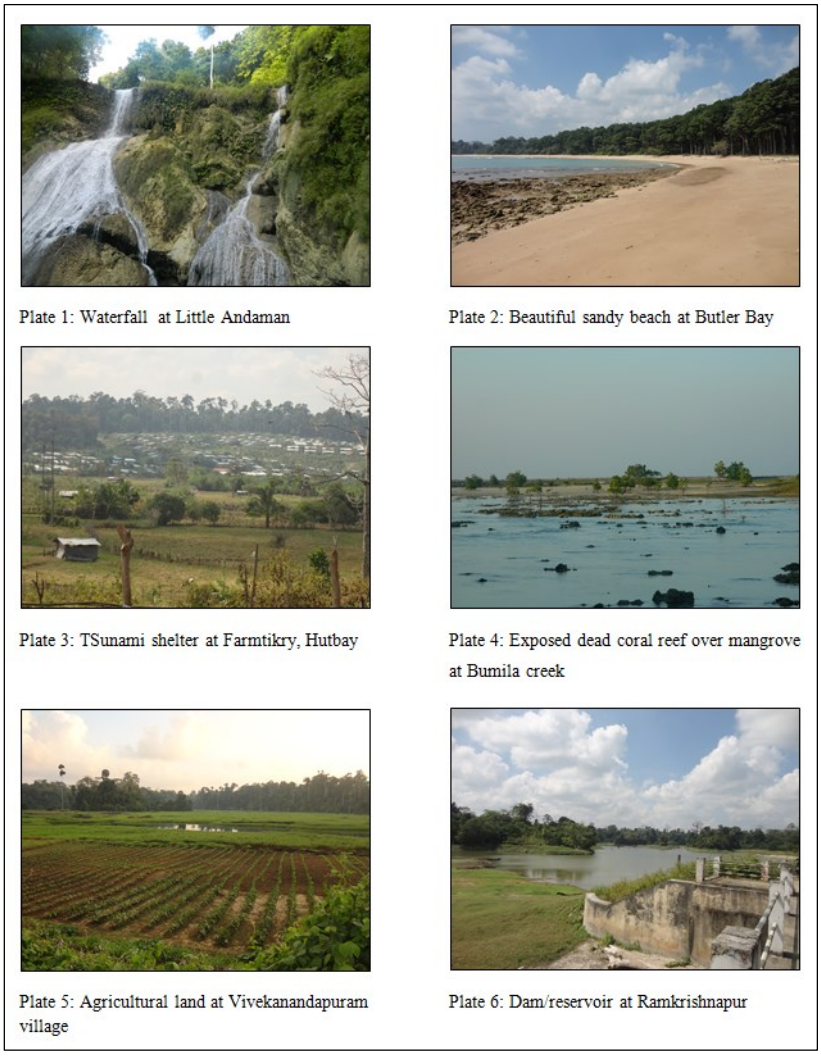

Figure 4: Field photos of LULC feature and scenic beauty of the Little Andaman island

From the field survey, it is observed that a good network of roads cover the island. Transport Department runs public bus service on the island. The Little Andaman has many tourist areas such as Harminder Bay (Nicobari settlement), Hut Bay waterfall, Christ Nallah waterfall (Elephant ride/safari), Oil Palm plantation, Palm oil processing unit, Butler Bay beach (boating through lagoons), Spices orchard, Ramakrishnapur and Rabindra Nagar Dams, wilderness trail through the tropical giant evergreen forests. Hence, the tourism industry has been increasing. Agriculture is the mainstay of the local people at Little Andaman, despite tourism, fishing activities (Figure 4). Major agricultural crops in Little Andaman are arecanut, red oil palm, paddy, vegetables, coconut and fruits. The arecanut plantation is observed in Vivakanandapur and Rabindranagar villages while large area under coconut plantation is observed in the south of Hutbay village.

4.2 Forest

The forest area, which is the largest component of the LULC of the island gradually decreased from 87.59% (623.65 km^2) in 1976 to 86.72% (617.48 km^2) in 1989 and 84.29% (600.13 km^2) in 2005 and further it reduced to 83.29% (593 km^2) in 2017. It is observed that the forest area in Little Andaman is well protected. According to Forest Code (2011) total forest area of Little Andaman is 703.65 km^2 (95% of geographical area) and the forest is classified as reserved forest. While analyzing the temporal changes for forest class between 1976 to 2017, there are no remarkable changes observed in the forest class and in general, it shows 1 to 4 percent of decrease in last 41 years. To produce more edible oil in the country, the Government of India sanctioned a project for raising Red Oil Palm plantation in Little Andaman Island. Under this programme, an area of 15.93 km^2 has also been brought under Red Oil Palm plantation in 1979 (Department of Environment & Forests, Andaman and Nicobar Islands, 2011).

The protection of forest in the island is achieved by the strong legal provisions existing in India. The responsibility of Indian citizen to protect forest is very well stipulated in the Constitution of India and it is the fundamental duty of every citizen of India to protect the forests of our country. Article 51-A (g) of Constitution of India says that “It shall be the duty of every citizen of India to protect and improve the natural environment including forests, lakes, rivers and wildlife and to have compassion for living creatures”. The Government of India issued forest policies in different time periods. The first National Forest Policy was enacted in 1894. Thereafter, it was revised and new National Forest Policy was published in 1952 by the Ministry of Food and Agriculture. Then, the National Forest Policy, 1988 (NFP)

was enacted with the basic objectives of maintenance of environmental stability, restoration of the ecological balance. It laid emphasis on people's participation through Joint Forest Management Programme and together with Forest (Conservation) Act, 1980 helped in stabilization of country's forest area in spite of huge demand on forest land for development and the ever increasing pressure for forest produces.

The major forest types of Little Andaman include tropical evergreen, semi-evergreen, moist-deciduous and littoral forests (Champion and Seth, 1968). Among the tree species recorded in Little Andaman, the dominant species include *Dipterocarpus spp*., *Knema andamanica*, *Fagraea racemosa*, *Elaeocarpus rugosus*, *Ficus hispida*, *Euodia glabra* under the evergreen forest. Species such as *Canariun euphyllum*, *Pterocymbium tinctorium*, *Oroxylum indicum*, *Terminalia procera*, *T. bialata* and *Neonauclea gageana* are dominant in semi-evergreen forest. Further, species viz., *Tetrameles nudiflora*, *Bombax insigne*, *Terminalia bialata*, *Pterocymbium tictorium* and *Anthocephalus chinensis* are dominant in deciduous forest. Whereas the littoral forest, species in *Manilkara littoralis*, *Gyrocarpus americanus*, *Pongamia pinnata*, *Terminalia catappa*, *Ficus nervosa* and *Bombax insigne* are dominant (Rasingam & Parthasarathy 2009). The conversion of forest land to the other LULC classes between 1976 to 1989, 2005 and 2017 is shown in table 3.

Table 3: Pattern of forest change from 1976 to 2017

Forest area change into following classes (area in km^2)	1976 to 1989	1989 to 2005	2005 to 2017
Built up area	5.03	17.29	3.28
Palm oil plantation	16.52	0	0
Dam/reservoir	0	0.85	0
Coconut plantation	0	0	4.04
Mining area	0.04	0.05	0.04

The study reveals that according to the LULC map of 1989, about 16.52 km^2 area of palm oil plantation and 5.03 km^2 area of built up area were previously (1976) forest land. The study found that about 17.29 km^2 built up area and about 0.85 km^2 dam/reservoir in 2005 LULC map were previously forest area. Similarly, about 3.28 km^2 built up area, 4.04 km^2 coconut plantation and 0.04 km^2 mining area in 2017 were previously forest land. The driving forces of forest cover change are numerous. Some forces act slowly (and often obscurely) over centuries, while others trigger quick and visible events. The major reasons for forest changes were the government policies. They are (a) colonization policy of 1954, 1972, (b) tsunami rehabitation shelter, (c) infrastructure development programme such as expansion of road, (d) tourism development programme, (e) agricultural development programme etc. other reason are natural calamities such as cyclone, tsunami etc.

4.3 Coral reefs

Coral reefs are among the most productive and biologically diverse ecosystems on earth (Moberg & Folke, 1999). Little Andaman exhibits narrow, linear and extensively well-developed fringing reefs all around the island except at few locations in the east and western coast. Reef flat is generally broader on the western side and narrower on the eastern side. The coral reefs cover an area of about 21.37 km^2 in 1976. The reef area has increased to 22.76 km^2 in 1989. It further increased into 23.42 km^2 and decreased to 22.54 km^2 in 2017. According to Meltzner et al., (2006) due to December 2004 Indian Ocean tsunami, entire island of Little Andaman rose, with the eastern part (including Hut Bay) up at least by 18 cm based on analysis of satellite images acquired on 1 January 2004 and 3 January 2005. This lead to exposure of coral reef surrounding the island. According to the report by Obura et al., (2008), 12.85 km^2 reef area was damaged in Little Andaman due to uplift of 24th December 2004 Indian Ocean Tsunami.

4.4 Mangroves

Mangroves are coastal forests found in sheltered estuaries, along river banks and lagoons in the tropics and subtropics. The term 'mangrove' describes both the ecosystem and the plant families that have developed specialized adaptations to live in tidal environment (Tomlinson, 1986). Mangrove of Little Andaman are mainly estuarine associated with creeks. Mangroves are found in the northern portion on Bumila creek, western side in Jackson creek and eastern side in Dugong creek. Broadly the mangrove species belong to the genus of Rhizophora and Bruguiera. The study found that mangrove covering an area about 5.39 % (38.36 km^2) in 1976, 5.56% (39.58 km^2) in 1989 and it has decreased to 5.54% (39.44 km^2) in 2005, because of the impacts of the Indian Ocean tsunami of December 2004. It has increased into 42.36 km^2 (5.95%) in 2017 due to natural recruitment and plantation in the tsunami affected areas particularly in the northern Bumila creek and western side of Jackson creek.

4.5 Other classes

The other classes viz., creek and sandy beaches or sand dune do not show any major change. It is observed that the sandy beach/ sand dune area which occupied about 0.37% (6.89 km^2) of area in 1976 has decreased to 0.72% (5.13 km^2) by 1989 but increased to 0.86 % (6.11 km^2) by 2005. It further decreased to 5.51 km^2 (0.77%) in 2017. Rock mining/quarrying which is observed south of Hut Bay has gradually increased from 0.19 km^2 in 1976 to 0.26 km^2 in 2017. This quarry is maintained by the Andaman and Lakshwadeep Harbour Works (ALHW) and named as Andaman and Lakshadweep Harbor Works Limestone Quarry.

The Ministry of Environment, Forest & Climate Change, Government of India has published the Island Protection Zone (IPZ) Notification, 2011, to ensure livelihood security to the local community, to promote conservation and protection of island unique environment and to promote development through sustainable integrated management plan of the Andaman & Nicobar (A&N) and Lakshadweep group of Islands (MoEF & CC, 2011). This

IPZ Notification, 2011 has two major components i) the Island Coastal Regulation Zone (ICRZ) and ii) the Integrated Island Management Plan (IIMP). The ICRZ is regulatory in nature and is predominantly prepared to delineate areas along the coast as ecosystem dominant (ICRZ I), urban (ICRZ II), rural (ICRZ III) and waterbody (ICRZ IV). The Little Andaman island fall under the ICRZ category. As all the development activity along the coastal area of this island are to be regulated by the ICRZ plan, there is a need to follow the guidelines of IPZ notification 2011. In order to prepare island management plan or resource management plan of this island, information of coastal land use and land cover, its present status and changes over a period of time is highly required. In the present study, land use and land cover changes are analyzed in detail and may be used to prepare ICRZ zonation and preparation of resource management plan such as mangrove restoration or plantation, conservation of coral reef area, prohibition of mining of sand from beaches etc.

5. Conclusions

Spatio-temporal dynamics of land use and land cover of Little Andaman are studied by using Landsat satellite images over the past 41 years. Results show that forest area, which is the largest component of the island, has gradually decreased from 87.59% (623.65 km^2) in 1976 to 83.29% (593 km^2), whereas the built up area which occupied about 16.64 km^2 (2.32%) in 1976 increased to 42.58 km^2 (5.98%) in 2017. This may be attributed to natural calamity such as cyclone, tsunami and anthropogenic activities such as an increase in the population, infrastructure development, agriculture development by construction of two dams/reservoirs, tourism development by construction of hotel, guest house, resort, good communication with Port Blair, and establishment of tsunami shelter, etc. The prominent changes in LULC are observed after the 24 December 2004 Indian Ocean tsunami. This assessment would help the Andaman Administration for policy formulation towards resource management and land use planning of the island. The study suggests the integration of ICRZ regulation along with the land use plan may help in sustainable development of the region.

Acknowledgements

This study was undertaken as part of the research study on "Preparation of Island Coastal Regulation Zone (ICRZ) plans for A&N Islands" (research study code - IR12010). The authors acknowledge the financial and technical support of the Ministry of Environment, Forest and Climate Change, Government of India and the World Bank under the ICZM Project of India. The authors express their sincere thanks to the Director, National Centre for Sustainable Coastal Management (NCSCM) for providing support for the research work. The authors are thankful to the Department of Environment and Forests, UT of Andaman and Nicobar for providing necessary permission for conducting field survey in the islands.

References

Burrough, P.A. and R.A. McDonell (1998). Principles of Geographical Information Systems, Oxford University Press.

Census of India (2011), http://www.censusindia.gov.in/2011census/dchb/3500_PART_B_DCHB_ANDMAN%20&%20NICOBAR%20ISLANDS.pdf, accessed on 5 January 2015.

Champion, H.G. and S.K. Seth (1968). A Revised Survey of the Forest Types of India, Manager of Publications, New Delhi, 404.

Department of Environment & Forests, Andaman and Nicobar Islands (2011), Forest Code 2011 http://forest.and.nic.in/ActsNRules%5CAnNFDC-2011.pdf, accessed on 30 June 2016.

Fabbri, K.P (1998). A methodology for supporting decision making in integrated coastal zone management, Ocean & Coastal Management, 39(1), 51-62.

Foley, J. A., R. DeFries, G.P. Asner, C. Barford, G. Bonan, S.R. Carpenter, F. S. Chapin, M.T. Coe, G. C. Daily, H.K. Gibbs, J.H. Helkowski, T. Holloway, E. A. Howard, C.J. Kucharik, C. Monfreda, J. A. Patz, I.C. Prentice, N. Ramankutty and P. K. Synder (2005). Global consequences of land use, Science, 309(5734), 570-574.

ICMAM (2005). Preliminary Assessment of Impact of Tsunami in Selected Coastal Areas of India, Integrated Coastal and Marine Area Management, Chennai, http://moes.gov.in/writereaddata/files/tsunami.pdf, accessed on 3 July 2016.

Jayaraj, R.S.C. and H.V. Andrews (2005). Andaman and Nicobar Islands Union Territory Biodiversity Strategy and Action Plan. Under the National Biodiversity Strategy and Action Plan, Government of India–UNDP (ANET, Port Blair), 154.

Lambin, E. F., H.J. Geist and E. Lepers (2003). Dynamics of land-use and land-cover change in tropical regions, Annual Review of Environment and Resources, 28(1), 205-241.

Liu, J., M. Liu, D. Zhuang, Z. Zhang and X. Deng (2003). Study on spatial pattern of land-use change in China during 1995–2000, Science in China Series D: Earth Sciences, 46(4), 373-384.

Mageswaran, T., V. Sachithanandam, R. Sridhar, E. Thirunavukarasu and R. Ramesh (2015). Mapping and monitoring of land use/land cover changes in Neil Island (South Andaman) using geospatial approaches, Indian Journal of Geomarine Sciences, 44(11), 1762-1768.

Mahapatra, M., R. Ramakrishnan and A.S. Rajawat (2013). Mapping and monitoring of land use and land cover changes using Remote Sensing and GIS techniques, International Journal of Geomatics and Geosciences, 4(1), 242- 248.

Meltzner, A. J., K. Sieh, M. Abrams, D.C. Agnew, K.W. Hudnut, J.P. Avouac and D.H. Natawidjaja (2006). Uplift and subsidence associated with the great Aceh-Andaman

earthquake of 2004, Journal of Geophysical Research: Solid Earth, 111(B2), 1-8.

Moberg, F. and C. Folke (1999). Ecological goods and services of coral reef ecosystems, Ecological economics, 29(2), 215-233.

MoEF and CC (2011). Island Protection Zone (IPZ) Notification 2011, Ministry of Environment, Forest & Climate Change, Government of India, New Delhi, http://www.moef.nic.in/sites/default/files/so20e.pdf, accessed on 20th January 2015.

Nayak, S. and A. Bahuguna (2001). Application of remote sensing data to monitor mangroves and other coastal vegetation of India, Indian Journal of Marine Science., 30(4), 195-213.

Obura, D.O., J. Tamelander and O. Linden (2008). Ten years after bleaching–facing the consequences of climate change in the Indian Ocean, CORDIO Status Report 2008. Coastal Oceans Research and Development in the Indian Ocean: Mombasa, Kenya at https://cmsdata.iucn.org/downloads/cordio_status_report_2008_1.pdf, accessed on 22nd January 2016.

Prasad, P. R. C., K.S. Rajan, C.B.S. Dutt and P.S. Roy (2010). A conceptual framework to analyse the land-use/land-cover changes and its impact on phytodiversity: a case study of North Andaman Islands, India, Biodiversity and Conservation., 19(11), 3073-3087.

Rasingam, L. and N. Parathasarathy (2009). Tree species diversity and population structure across major forest formations and disturbance categories in Little Andaman Island, India, Tropical Ecology, 50(1), 89-102.

Rawat, J. S. and M. Kumar (2015). Monitoring land use/cover change using remote sensing and GIS techniques: A case study of Hawalbagh block, district Almora, Uttarakhand, India, The Egyptian Journal of Remote Sensing and Space Science, 18(1), 77-84.

Reis, S. (2008). Analyzing land use/land cover changes using remote sensing and GIS in Rize, North-East Turkey, Sensors, 8(10), 6188-6202.

Roy, P. S. and A. Giriraj (2008). Land use and land cover analysis in Indian Context, Journal of Applied Sciences, 8, 1346-1353.

SAC (1991). Manual for Mapping of Coastal Wetlands/land forms and Shoreline Changes Using Satellite Data. Technical Note, Space Applications Centre (SAC), Ahmedabad. IRS-UP/SAC/MCE/SN/32/91, 63.

Tomlinson, P.B. (1986). The Botany of Mangroves, Cambridge University Press, 441.

Turner, B. L., W.B. Meyer and D.L. Skole (1994). Global land-use/land-cover change: towards an integrated study, Ambio, 23(1), 91-95.

Turner, B.L., W.C. Clark, R.W. Kates, J.F. Richard, J.T. Mathews and W.B. Meyer (1990). The Earth as Transformed by Human Action. Global and Regional Changes in the Biosphere over the past 300 Years, Cambridge University Press, Cambridge, New York, 707.

Yuvaraj, E., D.K. Saravanan and K. Dharanirajan (2014). Assessment of land use and land cover changes in South Andaman Island using remote sensing and GIS. International Journal of Geomatics and Geosciences, 5, 171-181.

Journal of Geomatics Vol. 13, No. 2, October 2019

Assessment of GPS, GLONASS and GPS+GLONASS processing solutions at different baseline lengths

Abdallah Ahmad Saad and Khaled Mahmoud Abdel Aziz*
Department of Surveying Engineering, Shoubra Faculty of Engineering, Benha University, Cairo, Egypt
Emails: abdallah.saad@feng.bu.edu.eg, *Khaled.Mahmoud@feng.bu.edu.eg

(Received: Mar 30, 2019; in final form: Dec 8, 2019)

Abstract: Nowadays, using GNSS constellations in many applications is clear. The increasing of the satellites availability at any place of the world from different GNSS constellations is compared against using GPS only for improving the positioning accuracy. In this research, the availability of complete GNSS constellations (GPS and GLONASS) at some of IGS stations are illustrated. Performance with different baseline lengths are assessed using observations from GPS only, GLONASS only and (GPS+GLONASS) using different duration times. The processed data are collected at the same day in two different years. The results indicate that using GLONASS only does not give the best accuracy compared to (GPS only and (GPS and GLONASS). Finally, the results obtained by the GPS only are close to a large extent with the (GPS and GLONASS) results.

Keywords: Trimble Business Centre (TBC) software, International Terrestrial Reference Frame (ITRF), Vector Length Errors (VLE) and International GNSS Service (IGS)

1. Introduction

The four global satellite navigation systems, Global Positioning System (GPS), Global Navigation Satellite System (GLONASS), Galileo Satellite Navigation System (Galileo), and Beidou Satellite Navigation System (BDS) have enabled a wide range of applications for positioning, navigation and timing (Zhang et al., 2018). Two new global systems, Beidou in China and Galileo in Europe, are currently under development (Januszewski, 2018). The principle of GPS in position determination has not changed in GNSS but an expectation of achieving greater accuracy and precision with GNSS is envisaged. Baseline processing, the fundamental principle of satellite based positioning is still applicable with the GNSS system both in PPP and differential positioning. The baselines spans from short to long ranges with various error compensations and corrections applied to longer baseline to achieve desired precision and accuracy with the use of various commercial GNSS data processing softwares (Okorocha and Olajugba, 2014). The performed research on GPS-only, GLONASS-only and combined (GPS and GLONASS) daily static observations with usage of PPP technique in different sky visibility level shows that currently existing software does not improve results significantly comparing GPS-only solutions with multi-GNSS. Adding GLONASS signals to GPS does not affect noticeable improvement of coordinates' accuracy and in some cases even caused accuracy's deterioration (Maciuk, 2018).

2. Study area and data collection

One same day of data collected by IGS stations in two different years 2014 and 2018 are used in this research. Firstly, five IGS stations (NZRT, ELAT, ISBA, NICO and RAMO) on 18-04-2014. Secondly eight IGS stations (NZRT, ARUC, ELAT, ISBA, MATE, MERS, NICO and RAMO) on 18-04-2018 (Figure 1). The different baseline lengths are processed by fixing NZRT as a base station. Choosing of these stations depended on the same criteria. At each receiver, the signals from GPS and GLONASS are collected for 24 Hours session.

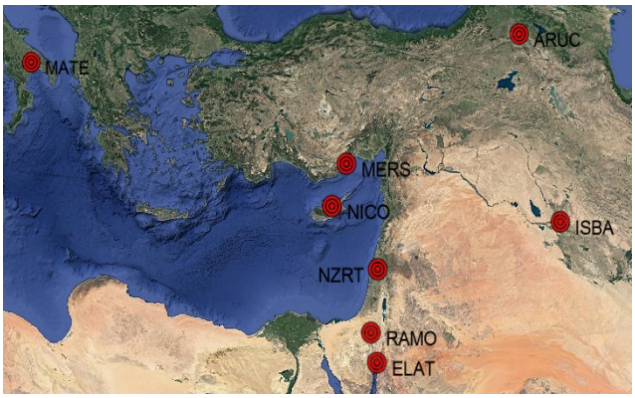

Figure 1: IGS stations used in this study

The baselines with different lengths are processed by using Trimble Business Center version 3.5 (TBC) commercial software. RINEX observation files of IGS stations downloaded from (CDDIS Daily 30-seconds data, 2019) and the broadcast and precise satellite ephemeris for GPS and GLONASS observations on these days obtained from (CDDIS Daily 30-second data, 2019) and (CDDIS GNSS Orbit Products, 2019).

3. Precise Point Positioning (PPP) and differential GPS positioning

Precise point positioning to achieve high positioning accuracy involves removal of all potential errors in the space segment, signal propagation, ground environment and receiver segment. In the differential GPS positioning, the reason that millimeter-level accuracy can be achieved is because some common errors can be fully or partially removed by differencing observations between two stations. However, this differential technique can't be used in PPP due to the fact that only observations from a single receiver are available. Therefore, all errors must be handled in PPP in order to achieve centimeter-level accuracy. The others include the special error sources that need to be mitigated specifically to PPP, such as the satellites and receiver antenna phase center offsets, phase wind up, relativistic

effect, Earth tide, ocean tide loading, and atmosphere loading. Most of these errors can be mitigated to some extent through modeling (Cai, 2009). The AUSPOS provides accuracies of several millimeters in the horizontal component and a couple of centimeters in the vertical component. In addition, this capability can also support high precision applications and research into crustal deformation monitoring. Typical examples of crustal deformation monitoring and establishment of a local control networks using AUSPOS for multiple days' data sets collected from multiple sites (Jia et al., 2014) and the relative GPS solution software (TBC) are observed to give better result at all observation times (Abdel Aziz, 2018). The maximum vector length errors obtained by using TBC, Trimble RTX, AUSPOS and CSRS-PPP at 1 hour are 0.015 m, 0.093 m 0.235 m and 0.075 m respectively, at 2 hours are 0.009 m, 0.066 m, 0.033 m and 0.061 m respectively, at 3 hours are 0.008 m, 0.017 m, 0.033 m and 0.016 m respectively and at 4 hours are 0.005 m, 0.019 m, 0.014 m and 0.021 m respectively, by using the different baseline lengths 17.52 km, 48.793 km, 91.279 km and 102.777 km.

The following steps illustrate how to use the AUSPOS - Online GPS Processing Service:

i) Selection of RINEX file (s), one wishes to submit,
ii) Second step, enter the RINEX information - repeat for each of the RINEX files,
iii) Third step is to provide Email address and
iv) Fourth step is submission of the RINEX files.

Finally, the results are sent to the e-mail that was recorded on the site (AUSPOS - Step by Step Guide, 2019).

4. Reference Systems and ITRF

The international civil coordinate reference standard is the International Reference Frame (ITRF), each GNSS has its own reference frame, which depends on the control stations coordinates hence guaranteeing independence among systems. The reference frame for GPS system is World Geodetic system 1984 (WGS84), its present version is almost identical with the latest version ITRF. The coordinates in GLONASS system are based on the parameter of the Earth 1990 (PZ-90) frame, since 2014 in version 90.11, also known Parametry Zemli 1990 (PZ-90). The new system is already coordinated with the ITRF at the centimeter level (Mikulski, 2014).

5. Methodology

In this research, GPS, GLONASS and combined GPS and GLONASS dual carrier phase observations are used to assess all satellites constellations with different baseline lengths and duration times on two different years. The following illustrates the work steps: -

- Processing the RINEX observation file of NZRT IGS station by AUSPOS Online GPS Processing Service (version: AUSPOS 2.3) on ITRF 2014 from (AUSPOS - Online GPS Processing, 2019), on two days 18-04-2014 and 18-04-2018.
- Firstly, processing the different baseline lengths by using Trimble Business Center (TBC) for five IGS stations in 18-04-2014 at three different solutions using (GPS only, GLONASS only and combined GPS + GLONASS) by fixing the NZRT station and processing the four IGS stations (ELAT, ISBA, NICO and RAMO) to the NZRT station at 24 Hrs. duration time of observations on ITFR 2014.
- Processing the different baseline lengths at different duration times of observations (4, 8, 12, 16, 20 Hrs.) for the three above mentioned solutions.
- Determining the Vector Length Errors (VLEs) for the different baseline lengths by computing the difference between the positioning of IGS station obtained by 24 Hrs. duration time of observations and the positions of these IGS stations at different processing period times by using three different solutions.

$$VLE = \sqrt{(x - x_r)^2 + (y - y_r)^2 + (z - z_r)^2}$$

where: x, y and z: the position of IGS station at different processing period times. x_r, y_r and z_r: the position of the same IGS station obtained by 24 Hrs. duration time of observations.

- Repeating the same last steps on the 18-04-2018 to determine the VLE.

6. Results and analysis

The aim of this research is to assess the contribution of the modernization of GNSS signals and study the complete GNSS systems (GPS and GLONASS) in processing different baseline lengths on the same day at two different years. The VLE generally is depending on the baseline length but there are some factors that affect VLE for examples (DOP and the common time between base and rover).

The baseline lengths are NZRT-RAMO is 248.181 km, NZRT-NICO is 316.879 km, NZRT-ELAT is 365.015 km and NZRT-ISBA is 852.461 km.

The VLE of different baseline lengths obtained from the two solutions of GPS and combined (GPS and GLONASS) gave the best results shown in figure 2, but the results derived from GPS are the best at all baseline lengths except the baseline NZRT-NICO because the maximum PDOP was 2.205 in combined (GPS+GLONASS) and it was 5.026 in the case of GPS only.

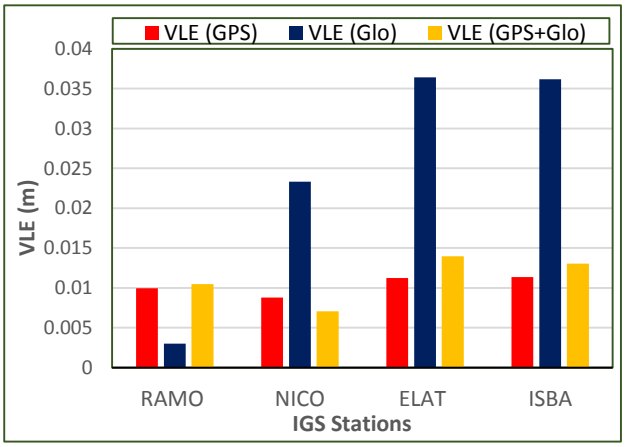

Figure 2: Vector Length Errors (VLE) for different baseline lengths by using the three solutions (4 hrs) in 2014

Figures 3 and 4 shows the duration of processing time of 8 and 12 hours respectively. Figure 3 shows the accuracy of 8

hours session compared to 4 hours session. Figure 4 also shows the accuracy of 12 hours' session compared to 8 hours' session. Still in both figures, GPS is the best than GPS+GLONASS and finally GLONASS with noticeable difference. The accuracy of GLONASS in using 12 hours' session is better than GPS and GPS+GLONASS and became more close to them. The baseline NZRT-NICO has not improved with increasing the session time in the cases of GPS and GPS+GLONASS and has improved in the case of GLONASS.

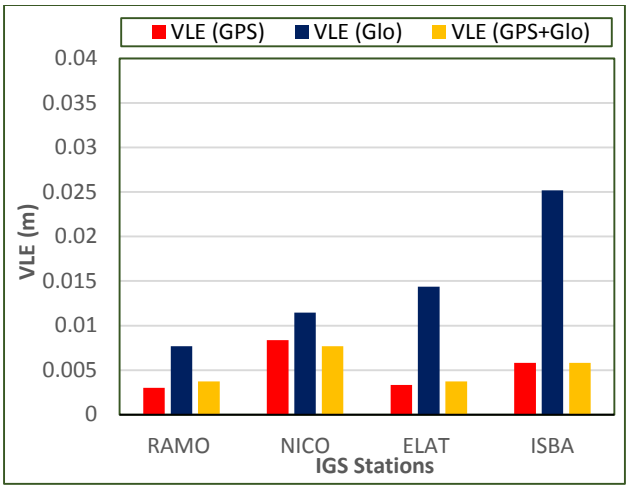

Figure 3: Vector Length Errors (VLE) for different baseline lengths by using the three solutions (8 hrs) in 2014

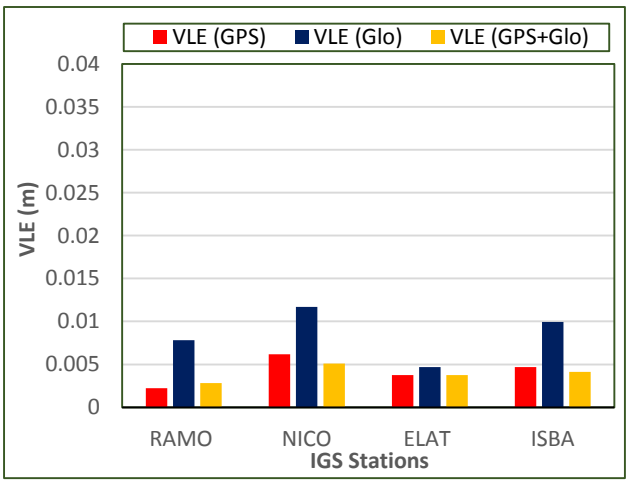

Figure 4: Vector Length Errors (VLE) for different baseline lengths by using the three solutions (12 hrs) in 2014

Figures 5 and 6 illustrated the results obtained by two period processing times 16 and 20 Hrs. The accuracies in both cases are equal. In both cases the accuracies much improved compared to the case of 12 hours. The three cases of GPS, GONASS and GPS+GLONASS became very close to each other. The results showed that achieving the accuracy of GPS by using GLONASS only requires 16 hours session.

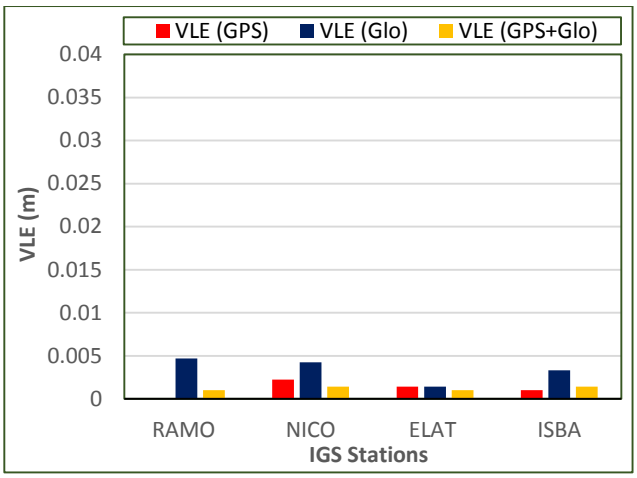

Figure 5: Vector Length Errors (VLE) for different baseline lengths by using the three solutions (16 hrs) in 2014

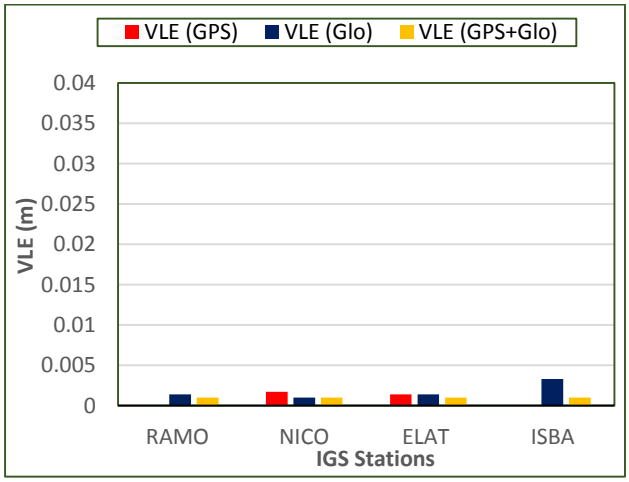

Figure 6: Vector Length Errors (VLE) for different baseline lengths by using the three solutions (20 hrs) in 2014

The following graphs illustrate the results obtained by processing the different baselines lengths at 2018 on same day used of 2014, but in 2018 was added a set of different baseline lengths to clarify the extent to take advantage of the development that occurred in these systems, either combined or individually.

In year 2018, three lines were added to previous baselines, NZRT-MATE is 1873.805 Km, NZRT-ARUC is 1142.405 Km and NZRT-MERS is 431.174 Km.

In Figure 7 it was detected that in most lines, when using GLONASS in processing, the solution is float. This is represented in the figure by the blue dashed line, which represents the VLE. When the duration time of processing was 4 hours in case of GLONASS, there were not enough available satellites. The VLE of baseline NZRT-RAMO is 0.738 m, because the processing duration time is less than one hour.

It is clear, in 4 hours session, that the VLE of different baseline lengths in 2018 is less than their corresponding values of 2014. The improvement was about 1 cm in both cases of GPS and GPS+GLONASS.

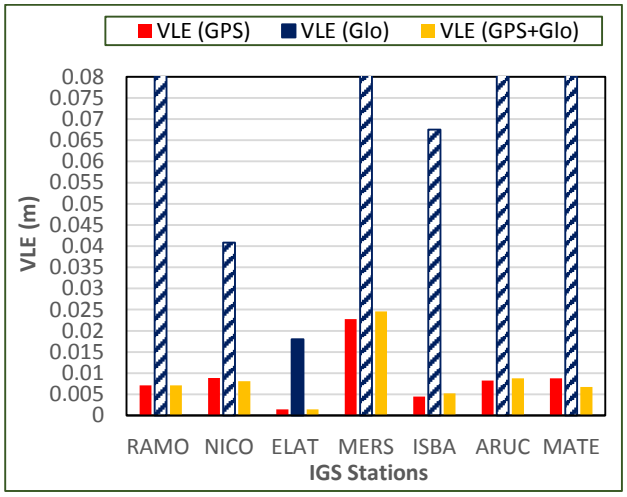

Figure 7: Vector Length Errors (VLE) for different baseline lengths by using the three solutions (4 hrs) in 2018

In figure 8, it is noted that when using GLONASS solution some baselines gave a float solution. Some other baselines gave a fixed solution with improved accuracy and sometimes not compared to the corresponding results from 2014.

In the case of using GPS and (GPS+GLONASS) solutions for 8 hours, there was an improvement in the values of VLE within 5 mm compared to the corresponding values of 2014.

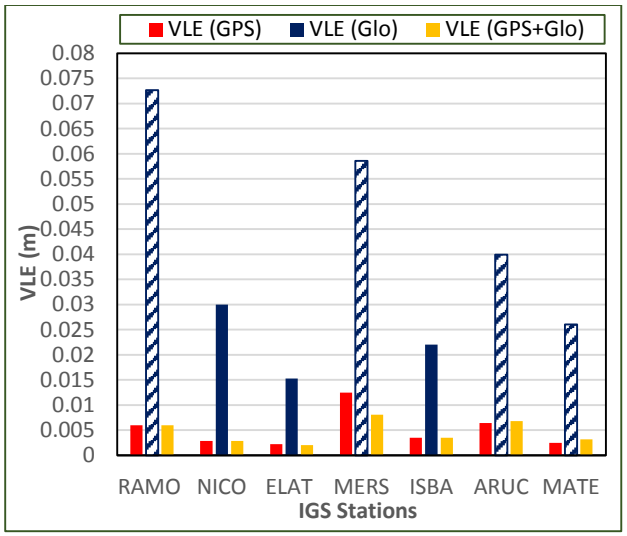

Figure 8: Vector Length Errors (VLE) for different baseline lengths by using the three solutions (8 hrs) in 2018

Figure 9 shows that GLONASS from 12 hours' session got fixed solutions but still have VLE larger than the other two cases. Also the VLE of GLONASS baselines in 2018 is larger than their corresponding values of 2014 in most baselines.

The differences between results obtained by processing the different baselines using GPS and (GPS+GLONASS) at 2014 and 2018 are within 2 mm.

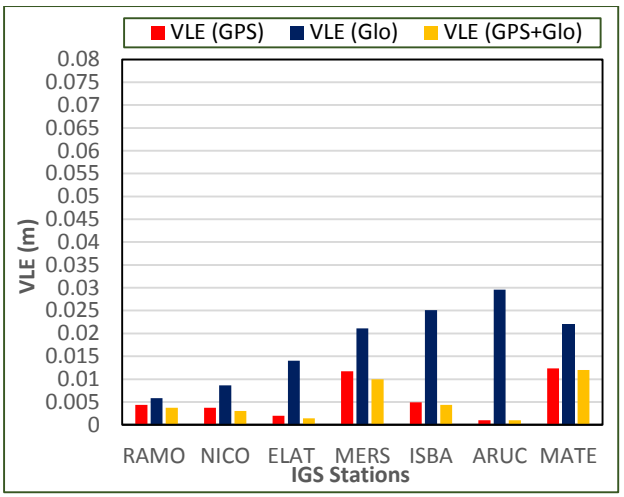

Figure 9: Vector Length Errors (VLE) for different baseline lengths by using the three solutions (12 hrs) in 2018

Figure 10 illustrates that VLE obtained by GLONASS solution is still larger compared to other two solutions except for one baselines. The results of GLONASS also showed that the VLE obtained in 2018 is larger than those of 2014.

The results obtained by processing the different baselines using GPS and (GPS+GLONASS) of 2018 have larger values of VLE compared to the corresponding values of 2014.

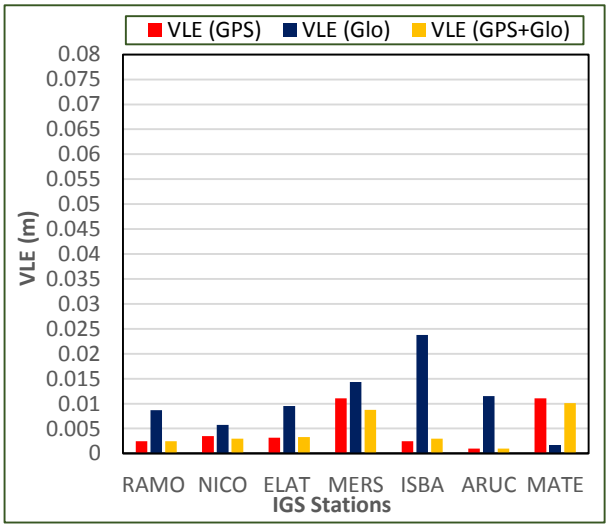

Figure 10: Vector Length Errors (VLE) for different baselines lengths by using the three solutions (16 hrs) in 2018

In figure 11, after 20 hrs duration time of processing, GLONASS solution became close or better in VLE than the other two solutions. The processing of different baselines using (GPS and GPS+GLONASS) gave VLE less than 5 mm for most baselines.

Results obtained are closely correlated with results obtained in 2014.

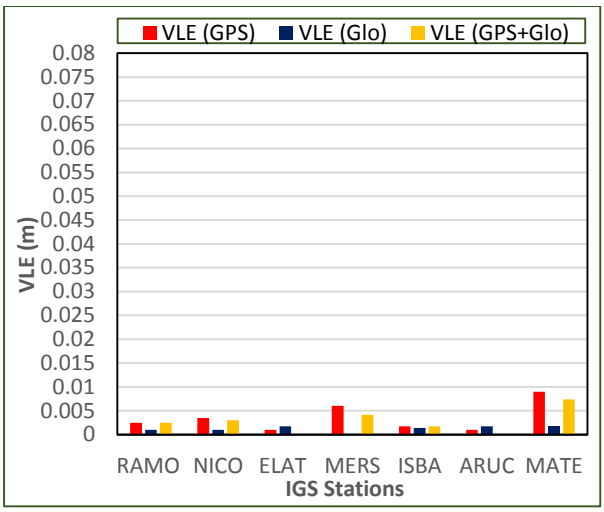

Figure 11: Vector Length Errors (VLE) for different baseline lengths by using the three solutions (20 hrs) in 2018

The tables 1-7 given below illustrates the Vector Length Errors (VLEs) for different base line lengths at different times of processing in two years 2014 and 2018.

Table 1: Vector Length Errors (VLE) of baseline NZRT- RAMO by using the three solutions at different processing times in 2014 and 2018

Base Line	Year / Times	2014 VLE (m)			2018 VLE (m)		
		GPS	GLO	GPS+GLO	GPS	GLO	GPS+GLO
NZRT-RAMO	4 Hrs.	0.01	0.003	0.01	0.007	0.738	0.007
	8 Hrs.	0.003	0.008	0.004	0.006	0.073	0.006
	12 Hrs.	0.002	0.008	0.003	0.004	0.006	0.004
	16 Hrs.	0	0.005	0.001	0.002	0.009	0.002
	20 Hrs.	0	0.001	0.001	0.002	0.001	0.002

Table 2: Vector Length Errors (VLE) of baseline NZRT- NICO by using the three solutions at different processing times in 2014 and 2018

Base Line	Year / Times	2014 VLE (m)			2018 VLE (m)		
		GPS	GLO	GPS+GLO	GPS	GLO	GPS+GLO
NZRT-NICO	4 Hrs.	0.009	0.023	0.007	0.009	0.041	0.008
	8 Hrs.	0.008	0.011	0.008	0.003	0.03	0.003
	12 Hrs.	0.006	0.012	0.005	0.004	0.009	0.003
	16 Hrs.	0.002	0.004	0.001	0.003	0.006	0.003
	20 Hrs.	0.002	0.001	0.001	0.003	1E-03	0.003

Table 3: Vector Length Errors (VLE) of baseline NZRT- ELAT by using the three solutions at different processing times in 2014 and 2018

Base Line	Year / Times	2014 VLE (m)			2018 VLE (m)		
		GPS	GLO	GPS+GLO	GPS	GLO	GPS+GLO
NZRT-ELAT	4 Hrs.	0.011	0.036	0.014	0.001	0.018	0.001
	8 Hrs.	0.003	0.014	0.004	0.002	0.015	0.002
	12 Hrs.	0.004	0.005	0.004	0.002	0.014	0.001
	16 Hrs.	0.001	0.001	1E-03	0.003	0.01	0.003
	20 Hrs.	0.001	0.001	0.001	0.001	0.002	0

Table 4: Vector Length Errors (VLE) of baseline NZRT- ISBA by using the three solutions at different processing times in 2014 and 2018

Base Line	Year / Times	2014 VLE (m)			2018 VLE (m)		
		GPS	GLO	GPS+GLO	GPS	GLO	GPS+GLO
NZRT-ISBA	4 Hrs.	0.011	0.036	0.013	0.004	0.067	0.005
	8 Hrs.	0.006	0.025	0.006	0.003	0.022	0.003
	12 Hrs.	0.005	0.01	0.004	0.005	0.025	0.004
	16 Hrs.	1E-03	0.003	0.001	0.002	0.024	0.003
	20 Hrs.	0	0.003	0.001	0.002	0.001	0.002

Table 5: Vector Length Errors (VLE) of baseline NZRT- MERS by using the three solutions at different processing times in 2018

Base Line	Year / Times	2018 VLE (m)		
		GPS	GLO	GPS+GLO
NZRT-MERS	4 Hrs.	0.023	0.092	0.025
	8 Hrs.	0.012	0.059	0.008
	12 Hrs.	0.012	0.021	0.01
	16 Hrs.	0.011	0.014	0.009
	20 Hrs.	0.006	0	0.004

Table 6: Vector Length Errors (VLE) of baseline NZRT- ARUC by using the three solutions at different processing times in 2018

Base Line	Year / Times	2018 VLE (m)		
		GPS	GLO	GPS+GLO
NZRT-ARUC	4 Hrs.	0.008	0.155	0.009
	8 Hrs.	0.006	0.04	0.007
	12 Hrs.	0.001	0.03	1E-03
	16 Hrs.	0.001	0.012	0.001
	20 Hrs.	0.001	0.002	0

Table 7: Vector Length Errors (VLE) of baseline NZRT- MATE by using the three solutions at different processing times in 2018

Base Line	Year / Times	2018 VLE (m)		
		GPS	GLO	GPS+GLO
NZRT-MATE	4 Hrs.	0.009	0.104	0.007
	8 Hrs.	0.002	0.026	0.003
	12 Hrs.	0.012	0.022	0.012
	16 Hrs.	0.011	0.002	0.01
	20 Hrs.	0.009	0.002	0.007

Due to the float solutions which obtained by processing the different baselines at processing duration (4H and 8H) by using the GLONASS system in 2018 compared to the same baselines in 2014 which obtained the fixed solutions. The table 8 -11 given the maximum PDOP and the actual processing duration for different baseline lengths at (4H and 8H) in two years 2014 and 2018 by using the GLONASS solution. When using the time of processing (4H) at 2014 that gives the largest maximum PDOP for baselines NZRT – ISBA and NZRT – ELAT compared to the remaining baselines, but the solutions are fixed. At (8H) the maximum PDOP is large at all baselines, but due to increasing the times of processing we obtained the fixed solution for all baselines.

In 2018 when processing duration are (4H and 8H) the maximum PDOP is large for most baselines and given a float solution which appear on the form of large VLE. The

accuracy of these baselines is improved when increasing the processing time into 12H.

Table 8: The maximum PDOP and the actual processing duration by using the GLONASS solution (4 hrs) in 2014

Baseline observation	Maximum PDOP	Processing Duration (H:M:S)
NZRT - RAMO	05.545	03:59:30
NZRT - NICO	05.545	03:59:30
NZRT - ISBA	19.260	03:59:30
NZRT - ELAT	19.767	03:59:30

Table 9: The maximum PDOP and the actual processing duration by using the GLONASS solution (8 hrs) in 2014

Baseline observation	Maximum PDOP	Processing Duration (H:M:S)
NZRT - RAMO	18.905	07:59:30
NZRT - NICO	13.425	07:59:30
NZRT - ISBA	19.26	07:59:30
NZRT - ELAT	19.767	07:59:30

Table 10: The maximum PDOP and the actual processing duration by using the GLONASS solution (4 hrs) in 2018

Baseline observation	Maximum PDOP	Processing Duration (H:M:S)
NZRT- ARUC	19.926	03:28:00
NZRT- MATE	19.843	03:17:30
NZRT - RAMO	03.651	00:55:30
NZRT - MERS	19.837	03:33:30
NZRT - NICO	19.305	03:41:00
NZRT - ISBA	15.887	03:02:00
NZRT - ELAT	18.753	03:30:00

Table 11: The maximum PDOP and the actual processing duration by using the GLONASS solution (8 hrs) in 2018

Baseline observation	Maximum PDOP	Processing Duration (H:M:S)
NZRT- ARUC	19.926	07:59:00
NZRT- MATE	19.843	07:36:00
NZRT- RAMO	19.462	05:01:00
NZRT- MERS	19.837	07:59:30
NZRT- NICO	19.370	07:59:00
NZRT- ISBA	19.554	07:59:30
NZRT- ELAT	19.530	07:59:30

7. Conclusions

- Most of the baselines (with variant lengths) that were processed by using two solutions GPS and (GPS+GLONASS) gave VLE within 1 cm at duration time of processing (4 Hrs) for both 2014 and 2018 years data.
- Our use of GPS observation only in processing is enough to get the best results due to convergence of results obtained when processing the different baselines lengths by using GPS only or combined GPS+GLONASS.
- The use of GLONASS satellites only in processing different baseline lengths requires a duration time of processing up to 16 Hrs to reach into the same results obtained by using the GPS solution.
- The VLE obtained by processing baseline lengths do not depend on the length of the baseline and time span only but also depended on the PDOP.
- The PDOP is an effect on accuracy of baseline lengths. By using the long processing duration can minimize this effect.

References

Abdel Aziz, K. (2018). Accuracy assessment of free web-based online GPS Processing services and relative GPS solution software, Journal of Geomatics, 12(1), 82-88.

AUSPOS - Online GPS Processing (2019). web page, http://www.ga.gov.au/bin/gps.pl.

AUSPOS - Step by Step Guide (2019). Web page, https://www.ga.gov.au/scientific-topics/positioning-navigation/geodesy/auspos/step-by-step.

Cai, C. (2009). Precise point positioning using dual-frequency GPS and GLONASS measurements. Master of Science, Department of Geomatics Engineering, Galgary, Alberta, August, 2009.

CDDIS Daily 30-second data (2019). web page, ftp://cddis.nasa.gov/gnss/data/daily/.

CDDIS GNSS Orbit Products (2019). web page, https://cddis.nasa.gov/Data_and_Derived_Products/

Januszewski, J. (2018). GNSS frequencies, signals, receiver capabilities and applications. Scientific Journals of the Maritime University of Szczecin, 15.06.2018.

Jia, M., J. Dawson and M. Moore (2014). AUSPOS: Geoscience Australia's on-line GPS positioning service. Geoscience Australia, Canberra Australia, https://www.researchgate.net/publication/288575085.

Maciuk, K. (2018). GPS-only, GLONASS-only and combined GPS+GLONASS absolute positioning under different sky view conditions. Technical Gazette 25(3), 933-939.

Mikulski, J. (2014). Telematics - support for transport. 14th international conference on transport systems Telematics, TST 2014, Katowice/Krakow/Ustron, Poland.

Okorocha, C. and O. Olajugba (2014). Comparative analysis of short, medium and long baseline processing in the precision of GNSS positioning. FIG Congress 2014. Kuala Lumpur, Malaysia.

Zhang, Q., W. Yang, S. Zhang and L. Yao (2018). Performance evaluation of QZSS augmenting GPS and BDS single-frequency single-epoch positioning with actual data in Asia-Pacific region. ISPRS Int. J. Geo-Inf. 2018.

PREFACE

Special Section (Part-II) on National Symposium on Advancements in Geospatial Technology for Societal Benefits, Dec 03-07, 2018

(Part-II)

It has been a long journey for remote sensing in India which started with a humble beginning of Earth observation from the experimental satellite Bhaskara-I launched in 1979 to the recent operational Resourcesat, Oceansat, INSAT and Cartosat series of satellites. Geophysical products obtained through high resolution optical imaging, active and passive microwave sensing, altimetry and atmospheric sounding are providing valuable inputs in various models and scientific applications. Observations from Chandrayan-1/2 and Mars Orbiter Mission provided newer dimensions of understanding about our celestial neighbours.

Many interesting papers were presented in National Symposium on Advancements in Geospatial Technology for Societal Benefits during Dec 03-07, 2018 on different application of remote sensing and geospatial technology. The symposium was hosted by Indian Society of Geomatics, Ahmedabad Chapter (ISG-AC), Indian Society of Remote Sensing, Ahmedabad Chapter (ISRS-AC) and Space Applications Centre, ISRO, Ahmedabad at SAC campus, Ahmedabad.

Various themes which were deliberated in Symposium were Geosciences, Agriculture, Navigation and Mobile Apps, Planetary Sciences, Environment, Geospatial Technology, Soil/Land Degradation, Machine Learning, Forestry, Coastal Applications, Hyperspectral Applications Urban Applications, Marine Sciences, Microwave Applications, Advancements in Data Processing, Cryosphere and Water Resources. Few selected papers of the symposium were decided to be published as special section in two parts. The Part-I covered 12 papers in previous issue (April 2019) of the Journal. 15 selected papers are being published in Part-II of special section in current issue.

We are extremely grateful to all the authors who have contributed in this special section. We thank all the reviewers for providing their valuable suggestions and comments timely.

R.P. Singh
R. Ratheesh
Surisetty.V.V. Arun Kumar

-Editors

Journal of Geomatics Vol. 13, No. 2, October 2019

Use of transportation network analysis for bus stop relocation, depiction of service area and bus route details

Subham Kharel[*,1], P. Shivananda[1], K. S. Ramesh[2], K. Naga Jothi[2] and K. Ganesha Raj[2]
[1]School of Civil Engineering, REVA University, Bengaluru
[2]Regional Remote Sensing Centre-South, Indian Space Research Organization, Bengaluru
*Email: kharelsubham1@gmail.com

(Received: Dec 20, 2018; in final form: Oct 10, 2019)

Abstract: The growing population and urbanization are the major problems faced by the developing countries in the world today. Increase in traffic congestion is a critical issue. The main focus of this paper is on improving traffic situations and making travelling easy to a user by using network analysis modules of Arc GIS. The location allocation module of Arc GIS is used to shift the location of existing bus stops taking into consideration different factors such as traffic signals, traffic constraints, etc. Bengaluru's bus system is operated by Bangalore Metropolitan Transport Co-operation (BMTC) which has introduced different buses for different routes in the city. A network service area is a layer that shows all areas that are within the reach of a facility, e.g., the three kilometres service area for a point on a network will include all the streets that can be serviced by the identified facility within three kilometers. The service area helps to calculate the accessibility of a facility or to choose the nearest facility among facilities within the service area. As distance increases, accessibility to/from the facility decreases. The transport network analysis provides the information of bus routes with bus stops in between the starting point and the destination point to a person who wants to plan his travel from one place to other. This system is designed in such a way that a person can plan his travel based on the bus route details e.g. to use public/private mode of travel optimally and well in time.

Keywords: Geographic Information System, Arc Info, Network Analysis, Service Area, Location- Allocation

1. Introduction

India is the second largest populated country in the world. The growing population, environmental issues and urbanization are the major problems the country is facing today. In addition to the above, traffic problems are creating more havoc. Bengaluru is the third largest metropolitan city in India. Due to increase in IT companies, industries and other business sectors, a large number of people have migrated in the recent years from all over the world to the city. Due to this, vehicle population has increased drastically leading to the increase in traffic problems. In addition to all these factors, private cab companies such as Ola and Uber also started in recent years which are adding to the problem. Travel time has increased, comfort of passengers has reduced and travel costs have increased due to the same. If this problem is not controlled, travelling from one part of the city to other will become a difficult task. The main focus of this study is to use GIS to provide solutions to reduce traffic congestion in the city and facilitate better mobility for the public. Using Geographic Information System (GIS) in the field of transportation opens up a wide range of possible applications, as diverse as the field of transportation itself. The main objective of this project is to use GIS modules in modeling the transportation system for better mobility of traffic. Network Analysis is used for transport planning during the study. The traffic congestion at the signalized intersections is caused mainly due to piling up of vehicles at bus stops which are very near to the traffic signals. Hence, it is very important to monitor the location of an existing bus stop and shift it to a more accessible location.

Bengaluru's bus system is operated by Bangalore Metropolitan Transport Co-operation (BMTC) which has introduced different buses for different routes in the city. They have assigned different bus numbers for buses moving from/to different locations in which the bus numbers are specified in the format number-alphabet(s) or vice-versa. A person who wants to travel from one place to other, will need to know the starting point, end point and different stops in between the two points. This system is designed in such a way that a person can get all the above information after providing the given route number as an input information well in advance. The Network Analysis module is a function of Arc GIS which is basically developed for Urban and Transport planning. It helps transport planners to have a better understanding of the road network and its components. A transport planner can plan his objectives and execute them in this platform to achieve more efficient results.

2. Objectives

The following objectives were set up during the study:

- To find the accessibility of a service by a person from his current location in terms of time or distance.
- To relocate bus stops which are prone to choking of traffic near signals in certain stretches.
- To locate all the bus stops along a desired bus route and developing a decision support system to help a passenger to use public/private mode of transportation based on current location and the availability of time & resources.
- Providing access to similar service by government and private oriented transport services.

The following are the parameters that were required for carrying out the study:

- Time attribute: traversal time along elements of the

network
- Distance attributes: to determine the lengths along the elements of the network
- Capacity Count: they are required to describe the relevant limit of the vehicles
- U-Turn at Junctions
- Satellite data for validation of the dataset.

3. Study area

The area chosen for the study was Bengaluru which is popularly known as the IT capital of India displayed in figure 1. Currently, Bengaluru has a population of over ten million people and is the second fastest-growing metropolis of India. The longitude and latitude extent of the region is 77°25'00"E to 77°44'00"E and 12°49'00"N to 13°04'00"N respectively. In 1971, the city's population was around 16.64 lakh and vehicle population was approximately one lakh. With the growth of population, urbanization and increase in IT sectors, the vehicle population drastically boomed to 67.22 lakhs as recorded in Census 2011(http://www.censusindia.gov.in) leading to rise in traffic problems. As of today, the vehicle population is around 73 lakhs. Today, Bengaluru's major problem is traffic congestion. Researchers all over a city are searching for solutions to overcome the problem.

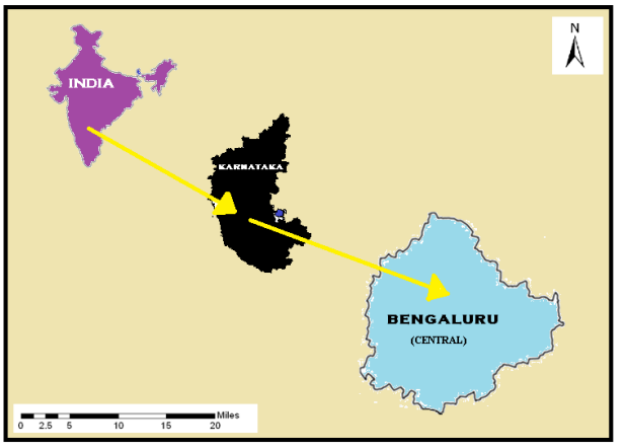

Figure 1: Study Area

4. Literature review

Kharel et al. (2018) in their paper discussed about using Network Analysis for solving problems related to best routes and closest facility which was petrol pumps in their case. They took the study area as CBD of Bengaluru City for their analysis. Their results showed that network analysis was very efficient in solving problems related to transportation. Yue et al. (2016) said that it was difficult to get the traffic values from video data and use it for traffic integration. Ranya et al. (2016) introduced a technique of establishing a spatial based location allocation computer program for emergency cases. Bigger cities have traffic problem often and finding the shortest path to reach a point is a big task. This was done by utilizing the different tools available in GIS. Ejiagha et al. (2012) in their paper described about an analysis on locating nearby health facilities such as hospitals, clinics, etc. and recommends that Healthcare facility should be provided to those deprived areas and GIS unit should be a basic component of all agencies responsible for administration of healthcare facility. Kumar et al. (2016) described the use of network analyst to find out service areas for different facilities required in day to day life in Chandigarh city. Ramos et al. (2012) showed in their paper a critical mission of an I.T.S. is to make efficient, safe and environment friendly transportation networks. Sidhtharthan and Durgadevagi (2016) reported that network analysis in GIS aims at finding solutions to routing problems related to traversibilty, rate of flow and network connectivity. Namoun et al. (2013) described an integrated approach for modeling transport infrastructure and optimizing traffic in urban areas. You and Kim (1998) gave a view about the integration of transportation modeling procedure beginning right from the data inventory to meeting the future demands of traffic. Arora and Pandey (2011) discussed about finding the solutions for routing problems related to traversing, flow and route connectivity. Visser and Wees (2000) discussed about a general simulation concept which was formulated to evaluate the performance of an intelligent transport system and introduce the virtual sensor concept as a concept for sensor system modeling. This idea was inspired from Electronic Fee Collection.

5. Data collection and organization

Open Street Map data which included the road and rail networks, bus stops, traffic signals, railways stations, traffic, etc. was used to prepare the spatial database for the study. Major routes such as ring roads were picked up for the study to ensure validity of data and ease of understanding. The main study area Majestic – Whitefield stretch has most congested traffic patterns. In addition to this, ancillary data like traffic volume counts, bus stops, traffic signals, etc. were collected from centers like BMTC, BBMP, Traffic Management Centre, Directorate of Urban Land Transport (DULT) and Bangalore Traffic Police. Information on latitudes and longitudes of the bus stops was obtained from Google. Different features of Network Analysis module were used to achieve the desired results during the course of the study. Figure 2 displays the overall methodology used during the study to achieve the desired results.

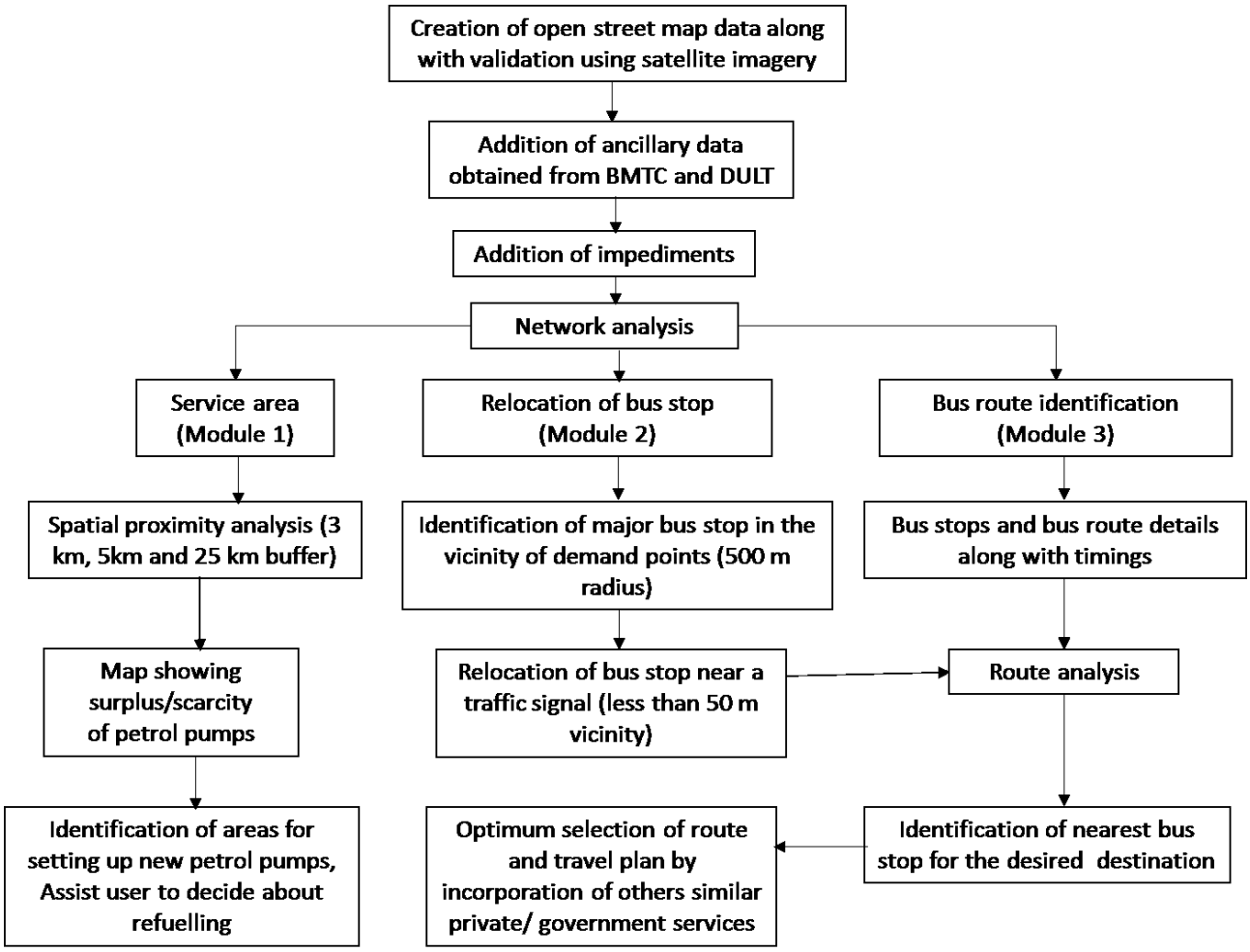

Figure 2: Methodology flowchart

6. Methodology

The methodology followed during the study is explained as listed below:

- The Network Analysis module of Arc GIS was used to carry out the study.
- The network dataset was created and the data to be used was validated using satellite imagery.
- Impediments/barriers were added to strengthen the above dataset (e.g. point, line and polygon barriers).
- Buffers were generated for creating service area polygons.
- The bus stops which had chances of increasing traffic congestion were relocated virtually taking into consideration various factors such as traffic, traffic signals, availability of facilities, etc. CCTV cameras mounted near signals will also facilitate in re-locating the bus stops. One of the bus stops was relocated based on CCTV footage available through downloading from Internet.
- All the bus stops along a bus route were located and a decision support system (DSS) was developed to help a passenger to use public/private mode of transportation based on current location & availability of time and resources.

6.1 Satellite images used during the study

The following satellite images were used during the study:

- Indian Remote Sensing Satellite, Cartosat-2 panchromatic images (2016-2017) of 1.0 m spatial resolution.
- Indian Remote Sensing Satellite, LISS 4 image (2017) of 5.8 m spatial resolution

The above two datasets were merged to obtain a hybrid merged image of 1.0 m resolution in colour.

6.2 Software packages and web mapping services used for the study

1) The software packages used during the study are listed below:
   a) ArcGIS software package – Used for digitization, topology and network analysis of the data that was collected from different sources.
   b) MS Excel 10 – Used for creating, adding, removing or manipulating the attribute tables of obtained data through web survey and data collection.
   c) MS word 10 – Used for the write up of the paper.

2) The online web mapping services used during the study are listed below:
   a) Open Street Maps – Used for downloading the basic data required for the analysis.
   b) Google Maps – For collecting the coordinates of

different points
c) Google Earth

7. Modules adopted

7.1 Service area

It is very important for a driver to keep note of the fuel and number of nearby petrol pumps. This module helps a user to identify the number of petrol pump in the vicinity of his location and decide whether he needs to refuel immediately. Hence, proximity analysis was carried using major road networks and existing petrol pumps in the city. It is briefly described below:

- Study area is initially crowded spatially with existing Indian oil petrol pump locations of the city.
- Proximity analysis in between existing petrol pumps are carried out using a special proximity analysis tool specially designed for proximity of objects in a transportation network.
- Multiple buffers of 3 km, 15 km and 25 km were taken into consideration as the distribution of facilities within an area depends upon the buffer value.
- GPS locations were used to identify the current location of a user on the map.
- This informs a user about his current location and the options available for him to refuel. Depending upon this, the user will be facilitated to know his nearby petrol pumps and his needs to refuel.

7.2 Relocation of bus stops

Bus stops and demand points (areas where a bus stop is essentially required such as railway stations, temples, schools, etc.) are needed to be in synchronicity with each other but in most cases this synchronicity is altered by the presence of impediments. In Bengaluru city, it was observed that most of the major bus stops are near to existing junctions / traffic signals (in a radius of less than 50 meters) making them one of the major causes of traffic congestion in the city as most signals in the city are fixed time signals and the presence of nearby bus stops creates unusual traffic queues which ultimately result in the traffic accumulation at the signalized junctions. In order to give a potential solution to this problem, Network Analysis was used during the study in which major bus stops were located using location allocation module of Arc GIS.

The procedure followed is briefly described below:

- An initial buffer of 500m radius was generated around each bus stop in order to locate all facilities within the vicinity of 500m from the existing bus stops which helped the location allocator to come up with important bus stops (depending upon the number of facilities in and around the bus stops and the distance between the facilities and the bus stops).
- These facilities were taken as demand points using which location allocator optimized the most important bus stops.
- Later a buffer of 50 m was generated around all existing traffic signals (as the nearness of the bus stops to the traffic signals was the major cause of traffic congestion as identified in the city).
- All bus stops that were within the buffer generated around the signals were manually shifted outside the buffer also taking into consideration the distance between two bus stops does not get drastically reduced since there will be a possibility of evolving traffic jams in between the two bus stops.

7.3 Decision Support System (DSS) for boarding a bus from any desired location

Bengaluru's bus system is operated by Bangalore Metropolitan Transport Co-operation (BMTC) which has introduced different buses for different routes in the city. They have assigned different bus numbers for buses moving from/to different locations in which the bus numbers are specified in the format number-alphabet(s) or vice-versa. For a person who wants to travel from one place to other he will need to know the starting point, end point and different stops in between the two points. This system is designed in such a way that a person can get all the above information after providing the given route number as an input information.

- Bus 335-E (Whitefield-Majestic) and 500-D (Hebbal to Silk Board) picking up passengers in the most congested routes as specified above were chosen for developing this methodology.
- Buses, bus stops and their respective bus numbers passing through each bus stop consisting of XY co-ordinates and bus numbers for all the buses passing through the routes were extracted using Google coordinates and ancillary data provided by BMTC.
- From a list of more than 500 bus stops, specific bus stops through which 335-E and 500-D buses along with their regular time of pass were loaded as a new shape file.
- Route analysis was integrated with bus stops information to direct a passenger towards the bus stop for catching the next bus well in advance.
- It was then left to the user to choose whichever mode of transportation he may desire for depending upon the availability of time and resources.

8. Results and discussion

The analysis was done for generating service area layers, bus stop location allocation and tracing buses by sorting their route numbers. The service area module was used to find the area served by existing petrol pumps. The area serviced by each petrol pump was displayed. The distribution of petrol pumps in the city is shown in figure 3. The blue color depicts petrol pumps in the center of the city and ad too many petrol pumps are nearby the distance between two nearby bus stops generated is less than 3 km. The pink color depicts that the distance between two nearby petrol pumps is less than 15kms and the third color code indicated there is no petrol pump in the area.

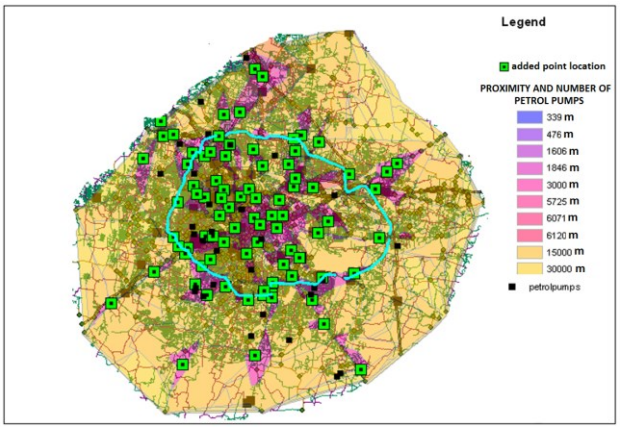

Figure 3: Area served by Indian Oil petrol pumps

This helps us identify a potential location for constructing a new petrol bunk in the city and facilitating the user to know his nearby petrol pumps and his needs to refuel.

Location allocation module helped in understanding the requirement of bus stops in the vicinity of different demand points and buffers around traffic signals helped in relocation problematic bus stops from their original position to a nearby position to help reduce traffic congestion as displayed in figure 4.

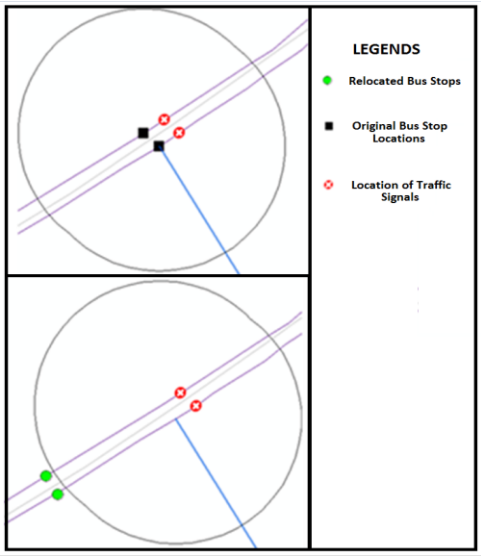

Figure 4: Example displaying relocation of bus stops

Bus numbers 335-E / 500-D were loaded from the attribute table and all bus stops through which the buses passed were traced. Integration of route analysis layer with bus routes and number helped to direct a passenger towards the bus stop for catching the next bus. It was then left to the user to choose whichever vehicle mode he wants to reach his destination depending upon his convenience and availability of resources.

Figure 5 displays an example of the decision support system showing the information about the origin, destination, nearest bus stop and the route the user needs to follow to reach his desired direction well in advance. After the analysis of the data, service area for facilities were found out, bus stop position was shifted and bus routes were traced out using bus numbers. The efficiency of GIS is clearly demonstrated by the above analysis. The network analysis tool is very efficient in solving different problems such as identifying routes, finding the closest facility, finding a service area, location-allocation, route tracing, vehicle routing problem, origin-destination matrix generation, and much more.

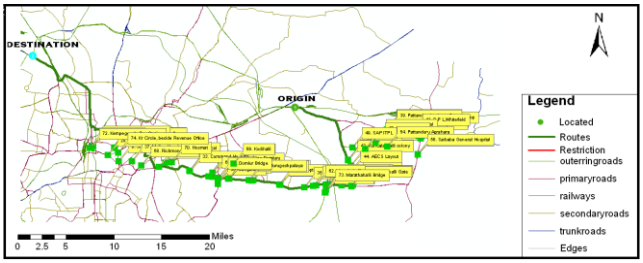

Figure 5: An example of route selection using Decision Support System

9. Future scope of study

Transport Network Optimization has a great scope of future study especially in developing countries. The collection of data for Origin-Destination Matrix creation is one of the most challenging tasks for a traffic planner. The study was only done for signalized intersections but planning needs to be done for un- signalized intersections too. These are some of the major tasks that could be taken up for future study. The study has been done for only one route of the city. Further research can be taken up on relocating bus stops on different routes of the city. Relocation of bus stops with respect to the metro stations and sub-urban railway stations is still a major task to be completed. In future, GIS can be used for transport planning and infrastructure development if more data is available for study. Integration can be done with respect to all modes of transport for better understanding of the traffic situations, provided more data is available. Web GIS applications can be developed to solve traffic related issues which will be very useful for public in upcoming years.

Acknowledgements

We sincerely acknowledge BMTC and Bengaluru Traffic Police Department for providing the data that was needed for our work. Sincere thanks to Dr. Ramalinga Reddy, Director, School of Civil Engineering, REVA University, Bengaluru for allowing Subham Kharel to work under RRSC-South, ISRO, Bengaluru. Authors are thankful to Dr. Santanu Chowdhury, Director, NRSC and Shri. Uday Raj, Chief General Manager, NRSC for their encouragement and support. We extend our sincere thanks to the technical as well as non-technical staff of RRSC-South for providing necessary support during the course of the study.

References

Arora, A. and M. K. Pandey (2011). Transportation network model and network analysis of road networks, 12th ESRI India User Conference, Gurgaon (Haryana, India), 7-8

December, 2011, 1-9.

Ejiagha, I.R., J.C. Ojiako and C.G. Eze (2012). Accessibility Analysis of Healthcare Delivery System within Enugu Urban Area Using Geographic Information System, Journal of Geographic Information System, 4, 312-321.

Kharel, S., P. Sivananda, K.S. Ramesh, K.N. Jothi and K.G. Raj (2018). Transportation network model for route and closest facility analysis in Central Bengaluru, International Journal of Application or Innovation in Engineering & Management (IJAIEM) 2319-4847, 7(4), 58-62.

Kumar, P. and D. Kumar (2016). Network analysis using GIS techniques: A case of Chandigarh city, International Journal of Science and Research (IJSR), 5(2), 409-411.

Namoun, A., C.A. Marlin, B.S. Germain, N. Mehandjiev and J. Philips (2013). A multi-agent system for modelling urban transport infrastructure using intelligent traffic forecasts, LNAI 8062, 175–186.

Ramos, A.L., Jose Vasconcelos Ferreira and Jaume Barcel (2012). Modelling and simulation for intelligent transportation systems, International Journal of Modeling and Optimization, 2(3), 409-411.

Ranya F.A.E., A. Elhog, S.E.K. Sideeg, A.E. Mohammed, N.A. Gism and M.S.A. Allah (2016). Route network analysis in Khartoum City, SUST Journal of Engineering and Computer Science (JECS), 17(1), 50-57.

Sidhtharthan, S. and S. Durgadevagi (2016). Road network analysis of Pondicherry Union Territory using GIS, International Journal of Technical Innovation in Modern Engineering & Science, 2(1), 32-41.

Visser A. and A.J.V.D. Wees (2000). Discrete event modelling methodology for intelligent transport systems. Proceedings of the 7th World Congress on Intelligent Systems, Italy, 2000.

You, J. and T. J. Kim (1998). An integrated urban systems model with GIS, Journal of Geographical Systems, 4(1), 305-321.

Yue, H., L.R. Rilett and P.Z. Revesz (2016). Spatio-temporal traffic video data archiving and retrieval system, Geoinformatica, 20(1), 59–94.

Journal of Geomatics Vol. 13, No. 2, October 2019

Disease control and combat mapping for tribal fortification using GIS –a case study for selected tribal blocks of Rayagada district, Odisha

P. K. Panda*,[1], M.L.Narasimham[1], I.V.Muralikrishna[2] and Sangeeta Sahu[3]
[1]Department of Civil Engineering, Centurion University of Technology and Management, Odisha
[2]Formerly JN Technological University, Telangana
[3]Department of Computer Science, Berhampur University, Odisha
*Email: prafullapanda@cutm.ac.in

(Received: Jan 02, 2018; in final form: Oct 10, 2019)

Abstract: Importance of health with respect to all living beings needs no special mention in the contemporary society. However, due to lack of awareness and health care services, many parts of our nation are still gravely affected due to several diseases, mostly the rural areas in general and much in particular the tribal villages. Most of the regions in India still have poor health protecting infrastructure facilities and as a result of which majority of the rural population is suffering from many diseases that could have been controlled with proper understanding of the disease causative process and possible preventive measures. In order to provide with better health care facilities in the Public Health Centres (PHCs), a data base of the disease causing agents and the remedial measures in the form of GIS maps will help in regularly monitoring the health level of rural public. An attempt has been made to map most common factors of prevalent diseases in rural and tribal regions in selected blocks spread over Rayagada district of south Odisha state and to develop a health care information system for the tribal regions. A well set methodology wherein the sum of the product of the weightage and rating considering various influencing parameters that result in an index referred as "Disease Vulnerability Index" (DVI) is evaluated for a number of villages in the selected blocks of the study area. Data analysis has been done for disease vulnerability mapping considering environmental factors, factors that are responsible for the sustenance of Disease Causing Vectors (DCVs) (Climatic factors), and factors that resist the growth of D.C.Vs (General Sanitation & Drainage). Each of the disease causing agents and disease spreading means has been assigned with a weightage factor indicative of the disease causing potential. Based on the relative levels of disease causing agents, each parameter has been assigned with a ranking on a 1 to 10 scale to assess the vulnerability level of the parameter at a certain location. Finally Disease Vulnerability Maps and Disease Control and Combat maps have been generated for each of the blocks under consideration using GIS layering. Number of villages with high % vulnerable values and low % vulnerability values for each block in the study area and number of villages with varying levels of disease controllability could be obtained.

Keywords: Disease Mapping, Disease vulnerability index, Geospatial Analysis, PHCs

1. Introduction

Importance of health with respect to all living beings needs no special mention in the contemporary society. Lack of awareness and availability of good health care services in tribal villages, in particular is a serious issue in India. In addition, illiteracy among tribal population, remoteness of the villages they live in, lack of clinical / pharmaceutical infrastructural services and the age old practices adopted for curing with reluctance for undergoing current day advanced treatment methods further aggravates the situation. As a result of all these factors, most of the tribal population in our country are falling a prey to several water borne and vector borne diseases(www.cips.org.in/documents/DownloadPDF/downloadpdf.php?id=66&category=Health).

Recent advances in GIS and Global Positioning System have created new opportunities for public health administrators to enhance planning, analysis and monitoring of vector born disease identification and elimination (https://nrhm-mis.nic.in/Orissa Health GIS_Mithun NRHM.pdf). However, the work related to geospatial health networking is in initial stages and has not spread over the width of the nation.

Most of the regions in India have still poor health protecting infrastructure facilities and as a result of which majority of the rural population is suffering from many diseases that could have been controlled with proper understanding of the disease causative process and the preventive measures (http://icmr.nic.in/annual/2014-15/RMRC_bhub.pdf). In order to provide with better health care facilities in the Public Health Centres (PHCs), a data base of the disease causing agents and the remedial measures in the form of GIS maps will help in regularly monitoring the health level of rural public. In the present context, an attempt has been made by a team of investigators belonging to Department of Civil Engineering, Centurion University of Technology and Management, supported by DST, Government of India, to generate maps that are indicative of disease vulnerability and possible control and combat of diseases in rural and tribal regions spread over two districts in South Odisha state (www.nrdms.gov.in, Project Report Submitted to DST: Project No.: NRDMS/01/41/014 (G, P-11) March 2018.). This paper deals with the analysis of the data collected w.r.t. selected blocks of Rayagada district of South Odisha. Five blocks of the district have predominant rural and tribal population. Preliminary study has observed that the general health conditions of these rural and tribal public are deteriorating due to the prevalence of certain diseases, which could have been prevented with a little understanding of the disease causing processes and the preventive steps. It has also been observed that there is no proper data base pertaining to these diseases in these regions.

2. Study area

The study area includes certain blocks of Rayagada district of the state of Odisha, India that lies between 19°0'00"N to 19°58'00"N latitude and 82°54'00"E to 84°02'00"E longitude. It covers a total geographical area of 7584.7 sq. km. As per 2001 census, total population of the district is 8,23,000 out of which 1,17,524 (14.28 %) are SC, 4,61,209 (56.04 %) are ST and 2,44,266 (29.68%) are OC. Density of population is 116 person/ sq. km. Literacy rate of the district is 35%. In the district of Rayagada more number of blocks have tribal population and it is a real requirement to provide health care services to all the tribal population of these blocks. The selected blocks are of B. Cuttack, Gudari, Munigada, Kashipur and K. Singpur since they happen to be the blocks with more tribal population in the district (Figure 1). The locations of PHCs and subcentres as mapped by NRHM, Government of India are also shown in figure 1. Hardly there is any study on the vulnerability of villages to major diseases along with information on the possible steps to be initiated to control the spread of diseases. In this context the proposed study is more or less first of its kind to collect data on the disease causing factors and those factors which will enable to assess the possibility of control of the spreading of diseases.

3. Objectives

This study addresses various problems associated with spreading of diseases in tribal regions and provide proper health information for sharing among all the concerned agencies and organizations. Since GIS platform is most suitable for information sharing and applicability, it is considered in the present study to generate the disease vulnerability and control information in the form of GIS maps. The mapping technologies can create interactive interfaces for users, with the support of GIS basic functions such as zoom in, zoom out, pan, and hyperlink. Thus, a geospatial-enabled approach has been performed in this study for semantic health information retrieval with the following specific objectives:

- Identification of most prevalent diseases causing health impairment in the tribal population in the study area.
- To map pockets those are most vulnerable for the diseases and evaluate disease vulnerability index for the study area

To prepare disease vulnerability index map and control and combat map for the study area.

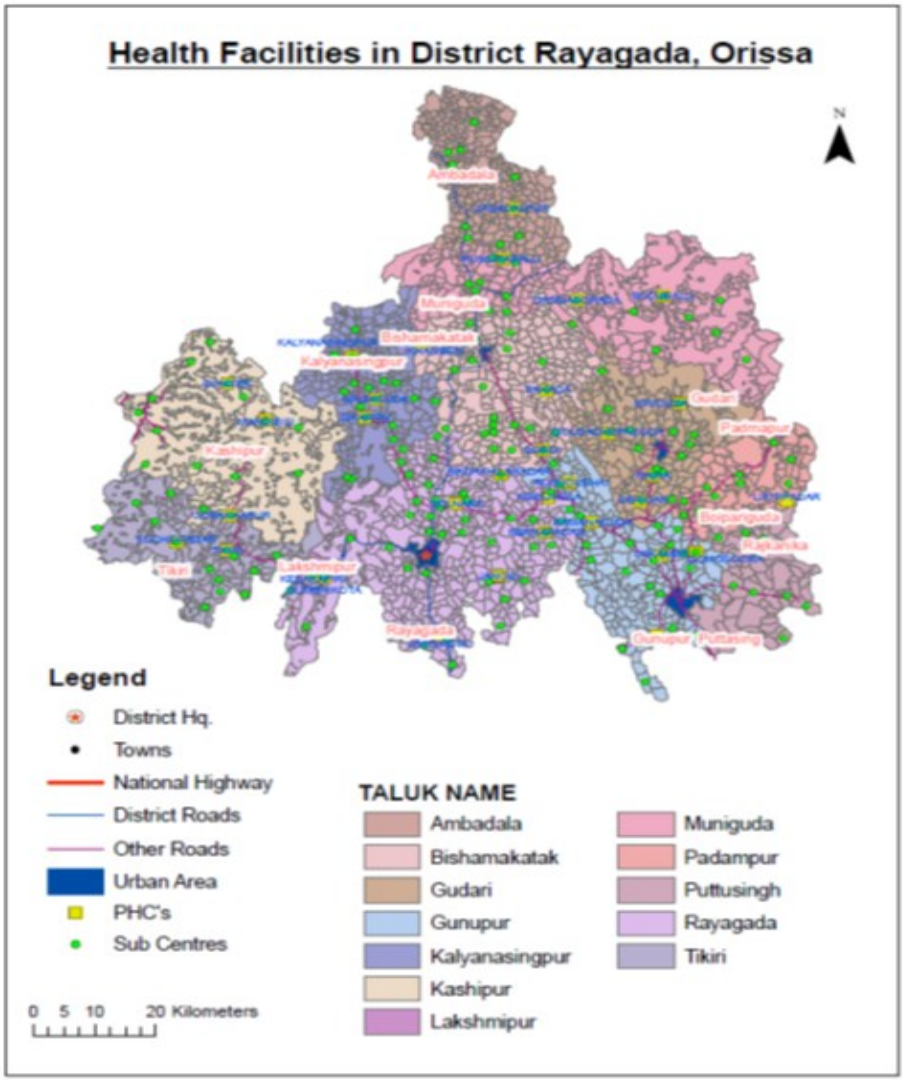

Figure 1: Study area map with locations of PHCs and subcentres

4. Methodology

The present study is a part of Geospatial Health Networking project of Department of Science & Technology (DST), Govt. of India, in which a sub-project on Disease Vulnerability and Disease Control mapping has been taken up. The study is based on availability of data related to rural health care services in the district and geographical accessibility of the health services. Important factors considered for baseline study and analysis are rural population, available health centres, roads, sanitary status, literacy, water bodies, drainage facilities etc. Preliminary discussions and interaction with district medical officers revealed that the most prevalent diseases in the selected tribal blocks are malaria, filariasis and anemia. Deliberations in a Workshop conducted with district medical officers and ground staff of PHCs and other related personnel concluded that the factors responsible for causing and sustenance of the identified diseases are more or less common. These can be categorized under three classes, viz., (i) Environmental factors, (ii) Climatic factors and (iii) General sanitation & drainage factors. Any one or combination of these factors would possibly be favourable to the growth of Disease Causing Vectors (DCVs). Awareness factors and preventive factors decide the possible extent of control the spread of diseases. Based on the nature of these factors each of them are assigned with a weightage in the scale of 1 to 10. Tables 1 and 2 given below indicate these Disease Vulnerability Factors (DVFs) and Disease Controlling Factors (DCFs) along with the assigned weightages. Subsequently, a questionnaire has been developed in consultation with district medical authorities for the identification of extent / level of impact of the disease causing factors as well as those factors that would possibly enable the control of the disease against its spreading, along with their relative level of impact. The questionnaire is developed in such a manner that it enables not only identifying the influencing parameters under the DVFs and DCFs but also their potential in assessing the vulnerability or control index. Each of the DVFs and DCFs are subdivided into several parameters that have high, medium and low weightage w.r.t. to disease vulnerability or control as the case may be. In tables 1 and 2 all the identified parameters have been listed along with their possible influence (high/ medium / low). Further, depending on the nature / level of each of the parameters in a particular village, a rating is fixed again in a 1 to 10 scale following the information gathered from the questionnaire (Table 3).

Table 1: Disease Vulnerability Factors (DVFs)

Nature of Factor	Parameters	Weightage@ (Numerical Value)	Remarks
Environmental Factors	Presence of Disease causing vectors	High (10)	More Vulnerable
	Water bodies	High (10)	Impact is more
	Toilets & Sanitation within the Dwellings	High (10)	Poor Sanitation worsens the situation
Factors responsible for sustenance of D.C.Vs (Climatic factors)	Rainfall	Low (1)	Normally less impact on sustenance of D.C.Vs
	Temperature	Medium (5)	Higher temperatures may favour the growth of D.C.Vs
	Humidity	Medium (5)	Higher humidity is many times favourable for the growth and sustenance of D.C.Vs
Factors that resist the growth of D.C.Vs (General Sanitation & Drainage)	General Sanitation in the Village	Medium (5)	Considered to have a medium influence in resisting the growth of D.C.Vs.
	Type of Dwellings	Low (1)	Normally the type of built houses will not have much influence on the D.C.V growth.
	Drainage & Roads	Medium (5)	Considered same effect as of general sanitation in the village.

Note: @The weightages are assigned by the project team as per their relative impact as indicated in the remarks column.

Table 2: Disease Control Factors (DCFs)

Nature of Factor	Parameters	Weightage@ (Numerical Value)	Remarks
Health Awareness Factors	General Literacy	Low (1)	Though literacy is important, the literacy level being normally low in the region, the level of literacy is considered to have a low impact.
	Health Awareness Programmes by Govt & Voluntary Organisations	Medium (5)	The health awareness camps & programmes though will educate the public its impact is considered towards motivation for better health care. Hence a medium impact is assigned.
	Vaccination programmes conducted	High (10)	If regular vaccination is carried out, it will have a high impact in controlling the spread of diseases.
	Availability of ASHA & ANGANWADI Workers	Medium (5)	Availability of the ASHA & Anganwadi workers will ensure continuous awareness creation and thus considered to have a medium impact on awareness creation.
	General Treatment & Religious Beliefs	Low (1)	Since the diseases of highly critical nature, the type of treatment and the religious practices will have a low impact.
Preventive Factors	Symptoms Identified & Reported	High (10)	Early identification and reporting of cases will have high influence in preventing the spread of the disease.
	Location of PHC	Medium (5)	Although the proximity of PHCs will control the spread of the disease, the general facilities within rural health centres will not improve the situation of controlling the disease and hence a medium weightage assigned.
	Availability of 108 Services	High (10)	Ready availability of 108 services will enable quick ontrol on the spread of the disease.
	Accessibility of Medical Practitioners	Medium (5)	Effect same as that w.r.t the PHC location.
	Availability of Qualified Pharmacist	Low (1)	General availability of qualified pharmacist in tribal villages is far from reality and hence this parameter will not have significant influence on controlling the disease.
	Road Connectivity with Headquarters	Medium (5)	Better road connectivity will provide a better chance to control the spread of the disease and hence a medium weightage is assigned.
Note: @The weightages are assigned by the project team as per their relative impact as indicated in the remarks column.			

Table 3: Parameter rating

S. No.	Category of parameter	Rating Assigned				Remarks
		(a)	(b)	(c)	(d)	
1	PHC Location	1	4	8	10	If present within village less vulnerable
2	Medical shop location	1	4	8	10	
3	Availability of Registered. Medical Practitioner	1	4	8	10	
4	Surface drainage system	1	4	8	10	Presence of canals provide better drainage
5	Habitat type	10	4	8	1	Presence of RCC habitats better clean climate
6	Sanitation in village	1	4	8	10	Better sanitation better control
7	Toilet facilities in village	1	4	8	10	Better type of toilets (with septic tanks) better control
8	Road facilities	1	4	8	10	Black top & RCC roads provide better control
9	Existence of schools	8	4	1	10	Higher educational facility better awareness
10	Anganwadis / Health care units	1	4	8	10	Proper organization better awareness
11	NGOs operating	1	4	8	10	If covered by NGOs better awareness

12	Vaccination Programmes	1	4	8	10	Regular vaccination better control
13	Health awareness camps by Govt. and NGOs.	10	8	4	1	More frequent camps better control & awareness
14	108 services	4	8	10	1	Availability in close proximity control spread
15	Types of treatment (Religious based)	10	8	4	1	Treatment based on religious beliefs lead to more ignorance and more vulnerability

The sum of the product of the weightage and rating result in an index which is referred here as "Disease Vulnerability Index" (DVI). A similar index is arrived by using the disease controlling parameter and the same is termed as "Disease Control Index (DCI)".

$$DVI = \sum_{i=1}^{n} [P_W]_i \mathrm{x} [P_R]_i \quad \text{- - (Eq. 1)}$$

where $[P_W]_i$ = Weightage assigned to i^{th} influencing parameter,
$[P_R]_i$= Rating of the i^{th} influencing parameter in a particular village and
n = total number of parameters.

The magnitude of DVI will reflect the relative vulnerability at a village. The values of DVI have been mapped for the selected block in the study area. The map thus generated is known as the disease vulnerability index map. Similarly, Disease Control and Combat Index has been arrived considering disease controlling parameters. The methodology is schematically shown in the flow chart (figure 2). As a part of the data collection for index evaluation and integrated map generation, data is gathered from several villages through the questionnaire.

5. Results

Information obtained from the questionnaire is converted in to numeric data required for assessing the ratings of each of the parameters identified under DVFs and DCFs. A ratings matrix for each of the factors is generated for different locations in the study area using the assigned ratings as per table 3. All the spatial data of the product of ratings and weightages are integrated into GIS environment for storage, retrieval, manipulation, analysis and generation of a composite map that is indicative of the disease vulnerability of the block as a whole.

General disease vulnerability maps have been derived separately for 5 Blocks of the Rayagada district using the computed values of DVI. Disease control and combat maps are also generated for these blocks. Figures 3a to 3e show the disease vulnerability maps for the blocks of K. Singhpur, B. Cuttack, Gudari, Kashipur and Muniguda generated through GIS technique. Similarly figures 4a to 4e show the disease controllability maps for the above mentioned blocks. Table 4 shows the number of vilages with percentages of high and low vulnerability in the above mentioned blocks in the Rayagada district. The information with regard to the disease controllability in the selected districts is presented in table 5. The outcome of the study creates necessary information bank for assessing the vulnerability of a location for general diseases and the possibility of its control with existing infrastructure and the environment.

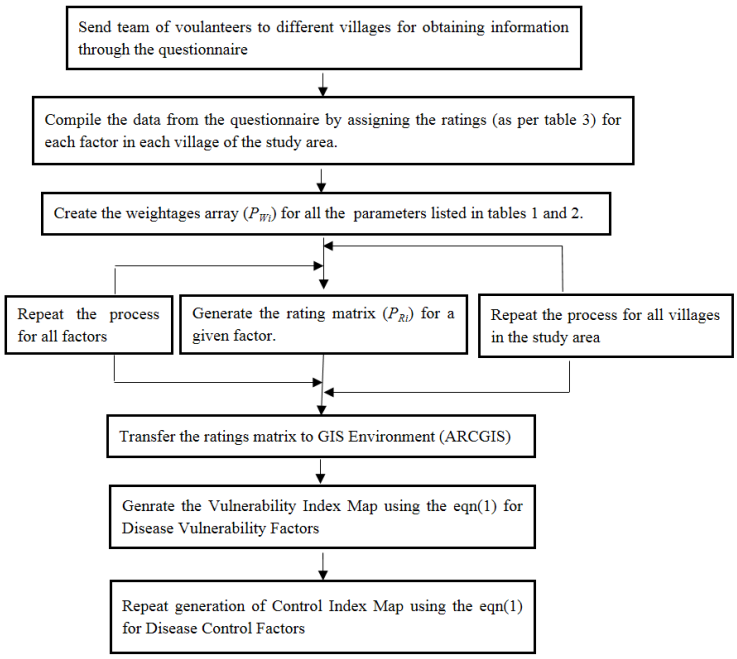

Figure 2: Flow chart

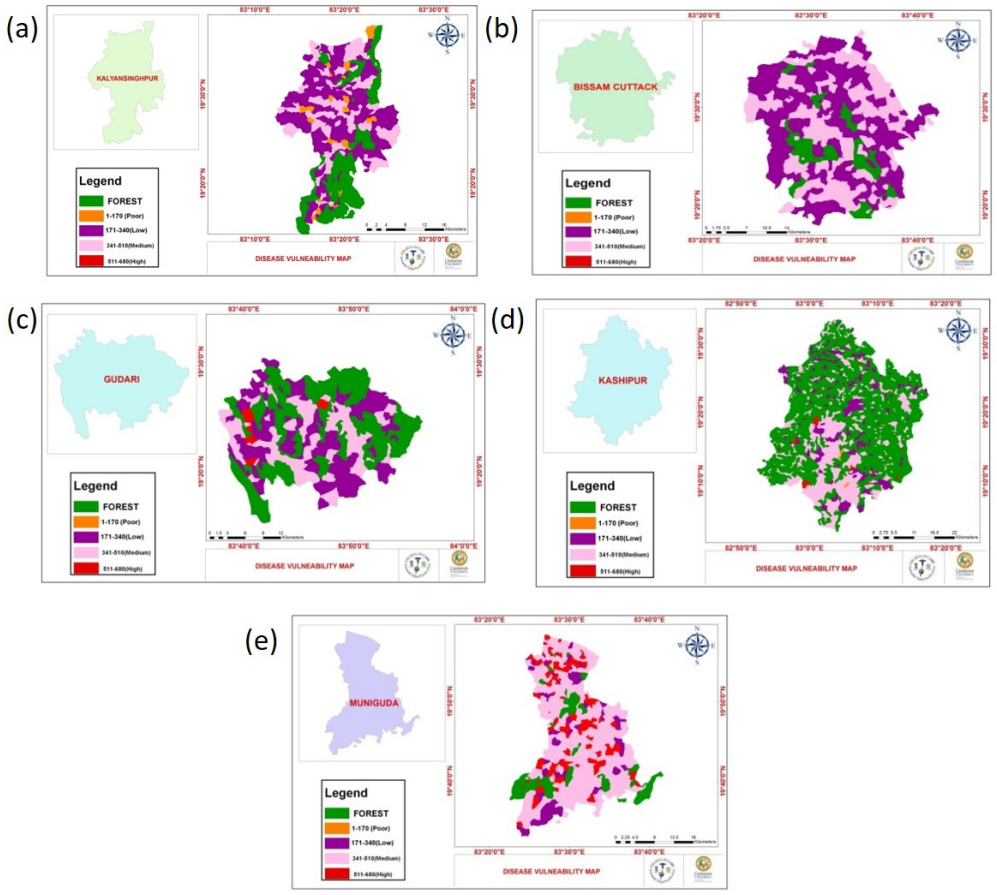

Figure 3: (a) DVI Maps for K. Singhpur Block, (b) B Cuttack Block, (c) Gudari Block, (d) Kashipur Block and (e) Muniguda Block

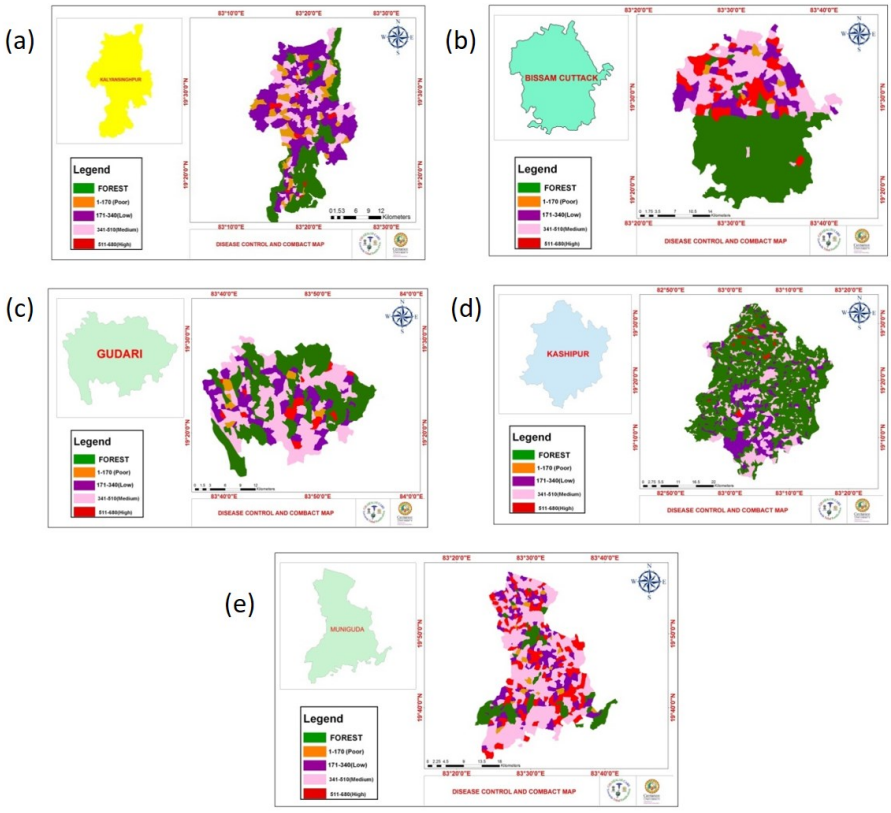

Figure 4: (a) DCI Maps for K. Singhpur Block, (b) B Cuttack Block, (c) Gudari Block, (d) Kashipur Block and (e) Muniguda Block

Table 4: Vulnerability information for selected blocks in Rayagda District

Block	Total no. of villages in the block	Villages High Vulnerability (DVI 511 - 600)		Villages with Least Vulnerability (DVI <170)	
		No	% In the Block	No	% In the Block
B. Cuttack	282	26	9.00	132	47.00
K.Singpur	223	29	13.00	132	59.00
Kashipur	406	45	11.00	201	50.00
Muniguda	366	43	12.00	198	54.00
Gudari	152	13	9.00	78	51.00

Table 5: Vulnerability Information for Selected Blocks in Rayagda District

Block	Total No of Villages in the Block	Villages High Control (Index: 511 - 600)		Villages with Control (Index: 341 - 510)		Villages with Less Control (Index: 170 - 340)		Villages with Least Control (Index: < 170)	
		No	% in the Block	No	% in the Block	No	% in the Block	No	% in the Block
B. Cuttack	282	65	23.05	103	36.52	105	37.23	9	3
K.Singpur	223	32	14.35	83	37.22	99	44.39	8	4
Kashipur	406	60	14.78	72	17.73	261	64.29	8	2
Muniguda	366	56	15.30	88	24.04	208	56.83	8	2
Gudari	152	14	9.21	43	28.29	82	53.95	14	9

7. Conclusions

The study enabled identification of several factors that are significant in disease spreading as well as its control. The parameters have been identified as Disease Vulnerability Factors and Disease Controlling Factors. These factors include different parameters with varying potential w.r.t disease spreading or control. Two indices are computed for each of the village in the selected blocks of the study area based on weight rating product summation methodology using parameters collected from field in form of a questionnaire. Disease Vulnerability maps and Disease Control maps for the blocks in the Rayagada district are developed from the computed values of DVI and DCI for the villages in each block in GIS environment. The vulnerability maps generated will help the district administration in readily identifying the villages in each block that have high vulnerability so that proper precautionary steps can be taken up. Similarly the control maps will help the district administration towards managing the infrastructure for disease control in an effective manner. Since the base maps are available in GIS, they can be used in dynamic nature by editing the data with updated status at any instance of time. Extension of the study in future will help in development of an information management system for optimized deployment of health services towards better treatment as well as prior control of diseases.

Acknowledgements

The work reported in this paper was carried out through the research project sponsored by Department of Science & Technology, Government of India under NRDMS, Geospatial Health Networking Scheme. The authors place on record the financial help provided by DST. The authors also thank the administration of Centurion University of Technology & Management, Odisha for the permission given for carrying out the project.

References

http://icmr.nic.in/annual/2014-15/RMRC_bhub.pdf

https://nrhm-mis.nic.in/Orissa Health GIS_Mithun NRHM.pdf

www.cips.org.in/documents/DownloadPDF/downloadpdf.php?id=66&category=Health

www.nrdms.gov.in, Project Report Submitted to DST: Project No.: NRDMS/01/41/014(G, P-11) March 2018.

Journal of Geomatics Vol. 13, No. 2, October 2019

Forecasting and visualization of NDVI series using statistical methods through Web-GIS

Ujjwal K. Gupta*[,1], Vidit Shah[2] and Markand P. Oza[1]
[1]Space Applications Centre (ISRO), Ahmedabad, 380015
[2]Ahmedabad University, Ahmedabad, 380009
*Email: ujjwal_gupta@sac.isro.gov.in

(Received: Jan 02 2019; in final form: Oct 10, 2019)

Abstract: Use of remote sensing derived information in agriculture sector plays an important role for decision makers to know status of vegetation on larger spatial scale. Researchers have developed various indices for this purpose. Normalised Difference Vegetation Index (NDVI) is one such indices that measures vegetation vigour of crop. Agricultural community has shown its uses in various applications viz. vegetation health monitoring, crop growth assessment, crop yield estimation etc. NDVI forecasting helps to make an educated guess, based on its temporal behaviour in past years, on likely vegetation condition ahead of time and thus supports decision makers to formulate mitigation strategy. In this paper, Moderate resolution Imaging Spectroradiometer (MODIS) satellite data is used for calculating NDVI and then, NDVI forecasting is performed based on 2002-2016 NDVI time series data. This paper uses two statistical approaches, (i) Conditional mean and variance based statistical approach and (ii) Auto Regression Integrated Moving Average (ARIMA) for forecasting. Forecast of NDVI values are compared with observed NDVI data for year 2016-2017 using mean absolute percentage error (MAPE). To investigate seasonal impacts on forecast of NDVI, average seasonal MAPE is calculated which is found to be 5-10% in Rabi (Winter season; Mid-October to March) and Zaid (Summer season; April to June) seasons over Gujarat region of India. This seasonal study of NDVI forecasting can be used to supplement the routine monitoring of environmental conditions for wide range of applications. The developed forecasting model is currently operationalized on VEDAS web portal (https://vedas.sac.gov.in).

Keywords: NDVI forecasting, ARIMA, MODIS, VEDAS, Web-GIS

1. Introduction

India is an agricultural dependent economy where farming is main activity. The impact of uncertainty of nature on the farming cannot be eliminated but the impact of nature can be reduced through proactive techniques. To keep track of progress of crop, remote sensing (RS) data can be used with its multi-spectral and multi-temporal observations. In tropical country like India where climate conditions varies a lot spatially, it becomes a challenging task to monitor vegetation status regularly. In such a scenario, it becomes evident to use satellite data through remote sensing to simplifying monitoring on both temporal and spatial scales.

Researches have derived a number of indices for showing vegetation status judiciously. One such index is Normalised Difference Vegetation Index (NDVI), a satellite derived indicator of vegetation vigour and its healthiness (Tucker, 1979). NDVI is derived as:

$$NDVI = \frac{(NIR - Red)}{(NIR + Red)}$$

where, NIR denotes near infrared region reflectance and red denotes reflectance in red region of electromagnetic spectrum, respectively. Agricultural community has shown its uses in various applications viz. vegetation health monitoring (Zhou et al., 2001, Sharma and Mishra, 2012), crop growth assessment (Oza, 2014), crop assessment and production forecasting (Sridhar et al., 1994, Parihar and Oza, 2006) etc.

For a country like India with multi-season crops, a seasonal understanding of vegetation becomes important apart from overall vegetation understanding. In India, there are mainly three crop seasons, Kharif (Monsoon season; July-Mid October), Rabi (Winter season; Mid-October to March) and Zaid (Summer season; April - June). Seasonal understanding also becomes more important in satellite based agriculture studies due to effects of seasonal climatic variation on quality of optical multispectral imagery.

Another important challenge is to develop a web based data visualization platform as decision support system that can ingest huge satellite data and help decision makers to judge their decision criteria in best available manner. A decision support system that not only gives present status of conditions but also shows picture of future conditions with certain confidence level is always preferred. It can be developed using Geographical Information System (GIS) technologies. Web-GIS is a special form of GIS that often uses web technologies to communicate among different components in its architecture containing at least one server and one client. A web-GIS based solution provides global reach, easy to use functionality and better cross platform capabilities. It enables diverse data at a unified place for convenience of decision makers.

2. Study area and dataset details

Moderate Resolution Imaging Spectroradiometer (MODIS) vegetation indices are designed to provide consistent spatial and temporal comparison of vegetation conditions. The 16-day Maximum Value Composite (MVC) NDVI product from MODIS-Terra (MOD13A1) is used in the present study (Didan, 2015). The MODIS

NDVI provides systematically processed data series. These are computed from atmospherically corrected bi-directional surface reflectances that have been masked for water, clouds, aerosols and cloud shadows. The spatial resolution of MODIS product used in the present study is 500 m. To determine the NDVI, red reflectance (0.645µm) and NIR (0.858 µm) reflectance are used.

For this study, Gujarat region is chosen which is located at the western side of India as shown in figure 1. It is preferred due to its diversified land use land cover (LULC) and triple crop cycle system (Mishra et al., 2017). Hence, it gives extra benefit to statistical models to learn in term of variance.

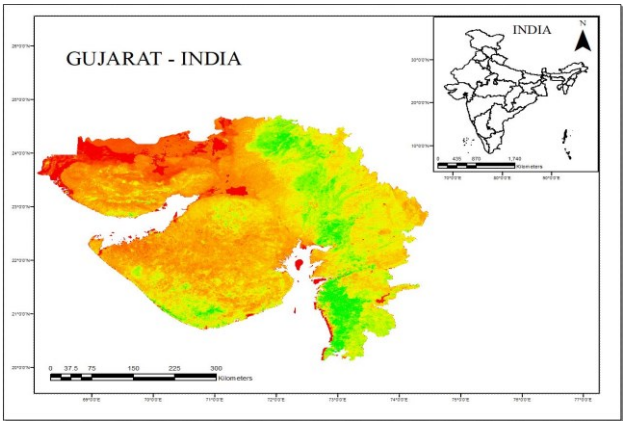

Figure 1: Classified image of Gujarat region of India based on NDVI values showing diversified vegetation in region

3. Methodology

Time series analysis in remote sensing helps in identifying the nature of the phenomenon represented by the sequence of the observation of RS data and exploit it to forecast future values of time series variables. MOD13A1 data has a temporal resolution of 16 days. To forecast NDVI values two methods are used: (1) Conditional mean and variance based statistical method (Oza, 2014), and (2) Auto Regression Integrated Moving Average (ARIMA) (Box and Jenkins, 1976).

3.1 Conditional mean and variance based statistical method

Let Y be a vector of length (n X 1) representing temporal profile of data, Y_1 be vector of length (n_1 X 1; such that $n_1 < n$) corresponds to observed temporal series and Y_2 be a vector of length (n_2 X 1; such that $n_2 = n - n_1$) corresponds to missing temporal profile. Then, mean temporal profile (M) using k samples can be calculated as given in eqn. (1),

$$M = k^{-1} \sum_{i=1}^{k} Y_i \quad ...(1)$$

and dispersion matrix (S) can be computed by using eqn. (2) as,

$$S = (k-1)^{-1} \sum_{i=1}^{k} [(Y_i - M)(Y_i - M)^T] \quad ...(2)$$

where, T denotes matrix transpose operation. Dispersion matrix, S is a square, symmetric and positive definitive matrix with size of n X n. It can be decomposed as,

$$S = \begin{bmatrix} S_{11} & S_{12} \\ S_{21} & S_{22} \end{bmatrix}$$

where S_{11}: submatrix of size n_1 X n_1, corresponds to observed data

S_{12}: submatrix of size (n_1 X n_2)

S_{21}: submatrix of size (n_2 X n_1)

S_{22}: submatrix of size (n_2 X n_2)

From mean temporal profile and dispersion matrix, unobserved data values (Y_2) can be conditionally computed from (Y_1) as given in eqn. (3),

$$E(Y_2/Y_1) = M_2 + S_{21}S_{11}^{-1}(Y_1 - M_1) \quad ...(3)$$

Here, E stands for expected value vector. The mean vector M_2 from observed time series corresponding to unobserved data period contains "apriori" information. The term $S_{21}S_{11}^{-1}$, derived from "hidden" pattern from data, controls the correction that is applied to "apriori" information. The more rough its history is more changes are required in "apriori" information.

3.2 Auto Regression Integrated Moving Average (ARIMA)

The ARIMA models are one of the classes of stochastic models for describing time series (Box and Jenkins, 1976). ARIMA models include three basic types: autoregressive (AR) models, moving average (MA) model and combined MA and AR model which is ARMA model. In ARIMA model approach, the past observations are analyzed to formulate a model describing the inner correlation among them. The acronym in ARIMA is descriptive and capturing key aspect of model itself. Briefly they are,

AR (p): Auto Regression. A sub-structure that uses dependent relationship between the current observation and number of lagged previous observations.

$$X_t = \sum_{j=1}^{p} \emptyset_j X_{t-j} + \omega_t$$

I (d): Integrated. The letter "I" in ARIMA indicates that the modeling time series has been transformed into a stationary time series. The 'd' value is used to remove the trend from given time series so that overall series becomes stationary.

MA (q): Moving Average. A sub-structure that uses the dependency between a current observation and a residual error (ϵ_j) from a lag observation.

$$X_t = \sum_{j=1}^{q} \emptyset_j \epsilon_{t-j} + \epsilon_t$$

Each of these components are explicitly specified in the model as a parameter. "ARIMA (p,d,q)" is the generalized notation where parameters are substituted in the integer value indicating which ARIMA model is being used.

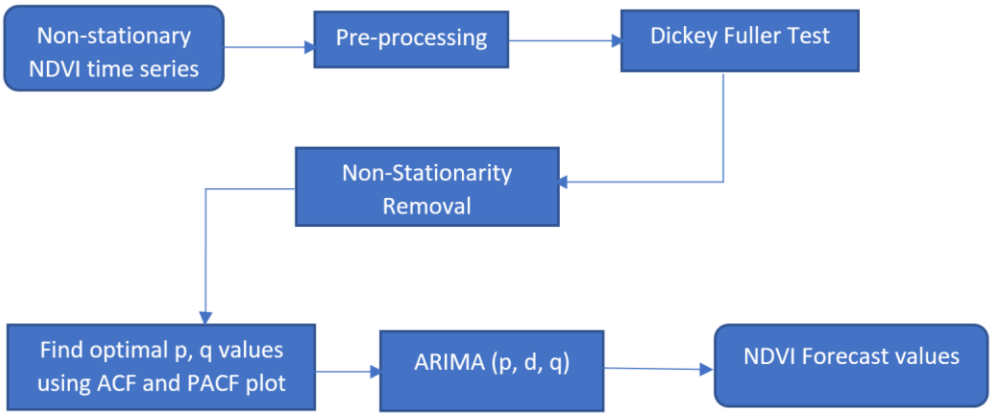

Figure 2: ARIMA methodology flow chart for NDVI forecast

3.3 Dickey Fuller Test of stationarity

A stationary time series can be defined when the data has a constant mean and no trend overtime. However, sometime time series may not be stationary and have trend line. In such cases, stationary is introduced by first order derivative, logarithmic operations etc. Stationarity of time series is tested by Dickey Fuller test (Said and Dickey, 1984).

Suppose there is an auto regressive time series:

$$y_t = \emptyset y_{t-1} + \in_t$$

It can be transformed by first order derivative into:

$$y_t - y_{t-1} = (\emptyset - 1)y_{t-1} + \in_t$$

If delta operator i.e. $\Delta y_t = y_t - y_{t-1}$ and $\beta = (\emptyset - 1)$ are set, above equation can be rewritten as,

$$\Delta y_t = \beta y_{t-1} + \in_t$$

This makes null and alternative hypothesis of this test as follows:

H_0 : Unit root is present in autoregressive model i.e. $\beta = 0$

H_1: The series has no unit root i.e. $\beta \neq 0$

The null hypothesis is rejected when p value of test is less than critical value i.e. series is stationary and vice versa. Here, critical value of 5% is selected for rejecting null hypothesis.

For making NDVI time series stationary, first derivative of series is used i.e. d=1. After removing seasonality, Auto Correlation Function (ACF) and Partial Auto Correlation Function (PACF) are plotted in order to get appropriate values of p and q in ARIMA (p, d, q) respectively. ACF plot is a bar chart of coefficients of correlation between a time series and lag of itself whereas PACF plot is a bar chart of partial correlation coefficients between series and its lag. From ACF and PACF plots, highest values of p and q values are figured out as 3 and 2 respectively.

A flow chart depicting ARIMA methodology is shown in figure 2.

For selecting best p and q values, randomly 1000 locations are selected in Gujarat state as shown in figure 3 and Akaike Information Criterion (AIC) value is calculated for each p and q pair. These AIC values are used as estimator of relative quality of statistical models. From AIC values of each pair, highest AIC value pair is selected as best model. Figure 4 shows p and q pair values with its frequency of occurrences as best model.

In this paper, Mean Absolute Percentage Error (MAPE) is used as a measure of accuracy of statistical forecast methods. MAPE is calculated as:

$$MAPE = \frac{\sum_{t=1}^{n} \left| {}^{(A_t - F_t)}/_{A_t} \right|}{n}$$

where, A_t is original value, F_t is forecast value for n number of sample points.

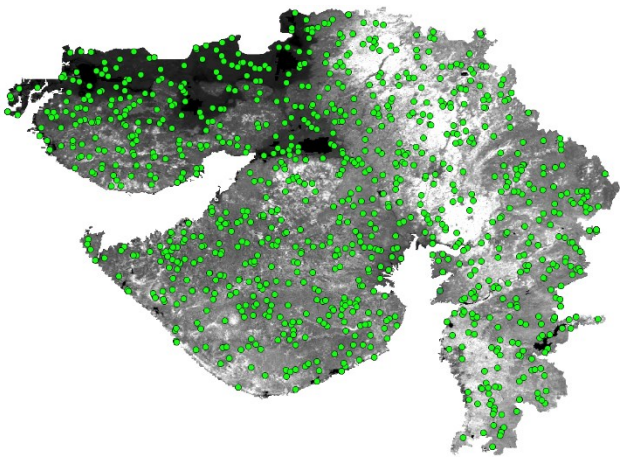

Figure 3: Randomly selected 1000 sample points over Gujarat region

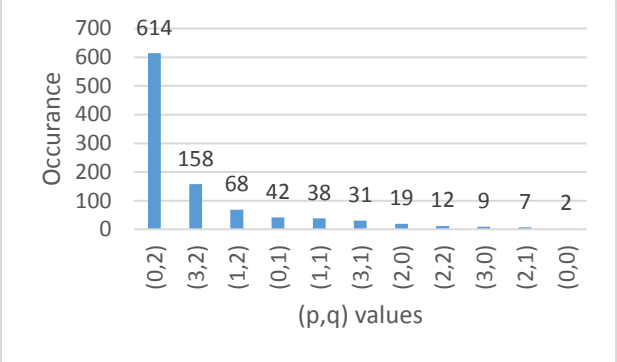

Figure 4: Frequency distribution for best model selection for each (p, q) pair

4. Results and discussion

Based on above discussed methodology, conditional mean and variance method as well as ARIMA are applied to MODIS NDVI time series data from 2002 to 2016, which was later verified with the NDVI data of 2016-2017. NDVI Forecast are done for up to next 3 forecast values corresponding to 16 days, 32 days and 48 days forecasts. Table 1 consolidates average MAPE results of both methods based on annual time series data for a sample date over Gujarat region. From table 1, it can be inferred that both the methods perform equally well in annual forecast.

Table 1: Mean Absolute Percentage Error (MAPE) for ARIMA and conditional mean and variance based method using annual time series for 08 JAN 2017

Forecast Days	Avg. ARIMA (0,1,2) MAPE	Avg. Conditional Mean & Variance MAPE
16	**3.02**	3.57
32	7.8	**7.2**
48	**9.47**	9.74

Table 2: Mean Absolute Percentage Error (MAPE) for ARIMA and conditional mean and variance based method using seasonal time series

Season	Forecast Days	Avg. ARIMA (0,1,2) MAPE	Avg. Conditional Mean & Variance MAPE
Rabi	16	**6.758**	8.74
	32	**8.936**	9.47
	48	12.457	**11.25**
Kharif	16	**19.871**	23.24
	32	**21.249**	26.95
	48	**26.478**	37.95
Zaid	16	**5.412**	8.82
	32	**6.451**	9.33
	48	**8.969**	9.89

For checking robustness of forecast methods under seasonal variations, average MAPE is calculated for Gujarat region. Table 2 summarizes seasonal effects on forecasting models.

It can be seen and analysed from table 2 that both forecasting models underperform in Kharif season. The reasons may be limitations of optical multispectral data in cloudy and foggy conditions. In other seasons, both methods give a satisfactory forecast error (MAPE) of 5-10% averaged over Gujarat region. In general, ARIMA performs well as compared to conditional mean and variance based forecast model under seasonal variations.

Currently, Annual ARIMA based NDVI forecast is implemented using MODIS NDVI time series pixel drilling. It is available at VEDAS web portal (https://vedas.sac.gov.in) through web GIS as Open Geospatial Consortium (OGC) compliant web map service. Figure 5 demonstrates a screenshot of operationalized model showing forecast result along with previous years NDVI time series data.

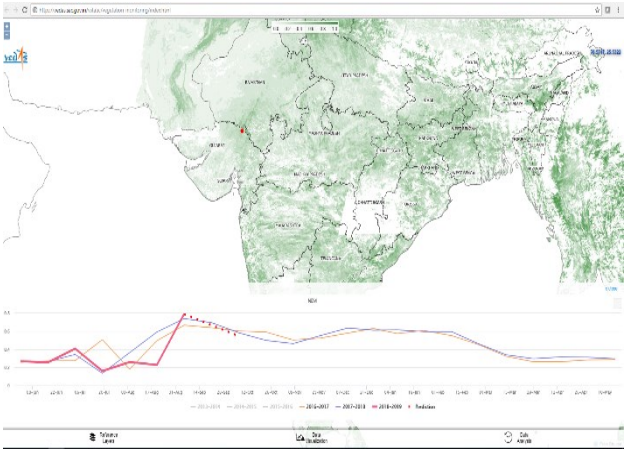

Figure 5: Forecast results of operationalized statistical model at VEDAS web portal through web-GIS

5. Conclusion and future work

In this paper, two standard statistical methods are used and found them suitable for NDVI forecast purpose with 5-10% seasonal MAPE in Rabi and Zaid seasons when averaged over Gujarat region for up to three forecasts. It was found that MAPE in Kharif season is more compared to other seasons which may be due to limitation of optical multispectral data in cloudy and foggy conditions. While forecasting NDVI values using annual timeseries data, both methods, (i) conditional mean and variance based statistical method as well as (ii) ARIMA method, are found to be performed at par to each other. NDVI forecast using statistical methods can be applied using remote sensing data at both temporal and spatial scales. These methods can be applied for forecast related to homogeneous cropping area for better understanding of phenological process of crop in future.

References

Box, G.E. and G. M. Jenkins (1976). *Time Series analysis: forecasting and control, revised ed*. Holden-Day.

Didan, K. (2015). *MOD13A1 MODIS/Terra Vegetation Indices 16-Day L3 Global 500m SIN Grid V006* [Data set]. NASA EOSDIS LP DAAC. doi: 10.5067/MODIS/MOD13A1.006

Mishra, S., M. P. Oza and S. A. Sharma (2017). Crop phenology identification using NDVI time-series and its dissemination using WebGIS, Proceedings of 38th Asian Conference on Remote Sensing (ACRS-2017), 23-27 October, New Delhi, India.

Oza, M. (2014). Use of Statistical Method to Remote Sensing Data for In-season Crop Growth Assessment. Journal of the Indian Society of Remote Sensing, 42(1), 243-248

Parihar, J. S., and M. P. Oza (2006). FASAL: an integrated approach for crop assessment and production forecasting. In *Agriculture and Hydrology Applications of Remote Sensing* (Vol. 6411, p. 641101). International Society for Optics and Photonics.

Said, S. E. and D. A. Dickey (1984). Testing for unit roots in autoregressive-moving average models of unknown order. Biometrika, 71(3), 599-607.

Sharma, S. A. and S. Mishra (2012). Web-GIS based monitoring of vegetation using NDVI profiles. Journal of Geomatics, 6(2), 109-112.

Sridhar, V. N., V. K. Dadhwal, K. N. Chaudhari, R. Sharma, G. D. Bairagi and A. K. Sharma (1994). Wheat production forecasting for a predominantly unirrigated region in Madhya Pradesh, India. Remote Sensing, 15(6), 1307-1316.

Tucker, C. J. (1979). Red and photographic infrared linear combinations for monitoring vegetation. Remote sensing of Environment, 8(2), 127-150.

Zhou, L., C. J. Tucker, R. K. Kaufmann, D. Slayback, N. V. Shabanov and R. B. Myneni (2001). Variations in northern vegetation activity inferred from satellite data of vegetation index during 1981 to 1999. Journal of Geophysical Research: Atmospheres, 106(D17), 20069-20083.

Journal of Geomatics Vol. 13, No. 2, October 2019

Evaluation and quality monitoring of SCATSAT-1 scan mode data

Maneesha Gupta*, Anuja Sharma, B. Kartikeyan
Image Analysis and Quality Evaluation Division, Signal and Image Processing Group
Space Applications Centre, Ahmedabad-380015
*Email: maneesha.nano@gmail.com

(Received: Jan 05, 2018; in final form: Oct 10, 2019)

Abstract: Accurate wind products generation, depends on the accuracy of sigma-0 estimation from the scatterometer data. Similar to Oceansat-2 (OSCAT) scatterometer, SCATSAT-1 scatterometer works on dual pencil beam (inner beam HH and outer beam VV) approach at 13.5 GHz frequency by conically scanning the earth surface and collecting the backscatter. The scatterometer data is signal processed on-board and radiometrically corrected on ground. In contrast to OSCAT-2 scatterometer, SCATSAT-1 sensor is designed with advanced techniques for providing better sigma-0 (directory.eoportal.org). This work discusses the quality aspects of SCATSAT-1 data (scan mode). Level-1B scan mode is the basic data and it is very significant to evaluate and monitor the quality of this data as it forms the basic input to the Level-2A cell-grid sigma-0, which in turn results in the formation of wind product (Level-2B). The level-1B product carries information about the radiometry (sigma-0, Signal to Noise Ratio (SNR)), geometry (azimuth angle, incidence angle, geolocation), calibration constant and sigma-0 quality flag at both slice and footprint level. For evaluation of data quality these parameters are categorised into static and dynamic parameters based on the sensor scan mechanism and the wave target interaction. Doppler frequency, X-Factor, Range, incidence angle and azimuth angle are the static parameters which varies systematically over the orbit data and shows consistency and are well within the specification. The dynamic parameters like sigma-0, SNR and brightness temperature (BT) are observed for the scan mode data acquired for each orbit/revolution. For calibration/validation, sigma-0 and BT of well-known calibrated sites (viz. Amazon rain-forest, Antarctica) are monitored and results show that variation in Sigma-0 over the Amazon rainforest is less than 0.3 dB, as expected. The results from trend analysis ensures that parameters are behaving well within the specifications and assures stability and consistency of system parameters. The analysis suggests that the products from the SCATSAT-1 can be taken for climate studies.

Key words: Sigma-0, Brightness Temperature, Footprint, X-Factor, Fore, Aft

1. Introduction

SCATSAT-1 is a continuity mission to Oceansat-2 Scatterometer (OSCAT-2) in providing Ku Band data to global user community. SCATSAT-1 mission was launched in September 2016 by ISRO's PSLV-C35, the payload carries a dual pencil beam scatterometer in Ku (13.5 GHz) band to study the ocean wind vector and associated phenomena. It operates day and night and covers the entire globe in two days. Like its predecessor Oceansat-2 scatterometer, SCATSAT-1 mission is a global science mission and its data is used by international agencies such as National Aeronautical and Space Administration (NASA), National Ocean and Atmospheric Administration (NOAA), Royal Netherlands Meteorological Institute (KNMI), European Organisation for the Exploitation of Meteorological Satellites (EUMETSAT) etc., (www.nesdis.noaa.gov/OPPA/indec-scatsat.php; OSI-SAF winds Team) to generate wind over the ocean and to forecast various phenomenon over the ocean such as storms, cyclones etc., which requires accurate sigma-0 data over the sea. For near real time monitoring and forecasting of weather phenomenon, it is required to analyse, assess and monitor the quality of the data at each level (Maneesha et al., 2011; Risien and Chelton, 2008).

The Data Quality Evaluation (DQE) system monitors the quality aspects at each level of data starting with the basic raw data to Level-2B global wind product in near real time. Further, if any anomaly or high deviation from the defined specifications is observed, DQE raises alerts to the concerned team for taking necessary actions. The key objective of DQE system is to ensure the dissemination of best quality of data to the end user.

The Level-1B data in SCATSAT-1 is acquired in every half orbit in contrast to its predecessor OSCAT-2, to improve the turn-around-time for data dissemination. In this paper, quality of Level-1B scan mode data is monitored using the in-house designed DQE software in an automatic manner. The results are interpreted based on the statistics from the slice and footprint data. Section 2 briefly defines the data sets used and the methodology to evaluate the data quality followed by results and analysis in section 3.

2. Data and methodology

The data used for this work is radiometrically corrected and geotagged Level-1B product at slice and footprint. The data is taken from operations generated through Data Product Generation System (DPGS) at National Remote Sensing Centre (NRSC) Hyderabad. The same data is shared at Meteorological and Oceanographic satellite data archival centre at Space Applications Centre Ahmedabad (www.mosdac.gov.in). It has both inner (HH) and outer (VV) beam data. The data of inner and outer beam has 281 and 282 footprints respectively.

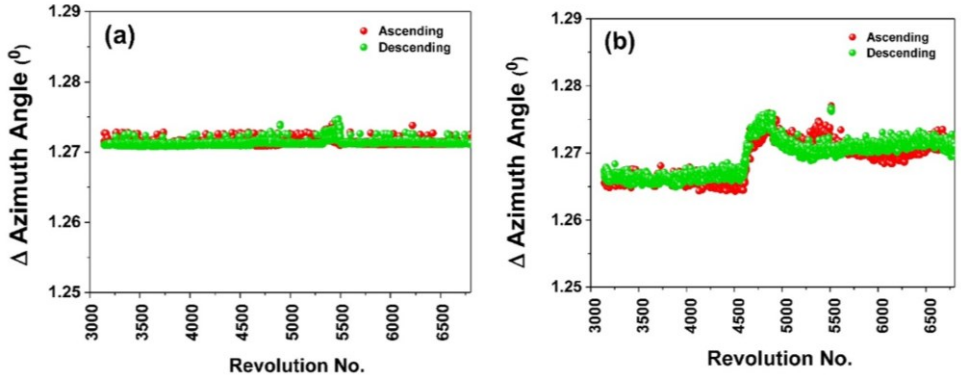

Figure 1: Footprint to footprint azimuth angle difference (a) HH and (b) VV beam

As scatterometer is an active sensor, the processing bandwidth of the signal processor and the 3dB power of the beam decides how many slices has to be taken to form the actual footprint on ground. Here, 9 inner slices and 14 outer slices are selected from the raw data to form the level-1B footprint along with appropriate weighting function. The basic data unit for Level-1B product is half orbit defined as north to south as descending and south to north as ascending (www.mosdac.gov.in/Scatsat-1-data-products). The data used in this work is generated from the SCATSAT-1 processing software version 1.1.2 from May 2017 to December 2017 and the analysis is based on each half orbit data, global cycle-wise data (two days) and long-term data.

The methodology used for evaluation and monitoring of quality metrics for SCATSAT-1 is based on identification and generation of quality metrics. The metric is categorized into static and dynamic parameters depending on the sensor scan mechanism and the wave target interaction (Maneesha et al., 2011). The static parameters are Doppler frequency, incidence angle, X-factor, azimuth angle, geolocation and kp whereas the dynamic parameters include SNR, sigma-0 (σ0) and Brightness Temperature (BT) explained elsewhere (Gupta et al., 2011). Behaviour of static parameters is monitored with respect to defined specifications (mentioned in Table 3.2) in half orbit revolution. The dynamic parameters are assessed in both half orbit and global one cycle data based on the sigma-naught quality flag which contains information of each slice/footprint in terms of location (land/sea), beam (inner/outer), node (ascending/descending), scan-direction (fore/aft), and sigma-0 quality (good/poor, valid/invalid). As scatterometer works for generating wind products which is governed by statistical averaging of Sigma-0. Thus to ensure the data quality and calibration aspects, the sigma-0 and BT are studied over the invariant sites and over land/sea using two days global cycle average.

3. Analysis, results & discussion

The analysis carried out on the parameters described in section 2 are discussed in this section. As per the quality metrics the results are shown in three categories namely (i) static parameter analysis (ii) dynamic parameter analysis (iii) invariant site monitoring.

3.1 Static parameters

In SCATSAT-1 there are certain parameters which are programmed for particular mode of operations and remains static within specifications. Range, X-factor, Incidence angle (inner and outer beam), Azimuth angle difference from footprint to footprint are the static parameters which varies within the defined specifications and depends on the geometry of the system. Figure 1 shows the azimuth angle difference for inner and outer beam footprints in ascending and descending passes. It varies within the defined limits ($1.27^0 \pm 0.01^0$) and is stable around 1.27^0 over the observed revolution data. In outer beam after revolution 4600 slight deviation of the order of 0.01^0 is observed which is highly stable as seen in figure1b, which might be the effect of orbit manoeuvring during the orbit-locking phase.

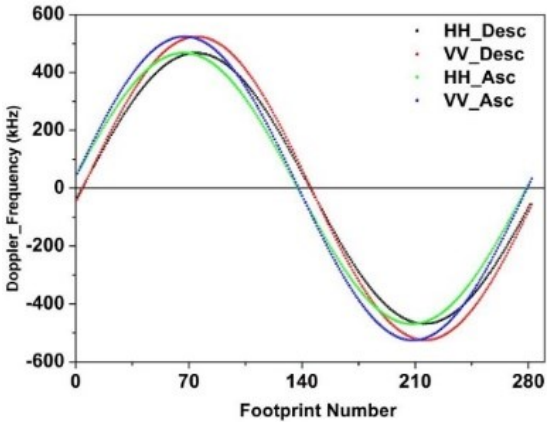

Figure 2: Doppler frequency (kHz) for half revolution data

Doppler frequency which is a function of scan forms a sinusoidal pattern for each scan and varies ±467 kHz for inner beam and ±523 kHz for outer beam. Figure 2 shows the typical plot of Doppler frequency shift over the footprints of a scan averaged over the half revolution data for revolution number 4773 (day-233). The expected sinusoidal pattern is observed for both inner (HH) and outer (VV) beam in every ascending and descending orbit. From the observed pattern (Figure 2), Doppler frequency at maxima is at footprint number 70 and 210, whereas the minima are at footprint number 1, 140 and 280 are analysed for multiple revolution data. Results are shown in figure 3(a) and 3(b) for inner and outer beam respectively.

Doppler frequency over the eight-month's data shows stable Doppler shift over the chosen footprints. At nadir, the Doppler for HH beam is less than VV beam by ~56 kHz.

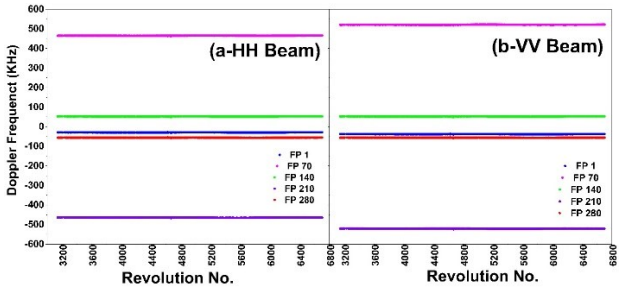

Figure 3: Doppler frequency (kHz) at different footprint locations over multiple revolutions data (FP –footprint)

Incidence angle is a static parameter for pencil beam scatterometer and form pattern with respect to ascending/descending pass and is a function of latitude due to spheroid shape of the earth. Figure 4 shows the incidence angle for both HH and VV beams is fixed at 49.06^0 and 57.96^0 respectively. It is observed to be stable in both ascending and descending node.

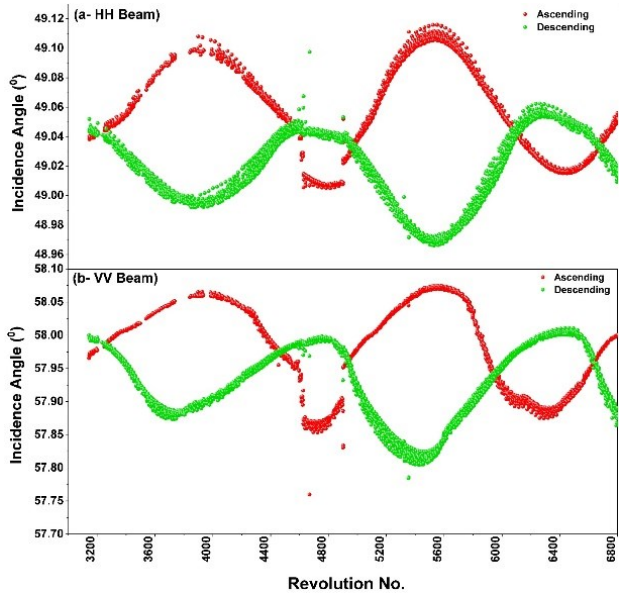

Figure 4: Incidence angle for inner and outer beam in both ascending and descending pass

Range and X-Factor from SCATSAT-1 is monitored for both HH and VV beam in ascending and descending revolutions are shown in figure 5 and figure 6 respectively. Similar patterns are observed for both beams in ascending and descending orbits. The range observed varies around 1241 km for outer and 1057 km for inner beam as expected. The variation in range is compensated in the calibration factor i.e. X-Factor and is shown in figure 6 (a & b). From the figure 5 a b there is a broadening in range seen and is compensated in cal factor (X factor). This broadening is due to orbit manoeuvring which took place during orbit 4600 and is confirmed from the satellite velocity and position (Figure 7).

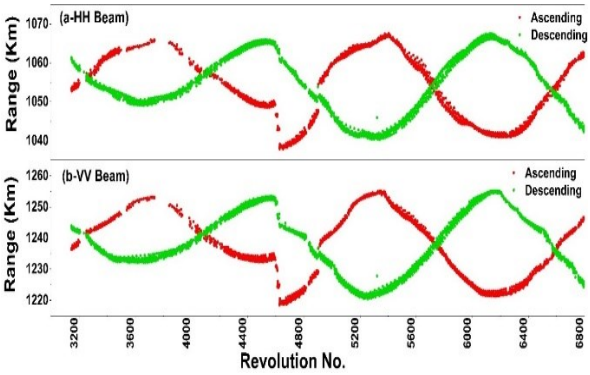

Figure 5: Range observed in SCATSAT-1

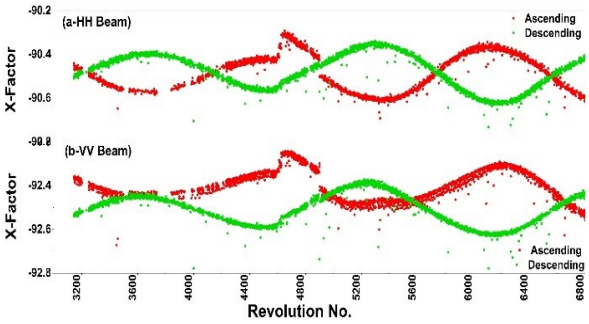

Figure 6: X-Factor from level-1b footprint data of SCATSAT-1

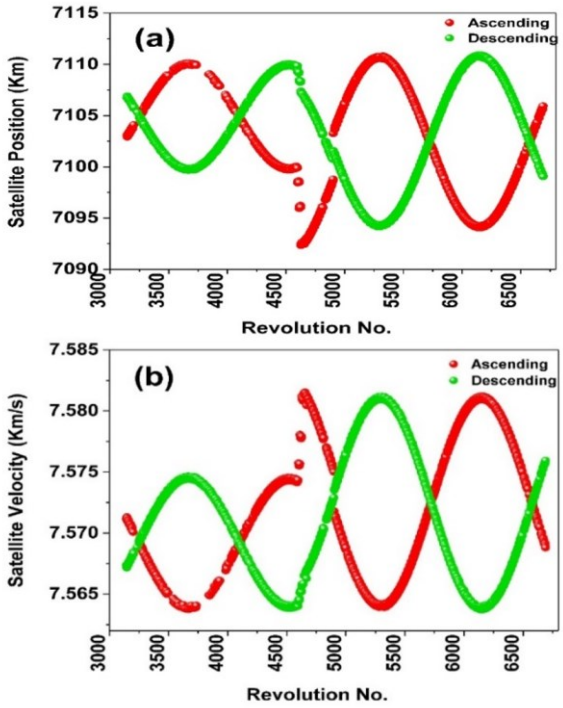

Figure 7: (a) Satellite position (b) Satellite velocity

The statistics from the long-term data (May- 2017 to December 2017) for static parameters is given in table 2. It is evident from the statistics that the behaviour of static parameters is stable with respect to time and is within the defined specifications mentioned in table 1.

Table 1: Specifications of static parameters

parameter	Range specifications (minimum and maximum)			
	Inner Beam (HH)		Outer Beam (VV)	
	Min	Max	Min	Max
Doppler Freq. (kHz.) sinusoidal pattern)	-467	467	-523	523
Incidence angle (deg)	48.95	49.15	57.8	58.1
Azimuth Angle (deg) (footprint to footprint variation)	1.25	1.29	1.25	1.29
X Factor(dBm)	-93	-88	-93	-90
Range(km)	1025	1095	1210	1260

Table 2: Statistics of static parameters

Parameter		Pass Node	HH beam Obs. value	VV beam Obs. value
Doppler Frequency (kHz)	*FP-1	D	-29.24	-37.84
		A	51.24	52.22
	FP-70	D	465.05	520.73
		A	466.94	523.57
	FP-140	D	52.32	52.25
		A	-26.89	-36.70
	FP-210	D	-464.07	-520.78
		A	-466.95	-523.05
	FP-280	D	-55.94	-56.16
		A	24.53	33.91
Incidence angle (degree)			49.05	57.96
Azimuth angle (variation footprint to footprint) (degree)			1.26	1.25
X Factor (dBm)		D	-90.49	-92.52
		A	-90.48	-92.40
Range (km)		D	1055.16	1239.74
		A	1055.15	1236.04

*FP is Footprint Number in a scan #D- Descending A- Ascending

3.2 Dynamic parameters

Level-1B Footprint data is made from slices i.e. 9 slices for inner beam and 14 slices of outer beam. The slices are a part of Level-1B data and are observed for each revolution data as these slices contribute in the collocation of footprint sigma-0 for both Level-1B scan mode footprints as well as Level-2A collocated footprints within the cell grid. Slices histograms are observed for sigma-0 at both sea and land for both beams. Peak of the histogram shows that there is less than 1dB variation among the slices for single orbit data. Results are shown in figure 8 for inner beam sea slices histogram (Figure 8 is histogram for inner beam slices (a) over sea; (b) is over land and (c) is histogram peak variation for land and sea).

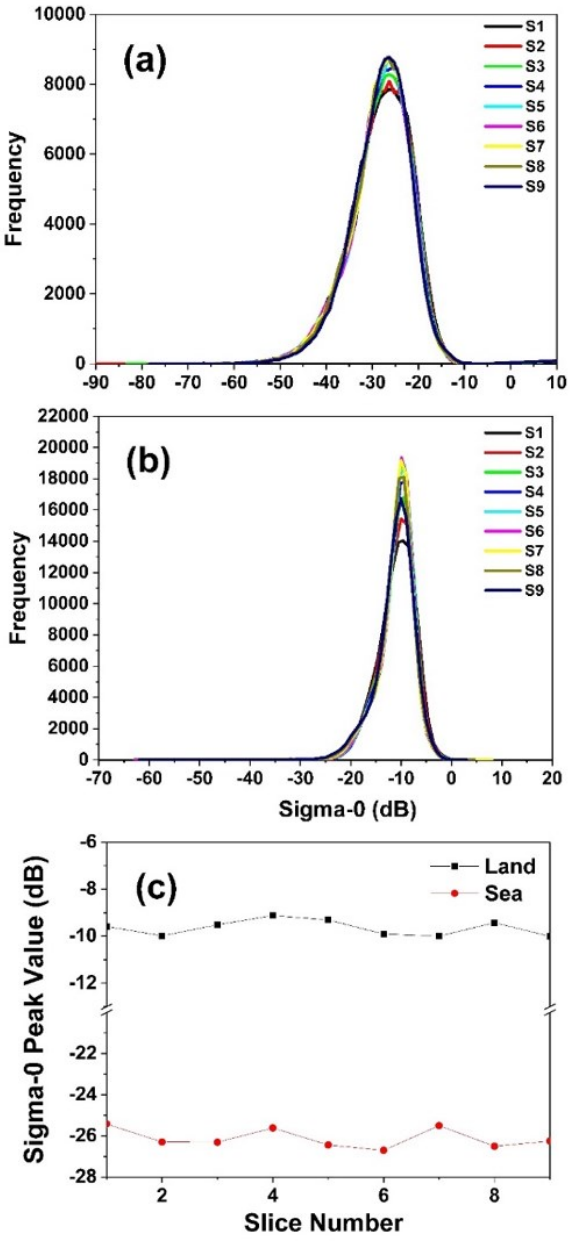

Figure 8: Sample snapshot of slices histogram of inner beam for revolution number 6339 in ascending pass (a) sea; (b) land and (c) histogram peak variation

Similar results are observed at land and sea for outer beam (figure not shown here). This analysis suggests that the SCATSAT-1 processor is picking slices (9 out of 40 in Inner and 14 out of 40 for outer) well within the specifications. As per specifications sigma-0 peak over land lies at -10.5±0.5dB (HH beam) and -11.5 ±0.5dB (VV beam) and for sea sigma-0 peak lies at -26±0.5dB (HH beam) and -23±0.5dB (VV beam).

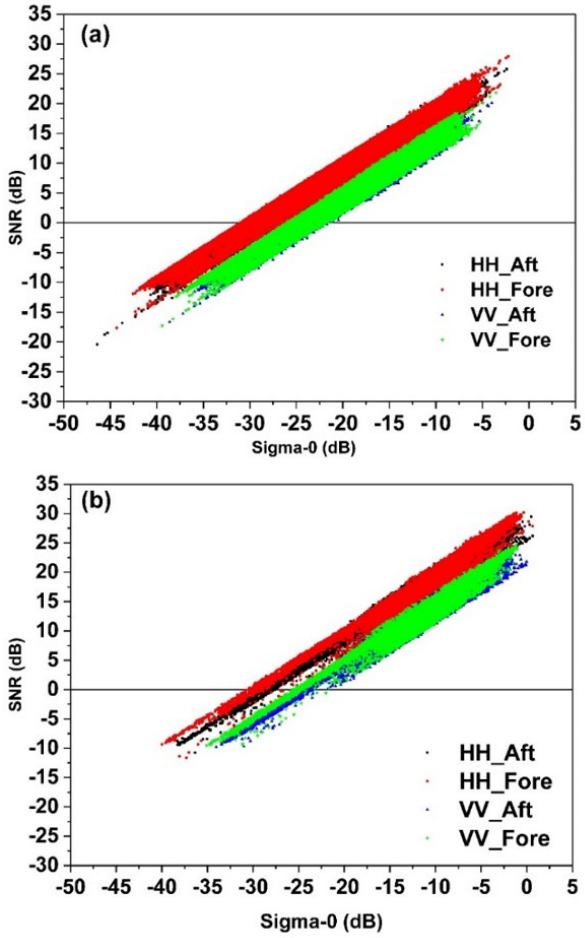

Figure 9: Sigma-0 vs SNR for inner and outer beam over (a) sea (b) land

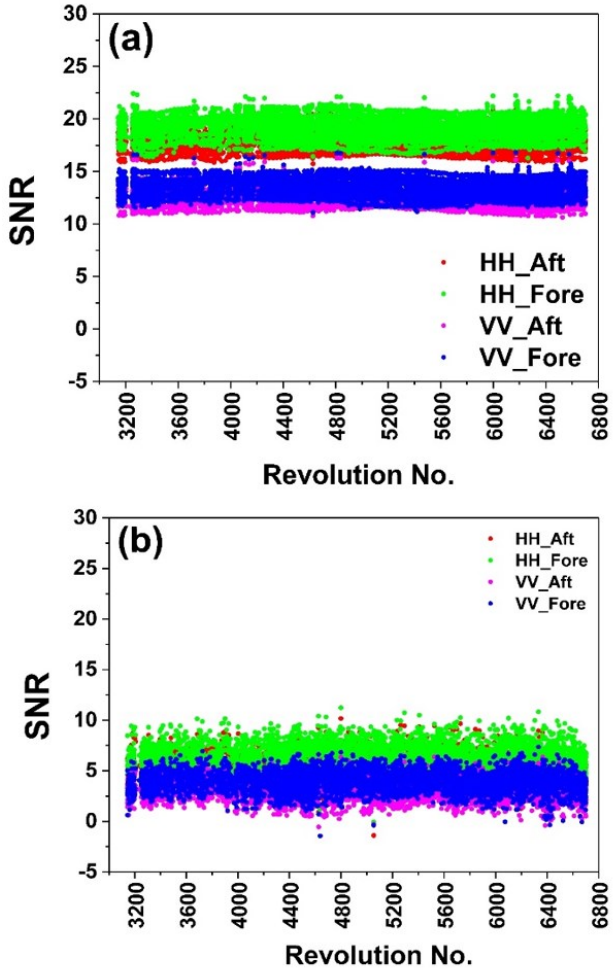

Figure 10: SNR behaviour for (a) land (b) sea

Figure 9 shows the linearity between the Sigma-0 and SNR for the defined range for both the beams. Interpretation based on plots of figure 9(a) over the sea, suggests that for positive SNR of ~25dB(Inner) and ~20dB (outer), sigma-0 reaches to -5dB and on the other side at negative SNR of -10dB sigma-0 covers the range of -40dB for Inner beam and 35 dB for outer beam. Thus, the data under study covers the dynamic range well within the specified dynamic range (+10 to -96dB globally) of sigma-0. Similar behaviour is observed over the land (figure 9 b) with a difference of 5dB over the dynamic range. SNR is further observed as the mean value independently over multiple revolution data and is shown in figure 10a for land and figure 9b for sea. SNR on sea is less than on land (because of the return in Ku band for HH and VV beam from water surface is less than that from land) which is as expected. Over the land, SNR is 5 dB higher for HH w.r.t. VV (figure 10a) and forms pattern over the revolutions data whereas on sea (figure 10b) SNR from both beams (HH and VV) overlap with a difference of 3dB. Also, both plots of figure 10 suggest SNR is 2dB higher in fore look in comparison to aft look over the globe.

Kp is the normalized standard deviation in sigma-0 and tells the quality of data. The low value of kp indicates better sigma-0 value. Figure 11 shows the mean kp variation over multiple revolutions. From plots, kp is nearly 0.1 for land and on sea it varies from 0.1 to 0.5 which is well within the defined specifications (0 to 1) and confirms the high-quality product of SCATSAT-1.

Figure 12 is the typical colour coded sample snap shot of sigma-0 and brightness temperature respectively seen from the global coverage of two days (20st and 21st August 2017) inner beam data. The grid used is 50 km x 50 km for both sigma-0 and BT display. It also supports, that the radiometry acquired by the sensor in the scan mode data is of good quality and the brightness temperature observed over the land, sea, sea-ice matches well with the specifications (Raj Kumar et al., 2011)

The overall time series of sigma-0 and BT are shown in figures 13 and 14 respectively over the global land and sea average. The sigma-0 plot (figure 13a) shows a seasonal pattern in sigma-0 (-21 to -22 dB for VV beam and -24 to -26 dB for HH beam). In the mid of September, a systematic shift of 1 dB is observed which is constant thereafter might be due to greater noise as brightness temperature data (figure 14 a) also suggest that noise is large which is still not significant as per system specifications (as per the specification 10 K variation in BT is within acceptable limits). The figure 13b shows a

constant behaviour of sigma-0 around -11.46 dB and -10.44 for land in HH and VV beam respectively which are well within specifications (discussed earlier). From figure 14(a, b) brightness temperature over the sea is stable and constant except getting down by 15 K in mid-September might be due to increase in noise for both HH and VV beams. Over the land an increase of Brightness temperature by 15K in VV beam is observed whereas in HH beam it is stable and within limits.

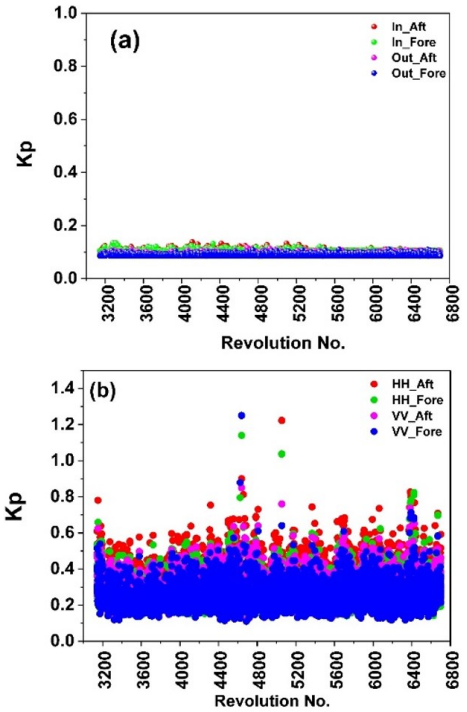

Figure 11: kp variation (a) land (b) sea (in-inner beam (HH), out-outer beam (VV), l-land, s-sea)

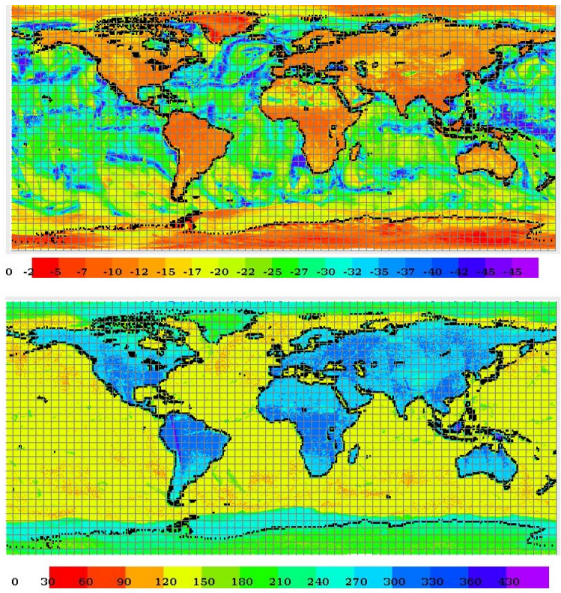

Figure 12: Cycle-wise global (top) sigma-0 and (bottom) brightness temperature (20-21st August 2017)

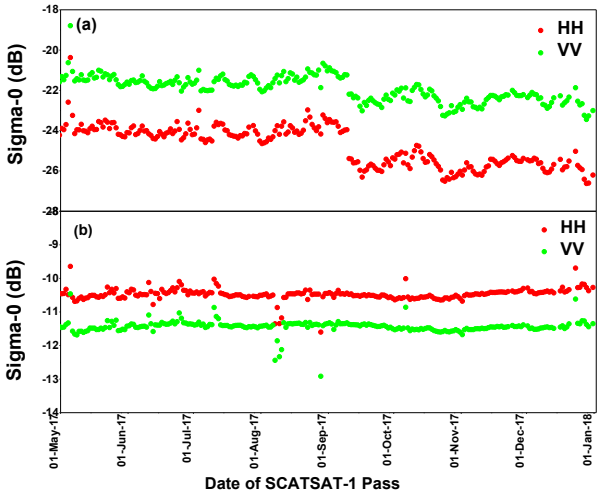

Figure 13: Time series of sigma-0 over (a) sea (b) land for both HHand VV beams

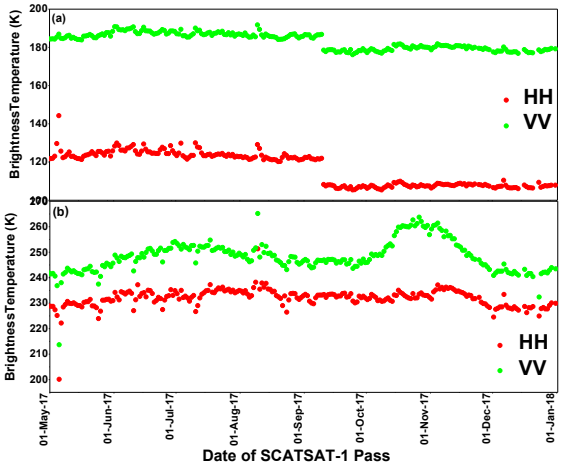

Figure 14: Time series of brightness temperature over (a) sea & (b) land for both HH and VV beams

3.3 Invariant site monitoring

For data calibration/validation, well-known calibrated sites (viz. Amazon rain-forest and Antarctica) are used for monitoring sigma-0 and brightness temperature (Raj Kumar et al., 2011). Figure 15a shows the sigma-0 Ascending pass and in fore/aft scan direction. Figure 15b shows the BT in ascending pass and in fore/aft scan direction over Amazon rain-forest for eight month's data. It is clear that BT is around 275 K over the Amazon rain-forest and is stable.

Detailed statistics (Minimum, maximum, mean and Standard deviation) of sigma-0 are shown in table 3. It shows that sigma-0 accuracy over the Amazon rain-forest is less than 0.25dB which is as expected and accuracy of BT in all categories is less than 12K. Results from trend analysis ensures that parameters are behaving well within the specifications (varies wr.t sites typically within ±0.5dB variation in sigma-0 and ±10K variation in BT) and assures stability and consistency of the system and product quality parameters.

Table 3: Amazon Sigma-0 and BT statistics from May 2017 to December 2017 over Amazon Rainforest

Beam	Node	Scan Direction	Sigma-0 (dB)				Brightness Temperature (K)			
			Mean	Min	Max	Std dev	Mean	Min	Max	Std dev
Inner	#Asc	Aft	-8.38	-8.90	-7.50	0.23	261.2	237.8	279.8	8.6
		Fore	-8.03	-8.55	-7.37	0.24	259.1	240.9	274.9	7.9
	^Des	Aft	-7.99	-8.66	-7.22	0.22	262.9	214.8	278.6	9.2
		Fore	-8.08	-8.68	-7.57	0.18	263.1	240.3	278.9	8.9
Outer	Asc	Aft	-9.42	-10.08	-8.64	0.24	270.7	258.8	286.4	6.3
		Fore	-9.16	-10.01	-8.17	0.30	266.7	252.9	281.6	7.0
	Des	Aft	-9.17	-9.99	-8.16	0.27	278.8	253.7	321.5	12.0
		Fore	-9.32	-9.92	-8.57	0.22	273.6	246.1	304.7	9.8

*Asc= Ascending and ^Dsc=Descending

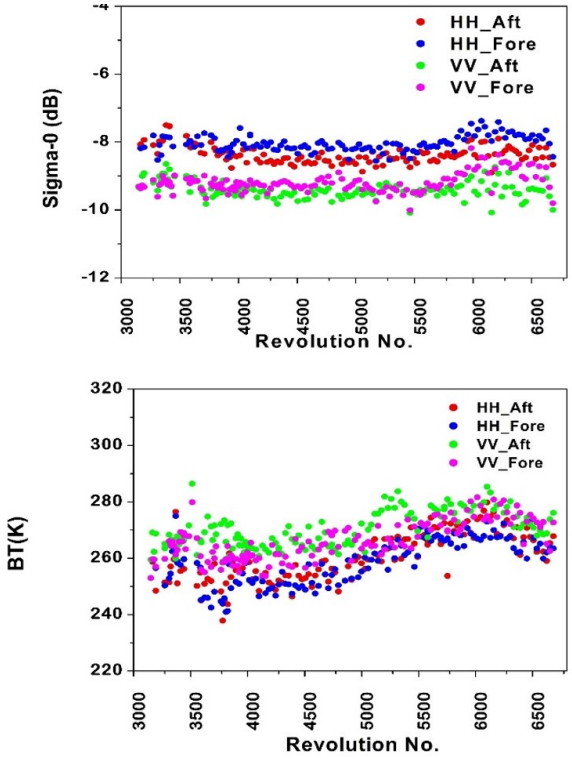

Figure 15: Temporal trend (a) sigma-0(dB) (b) BT for VV and HH beam in ascending pass

4. Conclusions

Data quality of SCATSAT-1 scatterometer scan mode data is discussed. Eight months of data is statistically analysed for monitoring the stability and accuracy of quality parameters. Results for the identified quality metrics show consistency in both fixed geometric parameters as well as dynamic radiometric parameters i.e. sigma-0, BT and SNR as per mission specifications. SNR, kp and sigma-0 are analysed for multiple revolutions data which shows as expected trends. The sigma-0 over the invariant sites is observed and found to be stable in defined range. Over Amazon rainforest, sigma-0 observation has an accuracy better than 0.24 dB in HH beam and 0.25 dB in VV beam. Also, Brightness temperature over the invariant sites is found to be stable with an accuracy better than 10 K suggesting that noise filter on board is stable. The analysis carried out in this paper will aid the end users in further analysis of the wind vector. The analysis clearly shows that SCATSAT-1 data is of very high quality and will be able to provide the climate quality products similar to QuikSCAT.

Acknowledgements

Authors would like to thank Shri D.K. Das, Director-SAC and Shri Debajyoti Dhar, Group Director-Signal and Image Processing Group for their consistent support towards this activity. Authors would like to acknowledge National Remote Sensing Centre data centre of ISRO for the datasets used in this work. Further, Authors would like to thank payload team, data products team and calibration validation team for technical and scientific interactions.

References

https://directory.eoportal.org/web/eoportal/satellite-missions/s/scatsat-1#sensors

https://www.mosdac.gov.in

Maneesha Gupta, Y. P. Desai, B Kartikeyan (2011). Strategy for quality evaluation of OSCAT data, 4th International Congress of Environmental Research (ICER-11), 15-17th Dec. 2011.

OSI-SAF winds Team; "Scatsat-1 wind product User Manual", Version1.3;05/06/2018, EUMETSAT OSISAF

Raj Kumar, S. A. Bhowmick, K. N. Babu, R. Nigam, and A. Sarkar (2011). Relative Calibration Using Natural Terrestrial Targets: A Preparation Towards Oceansat-2 Scatterometer, IEEE Transactions on Geoscience and Remote sensing, 49 (6).

Risien, C.M. and D. B. Chelton (2008). A Global Climatology of Surface Wind and Wind stress fields from eight years of QuikSCAT Data, Journal of Physical Oceanography, 38, 2379-2413.

www.mosdac.gov.in/Scatsat-1-data-products

www.nesdis.noaa.gov/OPPA/indec-scatsat.php

Journal of Geomatics Vol. 13, No. 2, October 2019

Deployment of blood bank information system in Delhi NCT using web mapping application

Anasua Chakraborty*[,1], Kankana Chakraborty[1] and Saurav Sengupta[2]
[1]Symbiosis Institute of Geoinformatics, Pune-411016
[2]Department of Geography, St. Xavier's College, The University of Burdwan, West Bengal
*Email: anasua40chakraborty@gmail.com

(Received: Apr 02, 2019; in final form: Oct 11, 2019)

Abstract: Blood bank is a storehouse for collection of blood, which is gathered by the procedure of donation, primarily for future or in emergency use. But the information regarding the blood storage and availability is of utmost important, otherwise the information unavailable at the right time is of no use. In order to have all the information starting from the blood bank location to its stock inventory, a platform has been built. Focus of this paper is to build a browser-based user-friendly application as a solution to problem, which is faced daily due to shortage of blood thus minimizing the efforts and maximizing the utility. The study aims at the availability of cumulative information of blood availability in the banks and hospitals especially for the administrative personnel at the time of any crisis.

Keywords: Geographic Information System (GIS), ESRI WebApp builder, operational surveillance, real time tracking, Survey123

1. Introduction

A Geographic Information System (GIS) is a browser-based system for storing, capturing, displaying and checking data related to positions on the Earth's surface. GIS relates seemingly unrelated data, which can help individuals and organizations better understand the spatial patterns and relationships. GIS technology is a crucial part of spatial data infrastructure, which has been described by the White House as the technology, policies, standards, human resources, and related activities, which is necessary to acquire, process, distribute, use, maintain, and preserve spatial data. GIS technology desegregates database operations like unparalleled visual imaging and geographical analysis extended by maps with interrogation and statistical analysis (Kim et al., 2018; Mostafa et al., 2014; Kanani et al., 2017).

The GIS in India works on bulk data creation of digital ground survey maps to site mapping, transitions and digital computation, analysis and providing custom made presentations based on survey data of an area. The dimensions of maps differ for each resource, sector, function and element. After collection of data, it is transformed and translated into knowledge. This in turn helps the information seekers to properly plan for the future, manage their resources efficiently, and make critical business decisions to expand the territories of business including health care, logistics, agriculture, oil & gas, telecommunication, public safety etc. (Premasudha et al., 2009; Priya et al., 2014; Kanani et al., 2017).

Considering health care, the methods for improving health by implementation of geospatial technologies has become widespread in many nations (Haynes et al., 2016), but India's adoption of these approaches has been fairly slow. There is no coordination between blood banks and hospitals (Debroy, 2017). Blood Bank Information System plays an integral part, considering the utility of GIS in today's health sector. The idea of creating such an information system was boomed by analyzing the amount of wastage of blood (figure 1) every year in India. The idea is to create a web application with the help of ESRI (Environmental System Research Institute) Webapp Builder, which shall provide a platform to the hospitals and the blood bank management authorities wherein all the blood stock related data (table 1) can be analyzed and updated at the same time.

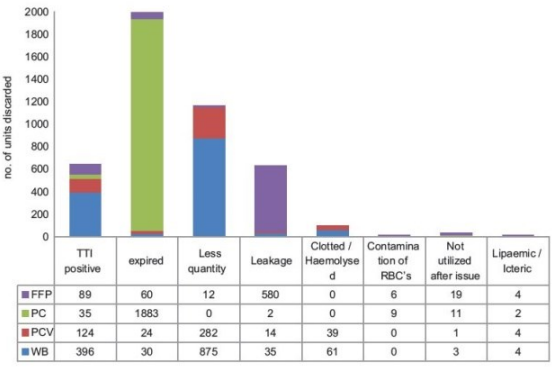

Figure 1: Graph showing blood discard reasons along with units (Source: Global Journal of Transfusion Medicine)

Table 1: Examples of blood use

Automobile Accident	50 units of blood
Heart Surgery	6 units of blood/6 units of platelets
Organ Transplant	40 units of blood/ 30 units of platelets
20 bags of Cryoprecipitate	25 units of fresh frozen plasma
Bone Marrow Plant	120 units of platelets/ 20 units of blood
Burn Victims	20 units of platelets

The platform shall contain information about the blood stock (updated by the blood banks from time to time), hospital data (who will be accessing the data), location of the blood banks (for nearest location identification). Real-

time updating of data is incorporated for continuous tracking and monitoring of blood stock, to have a clear idea about the demand and supply of blood for each group. The application will provide all necessary information to both blood banks and the hospitals at their fingertip.

2. Study area

Delhi, well known as the National Capital Territory of Delhi (NCT), is a city and a union territory of India. Delhi lies in North of India. It borders the Indian states of Haryana on the north, west and south and Uttar Pradesh to the east covering an area of 1,484 square kilometers (573 sq. mi). Being a capital region with its administrative prominence, huge population along with a well-connected transport network, this part has been considered as the area of study (figure 2).

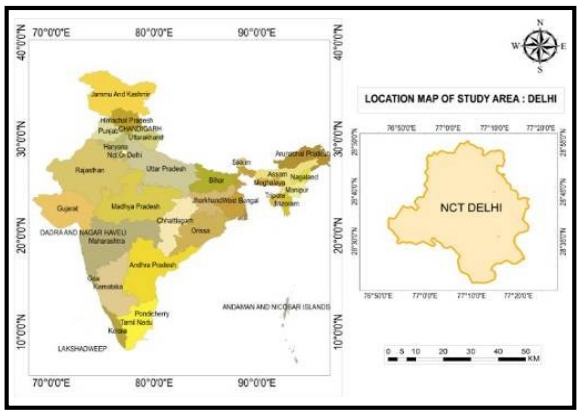

Figure 2: Location map of Delhi NCT

3. Objectives

The main objective of the study is to build an Automated Blood Bank Information system which could act as an operational surveillance system for hospitals and blood banks to optimize the work flow and bridge the gap between information exchanges when it comes to the requirement of blood. However, this system would also:

- Provide location-based blood bank information for easy accessibility.
- Provide stock information regarding individual blood groups.
- Provide a platform to understand the blood stocks, demand, peak time demand, real time updates of data etc. for instant action and one glance information purpose.
- Provide a common data collection method as Mobile Medical App which could be filled by all the blood banks for the information update of different blood groups and instant upload for real time update (Data collection both online and offline).

4. Materials and methodology

4.1 Database preparation

To undergo this study, we have used the following datasets:

- Administrative boundary of Delhi NCT.
- Blood Bank locations.
- Hospital locations along with patient details.
- Amount of blood available for each blood group at particular blood banks.

The blood bank location data was collected by taking the points from Google Earth in a KML (Keyhole Markup Language) format. This was then run through ESRI ArcMap to convert to shape file for further usage. The hospital locational data along with their domain of specialty was collected in the similar manner as that for the blood bank data (KML to shape file). Blood Banks and Hospitals detailed information (Figure 3) was collected from online governmental portal (https://data.gov.in/catalog/blood-bank-directory-national-health-portal; https://data.gov.in/catalog/hospital-directory-national-health-portal).

4.2 Data pre-processing

Pre-processing usually consists of a sequence of operations, the number and order of which is defined by the aim of the research and the type of data collected from various sources. The main steps followed are:

- Cleaning, sorting, filtering and appending of collected data in order to obtain an error free data for better analysis and representation.
- Conversion of generated KML file to shape file.
- Conversion of CSV files to point data and exporting it to shape file using ESRI ArcMap.
- Assigning of projections to each layer.
- Creation of ESRI ArcGIS online account for further accessibility and creating dashboards.

4.3 Data processing

The main focus was on building an application with the help of ESRI ArcGIS Web-App builder which would ease the process of monitoring and analyzing the demand, supply, and wastage of blood for different blood banks as per hospital requirements. After creating the Arc GIS account, the shape files created in Arc Map 10.5 were shared and published as a map package. The published shape files were built through ESRI Web Feature Services for further processing in order to build the web application.

Once the theme is decided, the next step is to configure the widgets of the application. The detailed workflow that has been ingested to provide a detailed insight of the process is shown in figure 4.

The selected theme of the application is displayed on the dashboard with different infographics based on the data for better visualization and analysis. The infographics are selected to show the relation between the different attributes of the data of the Blood Banks which includes pie, count, column, bar graph, line graph and filter.

The next agenda is to build the application in such a way that the user could access the data for information from the provided data. Operation dashboard was created on Arc GIS online which was later on integrated with the Survey123 form in such a way that the data which will be updated by the blood banks would immediately reflect on the dashboard by changing the graphs and counts (Figures 5 &)

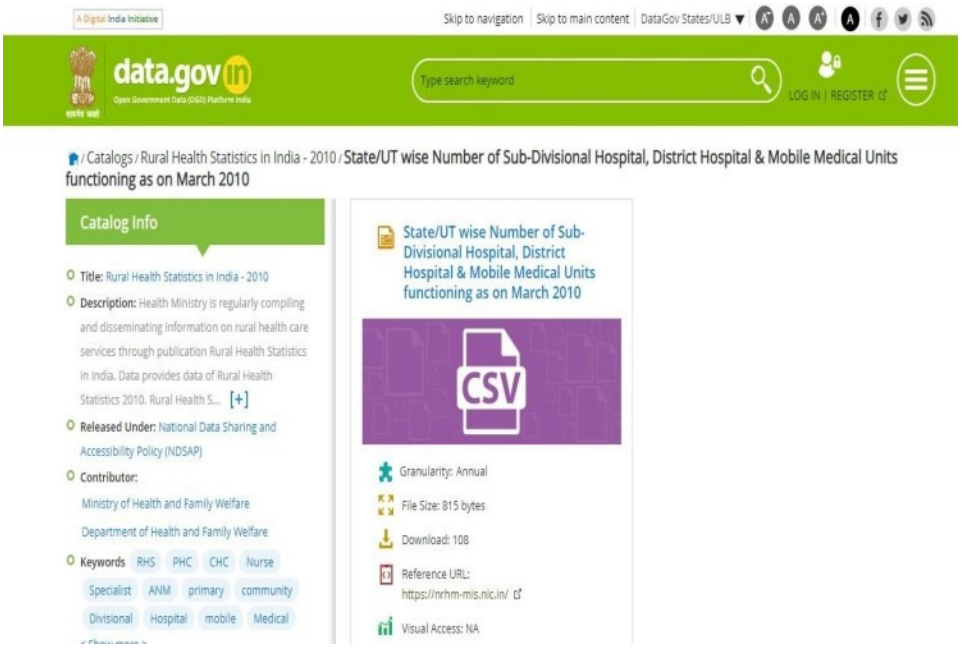

Figure 3: Data collection website

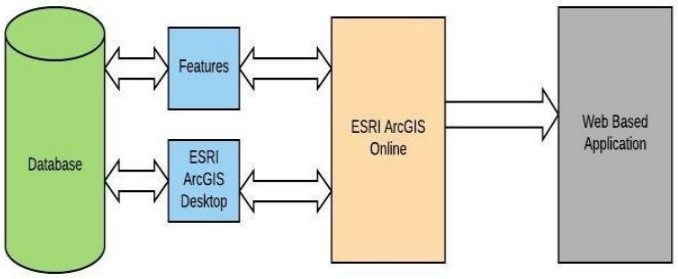

Figure 4: Web GIS architecture

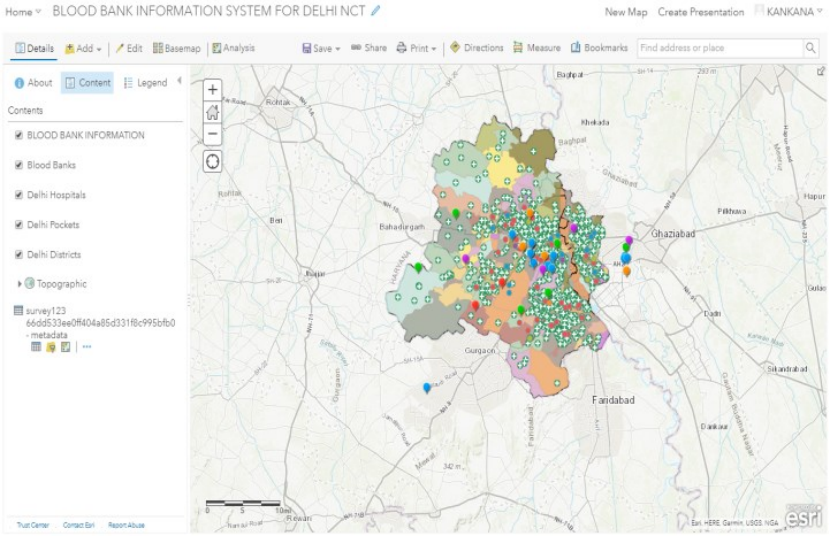

Figure 5: Web Map for Blood Bank Information System

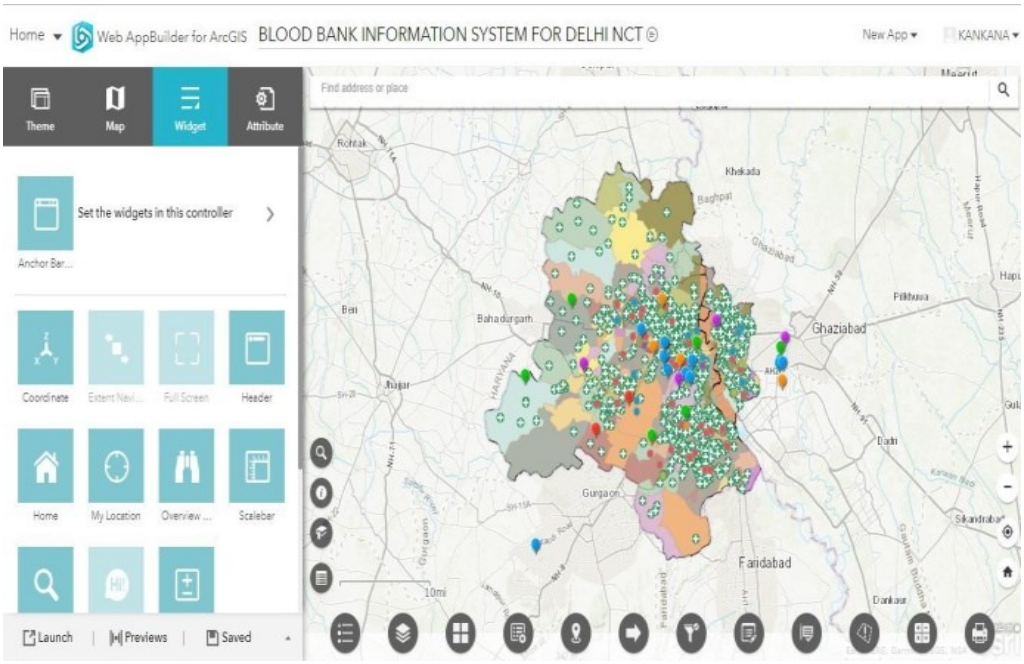

Figure 6: Configuring the widgets in web application

The Survey123 for Arc GIS was built with a motive that the blood bank organizations could fill up the built form with the details of their stock and other organizational details which was further integrated with the operations of the dashboard and web application, which would help in real time updating for a more well-built application.

5. Results and discussions

The application was intended to show the nearest facilities, the summary and analyze a particular situation. The resultant web mapping application and operation dashboard is showing satisfactory results which are intended to be achieved. Developed application can be helpful to mitigate the blood wastage every year. The Survey123 formis also integrated for real time update.

The web application can be accessed by both hospital and blood bank authority where data updating and viewing can be done from both the end as shown in figure 7.

The data was showing a trend in the infographic on the Operations Dashboard. Thus, accomplishing the main aim of this paper which was to build a platform wherein the hospitals and the blood could update their data and henceforth maintain the stocks, immediate requirement, past stocks, nearby facilities. The web application displays the final output along with the configuration which has been applied into it.

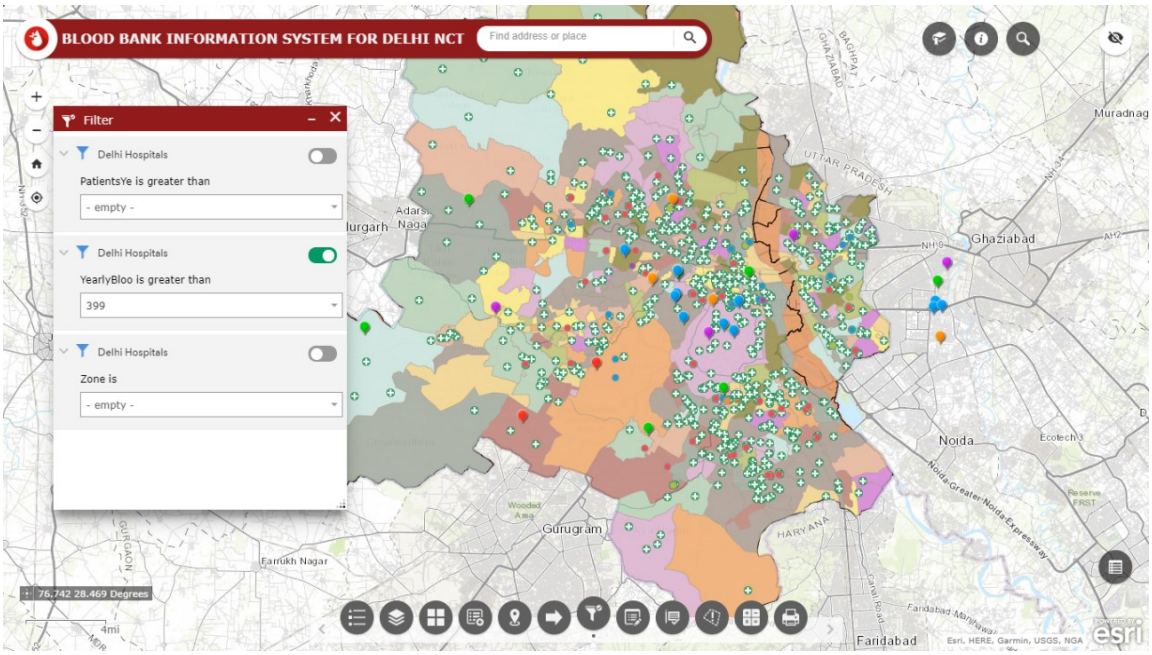

Figure 7: Web application user interface

The web mapping application can be accessed by the hospitals and the blood banks to get a clear idea regarding the information that have been stored by them. The different configured widgets will provide all the possible outcomes that the hospital or blood bank requires for any sort of analysis. The Surveillance Dashboard will show the initial graphical representation of the stored and updated data.

5.1 Blood bank information system

The blood bank information system is built mainly for the hospitals to have a clear picture about the existing information of all the hospitals in Delhi NCT (figure 8).

The web application shows all the information quarterly, its patients or the blood requirements.

The application can be accessed with the following URL: http://esriind-kankana.maps.arcgis.com/apps/webappviewer/index.html?id=a5c5726b4fdd49ad98edac79b0eb1826

5.2 Surveillance dashboard

The Surveillance dashboard is built for the blood banks to keep track or record of their blood stock information (for each blood group) along with license, apheresis etc. The information is collected quarterly. The dashboard shows the real time update of the stock, requirements, location etc. about blood banks (Figure 9).

The application can be accessed with the following URL: https://esriind-kankana.maps.arcgis.com/apps/webappviewer/index.html?id=ae401bcc744f41cc8deee3cb6066b bd8

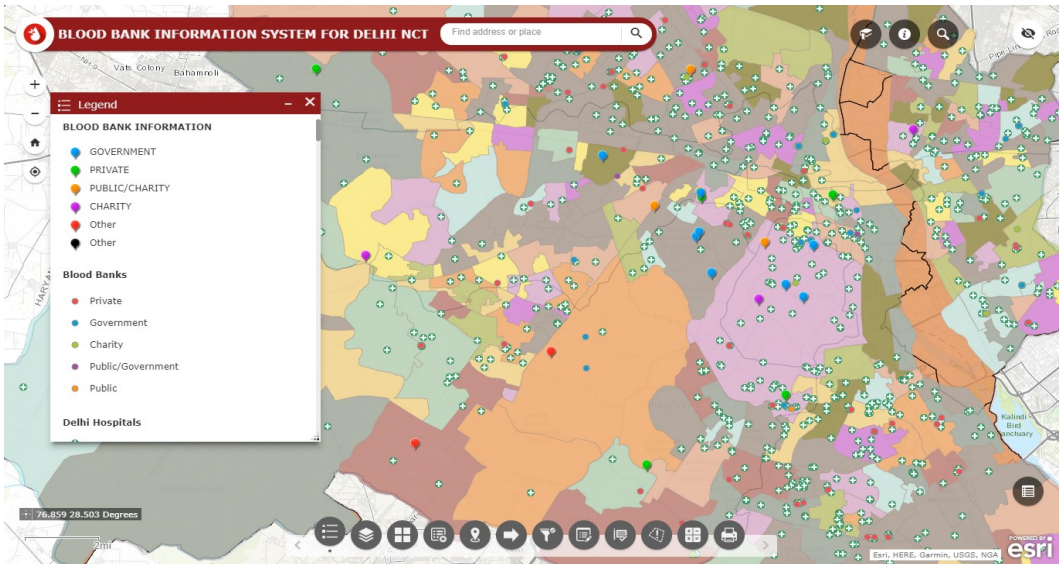

Figure 8: Zoomed view of nearest blood bank facility

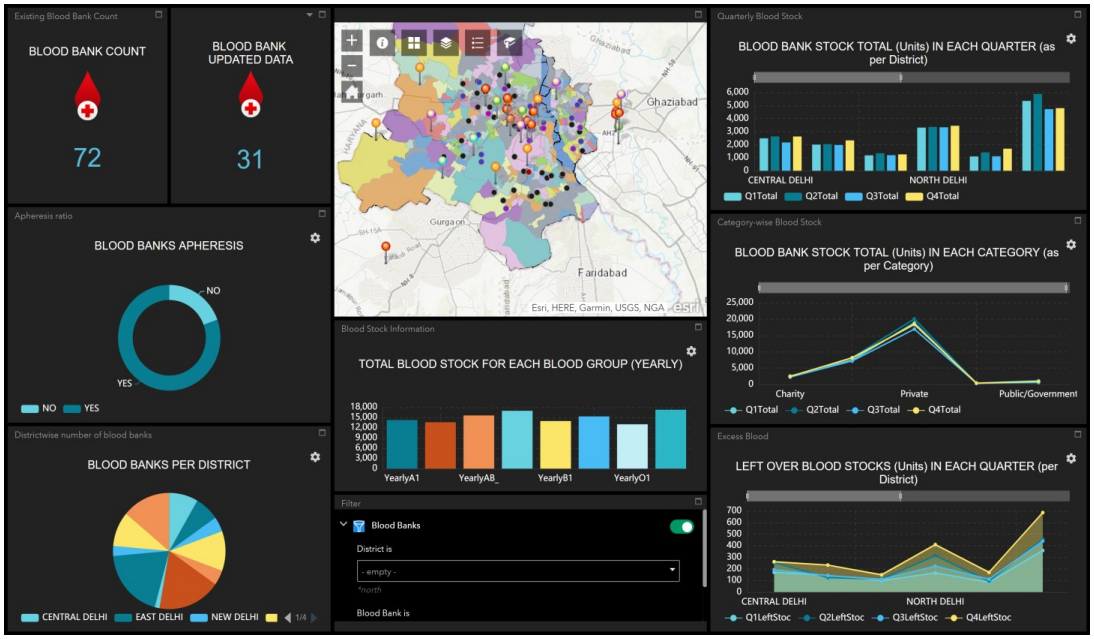

Figure 9: Dashboard view of web application

5.3 Blood bank information form

The blood bank information form was mainly made for collecting data on the fly and updating the same on the dashboard for real time visualization. The Survey123 form is for the blood banks over Delhi NCT to update their stocks, requirements etc. for easy monitoring (figure 10). The form can be accessed and filled using the following URL: https://survey123.arcgis.com/share/66dd533ee0ff404a85d331f8c995bfb0

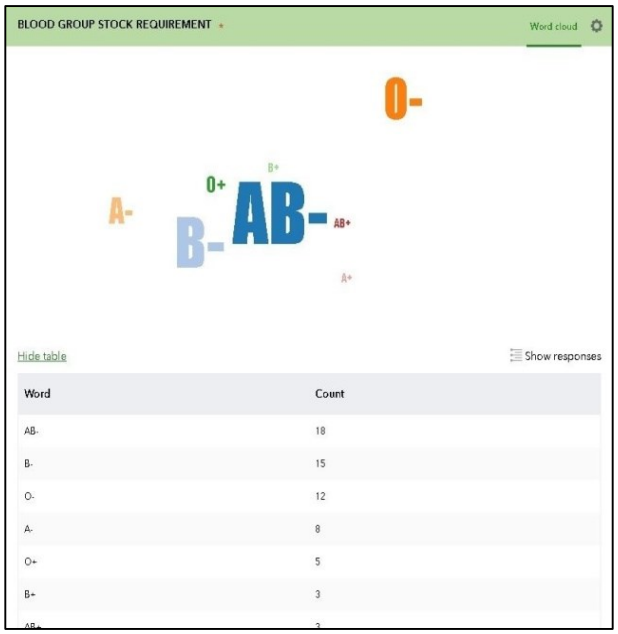

Figure 10: Word cloud in survey 123

6. Conclusions

Blood Bank Information System based on real time information has been developed along with an Operational Surveillance System and Mobile Medical Application. The proposed system facilitates a communication between the blood bank and different hospitals so that the appropriate answers can be received on a single platform. It also integrates the blood stock information for individual blood groups scattered among different blood banks and also the patient's blood group information from different hospitals to eradicate the blood exploitation. The Hospital Authority, Blood Banks and the Blood Bank Management Authority are able to use this Web Application to bridge the communication gap and provide necessary information for maintaining transparency. This reduces time which were usually taken to arrange a particular blood group in emergency situations and to keep a track of the blood availability. The application will help the user to locate the nearest blood banks, obtain information regarding the blood stocks etc. The Dashboard is built with an intension for real time data, updation for tracking, and report generation on blood groups most in demand and difficult to collect, graphical representation for stock as blood group, etc. Survey123 will help in field data collection and integration. It is believed that this will not only facilitate the users with valuable information but will extend its functionality in saving lives of many.

References

Debroy, S. (2017). No coordination between blood banks and hospitals, 6 lakh liters of blood wasted in five years, Available: https://timesofindia.com/india/no-coordination-between-blood-banks-and-hospitals-6-lakhs-liters-of-blood-wasted-in-five-years/articleshow/5833338.cms

Haynes, R., J. Andy, S.Violet and H. Zhao (2006). Validation of travel times to hospital estimated by GIS. International Journal of Health Geographics, doi: 10.1186/1476-072X-5-40.

https://data.gov.in/catalog/blood-bank-directory-national-health-portal

https://data.gov.in/catalog/hospital-directory-national-health-portal

Kanani, A.N., J.H. Vachhani, S.K. Dholakiya, S.B. Upadhyay (2017). Analysis on discard of blood and its products with suggested possible strategies to reduce its occurrence in a blood bank of tertiary care hospital in Western India. Glob J Transfus Med [serial online]. Available from: http://www.gjtmonline.com/text.asp?2017/2/2/130/214292

Kim, Y., Y.J. Byon, and H. Yeo (2018). Enhancing healthcare accessibility measurements using GIS: A case study in Seoul, Korea. PloS one, 13(2), e0193013. doi: 10.1371/journal.pone.0193013.

Mostafa, A., Y. Ahmed and A. Gamal (2014). A framework for a smart social blood donation system based on mobile cloud computing. Health Informatics - An International Journal. 3. 10.5121/hiij.2014.3401.

Premasudha, B. G., S. Swamy, and B.S. Adiga (2009). An application to find spatial distribution of blood donors from blood bank information system. International Journal of Information Technology and Knowledge Management, 2, 401-403.

Priya, P., V. Saranya, S. Shabana and K. Subramani (2014). The optimization of blood donor information and management system by technopedia. International Journal of Innovative Research in Science, Engineering and Technology, 3 (1), 390-395.

Journal of Geomatics Vol. 13, No. 2, October 2019

3D Volumetric change analysis in urban areas

Kriti Rastogi[1], A. P. Prathiba[2] and Gaurav V. Jain[1]
[1]Space Applications Centre, ISRO, Ahmedabad, India
[2]Indian Institute of Technology, Roorkee, India
*Email: kritirastogi@sac.isro.gov.in

(Received: Jan 04 2019; in final form: Oct 11, 2019)

Abstract: Urban planning demands a comprehensive understanding of urban development for efficient designing and expansion of urban areas. The 3- D model of urban area are popular among the urban planners. This study involves the development of 3-D model for part of Ahmedabad city for two time periods, year 2005 and 2015 and analyse volumetric change in urban development in one decade. The Digital Elevation Model (DEM) is generated using CARTOSAT-1 stereo pair data with 2.5 m spatial resolution for year 2005 and 2015. The building footprint is extracted for the study area from very high resolution merged product of CARTOSAT-2 series data using object based image analysis approach. The height is extracted from the generated DEM for year 2005 and 2015. The base height is extracted from the buffered area of 25 m around the buildings to extract the actual building height. The volumetric change in buildings in one decade is calculated by subtracting the building height of 2015 and 2005. The volumetric change in buildings are categorised into three types, i.e. reconstructed, new construction and unchanged built-up. The volumetric change in percentage for new construction, reconstruction and unchanged built-up areas are 4.47, 10.0 and 85.53, respectively.

Keywords: Building footprint, Volumetric change analysis, Stereo-pair data, Object based image analysis

1. Introduction

Urban planning demands a comprehensive understanding of urban development for efficient designing and expansion of urban areas. The effectiveness of planning is majorly contributed by the analysis of urban growth pattern. The 2-D map of urban areas limits the capabilities of visualization of 3-D urban structures. Hence, the 3-D model of urban area becomes increasingly popular among the urban planners. With the increase in populations and less availability of vacant land spaces, the city is rapidly expanding with tall structures. The integrated GIS and 3D volumetric analysis enhances the capabilities of urban planning and management (Haralik et al., 1973).

The 3-D volumetric analysis is beneficial in case of disaster events like flooding, earthquakes and tsunami. They play a vital role in the rescue operations for the development of the strategic planning which helps people to be rescued effectively (Kolbe et al., 2005). Most of the available sources for building 3-D model such as stereo aerial images, airborne LiDAR data, etc. are expensive when required to cover large urban area. The availability of very high resolution satellite data for large urban areas helps to investigate them in a fast and inexpensive manner. (Sharma et al., 2016).

In this study, 3-D model for two time periods for year 2005 and 2015 is generated for the study area and volumetric change analysis in urban area is analysed in one decade. The building footprints were extracted from a very high resolution fused multispectral data of CARTOSAT-2 series using object based image analysis approach. The elevation information is extracted from the digital elevation model generated from CARTOSAT-1 stereo pair data for year 2005 and 2015. The volumetric change from 2005 to 2015 is analysed and is categorised as new construction, reconstruction and unchanged classes.

2. Study area

Ahmedabad is the fifth most populous city of India with population of 55,77,940 as per the census of 2011. It is also the seventh largest metropolitan city of India. The city is geographically located at mean latitude of 23°02'25'' N and longitude 72°57'14'' E. It is major centre for trade and commerce in the western part of India. The city comprises of commercial, residential and educational structures. The study area is one of the sub-urban part of Ahmedabad. It comprises of congested residential and commercial structures within past few years, the development of this area took place during recent times and new high-rise residential buildings, commercial structure and educational institutes were developed. With the massive development, this study area is suitable for studying the horizontal and vertical expansion of the city (Figure 1).

3. Data used

The data used for the study is acquired by Indian Remote Sensing Satellite (IRS) launched by Indian Space Research Organisation (Table 1). CARTOSAT-2 series satellite provide panchromatic and multi-spectral (Red, Green, Blue and NIR) bands with spatial resolution of less than 1 m and 1.56 m, respectively. The merged product of panchromatic and multi-sensor images is used for building footprints extraction. CARTOSAT-1, first Indian Remote sensing satellite capable of providing stereo pair images with aft and fore angles of -5° and 26°, respectively and 2.5 m spatial resolution is used for generating DEM and ortho-rectified images for years 2005 and 2015.

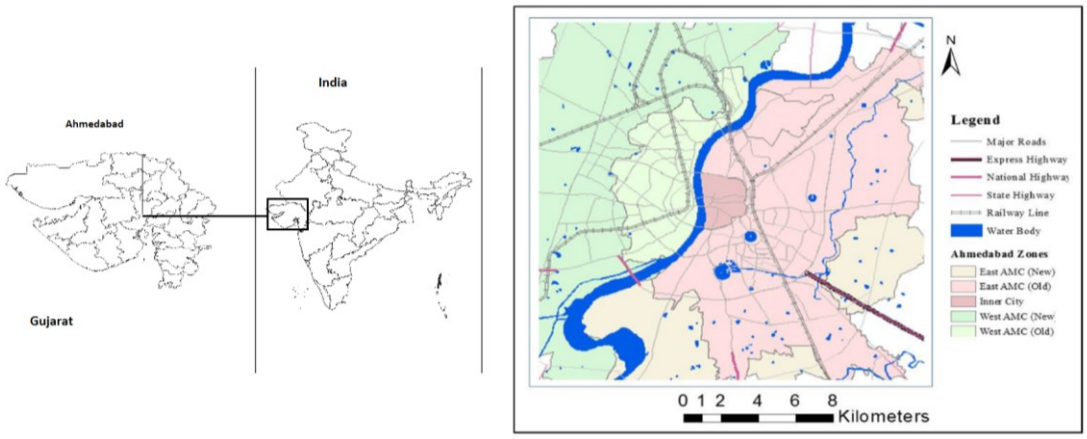

Figure 1: Study area location

Table 1: Specifications of data used

Sr. No.	Satellite	Bands	Spatial Resolution (m)	Date
1.	Cartosat-2	Pan +Multispectral Merged	<1	3/10/2016
3.	Cartosat-1	Stereo pair (Panchromatic)	2.5	24/12/2005
4.	Cartosat-1	Stereo pair (Panchromatic)	2.5	10/10/2015

4. Methodology

4.1 DEM generation

The DEM is generated from Cartosat-1 stereo pairs for year 2005 and 2015 using Leica Photogrammetry Suite (LPS). The DEM was generated with spatial resolution of 5 m. The Rational Function Model (RFM) coefficients, called RPCs, provided along the CARTOSAT data are used in generation of DEM and these are essentially a form of generalized sensor model. These sensor model parameters are terrain independent, have high fitting accuracy and are real time calculated (Tao and Hu, 2002).

4.2 Rational Function Model (RFM)

A sensor model relates 3D object point positions to their corresponding image positions through the collinearity condition. The RFM relates object space coordinates to the image space coordinates. The image pixel coordinates (x, y) are expressed as ratios of polynomials of ground coordinates (X, Y, Z). This method is independent of the sensor resolutions and sensor type and can be used for stereo reconstruction, DEM generation, large scale mapping, ortho-rectification and image registration (Tao, 2001). Generally, they are represented as third order polynomials. Ratios have a forward form as expressed in eq. (1) and eq. (2):

$$x = \frac{P_1(X;Y;Z)}{P_2(X;Y;Z)} \quad (1)$$

$$y = \frac{P_3(X;Y;Z)}{P_4(X;Y;Z)} \quad (2)$$

This equation is called upward RF. Usually, RF model is generated based on a rigorous sensor model. Pi (i =1, 2, 3 and 4) are the polynomial functions**.**

4.3 Data merging

In this study, panchromatic and multi-spectral bands (Red, Green, Blue and NIR) of CARTOSAT-2 are merged to produce the multispectral output with less than one meter using Brovey Transformation. Brovey transformation normalizes the colours of the image, the fused image retains its colour information. The fused image has clear edges, contour which helps to extract feature boundary, texture and ground feature information. (Rong, 2015). The generated image is georeferenced with ortho-rectified image of year 2015. The georeferenced image is used for the classification of building footprint using object based image classification (Figure 2).

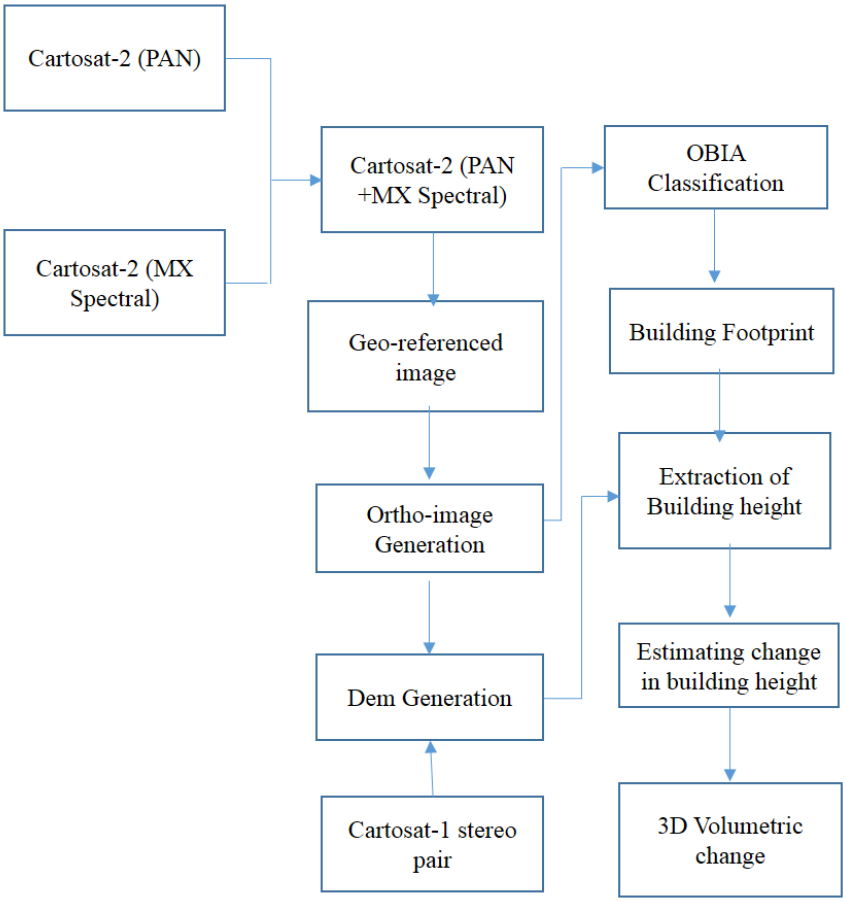

Figure 2: Methodology for volumetric change analysis

4.4 Object based classification

Object based image analysis (OBIA) classifies the images into meaningful group of pixels with homogeneous spectra. The classification of these objects can be done on the bases of its spectral, textural, contextual properties. In object based image classification, instead of classifying the individual pixels. The image is segmented to form image objects. Multi-resolution image segmentation is used to segment the image. This segmentation algorithm consecutively merges the pixels and existing objects. It is a bottom-up algorithm with an optimization approach that for the given number of image objects it minimizes the average heterogeneity and maximizes their respective homogeneity. The scale parameter determines the maximum allowed heterogeneity for the resulting objects. It denotes the size of the object, larger the size of the image object, higher the value of shape parameter. The smoothness and compactness parameter optimizes the resulting image object in regards to smooth borders and overall compactness within shape criteria respectively. For this study, the scale parameter of 15 is used and colour and shape of 0.7 and 0.3, respectively and smoothness and compactness are 0.5 each. Standard nearest neighbour algorithm is used for classify buildings with brightness feature and Gray level co-occurrence matrix (GLCM) homogeneity to classify objects in two types of buildings, i.e. brighter buildings and darker buildings. The mean brightness of an object is computed as in eq. (3):

$$c_k = \frac{1}{s_x \times s_y} \sum_{(x,y)} c(x,y)_k \quad (3)$$

where, c_k is the pixel intensity, s_x number of pixels in the x-direction, s_y number of pixels in the y-direction. The GLCM homogeneity of an object is computed as in eq. (4):

$$H = \sum_{i=1}^{Ng} \sum_{j=1}^{Ng} \frac{p(i,j)}{1+(i-j)^2} \quad (4)$$

where, $p(i,j)$ is the $(i,j)^{th}$ entry of the normalized GLCM, as given by eq. (5):

$$p(i,j) = \frac{P(i,j)}{\sum_{i,j} P(i,j)}, \quad (5)$$

where, $P(i,j)$ is the computed GLCM, N_g is the total number of grey levels in the image.

When calculating the GLCM, the pixels within the object are represented in the form of matrix, with pixel value and neighbouring pixel value as coordinates. The value of the matrix is a normalized number of pair occurrences (number of occurrences ÷ number of all pairs). Therefore, GLCM matrix values are always within the range [0, 1]. The GLCM homogeneity measures the smoothness of the grey level distribution of the image and it is inversely correlated with the contrast within the object, smaller the contrast larger the homogeneity within the object. This measure is used since the object contains nearly similar size having interior homogeneity (Flanders et al., 2003).

So, higher value of GLCM indicated the building objects. The objects are then classified to a class using the membership function. (Myint et al., 2011). The membership function determines the feature characteristics, which determines that the image objects belongs to a particular class or not by defining rule sets.

4.5 Building height extraction

The extracted building footprints using object based image analysis is used to evaluate the height information from the stereoscopic CARTOSAT DEM. Building footprints were overlaid on the DEM and the median value of the elevation inside the footprint were extracted using the zonal statistics in the GIS environment by selecting the mean parameter (Figure 3). To estimate the building height, the base value of the bottom of the building is to be computed as shown in figure 4. To compute the lower elevation of the building buffer of 25 m around the building were generated and the minimum value in the buffer is considered as ground elevation. The buffered region is the surrounding area which may represent the ground or surrounding roads or any other ground location representing ground elevation. The difference between the base elevation and average elevation of building represents the height of the building. The building height for 2005 and 2015 were extracted and the change in the height of building is evaluated by subtracting the height obtained from 2015 building footprint to 2005.

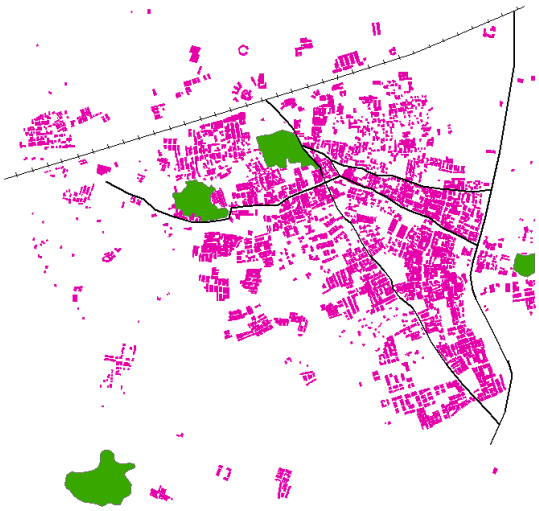

Figure 3: Building footprints extracted

4.6 Accuracy assessment

The accuracy assessment of change in building height was conducted on the sample of 28 randomly selected building in the study area. It was found that most of the buildings heights are identified correctly as shown in figure 6. Since the ground truth is done in 2018, most of the under constructed buildings are fully constructed, so maximum building selected for ground truth were old building and few new buildings. Photographs of two buildings are shown in figure 7.

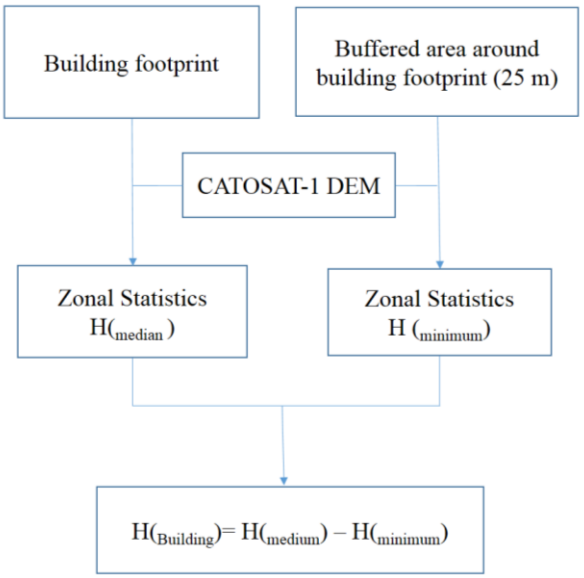

Figure 4: Methodology for building height extraction

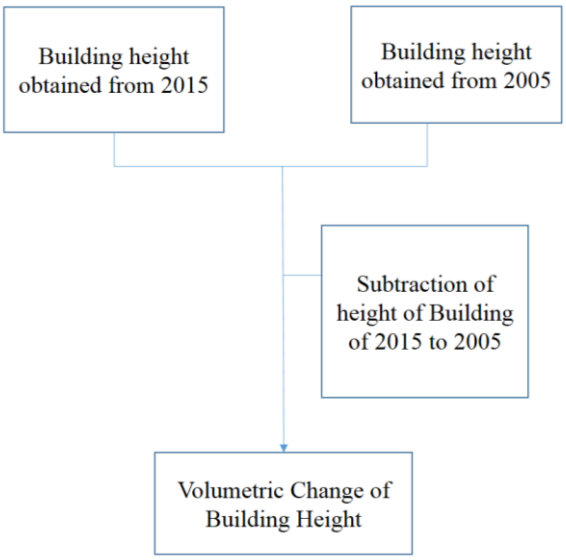

Figure 5: Volumetric change of building from year 2015 to 2005

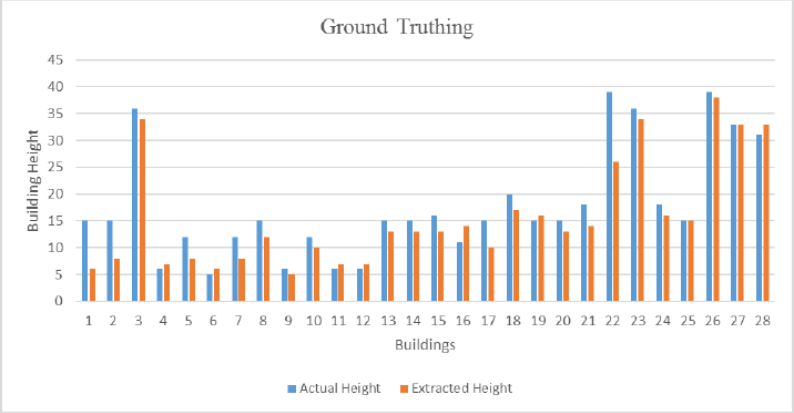

Figure 6: Variations in extracted and actual height

Figure 7: Photographs of buildings

5. Results and discussion

The 3-D volumetric change analysis of study area is carried out using CARTOSAT- 1 stereo pair data and CARTOSAT -2 series data shown in figure 5. The DEM model accuracy of the study area for year 2005 in Easting, Northing and Elevation were observed as 2.61 m, 2.69 m and 1.54 m, respectively. Similarly, the model accuracies for year 2015 were observed as 1.28 m, 0.96 m and 1 m, Easting, Northing and Elevation, respectively. The DEM of 2005 and 2015 year is shown in figure 8. The building foot print were extracted and congested slum area were masked as shown in figure 3. The building elevations were estimated by the median elevation value within the object. The elevation information of the building footprint is added and the building footprint were overlaid on DEMs. The 3-D model of the study area for year 2005 and 2015 is shown in figures 9 and 10, respectively. The volumetric change of urban areas is classified into three types: new construction, reconstruction and unchanged built-up area. The volumetric change in percentage for new construction, reconstruction and unchanged built-up area are 18.3, 7.8 and 73.9, respectively. The built-up areas change and volume change are shown in table 2. The volumetric change for buildings with heights less than 5 m, between 5-10 m, 10-20 m and 20-30 m and buildings with height more than 30 m is evaluated. There is volumetric change of 4.75% for buildings less than 5 m in height, 28.52% for 5-10 m, 60.5% for 10-20 m and 5.2% for 20-30 m and 1.72% for buildings with 30 m and above as shown in Table 3. The maximum volumetric change is observed in buildings with height between 10-20 m, this indicates that the highest development of medium rise buildings took place from 2005 to 2015. These buildings could be residential houses such as bungalows, apartments and educational institutes. Since the development of high rise buildings is observed in past few years, resulting the growth of buildings in vertical direction. The 2-D urban built-up change analysis can only infer the land use/ land cover change, but it limits the capability for analysing the high rise buildings. Since, 2-D mapping of urban area infers only about the area occupied by the urban built-up but 3-D model gives the additional information of the number of floors. The floor-wise information can further help for evaluating the floor area ratio (FAR). Higher the value of FAR, denser the area to live in sharing the common resources such as electricity, water supply, elevators, etc. The resource allocation problem can be solved through this information.

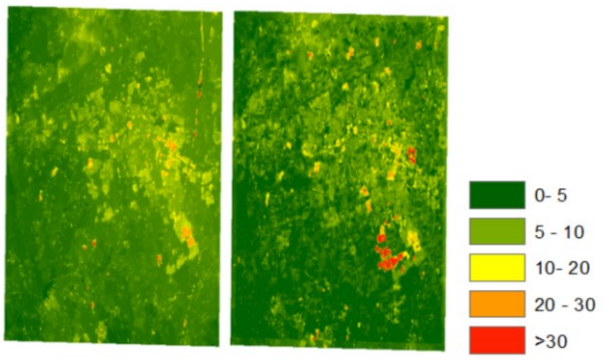

Figure 8: DEM for year (a) 2005 and (b) 2015

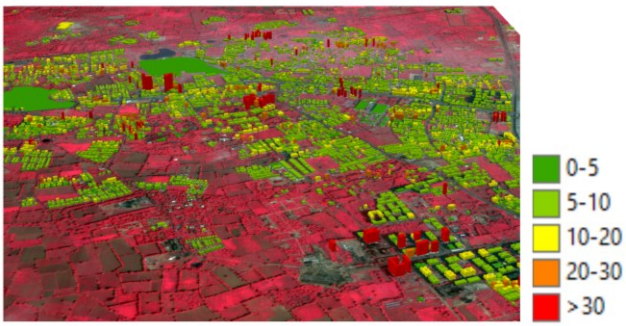

Figure 9: Building height extracted for 2005

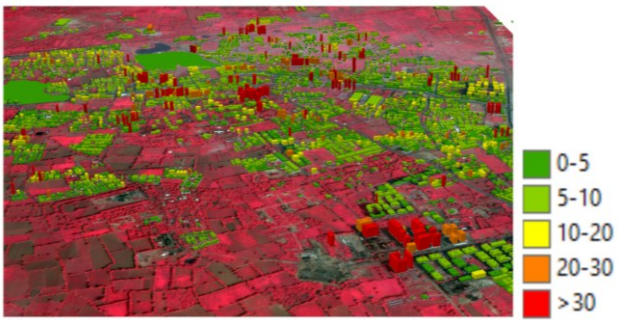

Figure 10: Building height extracted for 2015

Table 2: Built-up area change and volume change from 2005 to 2015

Building Type	Area change (hectare)	Area change (%)	Volume Change (%)
Newly constructed Building area	47.35	10	18.3
Reconstructed Building Area	21.17	4.47	7.8
Unchanged Building Area	405.05	85.53	73.9

Table 3: Volumetric change as per building height from 2005 to 2015

Building Type (Height in meter)	Volume Change (%)
<5	4.75
5-10	28.52
10-20	60.5
20-30	5.2
>30	1.72

6. Conclusions

This study highlights the significance of 3D model generation employing photogrammetric techniques. Building footprint were extracted using object based semi-automatic techniques, using the merged product of very high resolution satellite imagery. Through this study the volumetric change in urban areas is calculated in one decade from 2005 to 2015.The significant development of medium rise buildings were observed. Since the development of high rise buildings is observed in past few years, resulting of growth of buildings in vertical direction. The 2-D urban built-up change analysis can only infer the land use/ land cover change, but it limits the capability for analysing the high rise buildings. The study for urban built-up in 2-D is not sufficient for solving the urban modelling, with problems related to resource allocation. In future, the study of volumetric change analysis using FAR is planned to conduct for resource allocation problem.

Acknowledgements

The author would like to thank Shri D.K. Das, Director, Space Applications Centre (SAC), Ahmedabad for all the support and guidance during the course of the study. We would like to express our sincere gratitude to Dr. Raj Kumar, Shri Shashikant A. Sharma and Dr. Markand Oza for their valuable inputs.

References

Flanders, D., M. Hall-Beyer and J. Pereverzoff (2003). Preliminary evaluation of eCognition object-based software for cut block delineation and feature extraction. Canadian Journal of Remote Sensing, 29(4), 441–452.

Haralick, R.M., K. Shanmugan and I. Dinstein (1973). Textural Features for Image Classification. IEEE Transactions on Systems, Man and Cybernetics, SMC-3(6), 610–621.

Kolbe, T. H., G. Gröger and L. Plümer (2005). CityGML-Interoperable Access to 3D City Models. International Symposium on Geo-Informationon Disaster Management, Delft, the Netherlands, Springer.

Myint, S. W., P. Gober, A. Brazel, S. Grossman-Clarke and Q. Weng (2011). Per-pixel vs. object-based classification of urban land coverextraction using high spatial resolution imagery. Remote Sensing of Environment doi:10.1016/j.rse.2010.12.017.

Rong, C. (2015). The analysis of image fusion on improved Brovery Transform. International Industrial

Informatics and Computer Engineering Conference (IIICEC)

Sharma, S.A., R. Agrawal and P. Jayaprasad (2016). Indian Soc. Remote Sens. 44:187 https://doi.org/10.10007/s12524-015-0478-9

Tao, C. V. and Y. Hu (2002). Updating solutions of the Rational Function Model using additional control information. Photogrammetric Engineering & Remote Sensing, 68(7), 715–723.

Tao, C.V. (2001). A Comprehensive Study of the Rational Function Model for Photogrammetric Processing, PE&RS 67 (12), 1347-1357. http://www.geoict.yorku.ca/project/rationalmapper/pers2001_rfm.pdf

Journal of Geomatics Vol. 13, No. 2, October 2019

Carbon stock assessment in different land use sectors of Ziro valley, Arunachal Pradesh using geospatial approach

Bordoloi R*,[1], Das B[1], Yam G[2], Deka S[1], Tripathi OP[1]
[1]Department of Forestry, NERIST (Deemed to be University) Arunachal Pradesh
[2]Department of Zoology, Rajiv Gandhi University, Rono Hills, Arunachal Pradesh
*Email: ritashree.100@gmail.com

(Received: Jan 05 2018; in final form: Oct 11, 2019)

Abstract: Land use change particularly vegetation change is considered a major factor in reshaping the distribution of carbon stocks. The rapid changes in prevailing land use types tends to reduce forest cover thereby reducing the potential of carbon capture and storage. The study aims to calculate the amount of carbon stock in dissimilar land use of Ziro Valley in Arunachal Pradesh. Altogether 24 (0.1ha each) permanent plots were established under different land use viz; mixed forests, pine forests and agricultural land. To study the tree biomass and carbon under selected landuse, non-destructive biomass sampling approach was used. A total 102 species were recorded during the sampling. Species such as *Pinus wallichiana, Castonopsis indica, C. hystrics, Rhododendron hodgsonii, Elaeocarpus rugosus, Quercus myrsinifolia* were among the most frequent species. The stand density ranges from 440 to 770 stems/ha in the forest area. Species-specific volume equations were used to calculate the above ground biomass (AGB). The AGB recorded from the mixed forests ranged from 140.55 t/ha to 316.18 t/ha and in pine forests it was recorded 102.04 to 184.46 t/ha. The AGB recorded at shrub layer in the mixed forests varied from 4.71 to 7.29 t/ha and it was 5.38 to 13.46 t/ha in pine forests. The total carbon calculated for the mixed forests including soil organic carbon (SOC) was 131.35 tonnes /ha to 309.12 t/ha and it was recorded 129.66 t/ha to 203.02 t/ha in pine forests. The total soil carbon recorded in the agricultural field ranges from 11.53 t /ha to 61.45 t /ha. The present study reveals how the conversion of forest in to agriculture land will minimize the carbon capture potential of the forest land use. The different satellite data based modelling approach was also applied in this study to predict overall carbon stock of the study area.

Keywords: Carbon, Land use, Vegetation, Biomass, Pine forest, mixed forest.

1. Introduction

Terrestrial ecosystems are the storehouse of carbon reserved in the form of living biomass, litter, humus and soil organic matter, play a significant role in nutrient cycling including carbon cycle. Spatially and temporally variant carbon sources and sinks were also seen in Indian terrestrial ecosystem due to its diverse climate system; diversified by various land use distribution and other management practices. In terrestrial ecosystems, the carbon uptake takes place in both vegetation and soils. Soil contains about 75% of the global carbon and plays a vital role not only in crop production but also in managing carbon concentration in atmosphere (Schlesinger, 1999). Forest vegetation is important component of land cover and plays important role in carbon dynamics. The diverse structural composition of the forests, and other biotic disturbances and extractions of the trees contributes significantly in carbon cycle thereby shaping Global carbon resources (Bhat and Ravindranath, 2011). Land use changes tend to immediately bring disturbances in soil and ambient environment. The annual carbon fluxes to the atmosphere from land cover alterations aids in defining the global carbon budget (Le Quere et al., 2015) and offers the prospective to land administration in understanding the removal of carbon from atmosphere (Houghton et al., 2015). Arneth et al. (2017) reported historical CO_2 emissions from the terrestrial ecosystem resulted from land use changes and regarded to be perhaps larger than that assumed. Quantification of carbon stocks is very complex and in order to understand the complexity of the carbon cycle and its linkages, estimations are done through ground truth approach and carbon dynamics simulation through geospatial techniques. Remotely sensed data coupled with geospatial approaches plays a noteworthy role in present scenario in mapping and monitoring of land cover in shorter time span as compared to ground based approach (Jensen, 1986; Treitz and Rogan, 2004). Remote sensing images have revealed high correlation between spectral bands and vegetation which is in general the most important for estimation of above ground biomass (AGB) for large area (Nelson et al., 2000; Foody et al., 2003). The above technology is also capable in collecting data for areas which cannot be accessed due to undulating topography and other site variability. Keeping in mind the limited empirical analysis of land use changes in the context of major land cover C dynamics in the state of Arunachal Pradesh, the proposed objectives was carried out to calculate carbon stocks in major land use i.e., mixed forests, pine forests and agricultural land in the Ziro valley.

2. Study area

The Ziro valley is situated in Lower Subansiri district of Arunachal Pradesh (93º45´35.54´´ to 94º01´01.83´´ E longitudes and 27º25´25.36´´ to 27º38´22.8´´ N latitudes) having altitudinal range of 1,524 to 2,900 m asl. The Lower Subansiri district is bounded by Kurung Kumey and Upper Subansiri districts in the North, in the East by West Siang and Upper Subansiri districts, and Papum Pare district and the state of Assam to the South (Figure 1). The Ziro valley is frequently called as the Apatani plateau. The geographical coverage of study area is 3,460 km^2 of which about 33 km^2 areas is under agricultural lands and remaining area is either under forest cover, plantations or settlement

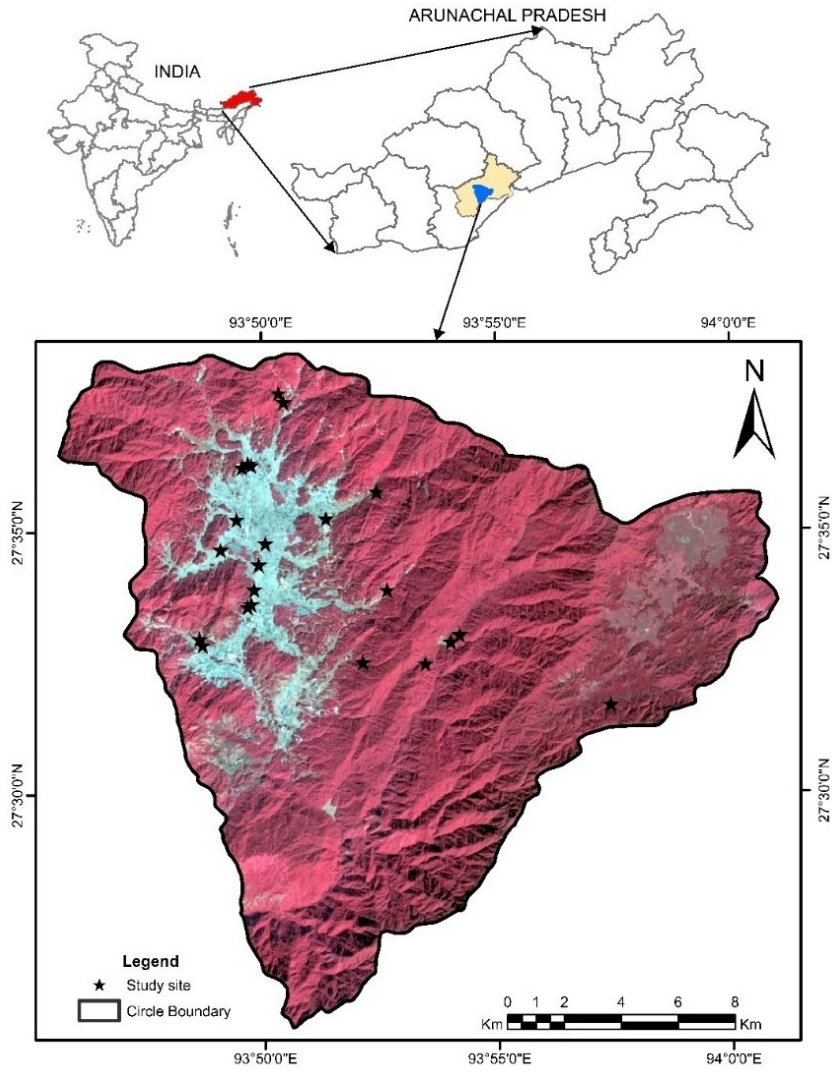

Figure 1: Location map of the study area

The area experiences warm subtropical to temperate climate. The Ziro valley experiences four seasons in a year i.e., cool winter, pre-monsoon, monsoon and post-monsoon seasons. Least temperature is recorded amid December and January and greater temperature amid summer in the July and August (Figure 2). The normal yearly precipitation of the study area for the year 2017 was recorded with low (5.76 mm) to high (496.51 mm) precipitation amid the May-July. The relative humidity remains high 78.16 % throughout the year, with the exception of winters when it slightly goes down (Figure. 2). The LULC map of the Ziro valley was prepared using LANDSAT OLI, 2017 satellite data and classified map is presented (Figure 3). The physiography of the study area had supported the rich vegetation having broad variety of forest resources.

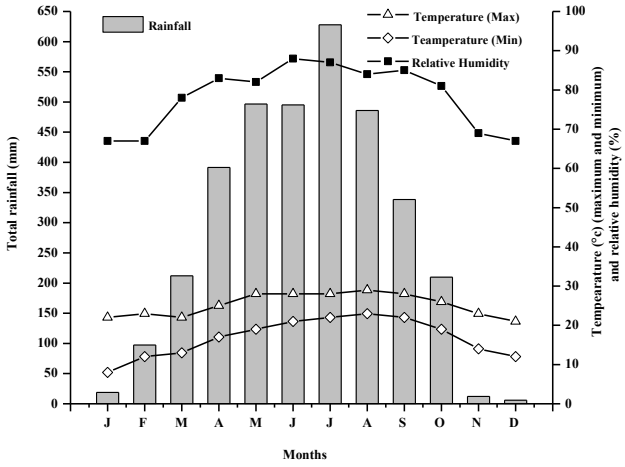

Figure 2: Climatogram of the study area

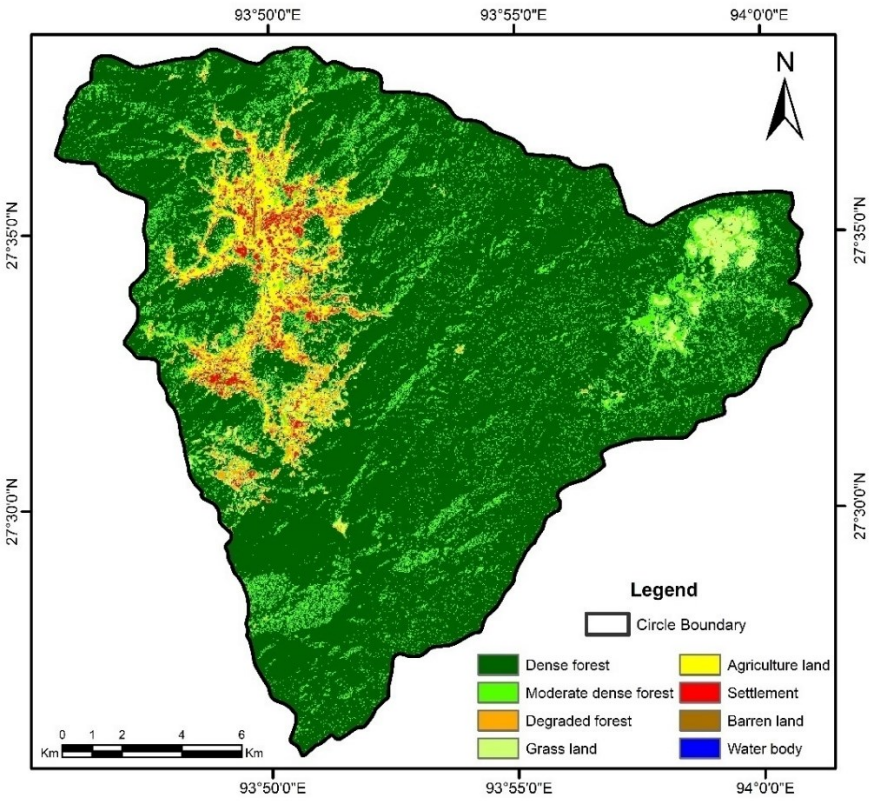

Figure 3: Land use land cover map of the study area

3. Data used and methodology

To measure the biomass, plots of 30m x 30m were sampled randomly from selected land cover and land use. The number of plots selected for all landuse types were primarily depending on the distributions/coverage and the variability in the carbon content in account. For the major land use, mixed forests, pine forests and agricultural lands were selected. The individual trees per ha, basal area and biomass (Mg/ha) were computed based on the sampled data. The AGB was estimated using volume equation (Appendix-I) of Forest Survey of India (FSI, 1996). The biomass of the under-storey (diameter less than 10 cm) were analysed in the sub plots of 5 m × 5m following NRSC-ISRO field manual and herb species were calculated using harvest methods (fresh weight basis) in sampled plots of 1m x1m within the nested plot of 30 m × 30 m. It was assumed that the above ground components have 55 % of Carbon (Mac Dicken, 1997). Random samples of soil from each 30m x 30m plot were collected in replicates. The soils were sampled to a depth of 45 cm and separated into different layers i.e., 0-15, 15-30 and 30-45 cm during the soil sample collection. Soil bulk density was measured using soil corer method as described by Anderson and Ingram (1993). Below ground biomass was calculated considering factor 0.29 of the AGB (IPCC 2005). Soil organic carbon was determined using the Walkley and Black (1934) method. The SOC content was calculated for bulk density and summed to estimate total SOC content.

3.1 Remote sensed data

Remote sensing permits to study the possessions and procedures of land uses and their temporal variability at different dimensions (Prince and Goward, 1995; Running et al*.,* 2000). The Landsat OLI image (5 Dec, 2017; Path 135, Row 41) of the study area was collected to calculate various vegetation indices. The collected initial satellite data for each OLI band were radiometrically calibrated to top of atmosphere surface reflectance. Further, processing of images involved several image processing techniques such as geometric correction, mosaicking and extraction of study area. Radiometric correction of each band was done through ERDAS imagine 9.1 following LANDSAT 8 user handbook. After radiometric correction all the images were re-projected to Universal Transverse Projection system followed by delineation of study area. Land use and land cover map was prepared using unsupervised classification through ERDAS imagine 9.1.

DN to Radiance Conversion

Images are processed in units of absolute radiance using 32-bit floating point calculations. These values are then converted to 16-bit integer values in the finished level 1 product. These values can then be converted to spectral radiance using the radiance scaling factors provided in the metadata file:

$$L\lambda = M_L * Qcal + A_L$$

Where: $L\lambda$ = Spectral radiance (W/(m2 * sr * μm)), M_L = Radiance multiplicative scaling factor for the band , A_L = Radiance additive scaling factor for the band , Qcal = Level 1 pixel value in DN.

Table 1: Vegetation indices used in current study

Vegetation Indices	Expression	Author
NDVI	$\text{NDVI} = \frac{\text{NIR} - \text{R}}{\text{NIR} + \text{R}}$	Rouse et al. (1974)
TVI	$\text{TVI} = \sqrt{\frac{NIR - R}{NIR + R}} + 0.5$	Deering et al. (1975)
SAVI	$\text{SAVI} = \frac{\text{NIR} - \text{R}}{\text{NIR} + \text{R} + \text{L}}(1 + \text{L})$	Huete (1988)

Top of Atmosphere Reflectance

Similar to the conversion to radiance, the 16-bit integer values in the level 1 product can also be converted to Top of Atmosphere (TOA) reflectance. The following equation is used to convert level 1 DN values to TOA reflectance:

$$\rho\lambda' = M\rho * Qcal + A\rho$$

where:

ρλ' : Top-of-Atmosphere Planetary Spectral Reflectance, without correction for solar angle. (Unit less)

Mρ : Reflectance multiplicative scaling factor for the band .

Aρ : Reflectance additive scaling factor for the band

Qcal l: Level 1 pixel value in DN

Note that ρλ' is not true TOA Reflectance, because it does not contain a correction for the solar elevation angle. This correction factor is left out of the level 1 scaling at the users' request); some users are content with the scene-centre solar elevation angle in the metadata, while others prefer to calculate their own per-pixel solar elevation angle across the entire scene. Once a solar elevation angle is chosen, the conversion to true TOA Reflectance is:

$$\boldsymbol{\rho\lambda = \rho\lambda'/\sin(\theta)}$$

where:

ρλ = Top-of-Atmosphere Planetary Reflectance (Unitless)

θ = Solar Elevation Angle (from the metadata, or calculated).

Above ground biomass: remote sensing approach

The current study emphasized three mostly used vegetation indices connected with satellite image change detection and biomass estimation was used. Vegetation indices are the best indicator of greenness of vegetation canopy and hence used to predict the above ground biomass estimation and prediction (Xue and Su, 2017) Almost all vegetation indices derived by the taking ratio of Near Infrared band (NIR) and Red band (R). The current study comprises indices (Table 1) of the normalized difference vegetation index (NDVI), which is the ratio of contrasting reflectance between the maximum absorption of the red wavelength and maximum reflectance of the infrared wavelength (Powel et al., 2010) and its value ranged between -1 to 1, the transformed vegetation index (TVI), which is the same as NDVI but values are always positive as addition of factor of 0.5 to absolute of NDVI and its value ranged in 0 to 1, the soil adjusted vegetation index (SAVI), which is similar to the NDVI but illuminates the soil brightness effect (Richardson and Wiegnad, 1977).

Spectral modeling of carbon stock estimation and prediction using satellite derived vegetation indices have been performed in the present study. The linear regression analysis done between fields based total carbon which was calculated by taking carbon observed in different plant component (AGB, BGB, herb, shrub and soil carbon) and vegetation indices.

4. Results and discussion

The results show the variations in biomass between the mixed forests and pine forests. Stand density, basal area and biomass showed noteworthy variation between the land use types. Altogether, 102 species were recorded from the present study area. Species like *Pinus wallichiana, Castonopsis indica, C. hysterics, Rhododendron hodgsonii, Elaeocarpus rugosus, Quercus myrsinifolia* were among the most frequent species. Based on the study it was observed that the basal area (m^2 /0.1ha) of the woody species ranged from 3.68 to 8.08 in the mixed forests and it was 2.60 to 4.45 in the pine forests. The stand density ranges from 440 stems/ha to 770 stems/ha in the mixed forests and 450 stems/ha to 600 stems/ha in the pine forests.

The volume equations were fitted to the data using diameter at breast height (dbh), height (H) and the combined variable dbh^2H as explanatory variables for the woody species. Species-specific biomass estimation was done for each plot. Biomass per plot (0.1 ha) was estimated by summing up the species present in the respective plots. The AGB ranges from 140.55 t/ha to 316.18 t/ha in the mixed forests whereas it varied from 102.04 to 184.46 t/ha in the pine forests. The findings of the present study are in conformity with the values reported of 7.25 t/ha to 287.047 t/ha in different vegetation types (Devagiri et al., 2013), 6.39 t/ha to 215.57 t/ha in tropical forest ecosystems (Khangar and Hirandhede, 2016). Evaluation of total AGB in the different land use types showed that the total AGB was higher in mixed forests as compared to pine forests and agricultural land. The biomass (t /ha) of the under-storey shrubs ranged from 6.07 to 9.40 whereas for herbs it ranged from 0.46 to 0.74 in the mixed forests on the other hand for plantation it was recorded 6.94-17.36 under-storey shrubs and 0.17-0.27 for herbs. The field-based findings showed a positive relation (R^2=0.94) between the basal area and woody species biomass. The overall allocation of SOC also varied amongst the three landuse types. The highest proportion of SOC content was deposited in the surface layer than the sub surface layer. The average total SOC content in the mixed forests was 29.63 t/ha, 50.27 t/ha in the pine forests and 31.10 t/ha in

the agricultural lands. The carbon stock sum of AGBC and SOC varied significantly over land use types. It ranges from 131.35 t/ha to 309.12 t/ha in mixed forests followed by 129.66 t/ha to 203.02 t/ha in pine forests and 11.53 t/ha to 61.45 t/ha in agricultural lands.

4.1 Spectral modelling of carbon stock

Satellite based biomass estimation of the study area was done through vegetation indices. NDVI values range between 0.08 to 0.42 among the sampled plots, 0.92 to 1.26 for the TVI, 0.12 to 0.62 for SAVI in the present study. Das et al. (2017) had reported NDVI value of 0.26 and SAVI value of 0.70 from different land use sectors of Arunachal Pradesh. To apprehend the relationship linear regression analysis was carried out between AGB and satellite derived different vegetation indices. The coefficient (R^2) of regression model between biomass and different vegetation indices were presented in Table 2 and the spatial variability map of selected land use types of the study area is given in figure 4.

Table 2: Coefficient for R^2 for biomass and different vegetation indices

Vegetation Indices	Equation	R^2
NDVI	Y = 685.57x – 23.262	0.75
TVI	Y = 432.89x – 282.82	0.41
SAVI	Y = 460.81x – 28.433	0.79

*Where x denotes the NDVI and Y denotes AGB

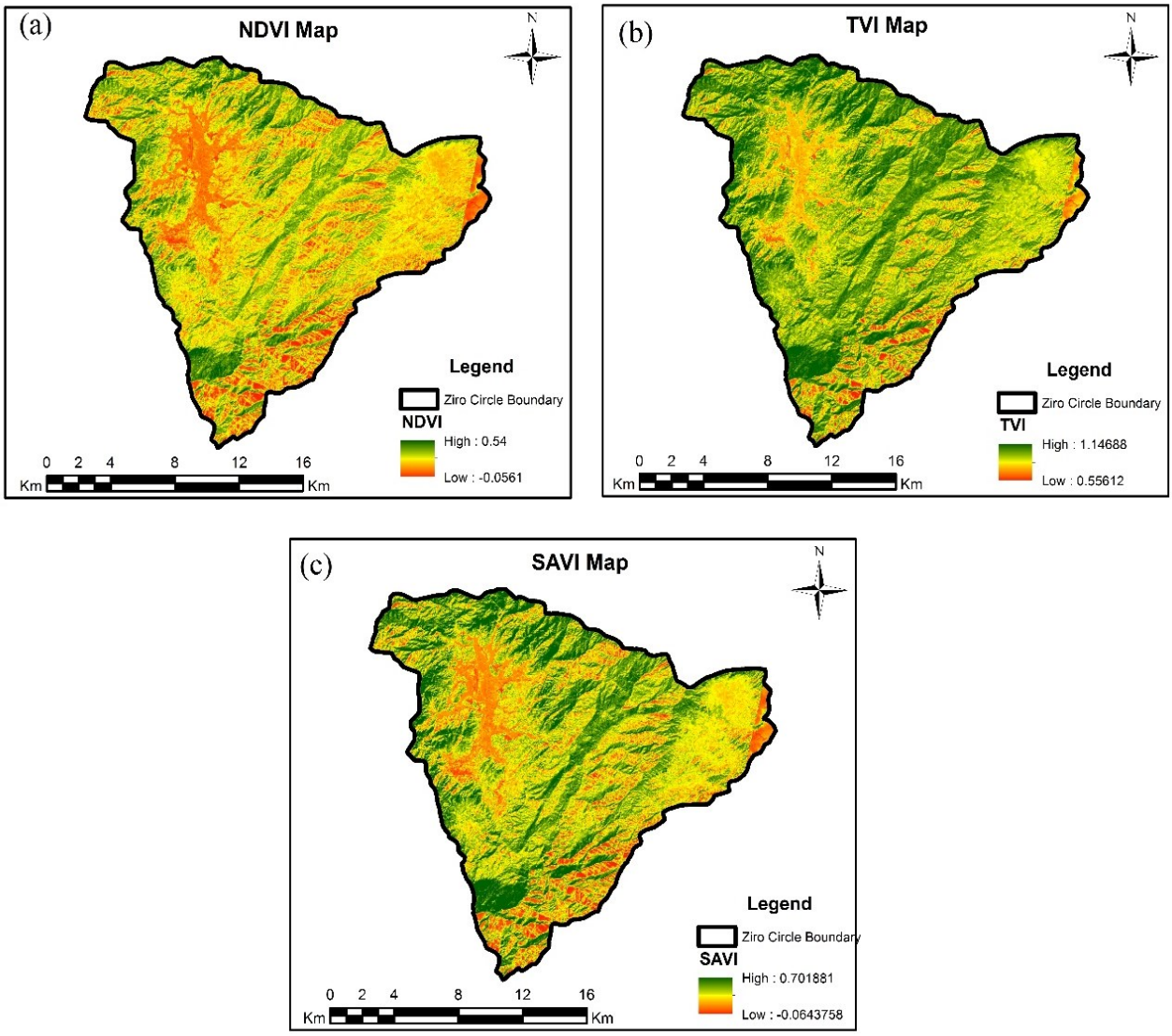

Figure 4: (a) NDVI map, (b) TVI map and (c) SAVI map of study area

The coefficient (R^2) value observed is 0.75 for NDVI, 0.41 for TVI and 0.79 for SAVI. The R^2 value observed for three vegetation indices was compared with values reported by different researchers around the world. Foody et al. (2003) had reported lower R^2 value of 0.082, 0.009 and 0.099, respectively from the Thailand, Brazil and Malaysia using Landsat TM satellite data than the values observed in the current studies. The R^2 value was also reported to be lower ($R^{2=}$ 0.046) by Zhou (2014) from South eastern Bangladesh using Landsat ETM+ bands. Rahman et al. (2008) had also reported the lower R^2 (0.138) value for NDVI. The R^2 value (0.51) reported by Mynard et al. (2007) found to be higher than the values of current study. Redowan et al. (2015) had also reported higher R^2 (0.768) value than current research. The R^2 value for TVI has very low relationship between biomass and TVI. The R^2 (0.173) value for TVI was reported by Rahman et al. (2008) from South eastern Bangladesh using Landsat ETM+ bands were lower than present observation. The higher R^2 value (0.639) was reported by Redowan et al. (2015) for Kahdimanagr national park, Bangladesh. The R^2 value ranged between 0.46 and 0.86 for south western part of Karnataka (Devagiri et al., 2013). The R^2value computed for SAVI is higher than the R^2value 0.52 reported by Zhou (2014). Ullah et al. (2012) had also studied the relationship between green biomass and SAVI and reported R^2 value (0.54) which is lower than the values observed in current study. Maynard et al. (2015) modelled the AGB using vegetation indices and reported the R^2 value of 0.51 for SAVI while in other study it was reported to be 0.029 by Rahman et al. (2008).

Though NDVI is widely used vegetation indices for biomass estimation but it showed low R^2 values in current study. NDVI has the draw backs of light scattering due to aerosols present in atmosphere which affects the biomass estimation (Ben-Ze'ev, et al., 2006). There is no significant difference in NDVI and TVI as both indices have same drawbacks. Also these two indices only use two bands (NIR and Red). In TVI, the values always show positive values and sometimes it goes beyond 1. SAVI perform better than former two indices, as it considers the soil brightness effect and correction factor was added to this which minimizes the error which was observed in NDVI.

4.1.1 Biomass and carbon stock prediction

The current study revealed that soil adjusted vegetation index (SAVI) have better relationship with the carbon stock. The best fit regression model Y = 460.81x – 28.433 (R^2 = 0.79) was used to predict carbon stock per sample plot (Figure 4). The predicted carbon stock was summed up and converted into stock per hectare. The predicted carbon stock for the study area was 118.79 t ha^{-1}. However, the carbon stock predicted for mixed forest was 177.43 t ha^{-1}, 169.23t ha^{-1} for Pine forest and it was 31.10 t ha^{-1} for paddy field. Devagiri et al. (2013) reported carbon stock of 3 Mt (mean carbon density of 33 t ha^{-1}) from Hassan district of Karnataka. Bhat et al. (2003) reported total carbon density (TCD) from 131.86 $Mgha^{-1}$ to 460.89 $Mgha^{-1}$, which indicates that the carbon density of forests reduces with increasing elevation in forest of Uttar Kannad in Western Ghats (Figure 5).

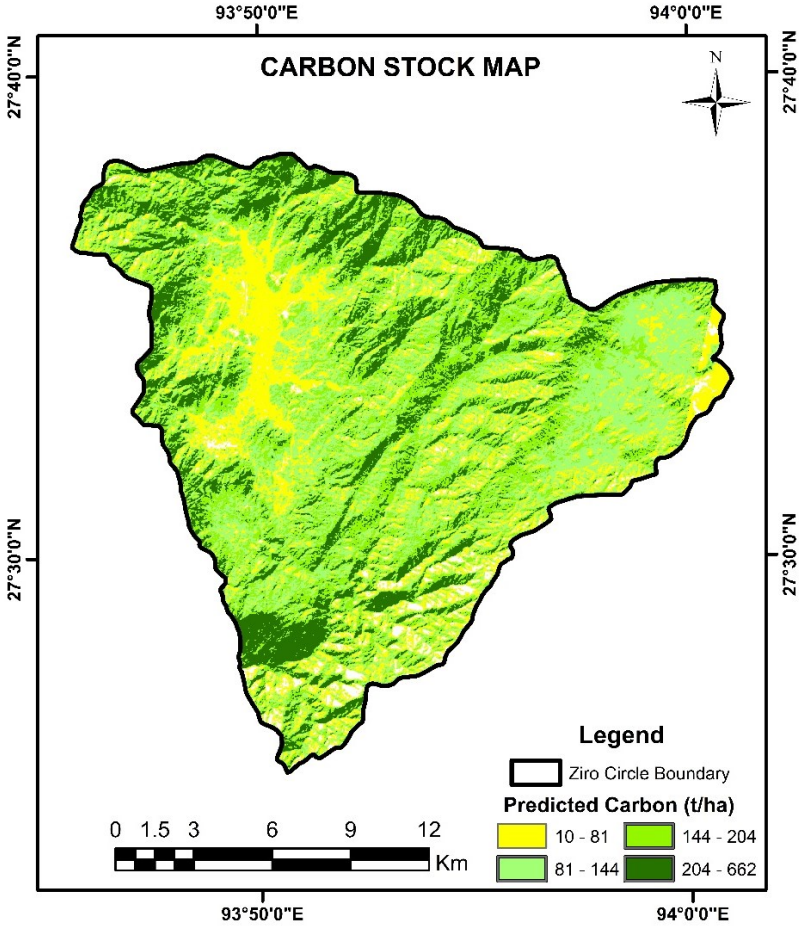

Figure 5: Predicted carbon stock for the study area

5. Conclusions

In the present study, the field based findings of the total carbon stock in the mixed forests was estimated 195.81 t/ha, it was estimated 162.26 t/ha in the pine forests and it was estimated 31.10 t/ha in agricultural lands whereas, the remote sensing based findings predicted carbon stock of the overall land use types of the study area to be 118.79 t/ha which is quite comparable with the field based findings.The difference in the biomass estimations between the observed values and predicted values might be due to the changes in the crown density and phenological conditions of vegetation types existing in the study area.This type of studies will be more successful if they are integrated with socioeconomic, ecological and political objectives for biodiversity conservation and biomass based livelihood enhancement opportunities to use forests as a part of CO_2 emission control strategy.

Dedication

This paper is dedicated to our beloved teacher Late Prof. R.S. Tripathi.

References

Anderson, J. M. and J. S. I. Ingram (1993). Tropical soil biological and fertility: a handbook of methods.

Arneth A., S. Stich, J. Pongratz, B.D. Stocker, *et al.,* (2017). Historical carbon dioxide emissions caused by land-use changes are possibly larger than assumed. Nature Geoscience, 10(2), 79–84

Ben-Ze'ev, E., A. Karnieli, N. Agam, Y. Kaufman, and B. Holben (2006). Assessing vegetation condition in the presence of biomass burning smoke by applying the Aerosol-free Vegetation Index (AFRI) on MODIS images. International Journal of Remote Sensing, 27(15), 3203-3221.

Bhat, D. M., K. S. Murali and N. H. Ravindranath (2003). Carbon stock dynamics in the tropical rainforests of Uttar Kannada district, Western Ghats, India. International Journal of Environment and Pollution, 19(2), 139-149.

Bhat, D.M. and N. H. Ravindranath (2011). Aboveground standing biomass and carbon stock dynamics under a varied degree of anthropogenic pressure in tropical rain forests of Uttara Kannada district, Western Ghats, India. Taiwaniam 56(2), 85-96.

Das, B., S. Deka, R. Bordoloi, P. K. Pandey, L. B. Singha and O. P. Tripathi (2017). Rapid assessment of above ground biomass in forest of Papum Pare district of Arunachal Pradesh: a geospatial approach, Malaya Journal of Biosciences,4(2), 48-55.

Devagiri, G. M., S. Money, S. Singh, V. K. Dadhwal, P. Patil, A. Khaplek, A. S. Devakumar and S. Hubballi (2013). Assessment of above ground biomass and carbon pool in different vegetation types of south western part of Karnataka, India spectral modelling. Tropical Ecology, 54(2), 149–165

Foody, G. M., D. S. Boyd and M. E. J. Cutler (2003). Predictive relations of tropical forest biomass from Landsat TM data and their transferability between regions. Remote Sensing of Environment, 85(4), 463–474.

FSI. 1996. Volume Equations for Forests of India, Nepal and Bhutan. Forest Survey of India, Ministry of Environment and Forests, Govt. of India, Dehradun

Houghton, R.A., B. Byers and A.A. Nassikas (2015). A role for tropical forests in stabilizing atmospheric CO2, Nature Climate Change, 5, 1022–1023.

IPCC, G.L (2005). Agriculture, Forestry and Other Land Use. IPCC Guidelines for national greenhouse gas inventories.

Jensen, J.R. (1986). Digital Image Processing. Prentice-Hall: New Jersey.

Khangar, H, and D.K. Hirandhede (2016). Studies on above ground biomass (AGB) for assessing vegetation carbon pool in tropical forest ecosystem of central India. International Journal of Pharmaceutical Sciences and Research, 7(11), 4588-91.

LANDSAT 8 (L8) Data Users Handbook Version 1.0 June 2015. (2015), 8(June).

MacDicken, K.G. (1997). A guide to monitoring carbon emissions from deforestation and degradation in developing countries: An examination of issues facing the incorporation of REDD into market-based climate policies. Resource for Future, Washington DC, 84.

Maynard, C. L., R. L. Lawrence, G.A. Nielsen and G. Decker (2015.). Modeling Vegetation Amount Using Bandwise Regression and Ecological Site Descriptions as an Alternative to Vegetation Indices, GIScience &Remote Sensing, (1), 68-81.

Nelson, R.F., D.S. Kimes, W.A. Salas, and M. Routhier (2000). Secondary forest age and tropical forest biomass estimation using Thematic Mapper imagery. Bioscience, 50, 419–431.

Prince, S.D. and S.N. Goward (1995). Global primary production: a remote sensing approach. Journal of Biogeograhy. 22(4), 815–835.

Quéré, C.Le., R. Moriarty, R.M. Andrew, J.G. Canadell, S. Sitch, J.I. Korsbakken, P. Friedlingstein, G.P. Peters, R.J. Andres …et al. (2015). Global Carbon Budget 2015. Earth System and Science Data. 7, 349-396.

Redowan, M., R. Akter, M. Islam and K. M. Masum (2015). Estimating growing stock volume in a Bangladesh forest site using Landsat TM and field-measured data, 6(2), 1607–1619.

Richardson, A.J. and C.L. Wiegand (1977). Distinguishing vegetation from soil background information, Photogrammetric Engineering and Remote Sensing, 43(12), 1541-1552.

Running, S.W., P.E. Thornton, R.R. Nemani, J.M. Glassy (2000). Global terrestrial gross and net primary productivity from the earth observing system. pp. 44–57. In Sala O, Jackson R, Mooney H, eds. Methods in Ecosystem Science. New York: Springer-Verlag.

Treitz, P. and J. Rogan (2004). Remote sensing for mapping and monitoring land-cover and land-use change-an introduction. Progress in planning, 61(4), 269-279.

Ullah, S., Y. Si, M. Schlerf, A. K. Skidmore and M. Shafique (2012). Estimation of grassland biomass and nitrogen using MERIS data International Journal of Applied Earth Observation, 19, 196–204.

Walkley, A. and I. A. Black (1934). An examination of Degtjareff method for determining soil organic matter and a proposed modification of the chromic acid titration method. Soil Science, 37, 29-37.

Xue, J., and B. Su (2017). Significant remote sensing vegetation indices: A review of developments and applications. Journal of Sensors, 2017.

Zhou, G. (2014). Determination of green aboveground biomass in desert steppe using litter-soil-adjusted vegetation index. European Journal of Remote Sensing, 47(1), 611–625.

Appendix-I: Species-specific equation used in present study (Source: FSI 1996)

Tree species	Volume eq. used
Abies densa	V=0.10744-2.09529*D+12.62008*D^2-1.61065*D^3
Acer accuminatum	SQRTV=-0.162945+3.109717*D
Acer sp.	SQRTV=-0.162945+3.109717*D
Acer caudatum	SQRTV=-0.162945+3.109717*D
Acer hookeri	SQRTV=-0.162945+3.109717*D
Alnus sp.	V=0.01115-0.11716*D+7.11672*D^2-4.54544*D^3
Alnus nepalenis	V=0.01115-0.11716*D+7.11672*D^2-4.54544*D^3
Alnus nitida	V=0.01115-0.11716*D+7.11672*D^2-4.54544*D^3
Altingia excelsa	V=0.09164-1.21122*D+7.76693*D^2+2.17361*D^3
Betula alnoides	V=0.15958-1.57976*D+8.25014*D^2-0.48518*D^3
Bombax ceiba	V=-0.10513+0.28329*D+6.11575*D^2
Castanopsis sp.	V=0.05331-0.87098*D+6.52533*D^2+1.74231*D^3
Chukrasia tabularis	V=-0.07559+9.23051*D^2
Cinnamomum bejolghota	V=-0.13819+2.28497*D-4.27569*D^2+11.3422*D^3
Cinnamomum camphora	V=-0.13819+2.28497*D-4.27569*D^2+11.3422*D^3
Cinnamomum tamala	V=0.1097-0.88668*D+6.097*D^2-1.62672*D^3
Cinnamomun cecidephne	V=-0.13819+2.28497*D-4.27569*D^2+11.3422*D^3
Citrus sinensis	V=0.15958-1.57976*D+8.25014*D^2-0.48518*D^3
Cyathea sp.	V=0.15958-1.57976*D+8.25014*D^2-0.48518*D^3
Cyperus torulosa	V=0.15958-1.57976*D+8.25014*D^2-0.48518*D^3
Debregeasia longifolia	V=0.15958-1.57976*D+8.25014*D^2-0.48518*D^3
Duabanga grandiflora	SQRTV=-0.05931+2.63098*D
Elaeocarpus rugosus	V=0.15958-1.57976*D+8.25014*D^2-0.48518*D^3
Elaeocarpus sp.	SQRTV=0.43483+5.72522*D-2.59907*SQRTD
Exbuclandia populnea	V=0.15958-1.57976*D+8.25014*D^2-0.48518*D^3
Ficus sp.	SQRTV=0.03629+3.95389*D-0.84421*SQRTD
Ficus auriculata	SQRTV=0.03629+3.95389*D-0.84421*SQRTD
Garcinia sp.	V=0.15958-1.57976*D+8.25014*D^2-0.48518*D^3
Gynocardia odorata	V=0.15958-1.57976*D+8.25014*D^2-0.48518*D^3
Irvingia gabonensis	V=0.15958-1.57976*D+8.25014*D^2-0.48518*D^3
Ligustrum robustum	V=0.15958-1.57976*D+8.25014*D^2-0.48518*D^3
Litchi sineisis	V=0.15958-1.57976*D+8.25014*D^2-0.48518*D^3
Lithocarpus sp.	V=0.15958-1.57976*D+8.25014*D^2-0.48518*D^3
Litsea monopetala	V=0.15958-1.57976*D+8.25014*D^2-0.48518*D^3
Maesa sp.	V=0.15958-1.57976*D+8.25014*D^2-0.48518*D^3
Magnolia campbelli	V=0.15958-1.57976*D+8.25014*D^2-0.48518*D^3
Magnolia sp.	V=0.15958-1.57976*D+8.25014*D^2-0.48518*D^3
Magnolia hodgsonii	V=0.15958-1.57976*D+8.25014*D^2-0.48518*D^3
Mahonia nepalensis	V=0.15958-1.57976*D+8.25014*D^2-0.48518*D^3
Mallotus sp.	V=0.14749-2.87503*D+19.61977*D^2-19.11630*D^3
Mangifera sylvatica	V=0.15958-1.57976*D+8.25014*D^2-0.48518*D^3
Michelia champaca	V=-0.11391+1.06784*D+5.36178*D^2

Michelia doltsopa	V=-0.11391+1.06784*D+5.36178*D^2
Michelia/magnolia oblonga	V=-0.11391+1.06784*D+5.36178*D^2
Moras alba	V=0.15958-1.57976*D+8.25014*D^2-0.48518*D^3
Myrica esculenta	V=0.15958-1.57976*D+8.25014*D^2-0.48518*D^3
Neolitsea zeylanica	V=0.15958-1.57976*D+8.25014*D^2-0.48518*D^3
Neolitsea pulcherima	V=0.15958-1.57976*D+8.25014*D^2-0.48518*D^3
Persea sp.	V=0.15958-1.57976*D+8.25014*D^2-0.48518*D^3
Phoebe pallida	V=-0.0432+0.3622*D^2H
Phoebe lanceolata	V=-0.0432+0.3622*D^2H
Phoenix sp.	V=0.15958-1.57976*D+8.25014*D^2-0.48518*D^3
Pinus wallichiana	V=0.22736-0.027394*D3+0.0012413*D^2(dia in cm)
Pinus roxburgii	V=0.22736-0.027394*D3+0.0012413*D^2(dia in cm)
Prunus sp.	V=0.15958-1.57976*D+8.25014*D^2-0.48518*D^3
Prunus nepalensis	V=0.15958-1.57976*D+8.25014*D^2-0.48518*D^3
Prunus persica	V=0.15958-1.57976*D+8.25014*D^2-0.48518*D^3
Pyrus sp.	V=0.15958-1.57976*D+8.25014*D^2-0.48518*D^3
Quercus dealbata	V=-0.04378+6.2342*D^2
Quercus glauca	V=-0.04378+6.2342*D^2
Quercus myrsinifolia	V=-0.04378+6.2342*D^2
Quercus lamellosa	V=-0.04378+6.2342*D^2
Quercus semiserrata	V=-0.04378+6.2342*D^2
Rhododendron hodgsonii	V=-0.08934+0.7073*D+2.13941*D^2
Rhododendron grande	V=-0.08934+0.7073*D+2.13941*D^2
Rhododendron dalhousiae	V=-0.08934+0.7073*D+2.13941*D^2
Rhododendron coxianum	V=-0.08934+0.7073*D+2.13941*D^2
Rhododendron subansirians	V=-0.08934+0.7073*D+2.13941*D^2
Rhododendron boothii	V=-0.08934+0.7073*D+2.13941*D^2
Rhododendron falconeri	V=-0.08934+0.7073*D+2.13941*D^2
Rhododendron kendrickii	V=-0.08934+0.7073*D+2.13941*D^2
Salvadora persica	V=0.15958-1.57976*D+8.25014*D^2-0.48518*D^3
Sapium buccatum	V=0.15958-1.57976*D+8.25014*D^2-0.48518*D^3
Saurauia nepalensis	V=0.15958-1.57976*D+8.25014*D^2-0.48518*D^3
Schima sp.	V=0.15958-1.57976*D+8.25014*D^2-0.48518*D^3
Schima wallichii	V=0.15958-1.57976*D+8.25014*D^2-0.48518*D^3
Symplocos theifolia	V=0.15958-1.57976*D+8.25014*D^2-0.48518*D^3
Taxus wallichiana	V=0.21869-2.04074*D+10.41713*D^2+1.85232*D^3
Toona ciliata	V=0.15958-1.57976*D+8.25014*D^2-0.48518*D^3
Trema orientalis	SQRTV=-0.09154+2.37257*D
Tsuga dumosa	

Journal of Geomatics Vol. 13, No. 2, October 2019

Hyperspectral subspace identification using eigen values

Dharambhai Shah and Tanish Zaveri*
Institute of Technology, Nirma University, Ahmedabad, Gujarat, India
*Email: ztanish@nirmauni.ac.in

(Received: Dec 20, 2018; in final form: Oct 16, 2019)

Abstract: Blind hyperspectral unmixing basically consists of three sub problems. First is Subspace identification that is finding the number of pure endmembers present. Second is endmember extraction and third is abundance estimation. There are many approaches for endmember extraction and abundance estimation in literature. But many approaches require prior information for the number of endmembers. In this paper, new approach based on eigenvalues of the hyperspectral image for subspace identification is proposed, which is best suitable for real-time application like wild land fire tracking, biological threat detection and monitoring of oil spills. We have compared our results with other state-of-art algorithms on the real and synthetic dataset which shows the effectiveness of the proposed work.

Keywords: Hyperspectral, Subspace identification, Eigen values, unmixing

1. Introduction

Hyperspectral devices or Imaging spectrometers captures tens to hundreds of narrow spectral bands of the scene from optical wavelength bands approximately at the same time. This technology represents the succeeding era in the spectral dimension of the progress of multispectral imaging sensors. Hyperspectral sensors can be applied to all major areas of earth and planetary science including land use (Kalluri et al., 2010), water characteristics (Mishra et al., 2017) and atmospheric characterization (Elwell et al., 2006) due to high spectral resolution. Land applications include all types of vegetation studies, soil science, geology, and hydrology (Chang, 2003). Hyperspectral sensors can be used in river, ocean, and lake for water quality, biochemical studies, and bathymetry analysis. Various parameter measurement, various analysis and characteristics of the atmosphere can be studied using hyperspectral sensors.

The scene depicted by a single pixel usually covers more than one different endmember or material due to multiple scattering, intimate mixing, and low spatial resolution. The spectral signature of different substances/objects is recorded into one mixed spectral response. The pixels that are composed of more than one spectrally distinct material are called mixed pixels. Depending on the spectral and spatial resolution of the hyperspectral sensor under the study, the mixed pixel may contain either different land-use or land cover types of dissimilar endmembers. Mixing can be linear or non-linear depending on how endmembers are related to each other in a single pixel. Decomposition of the mixed pixel is to extract subpixel level information is called spectral unmixing (Bioucas-Dias et al., 2012), as shown in figure 1. Automatic spectral unmixing chain consists of three stages. First is subspace identification which finds the number of pure spectral signatures present in the image. Second is endmember extraction which is extracting pure spectral signatures from the image itself. The final and third stage is abundance estimation to quantify various materials in a scene. Subspace identification is a very crucial step in unmixing chain as it provides initial information to subsequent stages. Real-time applications of hyperspectral image processing applications require fast approaches. There exist many approaches to hyperspectral subspace identification but all of them requires high processing time which is not suitable for real-time processing.

There are many popular subspace identification methods Principal Component Analysis (PCA), Singular Value Decomposition (SVD), Hyperspectral Subspace Identification by minimum error (Hysime), Harsanyi–Farrand–Chang (HFC). PCA (Jolliffe, 2011) is one of the statistical methods commonly used in signal and image processing for dimensionality reduction and decorrelation. PCA is a factor analysis approach with the consideration of the total variance in the data to convert the original variables into a lesser set of linear mixtures. Subspace for the hyperspectral image is calculated based on variances contained by principal components. SVD (Lange, 2010) finds singular values unlike principal components in PCA. But the method of finding subspace of SVD is same as in PCA. The only main difference is the principal component and singular values. HFC (Chang and Du, 2004) method is eigenvalue thresholding method using Neyman–Pearson detection to resolve subspace identification, which models the dimensionality estimation as a binary composite hypothesis testing problem and the subspace approximation error can be measured by ROC analysis. Hysime (Bioucas-Dias and Nascimento, 2008) uses the least mean squared error-based method to gather the signal subspace in hyperspectral images.

In this paper, we propose a new approach for subspace identification in the hyperspectral unmixing chain. The main advantage of our approach is fewer computations which is best suitable for real-time applications. Contributions from this paper are:

- We have developed new TE (Thresholding Eigenvalues) for subspace identification.
- Timing analysis for the proposed approach and other state-of-art approaches.

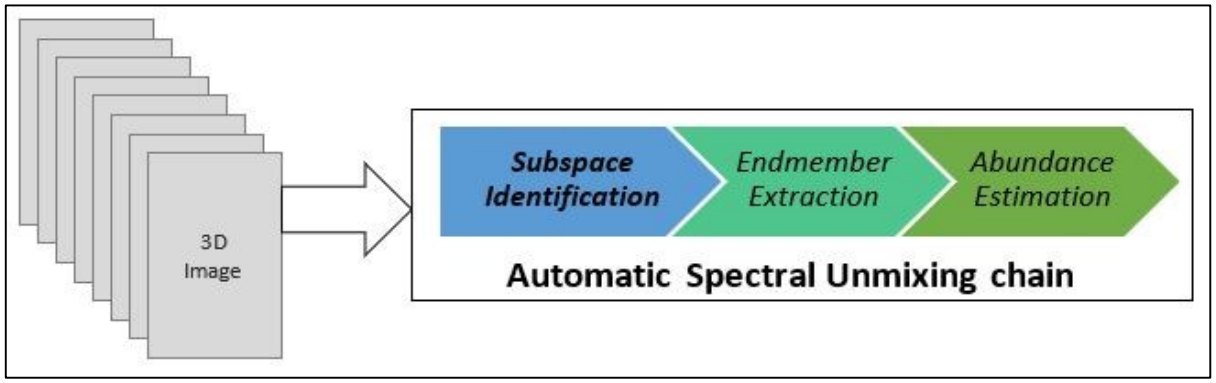

Figure 1: Automatic spectral unmixing chain

2. TE (Thresholding Eigenvalues)

Hyperspectral images are basically 3D-cube. Two dimensions are spatial and one dimension is spectral. To compute the correlation matrix easily, the two-dimensional image is required with one spatial and one spectral dimension. Y is the two-dimensional version of original three-dimensional hyperspectral image X. Y is having a size of M× B, where M is a number of pixels and B is the number of bands.

Correlation is a very basic operation in signal processing community to find similarity between two signals. Here, R is correlation matrix of Y, which represents bands similarity. Eigenvalues are invented with the purpose of finding the principal axes of a rigid body. As Eigenvalue represent principal axes, we can assume eigenvalues as the prime component. Higher eigenvalue means more basic component. If we find few eigenvalues, which represent whole data then that few numbers represent hyperspectral subspace dimension. E is eigenvalue set of correlation matrix R. Es is descending sorting of vector E. Es is calculated to find first major components which have more impact. L is normalized values of Es. Normalization is necessary to deal with a high dynamic range of eigenvalues.

The algorithm requires two variables for computation. One is two-dimensional hyperspectral image and second is the variance that needs to be preserved from eigenvalues. Var is a variable, which represents variance required. (Var/100) gives a value between 0 and 1. Variable Var value should be between 0 and 1 to compare it with normalized value of eigenvalues L. TE approach finds a value of N such that first N eigenvalues from L give variance greater than or equal to (Var/100). N is hyperspectral subspace dimension which represents the number of pure spectral signatures present in the image.

This TE approach requires few computations only to find N. The advantage of fewer computation in TE approach is very useful in real-time hyperspectral unmixing. Figure 2 shows the flowchart of the TE algorithm.

3. Results

We have performed two types of analysis on both real and synthetic dataset. First is timing analysis and second is subspace analysis (Figure 3).

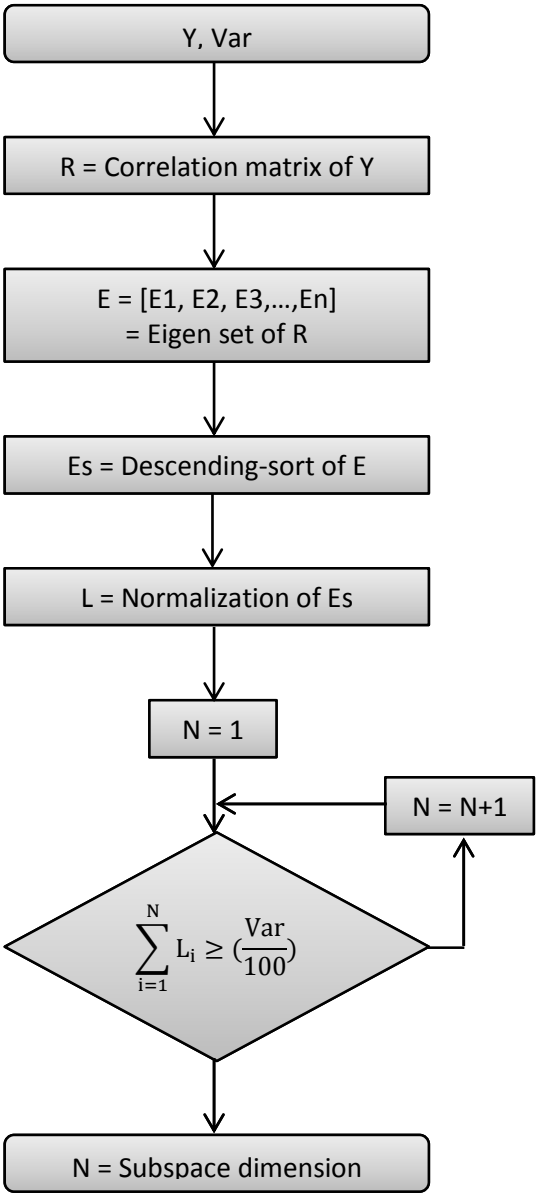

Figure 2: Flowchart of TE algorithm

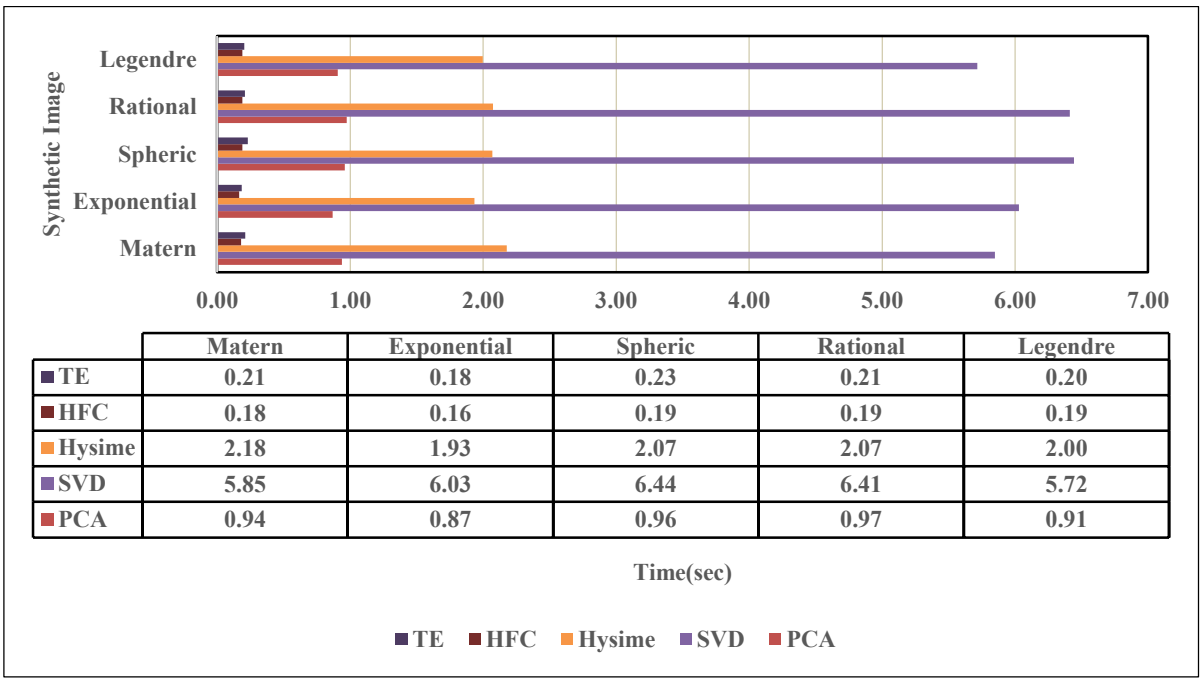

	Matern	Exponential	Spheric	Rational	Legendre
TE	0.21	0.18	0.23	0.21	0.20
HFC	0.18	0.16	0.19	0.19	0.19
Hysime	2.18	1.93	2.07	2.07	2.00
SVD	5.85	6.03	6.44	6.41	5.72
PCA	0.94	0.87	0.96	0.97	0.91

Figure 3: Timing Analysis for synthetic images

Cuprite image as shown in figure 4 is used as real dataset which can be downloaded from URL: https://sites.google.com/site/feiyunzhuhomepage/datasets-ground-truths. Cuprite image was taken by AVIRIS instrument which is an optical instrument that delivers images of the spectral radiance from 400 to 2500 nm wavelength range with overall 224 contiguous spectral channels.

We have used synthetic data generated from Hyperspectral Imagery Synthesis (EIAs) toolbox (Computational Intelligence Group, 2019). All these synthetic images are shown in figure 5 have been generated using 5 selected materials (asphalt, brick, fiberglass, Sheetmetal, vinyl-plastic from the USGS spectral library (Clark et al., 2007).

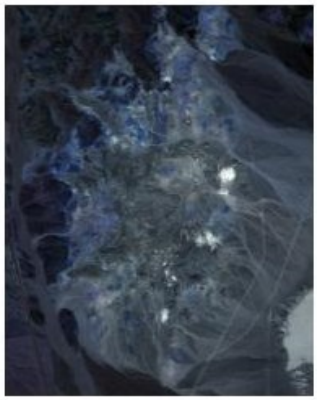

Figure 4: Cuprite image

Each image is of 128x128x431. Five synthetic images (Matern, Exponential, Spheric, Rational, and Legendre) as shown in figure 5 are generated using different modelling equations available in the toolbox (Computational Intelligence Group, 2019).

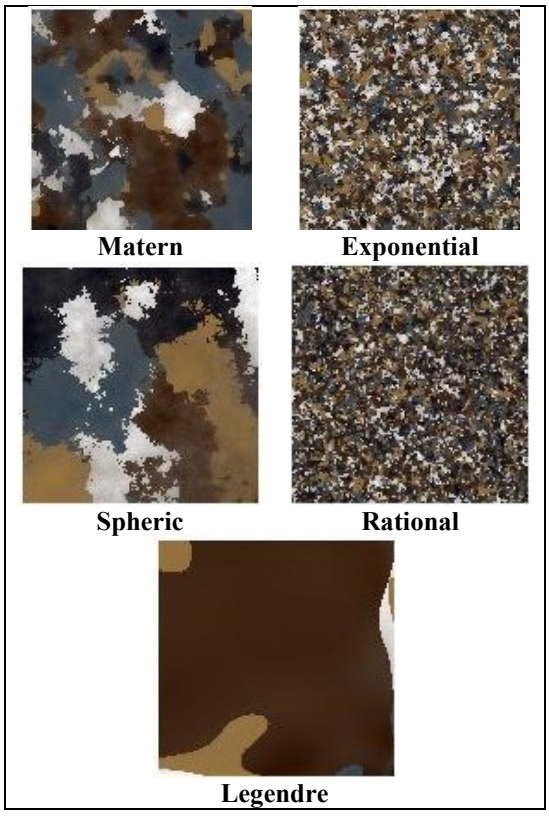

Figure 5: Synthetic images

3.1. Timing analysis

Processing time is very important for real-time applications. Some applications of hyperspectral images require less computation time. In this experiment, we have depicted processing time by each algorithm and compared with our approach as shown in figures 3 and 6. Processing

time for each algorithm on each synthetic image is shown in figure 3. It can be seen from figure 3 that processing time is very less by proposed method and HFC as compare to other algorithms. It can be also observed from figure 6 that proposed method and HFC requires less time compare to other algorithms.

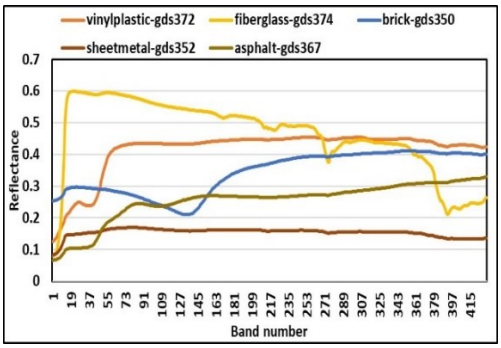

Figure 6: Spectral signatures used in the synthetic image

3.2. Subspace analysis

Subspace is also as important as timing in real time hyperspectral unmixing chain. Subspace provides the number of spectrally distinct signatures. Subspace analysis observes the number of pure signatures for the unsupervised spectral unmixing chain. Figures 7 and 8 show the subspace analysis experiment results for synthetic and real image respectively. As synthetic images are generated using the toolbox, we know the subspace dimensions. For our synthetic dataset, we have used five distinct signatures. So, reference data for all synthetic images is figure 5. We have compared subspace dimensions for our proposed approach and other approaches. All approaches except HFC gives perfect subspace dimensions. Reference data for cuprite image is 14 as mentioned in paper (Zhu et al., 2014).

We have compared subspace dimensions in figure 8 for cuprite image. It can be seen that HFC and our proposed algorithm gives the same result as GT (Figure 9).

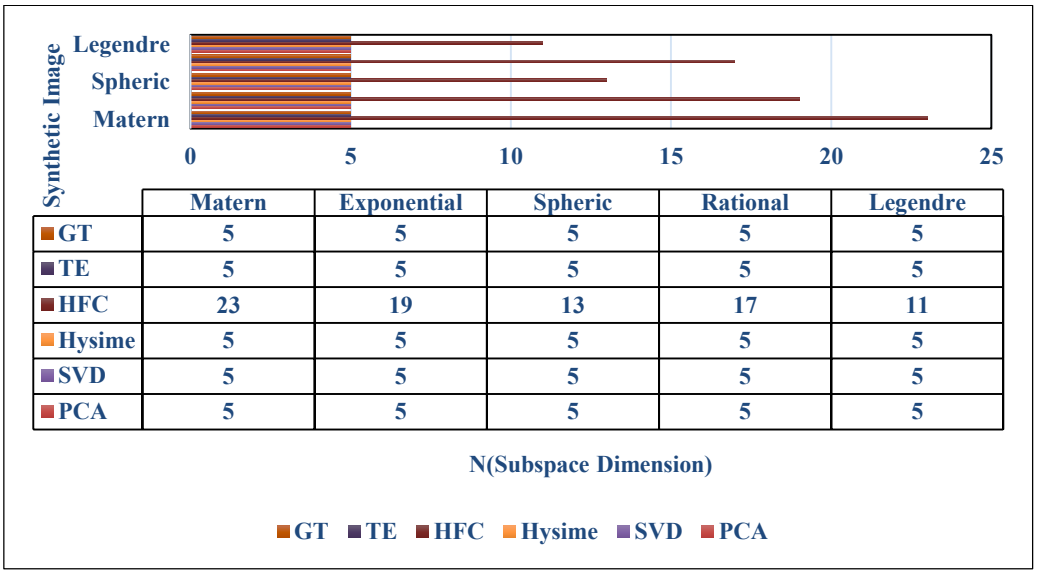

	Matern	Exponential	Spheric	Rational	Legendre
GT	5	5	5	5	5
TE	5	5	5	5	5
HFC	23	19	13	17	11
Hysime	5	5	5	5	5
SVD	5	5	5	5	5
PCA	5	5	5	5	5

Figure 7: Subspace analysis for synthetic image

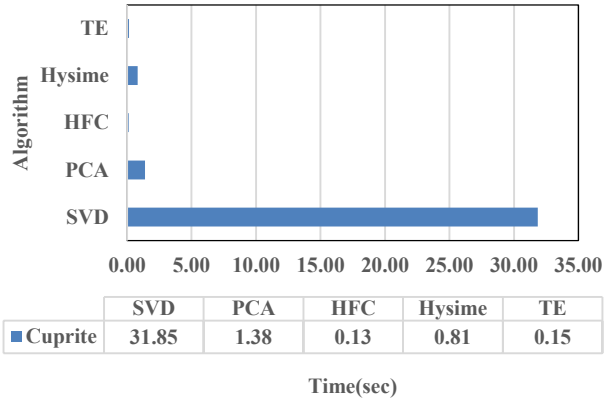

	SVD	PCA	HFC	Hysime	TE
Cuprite	31.85	1.38	0.13	0.81	0.15

Figure 6: Timing analysis for real image

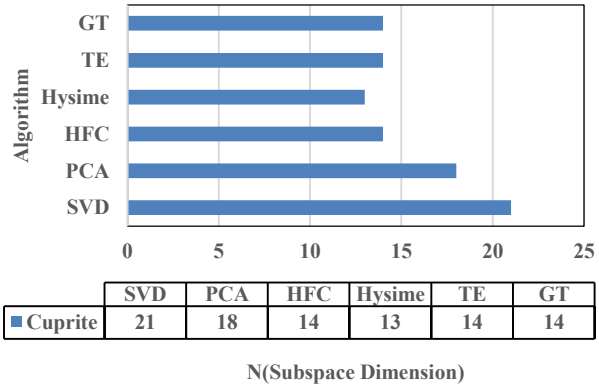

	SVD	PCA	HFC	Hysime	TE	GT
Cuprite	21	18	14	13	14	14

Figure 7: Subspace analysis for real image

4. Conclusions

In this paper, a new Thresholding Eigenvalues based to identify approach is proposed the subspace dimension of the hyperspectral image. The simulation results of the timing analysis and subspace analysis of proposed approach was computed form both synthetic and real dataset. TE approach computes subspace dimensions accurately and comparatively in less time. TE approach can be best suitable for real-time applications.

Acknowledgments

The authors of this paper are sincerely thankful to Nirma University and Institute of Technology, Nirma University, Ahmedabad, India for necessary support. This work has been carried out from the grant received from Visvesvaraya Ph.D. Scheme for Electronics and IT, Ministry of Electronics and Information Technology, Government of India.

References

Bioucas-Dias, J. M. and J.M. Nascimento (2008). Hyperspectral subspace identification. IEEE Transactions on Geoscience and Remote Sensing, 46(8), 2435-2445.

Bioucas-Dias, J. M., A. Plaza, N. Dobigeon, M. Parente, Q. Du, P. Gader and J. Chanussot (2012). Hyperspectral unmixing overview: Geometrical, statistical, and sparse regression-based approaches. IEEE journal of selected topics in applied earth observations and remote sensing, 5(2), 354-379.

Chang, C. I., and Q. Du (2004). Estimation of number of spectrally distinct signal sources in hyperspectral imagery. IEEE Transactions on geoscience and remote sensing, 42(3), 608-619.

Chang, Chein-I (2003). Hyperspectral imaging: techniques for spectral detection and classification, 1. Springer Science & Business Media.

Clark, R. N., G.A. Swayze, R. Wise, K.E. Livo, T. Hoefen, R.F. Kokaly and S.J. Sutley (2007). USGS digital spectral library splib06a. US geological survey, digital data series, 231.

Computational Intelligence Group, University of the BasqueCountry / Euskal Herriko Unibertsitatea (UPV / EHU),S., 2010. Hyperspectral imagery synthesis (eias)toolbox.http://www.ehu.es/ccwintco/index.php/Hyperspectral_Imagery_Synthesis_tools_for_MATLAB, online; accessed 28 March 2019

Elwell, J. D., G.W. Cantwell, D.K. Scott, R.W. Esplin, G.B. Hansen, S.M. Jensen (2006). A geosynchronous imaging Fourier transform spectrometer (GIFTS) for hyperspectral atmospheric remote sensing: instrument overview and preliminary performance results. In Infrared Spaceborne Remote Sensing XIV, 6297, 62970S. International Society for Optics and Photonics.

Hyperspectral Imagery Synthesis (EIAs) toolbox. (n.d.). Retrieved from http://www.ehu.es/ccwintco/index.php/Hyperspectral_Imagery_Synthesis_tools_for_MATLAB

Jolliffe, I. (2011). Principal component analysis. In International encyclopedia of statistical science, 1094-1096. Springer, Berlin, Heidelberg.

Kalluri, H.R., S. Prasad and L.M. Bruce (2010). Decision-level fusion of spectral reflectance and derivative information for robust hyperspectral land cover classification. IEEE Transactions on Geoscience and Remote Sensing, 48(11), 4047-4058.

Lange, K. (2010). Singular value decomposition. In Numerical analysis for statisticians,129-142. Springer, New York, NY.

Mishra, R., D. Shah, T. Zaveri, R. Ramakrishnan and P. Shah (2017). Separation of sewage water based on water quality parameters for south karnataka coastal region. Paper presented at the 38th Asian Conference on Remote Sensing - Space Applications: Touching Human Lives, ACRS 2017

Zhu, F., Y. Wang, S. Xiang, B. Fan and C. Pan (2014). Structured sparse method for hyperspectral unmixing. ISPRS Journal of Photogrammetry and Remote Sensing, 88, 101-118.

Journal of Geomatics Vol. 13, No. 2, October 2019

Concrete volume loss calculation of structures using Terrestrial Laser Scanner (TLS)

S.K.P. Kushwaha*, Hina Pande and S. Raghavendra
Photogrammetry and Remote Sensing Department, Indian Institute of Remote Sensing, Dehradun, India - 247667
*Email: s.k.p.kushwaha92@gmail.com

(Received: Dec 21, 2018; in final form: Oct 17, 2019)

Abstract: Buildings are one the major structures which have to be monitored appropriately with much importance. Any damage in the structure could be proved fatal if it is not rectified within the time. Over the course of time the structural material loses its strength. Concrete loss is a major concern as this may be a reason for the collapsing of the building. Thus the amount of concrete volume loss is an important factor to be monitored. In this research TLS (RIEGL VZ-400) has been used to serve this purpose, Terrestrial Laser Scanner (TLS) is an instrument which provides 3D point cloud of the targeted surface rapidly with more accuracy. The surface where there are abnormal depths can be found with help of variation in the points. The actual 3D surface and the simulated 3D idle surface are used to find out the exact concrete volume loss and this is compared with the ground truth validation. These results are helpful to remodify the building depending on the actual amount of materials required to renovate and to avoid further loss in the volume of the concrete, in the building. Using this technique 2 to 4 percentage of error was obtained.

Keywords: Terrestrial Laser Scanner (TLS), Point Cloud, Triangulated Irregular Network (TIN), Concrete Volume loss

1. Introduction

Buildings are one of the important structures which are to be monitored with great importance. Buildings where materials used were not good enough are more prone to the concrete loss damage. Buildings in the rural areas are less maintained than the buildings in the urban areas. Due to financial issues, non-availability of resources etc. So the livelihood in the rural are more prone in case the building collapses due to weakening of the structure, due to concrete loss in the building. This is the main area of research in this project. Due to different loads in the structure, due to water absorption, or other reasons due to which cohesive force of attraction between the concrete pile weakens (Santos et al., 2007) and fall off sometimes resultant in concrete loss. Thus concrete volume loss measurement is of much importance (Zhang et al., 2005). This measurement can be done with the help of TLS (Burton, 2007) and with much higher accuracy (Boehler & Marbs, 2003) than general method of estimation.

1.1 Terrestrial Laser Scanner (TLS)

TLS is a remote sensing instrument which can provide the information about the surface without being in direct contact with the target and gives us 3D point cloud of the targeted area which is to be studied. The basic principle of TLS is that it fires laser beam with high repeatability pulse and traces the return signal from the target (Pfeifer & Briese, 2007). In less time large amount of targeted area can be covered. It calculates the range, intensity, amplitude, RGB value (if the camera is mounted), etc. There has been many researches for volume estimation using TLS in the fields like soil erosion (Milan et al., 2007), estimation of waste dump (Tseng et al., 2016), excavation (Yakar et al., 2014). An automatic method for recognizing concrete mass loss using abrupt changes in the Gaussian and mean curvatures with TLS is discussed in Teza et al., 2009.

1.2 3D point cloud

3D data set in the form of points at discreet intervals can be referred as a point cloud. The discreet space between the points in the point cloud is due to the angular resolution, which is programmed before the scan of the target, lower the angular resolution, higher will be the space between the points and vice versa. Time period increases proportionally with increase in the angular resolution and vice versa. The Point cloud is an exact replica of the target, it's like virtual visualization of the real scenario in digital format where one can manipulate or process accordingly based on the requirement.

1.3 Concrete volume loss calculation

The amount of concrete that the building has lost is to be calculated. Gap between two 3D (simulated and actual) surfaces gives you the volume The range difference between the pixels of each surface multiplied by the surface area of the surface gives you the volume. In case of structure the volume difference is the amount of concrete loss that has occurred.

1.4 Accuracy assessment

The percentage of error in the calculation of concrete mass loss is calculated relative to the volume obtained by processing with the help of software and volume obtained from ground value inspection.

$$percentage\ of\ error = \frac{(V_{SOFTWARE} - V_{GROUND}) \times 100}{V_{GROUND}} \quad (1)$$

$V_{SOFTWARE}$ is the volume of concrete loss obtained using software

V_{GROUND} is the volume of concrete loss obtained using ground truth validation.

2. Study area and data acquisition

Three different types of concrete loss in a building were identified and were selected as study area. Study area 1, was taken at the edge of the building. Study area 2, was taken as the facia of a ventilation window. Study area 3, was taken as roof of a building (Figure 1). The positions of scans were planned accordingly to cover the whole concrete loss portion.

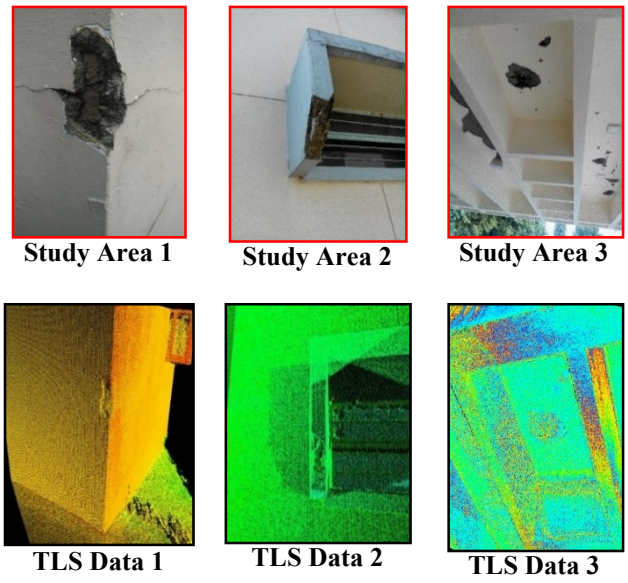

Figure 1: Study area and TLS data sets

3. Methodology

To get volume loss two surfaces are needed. One surface is the original (damaged) point cloud obtained from the TLS instrument with Laser Pulse Repetition Rate 100 kHz. The other surface is the simulated point cloud which is generated from the non-destructed similar surface of the structure, how it had been if there wasn't any concrete loss. Simulated point cloud was generated in cloud compare software. Noise were filtered out from the point cloud dataset and the damaged area were segmented out from the overall dataset. Simulated point cloud is the point cloud of the structure how the surface should have been. if no concrete loss had occurred. 3D point clouds were then converted into 2D raster's (continuous surface) as the point cloud is a discrete dataset which have spaces between them and to make the surface continuous. In some places pixels doesn't have values due to the absence of points in the point cloud or due to low density. These pixel values are interpolated with the neighbouring pixel value around it. Triangulated Irregular Network (TIN) surface is generated from the raster. From this Volume difference between two 3D surfaces are calculated with the help of software's (ArcMAP) and validated with the help of ground truth inspection (using clay models) (Figure 2).

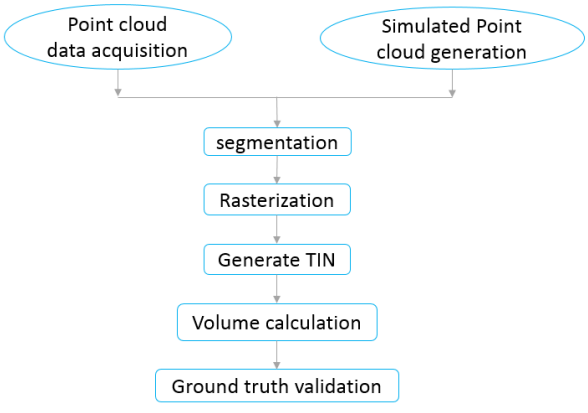

Figure 2: Methodology

4. Results and discussions

4.1 Study area 1: Volume

Volume computed using software was obtained as 303 cm^3. Whereas, volume obtained through manual process was 311.71 cm^3. Percentage of error was calculated using eq. 1 and as shown in figure 3 & 4.

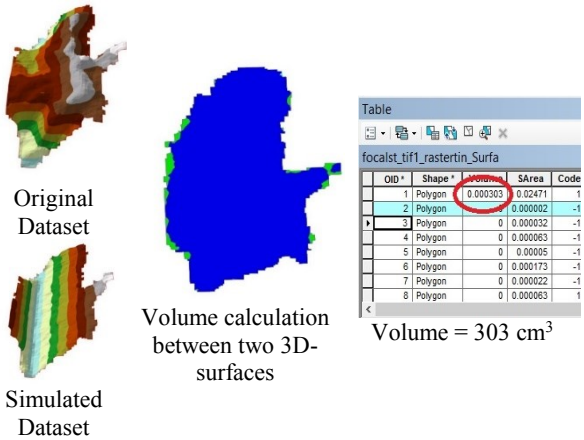

Figure 3: Volume computation using software

4.2 Study area 1: Validation

Clay was used to extract the shape of the destroyed portion, clay was made to take the actual shape by inserting into the structure and by preventing any voids between them. Then the clay was carefully removed and was filled into a container with known dimensions to get the exact volume. Proper care was taken to minimise all the voids. This procedure was followed for other two study areas also. The percentage of error in study area 1 = 2.79 %

Figure 4: Volume computation manually

The percentage of error in study area 1 = 2.79%

4.3 Study area 2: Volume

Volume computed using software was obtained as 2517 cm^3. Whereas, volume obtained through manual process was 2602.6 cm^3. Percentage of error was calculated using eq. 1 and as shown in figure 5 & 6.

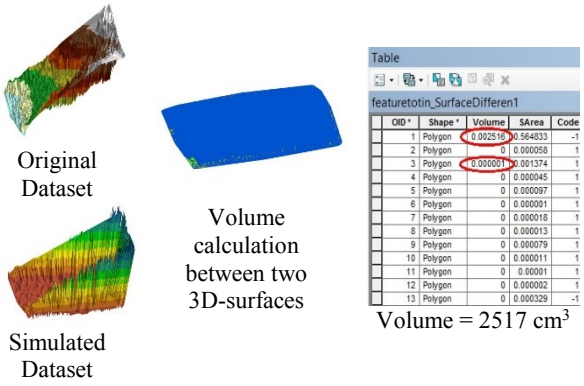

Figure 5: Volume computation using software

4.4 Study area 2: Validation

Validation process was repeated as mentioned earlier.

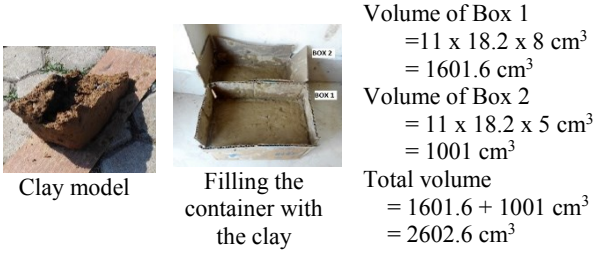

Figure 6: Volume computation manually

The percentage of error in study area 2 = 3.28%

4.5 Study area 3: Volume

Volume computed using software was obtained as 5622 cm^3. Whereas, volume obtained through manual process was 5640.576 cm^3. Percentage of error was calculated using eq. 1 as shown in figures 7 & 8.

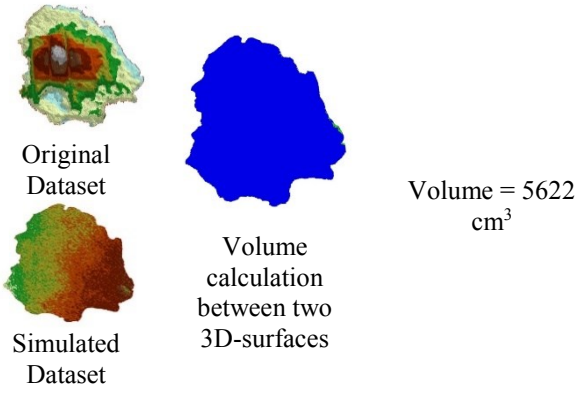

Figure 7: Volume computation using software

4.6 Study area 3: Validation

Validation process was repeated as mentioned earlier and as shown in the figures 7 & 8.

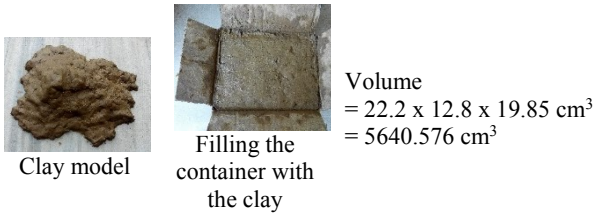

Figure 8: Volume computation manually

The percentage of error in study area 3 = 3.29%

5. Conclusions

The percentage error in concrete volume loss calculation in different study area 1,2 and 3 were obtained as 2.79 %, 3.28 % & 3.29 % respectively. Hence, TLS proves to be very effective instrument in measuring the concrete volume loss calculation of the structures.

TLS proves to be a fast, accurate and more reliable non-invasive technique to calculate the amount of concrete the building has lost. Concrete volume calculation with the help of this technique gives a more accurate amount of volume, that are needed to be used to refill or re modify to strengthen the building from further damage. TLS is a ground based instrument there may be few concrete losses above the field view of the instrument like concrete losses which can be visible only from the top of the structure. Those parts can be covered with the help of UAV Lidar. In this research, the overall accuracy of concrete volume loss estimation was obtained less than 4%.

Acknowledgements

We appreciate the support of the Indian Institute of Remote Sensing - ISRO for providing the access to the TLS (RIEGL VZ-400) instrument for the point cloud data acquisition. We also thank the Cloud Compare team for providing free access to the software for data processing.

References

Boehler, W. and A. Marbs (2003). Investigating Laser Scanner Accuracy. The International Archives of Photogrammetry Remote Sensing and Spatial Information Sciences, 34, 696–701. https://doi.org/10.1002/pbc.

Burton, G. (2007). Terrestrial laser scanner, 4, 45–48.

Milan, D.J., G.L. Heritage and D. Hetherington (2007). Application of a 3D laser scanner in the assessment of erosion and deposition volumes and channel change in a proglacial river. Earth Surf. Process, Landforms, 32, 1657–1674

Pfeifer, N. and C. Briese (2007). Norbert Pfeifer, Christian Briese. Scanning, 1–20. Retrieved from http://www.ipf.tuwien.ac.at/np/Publications/geosibirPfeifer.pdf

Santos, P. M. D., E.N.B.S. Júlio and V.D. Silva (2007). Correlation between concrete-to-concrete bond strength and the roughness of the substrate surface. Construction and Building Materials, 21(8), 1688–1695. https://doi.org/10.1016/j.conbuildmat.2006.05.044

Teza, G., A. Galgaro and F. Moro (2009). Contactless recognition of concrete surface damage from laser scanning and curvature computation. NDT and E International, 42(4), 240–249. https://doi.org/10.1016/j.ndteint.2008.10.009

Tseng, Y., Z. Shen and W. Chen (2016). Estimation of Waste Dump Volume Using Terrestrial Laser., proceedings of Asian Association on Remote Sensing.

Yakar, M., H.M. Yilmaz and O. Mutluoglu (2014). Performance of Photogrammetric and Terrestrial Laser Scanning Methods in Volume Computing of Excavation and Filling Areas. Arabian Journal for Science and Engineering, 39(1), 387–394. https://doi.org/10.1007/s13369-013-0853-1.

Zhang, X., J. Morris and R. Klette (2005). Volume Measurement Using a Laser Scanner, techreports/2005/CITR/NZ.

Journal of Geomatics Vol. 13, No. 2, October 2019

Performance evaluation of a newly in-house developed in-situ soil moisture sensor with standard industrial sensors and gravimetric sampling

Harsh Agrawal[*,1], Abhishek Dubey[1], Nikita Tiwari[2], Dharmendra Kumar Pandey[3], Deepak Putrevu[3], Arundhati Misra[3] and Raj Kumar[3]
[1]Nirma University, Ahmedabad
[2]National Institute of Technology (NIT), Raipur
[3]Space Applications Centre, (ISRO), Ahmedabad
*Email: harshag.96@gmail.com

(Received: Jan 01 2019; in final form: Oct 23, 2019)

Abstract: The calibration and validation of satellite derived soil moisture products heavily relies upon an accurate source of ground truth data as an accurate in-situ soil moisture information plays an important role in proper error estimation and further improvement in satellite derived soil moisture products. For proper validation of satellite derived soil moisture products at large scale, dense network of in-situ sensor with high accuracy and robustness under adverse conditions are required. In this work, In order to reduce the overall cost of such a dense soil moisture network of sensors, Smart Soil Sensor for Hydrology and land Applications (SHOOL) was designed and developed which is a highly compact and robust sensor, suitable for in-situ measurements of soil properties (dielectric constant, electrical conductivity, soil moisture, soil temperature etc. In-house developed SHOOL was further exclusively tested and validated using commercial probes and gravimetric sampling methods in various crop fields. Performance of in-house developed sensor was also evaluated using performance metrics which includes statistical measures R^2 (coefficient of determination), bias, ubRMSE and RMSE. The SHOOL performed satisfactorily over a large range of soil moisture (from dry to wet) with respect to gravimetric methods and commercial probes. It was observed that SHOOL has shown better performance and in good agreements with commercial probes. Overall, in-house developed sensor (SHOOL) has high potential to be a simpler and economical alternative to the industrial sensors and would be helpful in development of a dense sensor network for validation of satellite derived soil moisture products at various scales.

Keywords: Soil Moisture, Frequency Domain Reflectometry, Gravimetric sampling, Soil salinity.

1. Introduction

Soil moisture is one of the important parameters in the hydrological cycle to drive weather conditions, plant growth, groundwater storage, etc.; thus, it has a role in global climate (Vereecken et al. 2008). Soil moisture consists of only 0.05% of the total water in the global hydrological cycle (Robinson et al., 2008) and 0.001% of the total available freshwater (Drinkwater et al., 2009), but it has been declared as one of the Essential Climate Variable (ECV) due to its important role in the hydrological cycle.

Coarse scale at moderate temporal resolution global surface soil moisture can be obtained by satellite remote sensing, mostly by microwave sensors (Wagner et al., 2013). Currently several satellite missions provide global surface soil moisture products, such as: Soil Moisture Active Passive (SMAP) (Entekhabi et al., 2010) and METOP-A/B Advanced Scatterometer (ASCAT) (Wagner et al., 2013). Recently, Space Applications Centre (SAC), ISRO also adopted a modified version of ASCAT operational algorithm based on change detection (time series methodology) and developed daily operational soil moisture products using SMAP L-band brightness temperature data at 12.5 km grid resolution over India which is available at MOSDAC and VEDAS web portal of SAC (ISRO) (Pandey D. et al., 2016). Development of a time-series based methodology for estimation of large area soil wetness over India using IRS-P4 microwave radiometer data (Thapliyal et al., 2005), these Soil Wetness Index (SWI) and Soil Moisture (SM) data products have wide applications in agriculture productivity assessment, crop-water stress assessment, flood and drought monitoring and meteorological applications etc. Before their applications to solving various scientific or societal problems in different applications, satellite derived soil moisture data products have to be evaluated, and their validity and accuracy have to be assessed by using in-situ or reference data.

As a standard practice for validation of satellite derived soil moisture products, in-situ data are used as a reference, using field portable soil moisture probes or fixed station during field campaign. The validation of large-scale satellite-based soil moisture products from microwave radiometers typically faces the problem of the scale difference with in-situ observations because satellite derived products represents a field mean of large area. So in order to validate satellite derived soil moisture using in-situ data, more number of spatially distributed in-situ soil moisture measurements within satellite footprint are required to represents field mean of soil moisture. This brings us to the immediate need for designing and developing a cost effective soil moisture sensor which could be used to make dense soil moisture networks by installing more number of sensors within satellite footprint at low cost with required measurement accuracy as per the science requirement.

The study aims at the evaluation of newly developed in-house sensor having salient features of low cost, low weight, highly compact, field friendly, which can measure in-situ soil electrical properties, process it and directly transmit the data to the user via smartphone or ftp server. Probes are inserted in soil to provide soil dielectric, conductivity, moisture and temperature measurement with

a good accuracy. It is fully controlled and operated by android app which user can install and do the field measurements using smart phone. The device is compact and standalone with capability such as wireless interface for app, long lasting battery and robust for field applications. Field calibration and validation campaign was completed to evaluate the performance of the developed sensor for measurement of surface soil moisture.

2. Materials and methods

This study aims at performance evaluation of two industrial sensors; MP306 (ICT International) and Stevens Hydra Probe (Stevens Water) and a newly in-house (SAC-ISRO) developed in-situ soil moisture sensor. Frequency Domain Reflectometry (FDR) based Industrial measures soil dielectric constant and based on dielectric mixing model, calculates soil moisture in volumetric percentage. Inter-comparison and performance evaluation of probes are done through statistical parameters such as: Bias, Root Mean Square Error (RMSE), Unbiased Root Mean Square Error (ubRMSE) and Coefficient of determination (R^2).

2.1 Operating principles of sensors

Indirect measurement of soil moisture is popularized by the principle algorithms that process the raw Analog to digital converter (ADC) values to derived soil moisture equations or dielectric constant and conductivity (Figure 1). A comparative study and their use in standard field validation practices is described here.

2.2 Measurement of soil moisture by standard ICT probe

The MP306 moisture probe is used for measuring the moisture of soil and also moisture of material used in mining, roadways and buildings. The MP306 ICT Probe takes continuous measurement for a particular range of time using permanent or temporary burial and connection to a soil moisture meter. Soil moisture meter contain high frequency moisture detector which follows the property of standing wave principle that calculates the variation in incident and reflected wave. MP306 has a compact body with data logger for displaying the calculated parameters via the MP306 probe. Needles are arranged in one plane which makes it ideal for use in soil columns. Principally, it detects any change in the volume matrix ratio of water which substantially reflects change in the dielectric constant of the matrix. Change in dielectric constant is indicative of the change in water content of soil sample.

2.3 Measurement of soil moisture by standard Stevens Hydra probe

The Stevens hydra probe is the dielectric constant sensor which provides the simultaneous soil moisture, salinity of the soil, temperature, dielectric permittivity and electrical conductivity of the soil. Marine grade stainless steel tines using high grade epoxy potting makes hydra probe a robust sensor. It has basically three major components: cable, sensor and tines. Hydra probe has a wave guide which sends the electromagnetic waves which is received by the center tine. The body of hydra probe contains microprocessors, circuit boards and all the required electrical components. The four tines in hydra probe are 5cm in length that is suitable for surface measurements and wiring could be extended up to 2 meter based on use.

2.4 Measurement of soil moisture by in-house developed in-situ soil moisture sensor

The in-house developed sensor is an integrated smart soil sensor, which is designed based on modular approach. Voltage signal is sent across the active electrodes and raw ADC values are processed to get dielectric constant and electrical conductivity, which is further utilized in deriving soil moisture. High grade stainless steel probes are penetrated in soil for moisture measurement, multiple probes are multiplexed along a hub to increase the volumetric sample area and via a communication module data is sent to the in-house developed android app. Also the data could be uploaded to cloud servers via smart phone. Standard battery pack of 5V is enough to power the device and lasts a day long and an additional temperature sensor is provided to the device for measurement of soil temperature at the same depth which is used for correction of raw measured Dielectric Constant (DC) and Electrical Conductivity (EC).

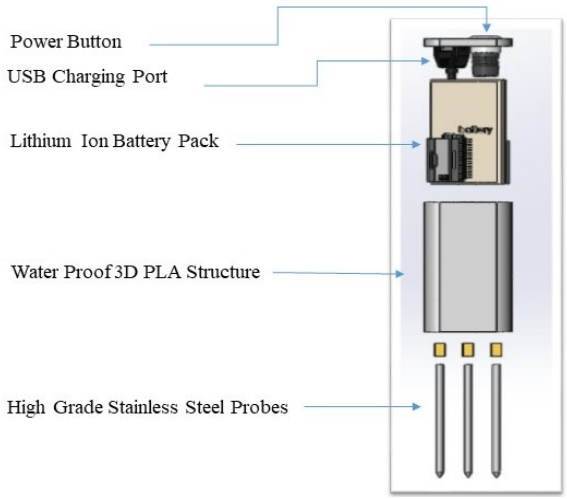

Figure 1: Concept Note

2.5 Data acquisition and processing

2.5.1 HYDRAMON App for Hydra Probe

Hydramon App is particularly used for the data logging of Stevens Hydra Probe which display the sampled readings (data) on the screen for review, received from the processor in Hydra probe. App could be interfaced with the Hydra probe via its Wi-Fi network named “Pogo”. This app makes Hydra Probe a modern sensor by eliminating the need of data logger as the data is logged in the smartphone itself. The Hydramon app has a front display screen that shows different parameters of the soil: raw ADC reading with derived pore water electrical conductivity, raw real dielectric permittivity, raw imaginary dielectric permittivity, soil temperature in Fahrenheit or Celsius, soil moisture percentage and bulk electrical conductivity. The soil measurement is stored in .csv format and can easily be emailed for further analysis.

2.5.2 ICT probe Data Logging:

MP306 has hand held meter for receiving the output which is connected through a cable length of 4.5 meter (can be

extended by using suitable cable) shows the volumetric water content present in the soil (VSW%). The meter provides power to the MP306 ICT for the reading, storage and to display the values. MP306 is connected to a set of chrome extension rods which have T handle on the end with connect the hand held meter when being used. Input voltage required for enabling the probe is 7-18 V DC unregulated.

2.5.3 Android App for in-house developed Sensor

In order to make the in-house sensor field friendly an app interface was developed to visualize the data (Figure 2). For field purposes the stop-&-go functionality is very important and the app designed aims to fulfil that. To sample a large area of field within a short duration, sampling time has to be reduced; therefore, digital data logging has an important role to play. For post processing purpose is logged in a tabular file format that could easily be taken up on laptop/PC for data analysis. Note-taking and field photograph capability is also embedded in the app as it is important to understand the field condition like soil properties, crop type, field undulations, rainfall, etc.

2.5.4 Features of the developed app

a) Bluetooth interface
b) Date & time of observation
c) Latitude and longitude of position
d) Dielectric permittivity (temperature corrected)
e) Soil moisture (in %)
f) Electrical conductivity (ds/m)
g) Soil temperature
h) Report field condition as notes
i) Data logging capability as .csv format
j) Data visualization through in-built viewer
k) Data sharing through Gmail, WhatsApp, Bluetooth etc.
l) Field photographs

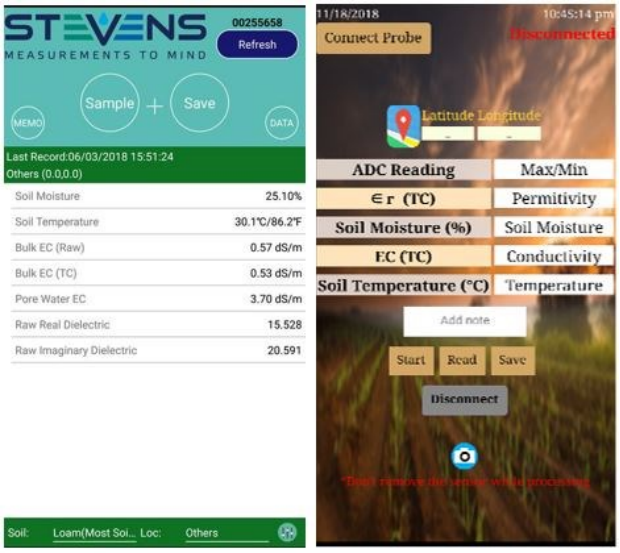

Figure 2: (a) Hydramon App; (b) Android app for in-house sensor

2.6 Measurement of soil moisture content by gravimetric method

Soil moisture measurement through gravimetric method represents the ratio of the mass of water content present in the soil sample to the dry weight (drying in the oven) of the soil sample or also it is defined as the ratio of volume of water to the total volume of soil sample. This can be achieved by calculating weight of the wet soil sample and second sampling after drying in the oven for at least 24 hours at 100°C to 110°C temperature. Difference between both the weights gives water mass. Temperature 100-110°C shows the boiling point of the water and it does not consider the physical and chemical property of the soil. For calculating soil moisture by gravimetric method some precision value of ±0.001 g is added to balance out the variations.

2.6.1 Material

1. Oven dry operating at 100-110°C
2. Tool to collect soil sample
3. Aluminum cans

2.6.2 Procedure

Weight of the can is calculated before taking the soil sample and recorded for further calculation. Soil sample is taken according to the size of can and weight is measured on a calibrated weighing scale. Can containing the sample is placed in the oven at the temperature of 100-110°C. After 48 hours (According to AAU observatory) sample is taken out and weight value is recorded (dry soil + can). Soil moisture is then calculated according by standard formula and procedure repeated for different soil samples.

$$Ratio = \frac{(Wet\ wt. - Can\ Wt.) - (Dry\ wt. - Can\ Wt.)}{(Dry\ wt. - Can\ wt.)}$$

$$\%SM = Wt.ratio * Bulk\ Density * 100$$

3. Validation

For absolute validation through gravimetric analysis, ground truth was carried out in and around Anand Agricultural University (AAU), Anand District, Gujarat (India). Anand Agricultural University has diverse field conditions and therefore it is suitable for validation. Most fields were harvested or being ploughed. Sandy-loamy soil is present with some amount of clayey soil. Gravimetric sampling facility available in observatory building was utilized for sampling and procedures. Sample collected from field was oven dried at 105°C for 48 hours. Soil moisture within Anand Agriculture University (AAU) varied from 10 to 35 volumetric percentage. Sensor Soil moisture measurement are plotted on single graph to create a comparative study. All the sensors follow similar pattern of variations which represents either field variability or some error in measurement when they are located within a 5 cm radii as shown in figure 3. Following graph is linear representation of measured soil moistures by various probes. Surface soil moisture measured using in-house developed sensor and commercial sensor was compared with gravimetric sampling techniques (Figure 4).

Figure 3: (a) Soil sampling at 5 cm, (b) Placement of sensors around sampling site and (c) Oven drying samples

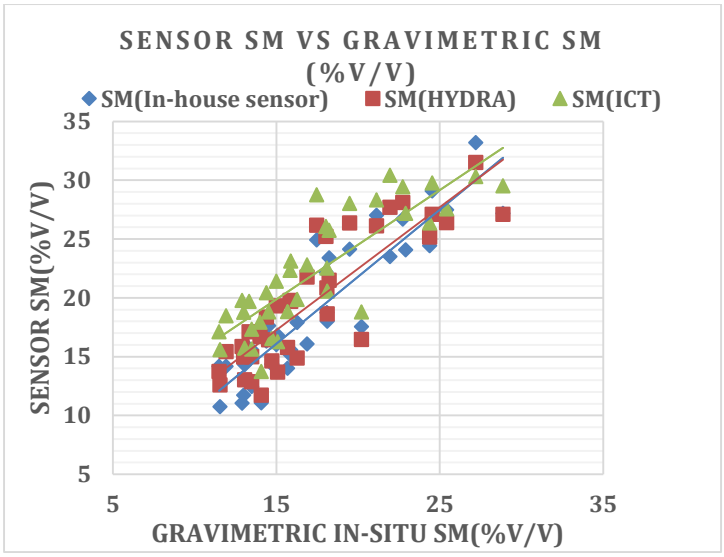

Figure 4: Graphical representation of Sensor measured SM Vs. Gravimetric measured SM

4. Statistical analysis

Performance matrix was generated to determine field capabilities of the sensors being tested. Comparatively in-house sensor showed least bias among the three sensors owing to its higher degree of calibration before field use and RMSE was found to be 2.94 which falls below prescribed accuracy standards of industrial SM measurement (Table 1).

Table 1: Performance Metrics for field validation of sensors

Comparison of in-house sensor & Commercial probes with Gravimetric samples			
Parameters	IN-HOUSE SENSOR	HYDRA	ICT
Bias(%)	1.45	1.68	4.7
RMSE	2.94	5.21	5.42
ubRMSE(%)	2.56	4.93	2.7
R^2	0.82	0.74	0.72

Unbiased RMSE (Instrument Prediction Error) is also found to be close to the other two sensors which validates the capability of in-house sensor to measure field soil moisture accurately. Results shows that based on the four parameters, sensor with extensive field calibration are able to perform estimation with better accuracy and capture field variation across various soil types. Therefore, it is suggested to calibrate the industrial sensor before approaching for in-situ accurate soil moisture measurement.

5. Results and discussion

Surface soil moisture measured using commercial and in-house developed sensor was evaluated across different fields by gravimetric sampling techniques (Figure 4). Results obtained were analyzed using performance metrics which includes statistical measures R^2 (coefficient of determination), bias, ubRMSE and RMSE (Table 1). The sensors performed satisfactorily over a large range of soil moisture with respect to gravimetric methods and in-house sensor has shown better performance and good agreement (Figure 5) with industrial requirements of soil moisture probes. This in-house developed sensor has high potential to be a simpler and economical alternative to the industrial sensors and would be helpful in development of a dense sensor network for validation of satellite derived soil moisture products at various scales.

Acknowledgements

Authors are grateful and highly acknowledge the overall support provided by Director, SAC, Deputy Director, EPSA. Authors are also thankful to “TREES Training

programme" for constant help and support. Support from Prof. Rucha Dave (Dept. of Basic Science and Humanities, B. A. College of Agriculture Anand Agricultural University, Anand) and her team was highly acknowledged for gravimetric field campaign.

References

Pandey D. et. al., (2016). Development of a Time Series–Based Methodology for Estimation of Soil Wetness Using SMAP Radiometer data: Preliminary results", SAC/EPSA/GHCAG/MHTD/TR/05/2016.

Drinkwater, M., K. Yann, F. Jordi and B. Michael (2009). Exploring the Water Cycle of the Blue Planet - The Soil Moisture and Ocean Salinity (SMOS) mission. ESA bulletin. Bulletin ASE. European Space Agency. 137.

Entekhabi, D., R.H. Reichle, R. D. Koster and W. T. Crow. (2010). Performance Metrics for Soil Moisture Retrievals and Application Requirements, J. Hydrometeor., 11, 832-840.

Thapliyal P.K., P. K. Pal, M. S. Narayanan, and J. Srinivasan (2005). Development of a time-series based methodology for estimation of large area soil wetness over India using IRS-P4 microwave radiometer data, Journal of Applied Meteorology, 44(1), 127-143.

Robinson, D. A., et al. (2008), Advancing process-based watershed hydrological research using near-surface geophysics: A vision for, and review of, electrical and magnetic geophysical methods, Hydrol. Processes, 22(18), 3604–3635.

Vereecken, H, K. Tamir, H. Thomas, K. Roy, H. Jan, H. Johan and V. Jan (2008). Comment on ``Field observations of soil moisture variability across scales'' by James S. Famiglietti et al. Water Resources Research. 44. 10.1029/2008WR006911.

Wagner, W., S. Hahn, R. Kidd, T. Melzer, Z. pari, S. Hasenauer, J. Figa-Saldana, P. de Rosnay, A. Jann and S. Schneider (2013). The ASCAT soil moisture product: A review of its specifications, validation results, and emerging applications. Meteorol. Z., 22, 5–33.

Journal of Geomatics Vol 13 No. 2 October 2019

Tidal effects on bio-optical variability in Gulf of Khambhat using ocean colour monitor on-board Oceansat-2

Rimjhim Bhatnagar Singh[1], Prakash Chauhan[2] and Mini Raman[1]
[1]Space Applications Centre, ISRO, Ahmedabad
[2]Indian Institute of Remote Sensing, ISRO, Dehradun
Email: rimjhim@sac.isro.gov.in

(Received: Dec 21, 2018; in final form: Nov 07, 2019)

Abstract: Every moment, Gulf of Khambhat witnesses a huge load of sediments as well as tremendous amounts of domestic and industrial discharge. Simultaneously, its typical tunnel-like structure leads to one of the highest tidal ranges thereby causing unique churning of the estuarine environment. To understand the complex waters here, bio-optical variability per se, a study was carried out using OCM-2 data. The data was interpreted for two months with simultaneous observations of tidal amplitude and tidal range. Routine observations from OCM-2 data was found to be helpful in monitoring the area covered under sediments thereby affecting the bio-optical signatures. Identification of the permanent turbidity zone as well as the maximum turbidity extent within this time frame was carried out which revealed ~ 110km of the gulf as permanently turbid while the maximum extent reaches ~300 km.

Keywords: Gulf of Khambhat, OCM-2, low and high tide, bathymetry, bio-optical

1. Introduction

India has a coastline of about 7,500 km, with nearly 560 million people living in the coastal districts and union territories (iomenvis.nic.in). According to the naval hydrographic charts, the Indian mainland consists nearly of 43% sandy beaches, 11% rocky coast with cliffs and 46% mudflats and marshy coast. The coastal area accounts for a very significant share of India's economic infrastructure. On the other hand, they are also subjected to recurrent natural disasters such as cyclones and floods which often lead to substantial changes in physical and biological characteristics. The west coast of India is a region of high wave activity during the southwest monsoon (Sanil Kumar et. al., 2006). At about 1600 km, Gujarat on the west coast has the longest coastline amongst the Indian states (iomenvis.nic.in). It has two Gulfs viz. the Gulf of Kutch and the Gulf of Khambhat. Gulf of Khambhat is a shallow and complex natural basin formed by south to north penetration of Arabian Sea. The entire gulf is relatively shallow, compared to Arabian Sea, with the maximum water depth of about 30m (Giardino et. al., 2014). The gulf is intercepted by many inlets of sea and creeks formed by confluence of many rivers like Sabarmati, Narmada, Mahi, Tapi and Shetrunji. These rivers form estuaries and download huge volume of sediments into the sea (Deshkar et al., 2012). The concentration of sediments in the surface water of Gulf of Khambhat is greater than 4mg/l and at the bottom more than 8mg/l (Vora et al, 1980). The typical funnel structure of the gulf experiences high tidal variations due to the combined effect of geometry and bottom friction. Tidal range varies from 10 m at Bhavnagar, Gulf of Khambhat to 0.5 m along the peninsular tip of India (Giardino et al., 2014; Kumar and Kumar, 2010). The measured current speed is roughly more than 3 m/s in the Gulf (Kumar et al, 2010). The high tidal energy along with a large number of fine sediments brought by the rivers makes the water always turbid with high suspended load (Sinha et al, 2010). High turbidity influences the oxygen content of the water and light penetration, thereby directly affecting the aquatic life (www.snh.org.uk), corals (https://scholarspace.manoa.hawaii.edu) etc. Moreover, the rivers also drain tremendous loads of domestic and industrial wastes into the gulf. Together, these have resulted in the degradation of the environment and decline in biodiversity of the otherwise significantly rich gulf.

Therefore, regular monitoring of estuaries is important for conserving aquatic life. So, in this direction data from Ocean Color Monitor, on-board Oceansat-2 was investigated for studying the optical variability of watercolour due to tidal influence.

2. Methodology

2.1 Study Area

The Gulf of Khambhat, Gujarat, lies in the west coast of India and north of the Arabian Sea between 20"00N−22"30N, and longitude 71"00E−73"00E (Figure 1). The longitudinal stretch of the Gulf is about 115 km. It is a home of many major rivers like Mahi, Narmada, Sabarmati and Tapti and many other rivulets.

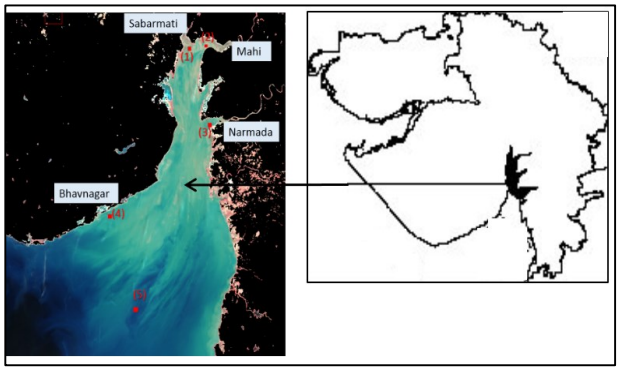

Figure 1: Study area-Gulf of Khambhat

2.2 Methods

Radiance data from Ocean Colour Monitor (OCM) onboard Oceansat-2 was used for this study. Oceansat-2 was launched in September 2009. It carried three payloads-OCM, ROSA and Ku band pencil-beam

scatterometer. OCM-2 is almost similar to OCM-1 except the fact that band 6, located at 670nm is shifted to 620nm and band 7 is shifted from 765nm to 740nm. The broad specifications of OCM are as tabulated in Table 1 below.

Table 1: **Specification of Ocean Colour Monitor on-board Oceansat-2**

No. of bands	8 (402-885nm)
Bands	B1=404-424nm B2=431-451nm B3=476-496 nm B4=500-520 nm B5=546-566 nm B6=610-630 nm B7=725-755 nm B8=845-885 nm
IGFOV (at nominal altitude)	360x250 m
Quantization	12 bit
LAC at 360m and GAC at 4km	

The geocoded data was available every alternate day for the study site. In this study, OCM data was studied for a period of two months, starting from January 1, 2017, until February 28, 2017. Land areas were masked using the data values in band 8.

Gulf of Khambhat was routinely observed vis-a-vis tidal table of Bhavnagar at Oceansat passing time of 12.00 noon. Tidal tables were generated using model WXtide32 version 4.7 (http://wxtide32.com). The low, as well as high tide, were matched with the extent of turbid area in the gulf. Also, as tidal range is directly related to turbidity (Uncles et al, 2002), this parameter is also evaluated over the test time frame of two months. Turbid water extent was also studied vis-à-vis bathymetry of the gulf. Shallow water bathymetry map was generated using gridded data from General Bathymetric Chart of Oceans (GEBCO) of British Oceanic Data Centre (www.gebco.net).

3. Results

Starting from January 1, 2017, till February 28, 2017, data from OCM-2 was obtained every alternate day. A total of five control points were taken to observe the variation in turbidity and changes in radiance pattern with time and tidal effects. The points were taken at each of the confluence regions of rivers Sabarmati, Narmada and Mahi, near Bhavnagar and at the far end of the funnel (shown in figure 1).

The true colour image is shown in figures 2a and 2b give an overview of the ocean colour over a period of two months. At the onset, it can be said that the waters within the Gulf of Khambhat are highly turbid. This indicates huge sediment deposition from three major rivers-Sabarmati, Narmada and Mahi. At the mouth of the gulf, a sudden change of watercolour is seen which indicates shallow regions of phytoplankton presence and finally leading to deep water. High turbidity is observed at most of the times. It may be attributed to high tidal range during the day or the occurrence of low tide, thereby revealing the underwater surface

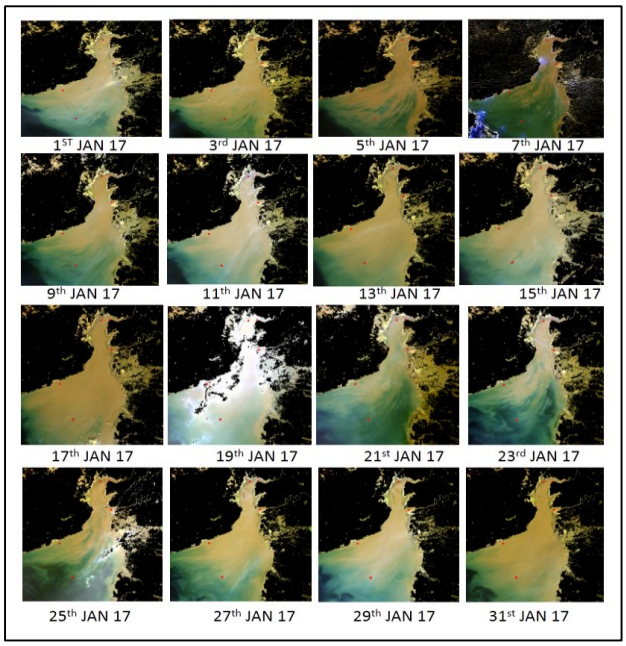

Figure 2a: OCM data focusing gulf of Khambhat along with five control points for the month of Jan-2017

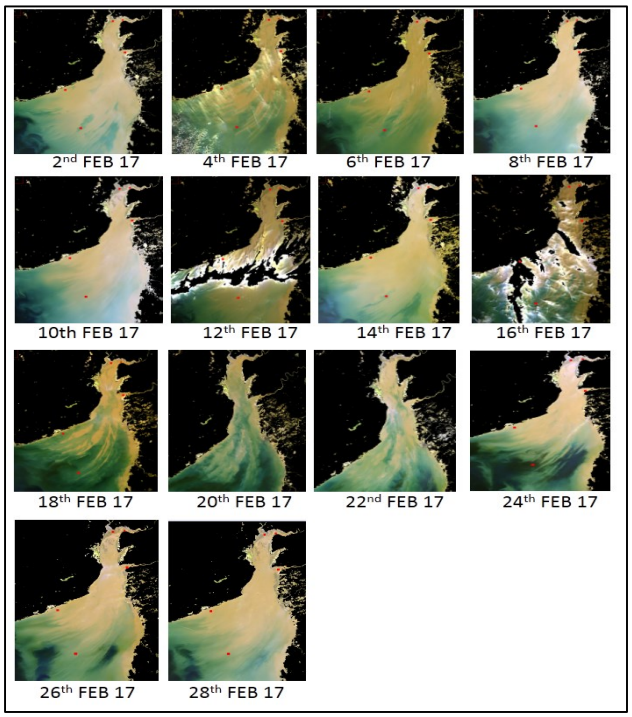

Figure 2b: OCM data of gulf of Khambhat along with five control points for the month of Feb-2017

To add to the visual clarity, density slicing of the study area was done, shown in figures 3a-b. Band 6 was used for density slicing and a total of five classes were made. It helps in identifying the boundary of sediment sweep under the tidal influences. Deep blue sea falls under 0-2 mW/sqcm/nm/str (blue) while highly turbid waterfalls under 4-5 mW/sqcm/nm/str (brown) class.

It may be seen from the figures that clear demarcation can be made for highly turbid and clean waters. Consequently, class distribution analysis was carried out as shown in figure 4.

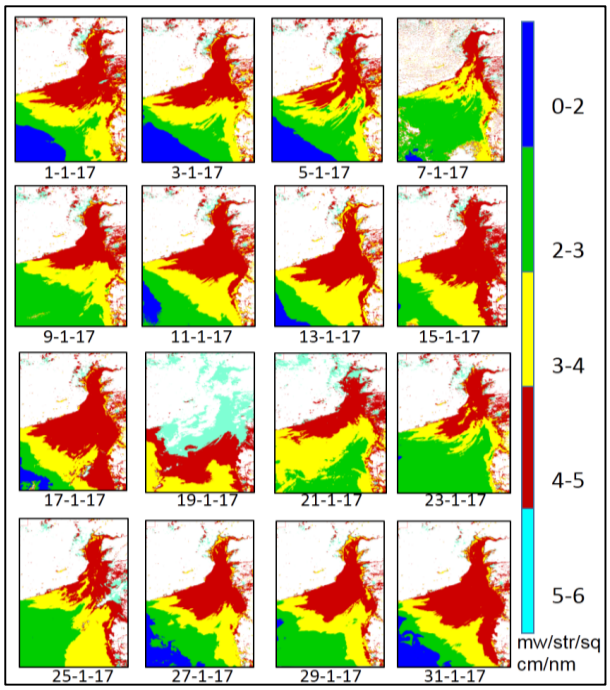

Figure 3a: Density sliced image for Gulf of Khambhat for the month of Jan-2017

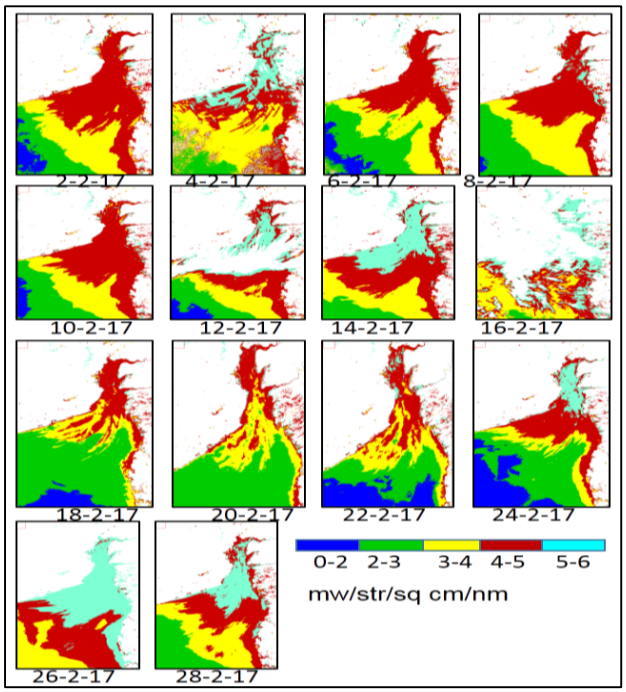

Figure 3b: Density sliced gulf of Khambhat image for the month of Feb-2017

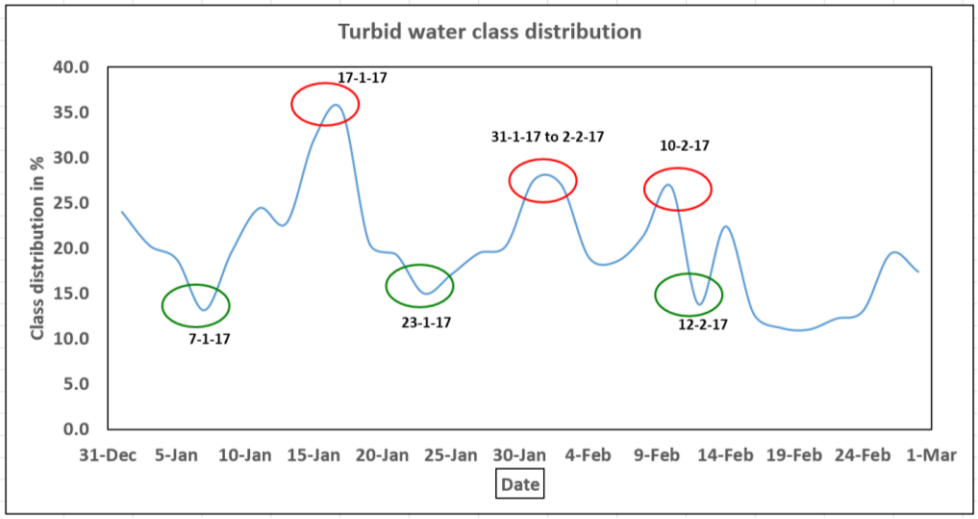

Figure 4: Turbid water plot for gulf of Khambhat during Jan-Feb 2017

For 17th January 2017, nearly one-third of the gulf was turbid while on 31-1-17 and 2-2-17, more than one-fourth of the gulf was turbid. This is shown in the three peaks of the graph, showing a high spread of sediments. On the contrary, three troughs are also noticed, where only around 10% of the gulf is turbid. This can be attributed to the occurrence of tidal cycle of significant amplitudes, shown in figure 6. For 17th Jan 2017, high tide of amplitude > 10m was encountered a couple of hours before the image capture. And when the water retreats, it takes away a lot of suspended soil with it. A similar pattern is seen for the other two dates. In case of the dates of low turbidity, high tidal amplitude is observed at the time of imaging. This exposes the massive tidal bars for the image on 7th January 2017. For the date of 12th Feb 2017, false trough is seen owing to a huge patch of cloud cover. This image is not considered for interpretation. From figure 5, it may be seen that the tidal bars correspond with the shallow regions of the gulf.

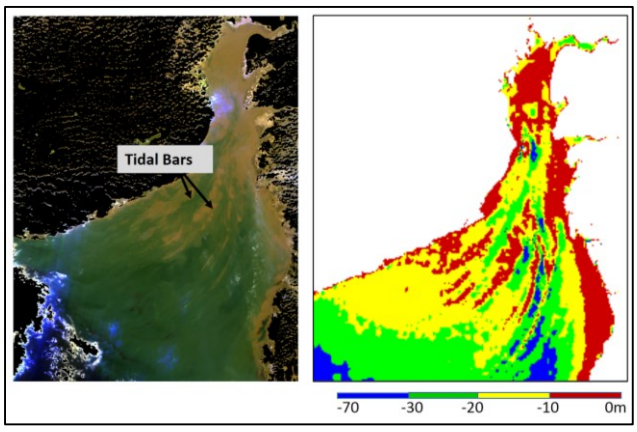

Figure 5: Tidal bars of image dated 7th Jan 17 (left) and bathymetry map (right)

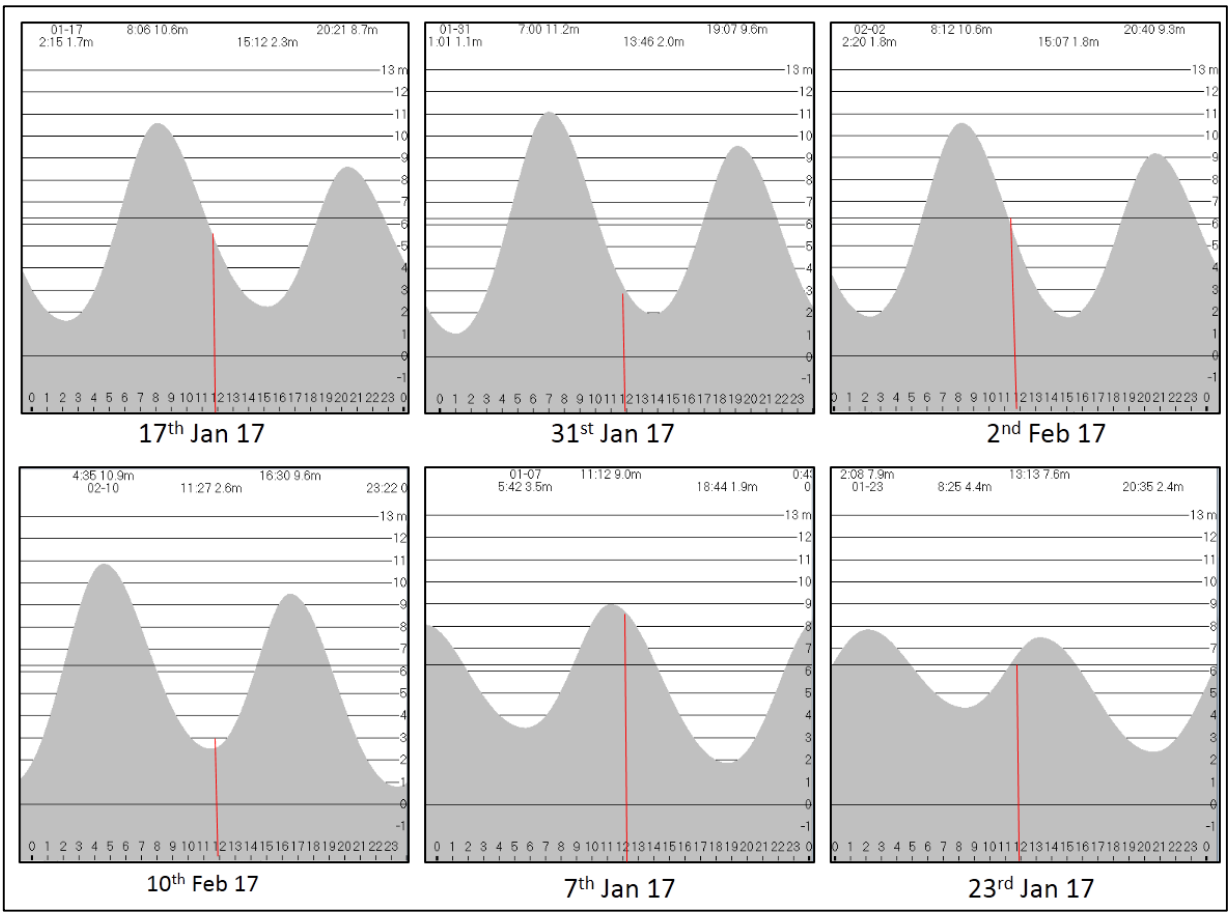

Figure 6: Tidal cycle for the dates of peaks and troughs

For the highest extent, > 300 km of the gulf is covered with turbid water while for the other case, ~150km of the gulf is turbid, for the tidal amplitude of <9m. It may be implied that in case of high tidal amplitude (>9m), the turbid extent of the gulf may further reduce. If one looks at the bathymetry map shown in figure 5, it becomes relevant to note that the turbidity dominates in the regions having bathymetry between 0 to -30m for the cases pertaining to case 1. In case 2, water remains highly turbid for bathymetry between 0 to -10m.

Furthermore, control points were observed for turbidity level, tidal amplitude and range for different dates, shown in table 2 in order to achieve more clarity about the interpretation. Here, visual observation of turbidity was recorded. Only two classes were made for this category- turbid (H) and non-turbid (L). On relating figures 4,5 and table 2 for January 1,3, 11, 13, 15, 17, 27, 29, 31 & February 2, 10,12, 14, 26 and 28, it is observed that at all control points, the turbidity level was high. This may be attributed to low tidal amplitude but high tidal range, thereby washing away huge loads of sediments. In cases like January 5, 7 and 9, where high tide is encountered, points 4 and 5 continue in low turbidity condition, particularly unaffected by the high tidal range

Table 2: Observations of turbidity level (low/high) and tidal amplitude at 12.00 noon for the time frames of study

No. of Control Point	Date	Turbidity level (Low(L) /(High (H))	Tidal amplitude, Tidal Range (m) (Bhavnagar)	Date	Turbidity level (Low(L) /(High (H))	Tidal amplitude; Tidal Range (m) (Bhavnagar)
1	Jan 1, 2017	H	3.2; 9.7	Feb 2, 2017	H	4.6; 8.8
2		H			H	
3		H			H	
4		H			H	
5		H			H	
1	Jan 3, 2017	H	4.5; 9.1	Feb 4, 2017	H	6.8; 7.6
2		H			H	
3		H			H	
4		H			L	
5		H			L	
1		H			H	

2	Jan 5, 2017	H	6.9; 7.5	Feb 6, 2017	H	8.4; 6.8
3		H			H	
4		L			H	
5		L			L	
1	Jan 7, 2017	L	7.8; 7.1	Feb 8, 2017	L	5.2; 8.4
2		L			L	
3		L			H	
4		L			H	
5		L			L	
1	Jan 9, 2017	H	7.5;7.1	Feb 10, 2017	H	2.7; 10
2		H			H	
3		H			H	
4		L			H	
5		L			H	
1	Jan 11, 2017	H	3.7; 10.4	Feb 12, 2017	H	2.1; 10.5
2		H			H	
3		H			H	
4		H			-	
5		H			H	
1	Jan 13, 2017	H	2.3; 11.4	Feb 14, 2017	H	2.7; 9.6
2		H			H	
3		H			H	
4		H			H	
5		H			H	
1	Jan 15, 2017	H	2.9; 11	Feb 16, 2017	-	4; 7.9
2		H			-	
3		H			-	
4		H			-	
5		H			-	
1	Jan 17, 2017	H	4.8; 8.9	Feb 18, 2017	H	5.8; 6
2		H			H	
3		H			H	
4		H			L	
5		H			L	
1	Jan 19, 2017	-	6.8; 6.7	Feb 20, 2017	L	7.2; 4.6
2		-			L	
3		-			L	
4		-			L	
5		-			L	
1	Jan 21, 2017	L	7.8; 5.3	Feb 22, 2017	L	6.1; 5.5
2		L			L	
3		L			H	
4		L			H	
5		L			L	
1	Jan 23, 2017	H	7; 5.5	Feb 24, 2017	L	4.2; 7.8
2		H			L	
3		H			H	
4		L			H	
5		L			L	
1	Jan 25, 2017	L	4.8; 7.3	Feb 26, 2017	H	2.4; 9.4
2		L			H	
3		H			H	
4		H			H	
5		L			H	
1	Jan 27, 2017	L	3.2; 9	Feb 28, 2017	H	1.7; 10.2
2		L			H	
3		H			H	
4		H			H	
5		H			H	
1		H				

2	Jan 29, 2017	H	2.6; 8.5	
3		H		
4		H		
5		H		
1	Jan 31, 2017	H	2.9; 10.1	
2		H		
3		H		
4		H		
5		H		

4. Conclusion

This study was predominantly aimed at broadly investigating OCM data for deriving meaningful interpretation of the oceanic waters. Hence, the focus was planned at the Gulf of Khambhat, which, pertaining to its unique geography, encounters heavy sediment load from three major estuaries and then opens up into deep ocean with wide funnel-shaped mouth. The area also encounters high tidal range due to structure for most parts of the month. The data was interpreted for two months with simultaneous observations of tidal amplitude at Oceansat passing time of 12.00 noon as well as tidal range within the time frame of twenty-four hours. It was found that for majority part of the study time frame, the waters towards narrow region of the funnel remain highly turbid, while the other part, following mixing with open water, becomes heavily rich in sediments. In future, this kind of study in larger time frames shall help in understanding the time-dependent variability in marine productivity of this region. It was also found that the turbidity dominates in the regions having bathymetry between 0 to -30m for the cases pertaining to case 1. In case 2, water remains highly turbid for bathymetry between 0 to -10m. Additionally, in waters of low turbidity, high tidal amplitude exposes the massive tidal bars, verified through the bathymetry of the region. Furthermore, this study indicates the use of OCM data for shoreline erosion studies also.

References

Deshkar, S., J. Lakhampurkar and D. Gavali (2012). State of three estuaries of Gulf of Khambhat, Indian Journal of Geo-Marine Sciences, 41 (1),15-25.

Giardino, A., E. Elias, A. Kumar and K. Karunakar (2014). Tidal Modeling in the Gulf of Khambhat based on a numerical and analytical approach, Indian Journal of Geo-Marine Sciences, 43(7), 25-36.

http://wxtide32.com/download.

https://scholarspace.manoa.hawaii.edu/bitstream/10125/4240/1/vol25n2-234-248.pdf.

Kumar, V. and K. Kumar (2010). Waves and Currents in Tide dominated location off Dahej, Gulf of Khambhat, India Marine Geodesy, 33(2-3), 218-231.

Sanilkumar, V., K.C. Pathak, P. Pednekar, N.S.N. Raju and R. Gowthaman (2006). Coastal processes along the Indian coastline, Current Science, 91 (4), 151-158.

Sinha, P. C., G. K. Jena, I. Jain, A.D. Rao and M.L. Husain (2010). Numerical Modeling of Tidal circulation and sediment transport in the Gulf of Khambhat and Narmada estuary, West coast of India, Pertanika Journal of Science and Technology, 18 (2), 293.

Uncles, R.J., J.A. Stephens and R.E. Smith (2002). The dependence of estuarine turbidity on tidal intrusion length, tidal range and residence time, Continental shelf research 22, 1835-1856.

Vora, K.H., A.R. Gujar and S.M. Karisiddaiah (1980). Soundwaves of the gulf of Khambhat, Indian Journal of Marine Science, 9, 90-93.

www.gebco.net/data_and_products

www.oceanservice.noaa.gov/eduactions/kits/estuaries/estuaries02_economy.html

www.snh.org.uk/publications/online/advisorynot

Journal of Geomatics Vol. 13, No. 2, October 2019

Influence of sea surface temperature and chlorophyll-a on the distribution of particulate organic carbon in the southwest Bay of Bengal

Priyanka Kandasamy*[1], Ranjit Kumar Sarangi[2], Saravanakumar Ayyappan[1], Deepraj Allimuthu[1], Shanthi Ramalingam[1] and Poornima Durairaj[1]
[1]Centre of Advanced study in Marine Biology, Faculty of Marine Sciences, Annamalai University, Tamilnadu
[2]Marine Ecosystem Division, BPSG/EPSA, Space Applications Centre (ISRO) Ahmedabad
Email: *annaipriyan@gmail.com

(Received: Jan 02, 2019; in final form: Nov 11, 2019)

Abstract: Particulate Organic Carbon (POC) plays a vital role in the ocean carbon cycle. POC is responsible for large fluxes of carbon and is linked to many important ocean biogeochemical processes. Nowadays, improved ocean colour sensor provides better understanding of the Sea Surface Temperature (SST), chlorophyll-a and POC distribution in the oceans with good spatial resolution. Better retrieval of POC from satellite data is envisaged to improve our ability to study the ocean biogeochemical cycle. In this context, the present study was carried out to understand the spatial and temporal changes of POC in the year 2017. Validation of VIIRS derived SST, chlorophyll-a and POC with in-situ measurements showed the better correlation of SST (R^2 = 0.77, Mean Normalized Bias (MNB) = ±0.004, Root Mean Square Error (RMSE) = ±0.23 and Standard Error of Estimate (SEE) = ±0.42), chlorophyll-a (R^2 =0.74, MNB = ±0.035, RMSE = ±0.13, and SEE =±0.23) and POC (R^2 =0.73, MNB = ±0.011, RMSE =±89.42, and SEE =±29.53) in the southwest Bay of Bengal respectively. The basin average of monthly composited VIIRS data showed the maximum chlorophyll-a (0.54 µgl-1) and POC (108.72 $mgCm^{-3}$) during monsoon in the month of November and minimum chlorophyll-a (0.25 µgl-1) and POC (62.60 $mgCm^{-3}$) observed during summer in the month of May. In contrast, monthly composite SST showed the minimum basin average (27.77°C) during monsoon in the month of December and the maximum (30.76°C) during summer in the month of May due to increased incoming solar radiation with cloud free sky compare to monsoon which experienced dense cloud cover with decreased light intensity at the surface of the ocean. The multiple regression analysis between POC, SST and chlorophyll-a demonstrated the better agreement between the variable with R^2 of 0.66 POC = 195.040 – 5.310 (SST) + 110.059(chl a) and suggested the strong positive influence of chlorophyll-a on the distribution of POC while the SST acted in a reverse manner in the southwest Bay of Bengal. The observed positive relationship between chlorophyll-a and POC in multiple linear regression analysis suggesting the influence of monsoon inputs and primary production on the distribution of POC. However, the negative relationship between SST and POC in MLR depicted that the increased SST hindered the primary production rate due to the strong stratification at the surface layers which results the unavailability of nutrients at the surface waters.

Keywords:SST, Chlorophyll-a, POC, validation, regression, southwest Bay of Bengal

1. Introduction

The exchange of carbon dioxide (CO_2) between the atmosphere and ocean is a critical component of the global carbon cycle and climate system (Sabine et al., 2004; Gruber et al., 2009). The ocean plays an important role in the global carbon cycle as it is a sink for about half of the anthropogenic carbon production (Sabine et al., 2004). An improved knowledge of the Particulate Organic Carbon (POC) reservoir is of interest to research on ocean biogeochemical cycles, ocean ecosystems, and climate studies relating to the ocean carbon cycle (Houghton, 2007).

POC plays a vital role in the ocean carbon cycle. The POC is responsible for large fluxes and is linked to many important ocean biogeochemical processes. The satellite ocean-color signal is influenced by particle composition, size and concentration and provides a way to observe variability in the POC pool at a range of temporal and spatial scales. There are many studies on the distribution of POC in the Pacific and Atlantic Ocean (Romankevich, 1984; Gordon and Cranford 1985; Yoro et al., 1997). However, little information is available on the distribution of POC (Bhosle et al., 1988) in the Indian Ocean in general, and in the Bay of Bengal in particular (Radhakrishna et al., 1978; Bhattathiri et al., 1980; Nandakumar et al., 1987).

Sea Surface Temperature (SST) is a fundamental variable at the ocean-atmosphere interface (Donlon et al., 2009). It affects the complex interactions between atmosphere and ocean at a variety of scales. Thus, SST datasets with high quality are needed for many applications, such as operational monitoring, numerical weather, and ocean forecasting, climate change research, and so on (Tu et al., 2015). SST data are often used in combination with chlorophyll-a to relate bloom events to mixed layer depths (Villareal et al., 2012) or upwelling zones (Thomas et al., 2012; Shi and Wang, 2007). Moreover, they are an important factor in marine carbon cycling and energy fluxes (Hedges, 2002; Hoikkala et al., 2015; Kuliński et al., 2014).

In many coastal regions, the resuspension of sediments is also an important source of POC. Bottom POC concentration in a shallow sea can rise up to three times under the influence of resuspension when the wind speed increases (Hung et al., 2000). Furthermore, physical mechanisms constitute important control factors for POC distribution. For example, convective mixing induced by decreasing temperature is the main reason for POC to

exhibit a uniform vertical profile in the water column (Zhao et al., 2003). Most importantly, evidence of sinking particles carrying POC out of the euphotic zone, a potential strategy to sequester CO_2 from the atmosphere, is still poorly understood. Bay of Bengal receives large influx of fresh water that decreases the sea-surface salinity. Moreover, the presence of weak winds (<10 m s -1) and warm sea-surface temperature (>28°C) results in strong stratification of the surface of the ocean and hence shallowing the mixed layer. SST and sea surface salinity (SSS) are directly related to surface heat and freshwaterfluxes. More importantly, these surface values are linked to atmospheric circulation, and their inter-annual variability, could have implications for larger-scale climate. As a result, low or no nutrients are injected into the surface waters thereby, influencing biological production (Kumar et al., 2007). However, the efficiency of the biological carbon pump to sequester atmospheric CO_2 and export particulate organic carbon from the surface is not well known. Nowadays, the availability of satellite derived ocean color products such as chlorophyll-a and POC has been the focus of numerous studies in the ocean observations at a large extent.

Although, the spatial distribution and seasonality of POC have been described in several reports (Gustafsson et al., 2014; Hoikkala et al., 2015; Kulinski et al., 2011; Maciejewska and Pempkowiak, 2014), only few studies are available in the validation of POC (Haeentjens et al., 2017; Szymczycha et al., 2017; Swirgon and Stamska, 2015). Similar such works are scanty in the Bay of Bengal that pertained on the POC distribution of and spatio-temporal variability. Hence our present study aimed to assess the spatial and temporal variability of POC and its interrelationship with SST and chlorophyll-a in the coastal waters of the southwest Bay of Bengal.

2. Materials and Methods

The Bay of Bengal is north-eastern part of the Indian Ocean, extended between the latitude 5°N to 30°N and longitude 80°E to 105°E (Figure 1). This is a semi enclosed basin alike the Arabian Sea, bounded by India on the west, by Bangladesh, Myanmar, and part of India on the north, and Burma and Malaysia in the east. The present study was carried out along the Tamilnadu coast falling in the southwest Bay of Bengal viz., transect of our study area are in Chennai, Cuddalore, Parangipettai and Nagapattinam, which are major prominent coastal stations in the east coast of Bay of Bengal.

1.1. In-situ measurements

In-situ SST,chlorophyll-a and POC were measured at five fixed sampling stations along the southwest coast of Bay of Bengal from 2nd February to 4th February 2018. On 2nd February Nagapattinam station was covered, 3rd February Parangipettai and Cuddalore stations were covered and 4th February Chennai station was covered. The stations were fixed with the help of Global Positioning System (GPS) at 5 km from shore and at an interval of 1 km between sampling point.Water samples were collected at the surface waters by using a Niskin water sampler. Sea Surface Temperature (SST) was measured using a digital multisensor of ±0.01°C accuracy (Merck Millipore-Multi 3420). The SST measurements were carried out using handeld multisensor temperature probe in the surface waters and the data was transmitted through USB interface. Chlorophyll-a concentration was measured by following the method of UNESCO (1994) using UV-VIS spectrophotometer (Shimadzu- UV 2450), calibrated previously with standard chlorophyll-a (Sigma – C6144), using 90% acetone. POC concentrations were determined by combustion of sample filters through pre treated 47mm Whatman GF/F filters and samples were treated with chromic acid fumes to remove the inorganic carbon and estimation were done by following the standard methods described by Parsons et al. (1984).

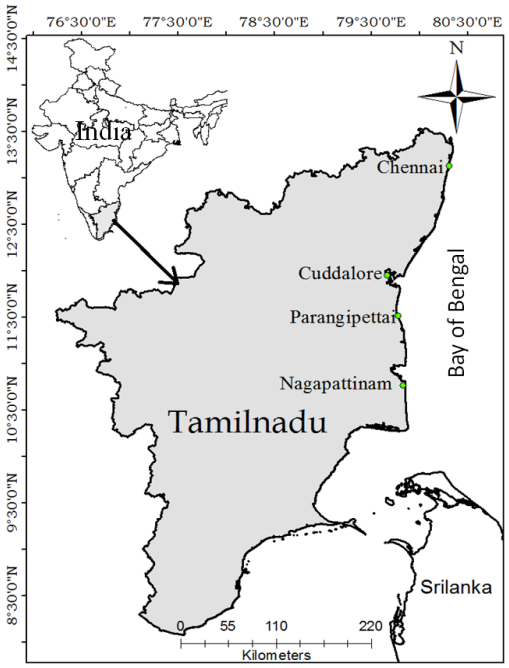

Figure 1: Map showing the study area

2.2. Remote sensing observations

Satellite measurements greatly increases the spatial and temporal extent of observations available for characterizing SST, Chlorophyll-a and POC dynamics and their relations to various dominant physical forcings to the surface ocean specifically POC from satellite images to understand the dynamics and cycling of carbon in the ocean.The Suomi National Polar-orbiting Partnership (SNPP) satellite Visible Infrared Imaging Radiometer Suite (VIIRS) derived 1 km SST, chlorophyll-a and POC image were acquired from the Ocean colour web for 3rd February 2018.The satellite derived images were processed by using SeaDAS 7.4 ver. software for interpretation and analysis. Validation of satellite derived SST, chlorophyll-a and POC products were done by using concurrent in-situ measured SST, chlorophyll-a and POC data in the southwest Bay of Bengal.

2.3.Statistical analysis

The evaluation process involved comparing satellite derived values with the field measurements. Statistical fitting was applied to these data using SigmaPlot (Ver.12.0) statistical software. Mean Normalized Bias

(MNB), Root Mean Square Error (RMSE) and Standard Error of the Estimate (SEE) were analyzed to test the performance between insitu and satellite. Standard error of the estimate (SEE) has been used to provide a numerical index in between satellite and insitu data performance and graphical criteria such as regression plots provide indication of the linear behavior of the fit.Mean normalized bias is a measure of the over or underestimation of the true values. Root mean square error provides a good measure of data scatter for normally distributed variables and gives useful information of the accuracy between satellite and in-situ data. These errors are defined as follows,

$$SEE = \sqrt{\frac{\sum(X-X^1)^2}{N}} \text{------ (1)}$$

$$RMSE = \frac{1}{N}\sum\sqrt{(X-X^1)^2} - - - (2)$$

$$MNB = \frac{1}{N}\sum\frac{(X-X^1)}{X^1} \text{-----(3)}$$

Where X = insitu data, X^1 = satellite data and N = number of points.

Multiple Linear Regression (MLR), is the simplest and most analogues to the bivariate techniques commonly used and thus provide the most readily interpretable results. It was carried out to calculate the values of a dependent variable, given a set of predicted variables which was used to determine the extent to how the variables contributed to the POC concentration.

3. Results and Discussion

The satellite images of SNPP-VIIRS derived SST, chlorophyll-a and POC were retrieved on 3rd February 2018 covering the southwest Bay of Bengal (Figure 2-4).

3.1. Validation of VIIRS derived SST

VIIRS derived SST data was validated with in-situ data to evaluate the performance of VIIRS and exhibited the good agreement with significant correlation co-efficient of R^2 = 0.77 with Standard Error of Estimation (SEE) of ±0.42, Mean Normalized Bias (MNB) of 0.004 and Root Mean Square Error (RMSE) of ±0.23 (Figure 2). The data points fall outside of the 95% confidence band suggests that the satellite derived values were higher or lower than they should be in natural waters. The relationship between the in-situ and VIIRS derived SST showed a highly significant relationship. Tu et al., (2015) investigated comparison between the VIIRS SST and in-situ SST, based on the overall comparison result showed that all types of in situ SST have very high correlation with the VIIRS SST. Similarly, our study also showed good correlation between in situ SST and VIIRS SST.

3.2. Validation of VIIRS derived chlorophyll-a

VIIRS derived chlorophyll-a data was validated with in-situ data to evaluate the performance of VIIRS and exhibited the good agreement with significant correlation co-efficient (R2) of 0.74 with SEE of ±0.24, MNB of 0.038 and RMSE of ±0.13 (Figure 3). The relationship between in-situ and VIIRS derived chlorophyll-a showed very less significant relationship due to uncertainties. VIIRS shows higher spatial coverage and detection accuracy than MODIS, after coefficient improvement. VIIRS is also able to predict chlorophyll-a with 53% accuracy (Zeng et al., 2016). Validation of the VIIRS ocean color products by inter-comparison with in situ observations, confirming good matchup of the water, leaving radiance between ship and VIIRS data (Arnone et al., 2012).

3.3 Validation of VIIRS derived POC

Validation of VIIRS derived POC showed good agreement with insitu estimations of POC (R^2=0.73, SEE = ±29.50, MNB = ±0.01 and RMSE = ±89.42). Recently (Everskings et al., 2017) five different POC empirical algorithms were validated with in situ data. Among the five algorithms, Stramski et al., (2008) found the better algorithm for the better retrieval of POC. It is therefore important to continue the validation work to improve the reliability of in-situ and satellite POC determinations. Haeentjens et al., (2017) validated the float POC with VIIRS and MODIS derived POC. Float-based POC estimates agree well with NASA's algorithm, but also exhibit a large spread (relativelylow prediction capability) in matchups. The uncertainty of the POC for both sensors(MODIS R^2 = 0.44 and VIIRS R^2 =0.40) is very close to the one from the algorithm used (Stramski et al., 2008) which has Root mean square differences (RMSD) =21.3 mg m-3, Root mean square relative deviation (RMSRD) =21.7%, R^2=0.87, for N=53 suggesting the POC derived from VIIRS agrees well with the float POC within uncertainty specified

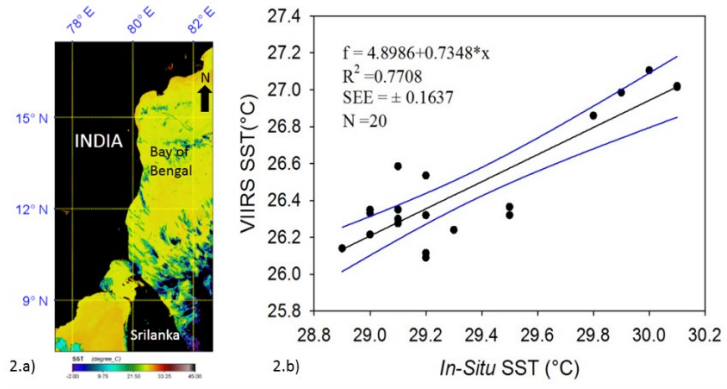

Figure 2: a) SNPP-VIIRS derived (3rd February 2018) image of SST; b) Regression plot of *in-situ* SST Vs VIIRS derived SST

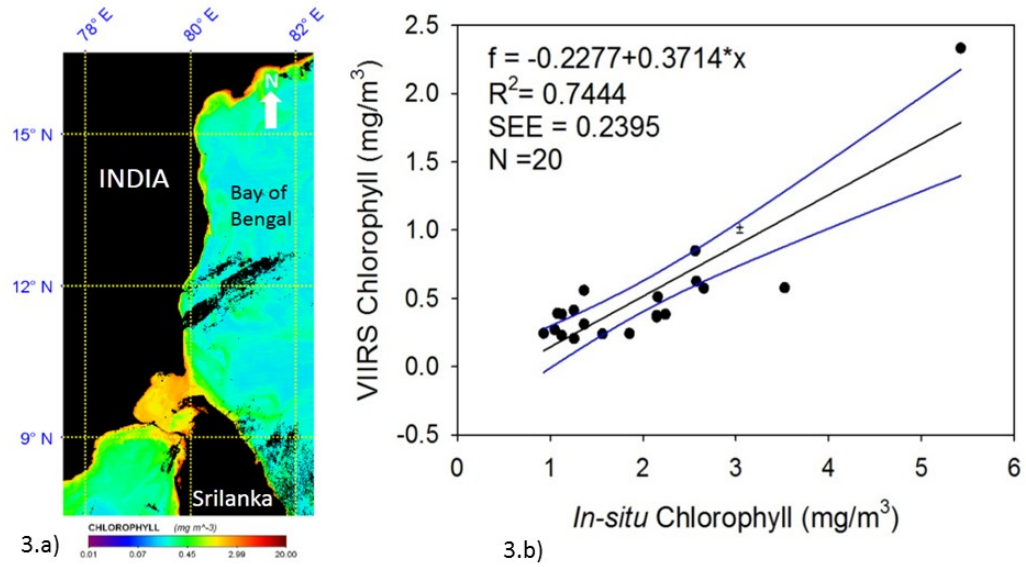

Figure 3: a) SNPP-VIIRS derived (3rd February 2018) image of chlorophyll-a; b) Regression plot of *in-situ* chlorophyll-a Vs VIIRS derived Chlorophyll-a

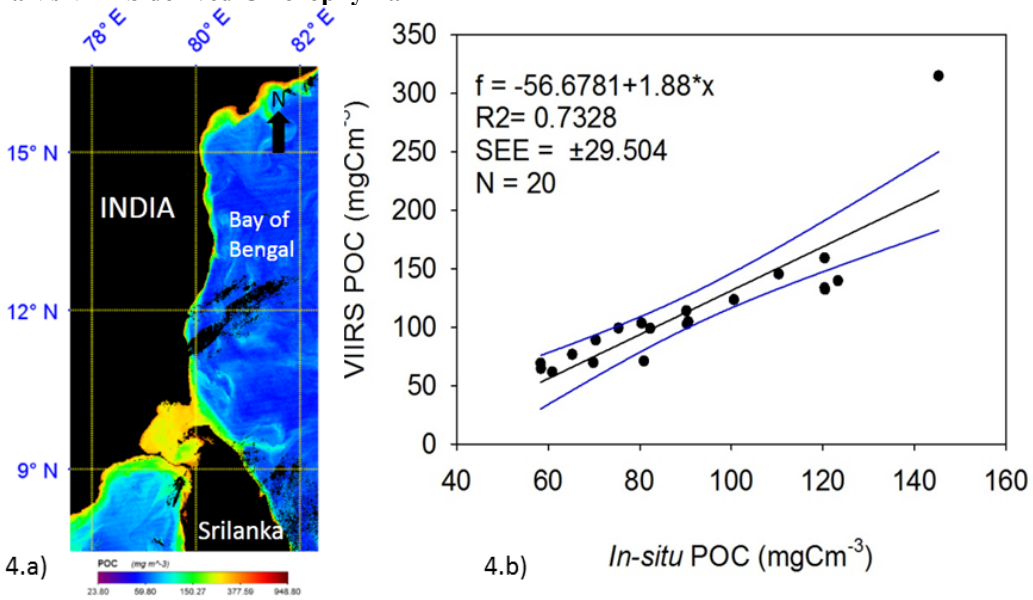

Figure 4: a) SNPP-VIIRS derived (3rd February 2018) image of POC; b) Regression plot of in-situ POC Vs VIIRS derived POC

3.4. Seasonal variability of SST

Seasonal variability of SST in the southwest Bay of Bengal was studied from the monthly composite images of VIIRS derived SST (Figure 5). The SST concentration has been varied from 26.7 to 31.1°C in the southwest Bay of Bengal and registered its highest concentration (31.1°C) at Nagapattinam during the Summer season and the lowest concentration observed during the Post monsoon (26.7°C) at Nagapattinam coastal waters.

The basin scale averages of SST in the southwest Bay of Bengal clearly indicate the seasonal pattern of SST with the maximum SST in the month of May (30.76^0C) (Figure 6) during summer season. The minimum SST concentration was observed during December (27.06^0C) month of monsoon followed by January (27.08^0C), February (27.25^0C) during the postmonsoon season. As SST increases in summer there is a concurrent thermal stratification of the water column in the vertical dimension and the thermocline (the strongest gradient of temperature) progressively deepens. In contradictory, SST decreases during monsoon and early postmonsoon of January and February vertical mixing is enhanced and thermal stratification reduced until well mixed conditions are reached in monsoon again. During the premonsoon season SST was moderately present in July, August and September around 29^0C. This process explains SST patterns at large latitudinal gradients depending on seasonal variation in atmospheric temperatures. This clearly depicted the well-known bi-modal distribution of surface temperature (Colborn, 1975) in the Bay of Bengal

.

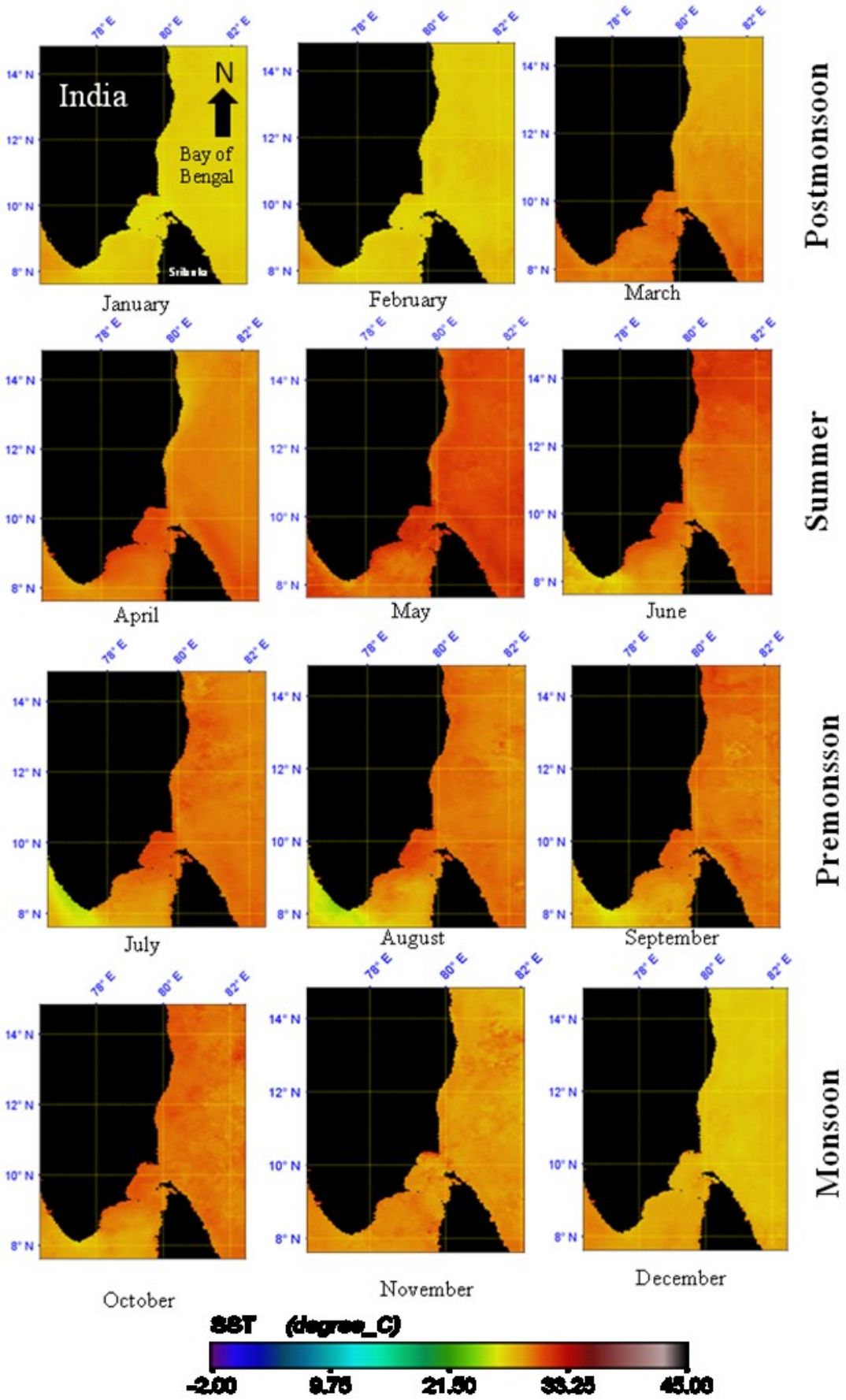

Figure 5: SNPP-VIIRS monthly composite of SST from January to December in the year 2017

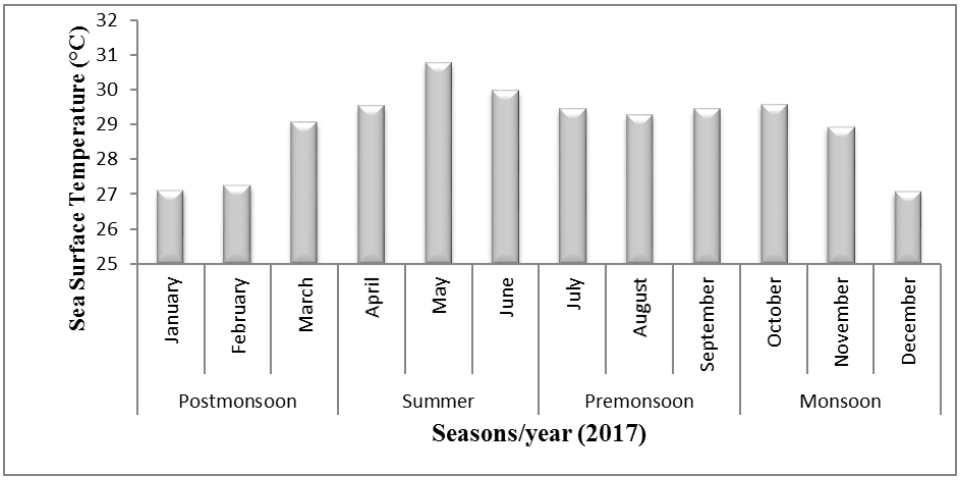

Figure 6: Seasonal variation of basin averaged SNPP-VIIRS derived Sea surface temperature in the southwest Bay of Bengal

3.5 Seasonal variability of chlorophyll-a

Seasonal variability of chlorophyll-a in the southwest Bay of Bengal was studied from the monthly composite images of VIIRS derived chlorophyll-a (Figure 7). The chlorophyll-a concentration has been measured as a representative of the phytoplankton biomass varied from 0.13 to 2.31 μgl^{-1} in the southwest Bay of Bengal and registered its highest concentration (2.31 μgl^{-1}) at Nagapattinam during monsoon season and the lowest concentration observed during the summer (0.13 μgl^{-1}) at Cuddalore coastal waters. However, the chlorophyll-a concentration was high in Palk Bay region throughout th year.

Monthly means of chlorophyll-a concentrations (Figure 8) shows clear seasonal pattern with the highest concentration (0.60 µgl-1) during premonsoon (September) followed by monsoon and the lowest value (0.25 µgl-1) was recorded during summer (May). Hence the annual variability indicated that the southwest Bay of Bengal was productive during premonsoon and monsoon seasons rather than the postmonsoon and summer seasons.Higher chlorophyll-a concentration is found during the premonsoon and monsoon due to wind-induced upwelling in the north Indian Ocean compared to other oceans (Yoder, 2001), and also the runoff from southern rivers could explain the enhanced level of nutrients and associated elevated chlorophyll-a (Kumar et al., 2010). During summer, the chlorophyll-a distribution was less due to the incoming solar radiation was higher because of cloud absence combining with low winds, resulting in highly stratified mixed layer depth. This inhibited any vertical mixing, and hence there was no input of nutrients from the subsurface to the upper ocean (Kumar et al., 2010).

3.6. Seasonal variability of POC

Seasonal variability of POC in the southwest Bay of Bengal was studied from the monthly composite images of VIIRS derived POC (Figure 9). The satellite derived POC concentration varied from 50.59 to 304.19 $mgCm^{-3}$ in the southwest Bay of Bengal. The POC level was found highest (304.19 $mgCm^{-3}$) during the monsoon season at Nagapattinam coastal waters, whereas the lowest POC concentration (50.59$mgCm^{-3}$) observed during summer season at Cuddalore coastal waters.

The mean values of POC obtained from spatial and temporal distribution pattern (Figure 10) shows moderate seasonal variation in Southwest Bay of Bengal. The highest POC value (111.163 $mgCm^{-3}$) is observed during early postmonsoon season is January 2017 followed by monsoon season (November 108.721 $mgCm^{-3}$). The distribution of POC was found minimum during summer season in May (62.599 $mgCm^{-3}$). During the premonsoon season POC concentration was moderate (90 - 100 $mgCm^{-3}$). Similar such distribution pattern was observed for chlorophyll-a also in Southwest Bay of Bengal, which clearly suggested the interrelationship between chlorophyll-a and POC.

The spatial distribution of the surface POC concentration in the ocean is generally governed by both the biological processes specifically in primary production and physical process particularly vertical mixing and advection (Stramska, 2014). The significance of the different processes can vary in time and space. Higher values were in fact present in monsoon season because surface primary production is high in the Bay of Bengal during monsoon (Qasim, 1977). Moreover large amount of suspended matter containing high organic matter is introduced into the Bay by major rivers flowing through the various geological formations of the Indian subcontinent (Rao, 1985). Probably this high amount of organic matter and primary production are responsible for the higher values of POC observed during monsoon season. In summer typically have low POC concentration because significant away from the source of nutrients, that the lower primary production might be inhibited due to water stratification (Huang et al., 2013). Accordingly, the POC concentrations are low during May and June, when the values of spatially averaged POC concentrations was 62.599 $mgCm^{-3}$. By November and December, POC concentrations in the Southwest Bay of Bengal are more often greater than 111.163 $mgCm^{-3}$

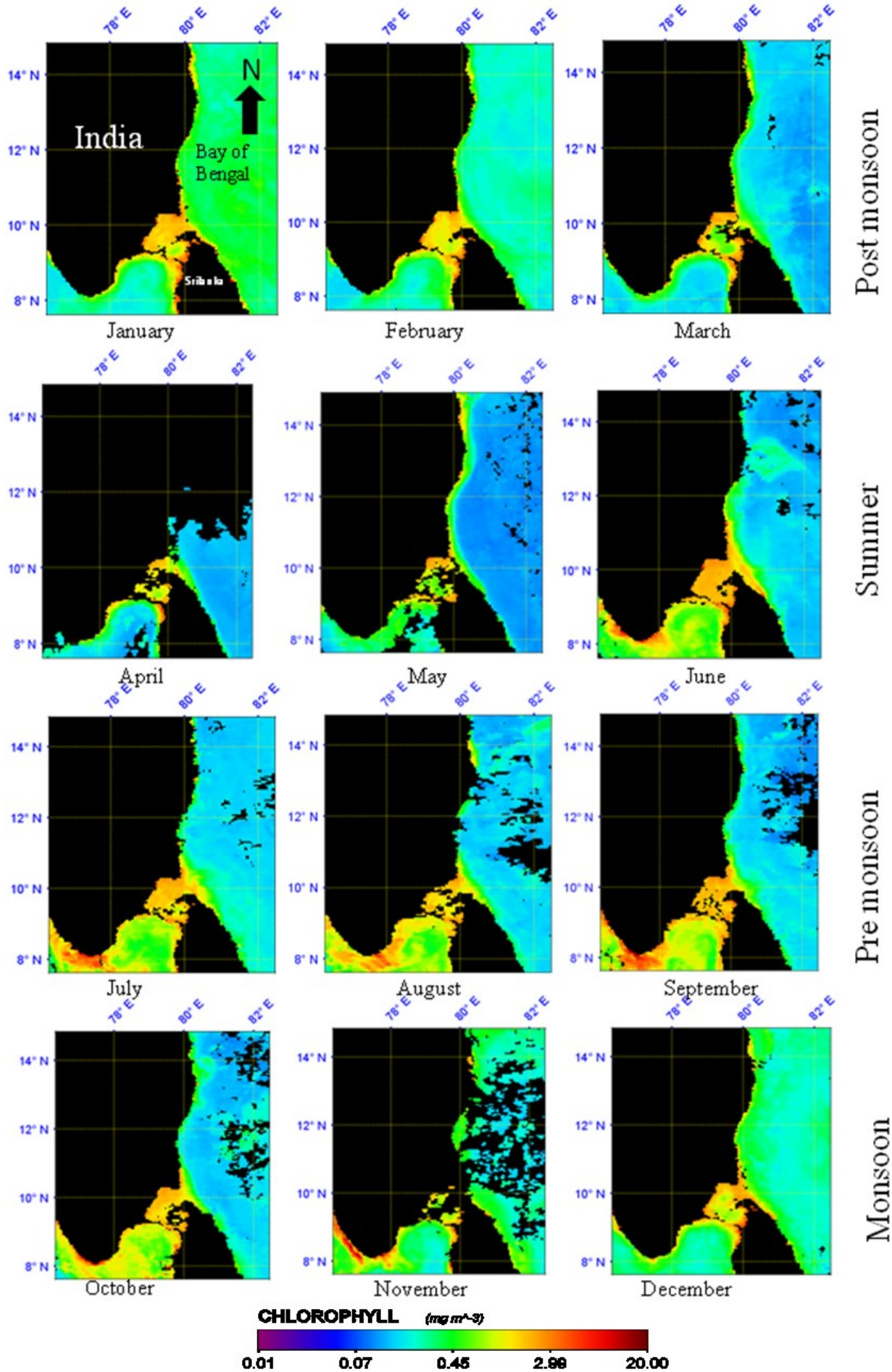

Figure 7: SNPP-VIIRS monthly composite of chlorophyll-a from January to December in the year 2017

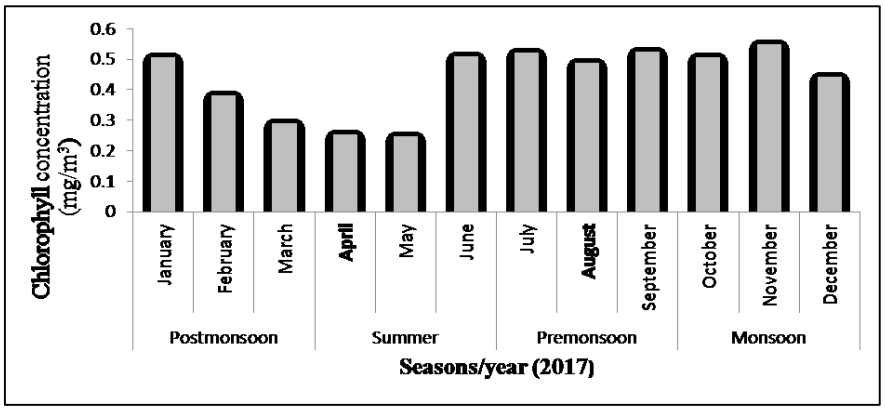

Figure 8: Seasonal variation of basin averaged SNPP-VIIRS derived Chlorophyll-a in the southwest Bay of Bengal

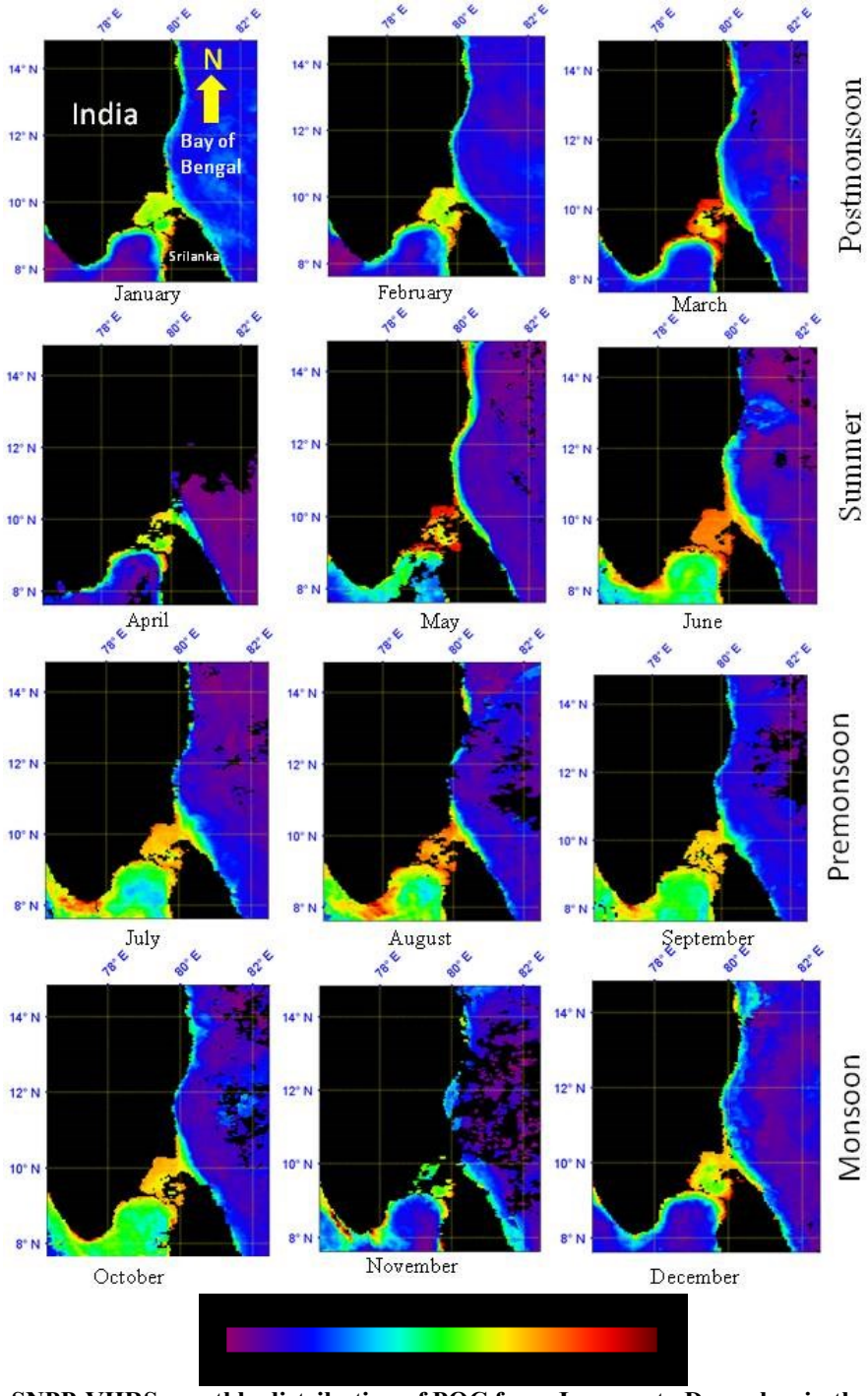

Figure 9: SNPP-VIIRS monthly distribution of POC from January to December in the year 2017

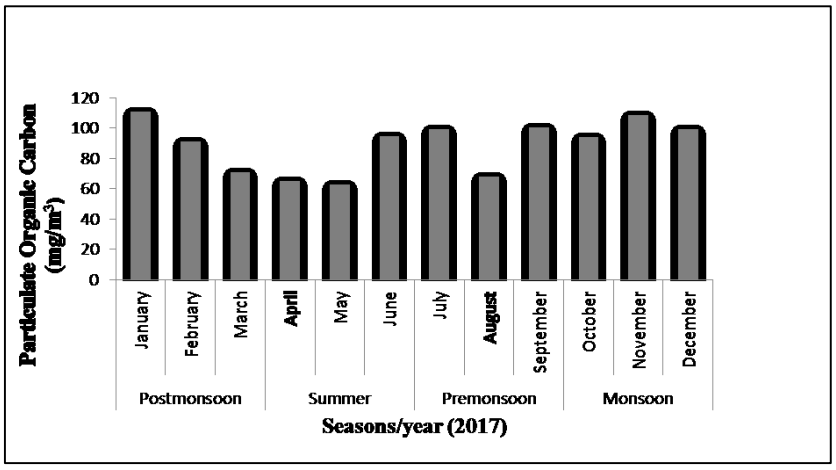

Figure 10: Seasonal variation of basin averaged SNPP-VIIRS derived Particular Organic Carbon in the southwest Bay of Bengal

3.7. Relationship between SST, chlorophyll-a and POC

The pixel/data points falling in the box of concurrent latitude 7.8–14.5N/longitude 77.2 to 82.5E covering the entire southwest Bay of Bengal was taken from the entire image. This was used to generate the mean value of monthly images of SST, chlorophyll-a and POC by using SeaDAS software. Monthly mean value for each dataset were plotted as bar plots to understand the variability in respective timescale and seasons in the figure 6, 8, 10. The resultant mean values of SST, chlorophyll-a and POC in the year of 2017 were analyzed by linear regression of variance on ranks using SigmaPlot (ver. 11) software to distinguish the effects of variables (Figure 11). The differences in the mean values among the different seasons was observed in the year of 2017. There was a statistically significant difference (P =<0.001) between seasons in the distribution of SST, chlorophyll-a and POC.

SST measurements are based on the quantification of infrared radiation leaving the ocean surface (Njoku, 1990) within the spectral range of 650–1200 nm. Water vapor is the largest source of uncertainty in space-borne SST measurements. In Bay of Bengal, (Poornima et al., 2018) stated there is no clear interannual variation in the SST and chlorophyll-a over the decade with the consistent seasonal pattern.

In this study an attempt was made to find the linear relationship between SST, chlorophyll-a and POC. The relationship was found inversely proportional to the SST and chlorophyll-a observed with the R^2 = 0.54, SEE = ±1.03. Similary, SST and POC also found a negative correlation of the R^2 =0.54, SEE = ±1.03.The better agreement between chlorophyll-a and POC observed with the R^2=0.58, SEE = ±1.02 relationship was found positive suggesting that the POC distribution in the southwest Bay of Bengal was highly dependent on the distribution of phytoplankton biomass rather than other physical parameter.

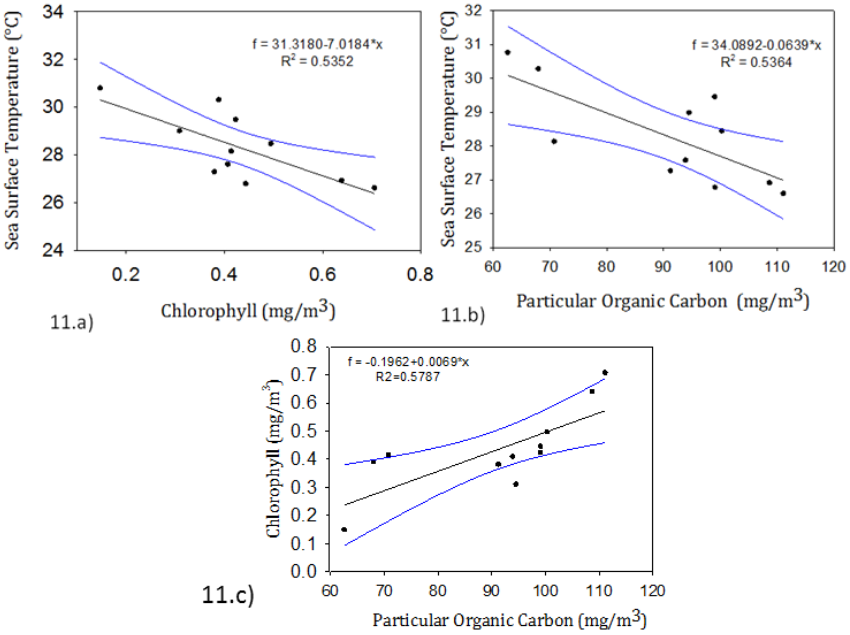

Figure 11: a) Regression analysis of Sea Surface Temperature and Chlorophyll-a, b) Regression analysis of Sea Surface Temperature and Particular organic carbon and c) Regression analysis of Chlorophyll-a and Particular Organic Carbon

3.7. 1. Regression analysis of SST and Chlorophyll-a

In this study an attempt was made to find the linear relationship between SST and chlorophyll-a observed the R^2 = 0.54, SEE = ±1.03 and the relationship was found inversely proportional to the SST and chlorophyll-a. Analysis of relationship between SST and chlorophyll-a increases our understanding of the productivity of the ocean. Satellite images provide reliable important information on oceanographic conditions and simultaneously support marine environmental monitoring and assessment (Nurdin et al., 2014). The present study showed the relationship between the SST and Chlorophyll-a was good around 29°C. When SST was high chlorophyll-a productivity is less. A similar relationship has earlier been reported from the Indian Ocean (Goes et al., 2005).

3.7.2. Regression analysis of Particulate Organic Carbon and SST

The regression analysis between SST and POC was found inversely correlated to the R^2 =0.55, SST = ± 1.03. The observed higher POC formation rate at low temperatures is in a good agreement with observations of (Kang and Cleasby 1995). The POC was less in summer obviously chlorophyll-a also less due to high temperature. Chlorophyll-a showed a fairly good significant positive co-relationship with POC (Fernandes et al., 2009). However, SST was a negative correlation with POC and Chlorophyll-a. Further more, physical mechanisms constitute important control factors for POC distribution. For example, convective mixing induced by decreasing temperature is the main reason for POC to exhibit a uniform vertical profilein the water column (Zhao et al., 2003; Delu et al., 2015).

3.7.3. Regression analysis of Particulate Organic Carbon and Chlorophyll-a

Chlorophyll-a and POC shows the significant relationship of R^2=0.52 and SEE=±0.07. This suggests that an important portion of the POC is composed of marine diatoms, dinoflagellates and/or brown algae which contain chlorophyll-a (Dougherty et al., 1970). Many studies have focused on the relationship between POC and Chlorophyll-a concentration (Morel, 1988; Buck et al., 1996; Legendre and Michaud 1999; Morel et al., 2006) and found the strong correlation between in-situ data with satellite data. They noted that, since chlorophyll-a is readily estimated from satellite data, such relationships provide a simple avenue for estimating POC from satellite data. They also pointed out the importance of POC in ecosystem models as the food source for zooplankton. Linear regression of POC on chlorophyll-a has been used to derive the phytoplankton fraction of the carbon from the slope of the fit, on the assumption that there is a back-ground of POC at sea that is not associated with phyto-plankton (Steele & Baird 1961, Townsend & Thomas 2002, Behrenfeld et al., 2005). The variability observed in the relationship between total carbon and chlorophyll-a arises from 2 main sources, variability in the proportion of non phytoplanktonic particulate carbon and variability in the phytoplankton carbon. The former type of variability is related to the status of the ecosystem as a whole, whereas the latter may be associated with changes in the phytoplankton community itself or with its acclimation to the light or nutrient regime.

3.8. Multiple Linear Regression (MLR)

Multiple regression was employed in order to ascertain the influence of SST and chlorophyll*a* with the dependent variable of POC.

POC = 195.040 – 5.310 (SST) + 110.059 (chl *a*)-------(4)

The above multiple regression equation represent the dependent variable of POC the distribution of chlorophyll-a was highly positively correlated and strongly negatively correlated of SST on the distribution of POC while the SST acted in a reverse manner in the southwest Bay of Bengal. Comparsions of VIIRS POC and Modelled POC (Figure 12) provided reasonably good performance on the POC derivations with RMSE = ± 84.06, Mean Relative Error(MRE) = 45.42 %. in the southwest Bay of Bengal. Moreover, the NASA standard POC algorithm has MRE of ~42% for the open ocean (Swirgon and Stamska, 2015) implies that the performance of present algorithm is acceptable for coastal waters.

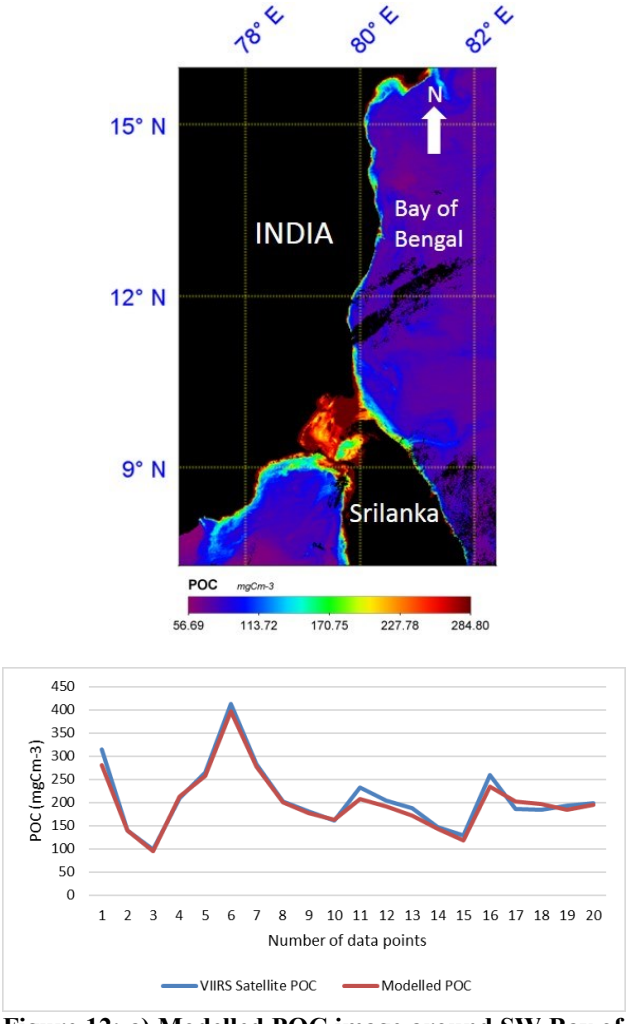

Figure 12: a) Modelled POC image around SW Bay of Bengal b): Comparision between VIIRS Satellite POC and modelled POC

Conclusion

Ocean colour remote sensing has long been recognized as a powerful means for the study of the world's oceans. The present study has clearly shown that *in-situ* Chlorophyll-a and POC concentration was high during monsoon compared to other seasons (POC= 108.72 mgCm-3 and Chl *a*= 0.54 µgl-1). In contradictory, SST decreases during monsoon and increases during summer due to vertical mixing is enhanced and thermal stratification reduced until well mixed conditions are reached in monsoon.

The observed positive relationship between chlorophyll-a and POC in multiple linear regression analysis suggesting the influence of monsoon inputs and primary production on the distribution of POC. However, the negative relationship between SST and POC in MLR depicted that the increased SST hindered the primary production rate due to the strong stratification at the surface layers which results the unavailability of nutrients at the surface waters. Moreover, the seasonal distribution of SST, chlorophyll-a and POC in the southwest Bay of Bengal is influenced by the seasonally reversed monsoon winds, especially southwest monsoon winds which play vital role in enhancing the primary productivity in the coastal waters. However, the northeast monsoon winds and seasonal rainfall also take part in enhancing the productivity during monsoon season.

Acknowledgements
The authors thank the Space Application Centre (SAC), ISRO, Government of India, Ahmedabad for financial assistance to the project as part of the Meteorology and Oceanography (MOP-2) Program of ISRO (MOP-II) and providing facilities for carrying out the work. Special thanks are to Dr. Mini Raman Division Head, Marine Sciences Division, SAC, ISRO, Ahmedabad for her timely help and support.

References

Arnone, R., G. Fargion, P. Martinolich, S. Ladner, A. Lawson, J. Bowers, M. Ondrusek, G. Zibordi, Z.P. Lee, C. Trees, C. Davis and S. Ahmed (2012). Validation of the VIIRS Ocean Color: SPIE Defense and Security Ocean Sensing and Monitoring IV, Baltimore, MD. 8372 83720G-1. https://doi:10.1117/12.922949.

Behrenfeld, M. J., E. Boss, D. A. Siegel and D. M. Shea (2005). Carbon based ocean productivity and phytoplankton physiology from space, Global Biogeochemical Cycles, 19, 1-14.

Bhattathiri, P.M.A., V.P. Devassy and K. Radhakrishna (1980). Primary production in the Bay of Bengal during southwest monsoon of 1978, Mahasagar-Bull. National. Institute of Oceanography, 13, 315–323.

Bhosle, N.B., V.M. Dhople and A.B. Wagh (1988). Distribution of particulate organic carbon in the central Arabian Sea, Procreeding Indian Academy Science, Earth Planetary Science, 97, 35-47.

Buck, K.R., F.P. Chavez and L. Campbell (1996). Basin-wide distributions of living carbon components and the inverted trophic pyramid of the central gyre of the North Atlantic Ocean, summer 1993, Aquatic Microbe Ecology, 10, 283–298.

Colborn, J. G., (1975). The upper layer thermal structure of the Indian Ocean, International Indian Ocean Expedition Monograph No. 2 Honolulu: East-West Central Press, University of Hawaii.

Delu, P, L. Qiong and B. Yan (2015). Review and suggestions for estimating particulate organic carbon and dissolved organic carbon inventories in the ocean using remote sensing data. Acta Oceanologica Sinica, 33(1),pp. 1–10.

Donlon, C. J., I. Robinson, K. S. Casey, J. Vazquez-Cuervo, E. Armstrong, O. Arino, C. Gentemann, D. May, P. LeBorgne, J. Piolle, I. Barton1, H Beggs, D. J. S. Poulter, C. J. Merchant, A. Bingham, S. Heinz, A Harris, G. Wick, B. Emery, P. Minnett, R. Evans, D. Llewellyn-Jones, C. Mutlow, R. Reynolds, H. Kawamural and N. Rayner (2009). The Global Ocean Data Assimilation Experiment (GODAE) high Resolution Sea Surface Temperature Pilot Project (GHRSST-PP), Oceangraphy Magazine.

Dougherty, R.C., H.H. Strain and W.A. Svec (1970). The structure, properties, and distribution of Chlorophyll Journal of American Chemical Society, 92(9), 2826–2833.

Eversking, H., V.M. Vicente, R. J. W. Brewin, G. D. Olmo, A. E. Hickman, T. Jackson, T. S. Kostadinov, H. Krasemann, H. Loisel, R. Rottgers, S. Roy, D. Stramski, S. Thomalla, T. Platt and S. Sathyendranath (2017).Validation and intercomparison of ocean color algorithms for estimating particulate organic carbon in the oceans, Frontier Marine Science, 4(251), 1-20.

Goes, J.I., P.G. Thoppil, R. Gomes and J.T. Fasullo (2005). Warming of the Eurasian landmass is making the Arabian Sea more productive, Science, 308(5721), 545–547.

Gordon, D. C. and P.J. Cranford (1985). Detailed distribution of dissolved and particulate organic matter in the Arctic Ocean and comparison with other oceanic regions, Deep Sea Research I, 32, 1221-1232.

Gruber, N., M. Gloor, S.E.M. Fletcher, S. C. Doney, S. Dutkiewicz, M. J. Follows, M. Gerber, A. R. Jacobson, F. Joos, K. Lindsay, D. Menemenlis, A. Mouchet, S. A. Muller, J. L.Sarmiento and T. Takahashi (2009). "Oceanic Sources, Sinks, and Transport of Atmospheric CO_2." Global Biogeochem. Cycles, 23, 1-21.

Gustafsson, E., Deutsch, B., Gustafsson, B.G., C. Humborg and C. M. Morth (2014). Carbon cycling in the Baltic Sea the fate of allochthonous organic carbon and its impact on air-sea CO_2 exchange. Journal of Marine System, 129, 289-302.

Haeentjens, N., E. Boss, and L. D. Talley (2017). Revisiting ocean color algorithms for chlorophyll-a and particulate organic carbon in the Southern Ocean using biogeochemical floats, Journal of Geophysics Research Oceans, 122, 6583–6593.

Hedges, J.I. (2002). Why dissolved organics matter. In: Hansell, D.A., Carlson, C.A. (Eds.), Biogeochemistry of Marine Dissolved Organic Matter. Elsevier Sci., San Diego, 1-33, http://dx.doi.org/ 10.1016/B978-012323841-2/50003-8.

Hoikkala, L., P. Kortelainen, H. Soinne and H. Kuosa (2015). Dissolved organic matter in the Baltic Sea. Journal of Marine System, 142, 47-61.

Houghton, R. A., (2007). Balancing the global carbon budget, Annual Review of Earth and Planetary Sciences, 35(1), 313–347.

Huang W-J, W.J. Cai, R.M. Castelao, Y. Wang and S.E. Lohrenz (2013). Effects of a wind-driven crossshelf large river plume on biological production and CO2 uptake on the Gulf of Mexico during spring, Limnology and Oceanography, 58(5), 1727–1735.

Hung, C.C., G. T. F. Wong, K.K. Liu, F.K. Shiah, and G.C. Gong (2000). The effects of environmental conditions on the relationship between nitrate reductase activity and NO_3^- uptake, field observations in the East China Sea, Limnology Oceanography, 45, 836– 848.

Kang, L.S. and J.L. Cleasby (1995). Temperature effect on flocculation kinetics using Fe(III) coagulant. Journal of Environment Engineering, 121, 893–901.

Kulinski, K., J. She and J. Pempkowiak (2011). Short and medium term dynamics of the carbon exchange between the Baltic Sea and the North Sea, Continental Shelf Research, 31 (15),1611-1619.

Kulinski, K., B. Schneider, K. Hammer, U. Machulik, and D. Schulz-Bull (2014). The influence of dissolved organic matter on the acid-base system of the Baltic Sea, Journal of Marine System, 132, 106-115.

Kumar, S.P., M. Nuncio, N. Ramaiah, S. Sardessai, J. Narvekar, V. Fernandes and J. T. Paul (2007). Eddy-mediated biological productivity in the Bay of Bengal during fall and spring intermonsoons, Deep Sea Research I, 54(9), 619-1640.

Kumar, S.P., J. Narvekar, M. Nuncio, A. Kumar, N. Ramaiah, S. Sardessai, M. Gauns, V. Fernandes and J. T. Paul (2010). Is the biological productivity in the Bay of Bengal light emitted?, Current Science, 98,1331-1339.

Legendre, L. and J. Michaud (1999). Chlorophyll-a to estimate the particulate organic carbon available as food to large zooplankton in the euphotic zone of oceans, Journal of Plankton Research, 21, 2067–2083.

Fernandes, L., B. Narayan, S.G. Bhosle, P. Matondkar and R. Bhushan (2009). Seasonal and spatial distribution of particulate organic matter in the Bay of Bengal, Journal of Marine Systems, 77,137–147.

Maciejewska, A., and J. Pempkowiak (2014). DOC and POC in the water column of the southern Baltic, Part I. Evaluation of factors influencing sources, distribution and concentration dynamics of organic matter, Oceanologia, 56 (3), 523-548.

Morel, A., 1988. Optical modeling of the upper ocean in relation to its biogenous matter content (case I waters), Journal of Geophysics Research, 93, 10749-10768.

Morel, A., B. Gentili, M. Chami, and J. Ras (2006). Bio-optical properties of high chlorophyll Case 1 waters and of yellow-substance-dominated Case 2 waters, Deep-Sea Research, I., 53,1439–1459.

Nandakumar, K., K., Venkat and N.B. Bhosle (1987). Distribution of particulate organic carbon in the central Bay of Bengal, Procreeding Indian Academy Science, (Earth Planetary Science), 96,189–193.

Njoku, E. G. (1990). Satellite remote sensing of sea surface temperature, In G. L. Geernaert & W. J. Plant (Eds.), Surface waves and fluxes, 2, 211–338.

Nurdin, S., M.A, Mustapha and T. Lihan (2014). The relationship between sea surface temperature and chlorophyll-a concentration in fisheries aggregation area in the archipelagic waters of spermonde using satellite images, Conference: Universiti-Kebangsaan-Malaysia, Faculty-of-Science-and-Technology.
DOI: 10.1063/1.4858699.

Parsons, T.R., Y. Maita and C.M. Lalli (1984). A manual of chemical and biological methods for seawater analysis, 1.7, Determination of Silicate. Pergamon Press,Oxford; New York, 25–27.

Poornima, D., R. Shanthi, L. Senthilnathan, T. Thangaradjou, A. Saravanakumar and R. K. Sarangi (2018). Decadal Pattern of Spatial and Temporal Variability of Nitrate Along the Southwest Bay of Bengal Using Remote Sensing Techniques, Journal of the Indian Society of Remote Sensing. doi.org/10.1007/s12524-018-0915-7(0123456789().,-volV)

Qasim, S. Z. (1977). Biological productivity of the Indian Ocean, Indian Journal of Marine Science, 6, 122-137.

Radhakrishna, K., P.M.A. Bhattathiri, and V.P. Devassy (1978). Primary productivity of the Bay of Bengal during August – September 1976, Indian Journal of Marine Science, 7, 94–98.

Rao, C. H. M., (1985). Distribution of suspended particulate matter in the waters of eastern continental margin of India, Indian Journal of Marine Science, 14, 15-19.

Romankevich, E.A., (1984). Geochemistry of Organic Matter in the Ocean, Springer-Verlag, Berlin, 304-336.

Sabine, C. L., R. A. Feely, N. Gruber, R. M. Key, K. Lee, J. L. Bullister, R. Wanninkhof, C. S. Wong, D.W.R. Wallace, Bronte Tilbrook, F. J., Millero, T.H., Peng, A., Kozyr, T. Ono and A. F. Rios (2004). The oceanic sink for anthropogenic CO2, Science, 305(5682), 367– 371.

Shi, W., and M. Wang, (2007). Observations of a Hurricane Katrina-induced phytoplankton bloom in the Gulf of Mexico, Geophysical Research Letters, 34.

Steele, J.H. and I.E. Baird (1961). Relations between primary production, chlorophyll-and particulate carbon, Limnology Oceanography, 6, 68–78.

Stramska, M., (2014). Particulate organic carbon in the surface waters of the North Atlantic, spatial and temporal variability based on satellite ocean colour, International Journal of Remote Sensing, 35(13), 4717–4738.

Stramski, D., Reynolds, R.A., Babin, M., Kaczmarek, S., Lewis, M.R., Rottgers, R., Sciandra, A., Stramska, M., Twardowski, M.S., B.A. Franz, and H. Claustre (2008). Relationship between the surface concentration of particulate organic carbon and optical properties in the eastern South Pacific and eastern Atlantic Oceans, Biogeosciences, 5,171–201.

Swirgon, M., and M. Stramska (2015). Comparison of insitu and satellite ocean color determinations of particulate organic carbon concentration in the global ocean, Oceanologia, 57, 25-31.

Szymczycha, B., A. Winogradow, K. Kulinski, K. Koziorowska and J. Pempkowiak. (2017). Diurnal and seasonal DOC and POC variability in the land-locked sea, Oceanologia., 59, 379-388.

Thomas, A.C., P.T. Strub, R.A.Weatherbee and C.James (2012). Satellite views of Pacific chlorophyll variability: comparisons to physical variability, local versus nonlocal influences and links to climate indices, Deep Sea Research Part II, Topical Studies in Oceanography, 77(80), 99-196.

Townsend, D.W. and M.Thomas (2002). Spring time nutrient and phytoplankton dynamics on Georges Bank, Marine Ecology Progess Series, 228, 57–74.

Tu, Q., D. Pan, and Hao (2015), Validation of SNPP VIIRS Sea Surface Temperature Retrieved from NAVO, Remote Sensing, **7**(12), 17234-17245.

Villareal, T.A. C. G. Brown, M.A. Brzezinski, J. W. Krause and C. Wilson (2012). Summer diatom blooms in the North Pacific Subtropical Gyre, 2008–2009, PLoS One 7, e33109.

Yoder, J.A., J.E.O. Reilly, A.H. Barnard, T.S. Moore and C.M. Ruhsam (2001). Variability in Coastal Zone Color Scanner (CZCS) chlorophyll imagery of ocean margin waters off the US east coast, Continental Shelf Research 21, 1191–1218.

Yoro, S.C., R. Sempere, C.M. Turley, M.A. Unanue, D. Durieu, X. Madron and M. Bianchi (1997). Cross-slope variations of organic carbon and bacteria in the Gulf of Lions in relation to water dynamics (northwestern Mediterranean), Marine Ecology Progress Series, 161, 255–264.

Zeng, C., H. Xu, and A.M. Fischer (2016). Chlorophyll-a estimation around the antarctica peninsula using satellite algorithms: hints from field water leaving reflectance, Sensors, 16, 2075, 1-14.

Zhao, J., H. Ji, and Z. Guo (2003). The vertical distribution of particulate organic carbon in the typical areas of the East China Sea in winter, Marine Sciences, 27(6), 59–63.

Journal of Geomatics Vol 13 No. 2 Oct 2019

Surveying and mapping of Gandhinagar city using IRNSS/NAVIC system

Jayrajsinh D. Jadeja and P.R Patel
Civil Engineering Department, Institute of Technology, Nirma University,
Email: jayraj.jadeja1121@gmail.com

(Received: Jan 09, 2019; in final form: Nov 18, 2019)

Abstract: Surveying and mapping are the most essential parts of any infrastructure project. The conventional method of surveying is very cumbersome, time-consuming and costly, as it requires a huge workforce to carry out the detailed survey. Due to advancement in space technology, various Regional and Global navigation satellite systems have emerged as an important tool for survey and mapping purpose. India has recently launched its own regional navigation satellite system called Indian Regional Navigation Satellite System (IRNSS) or NAVIC (Navigation with Indian Constellation). In this paper, an initial attempt is made to carry out surveying using high-performance Global Navigation Satellite Systems (GNSS) receiver. The objective of this research is to analyse the stability of the reference station and to prepare the map of Gandhinagar with reasonable accuracy by using the positional data collected from IRNSS/NAVIC system. Two stations, reference station and a temporal station was established at Nirma University campus. The true value and the observed value were measured between both stations using NAVIC receiver. The longer average mean of reference and temporal station were also calculated. The percentage error was 3.44% where true distance was 5.40m and observed distance was 5.22m. Surveying of Gandhinagar was done by using IRNSS/NAVIC receiver and collected data were imported on GIS Platform. The IRNSS/NAVIC receiver has been used here to generate a map, thus its potentials are needed to be explored for various mapping and navigation applications.

Keywords: IRNSS, NAVIC, True value, Observed value.

1. Introduction

In today's scenario, it is necessary to develop a low-cost method, which collects data from the field quickly and is robust in preparing Maps. Traditional methods are Time consuming and costly with many Limitations. In Difficult terrains, conducting survey with surveying instruments is very tedious and sometimes it causes human casualties. Since last two-decade use of Global Navigation satellite system (GNSS) (Geodesy, 1994) like Global Positioning System (GPS) and Globalnaya Navigazionnaya Sputnikovaya Sistema (GLONASS) has increased exponentially in the field of surveying and mapping. The advantages of using GNSS satellite systems over traditional instrumental surveying systems are that the satellite navigation systems are more reliable, economical, efficient and convenient over the conventional methods of surveying. Larger areas can be surveyed with great accuracy within a short time and map of the area can be made after processing the collected data. India has recently launched the navigation satellite system called Indian Regional Navigation Satellite System (IRNSS) or NAVIC (Navigation with Indian constellation). (ISRO-IRNSS-ICD, 2017) IRNSS is an autonomous regional navigation satellite system, which provides navigation and location service to its users. It's been developed by Indian space research organisation (ISRO), for navigation and military purpose. Primary Service area covered by it is Indian regional boundaries and it extended up to 1500 km from the Indian boundaries (Ravi, 2016). IRNSS consist of total three segments Space segment, Ground segment and a User segment. Space consist of 7 satellites, 3 in geostationary orbit and 4 are in geosynchronous orbit. The Ground Segment consists of the IRNSS Ranging and Integrity Monitoring stations (IRIM) and Navigation control centre (INC). The user segment consists of IRNSS receivers operating in different modes Single Frequency mode and Dual-Frequency mode (Ganesh, 2014). The two different services mode offered to IRNSS users are Standard Positioning Service (SPS) and Restricted Service (RS). SPS mode is free of cost to the users and the signals are unencrypted, RS mode is only for few authorised users and the signals are encrypted. There is a need to explore various applications of IRNSS. In this paper, an attempt is being made to develop a low-cost method to collect terrain data and prepare map with reasonable accuracy using IRNSS/NAVIC receiver.

2. Study area and methodology

The capital of Gujarat, Gandhinagar city have been chosen as the study area for this project. It is situated in the western region of India, 23 km north of Ahmedabad. It is also one of the planned city of India. The total area covered by Gandhinagar is 177 km^2 and it has a population of 2, 92,167 and a population density of Gandhinagar city is 1700/ km^2 as of census 2011. Figure 1 shows the coordinates describing the extent of the study area. Figure 2 shows the adopted methodology for surveying and mapping of Gandhinagar

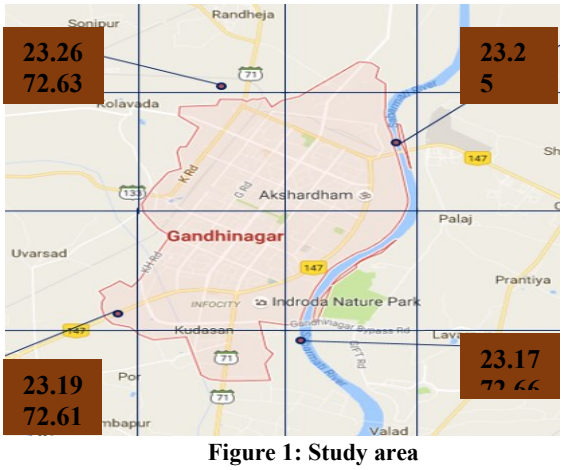

Figure 1: Study area

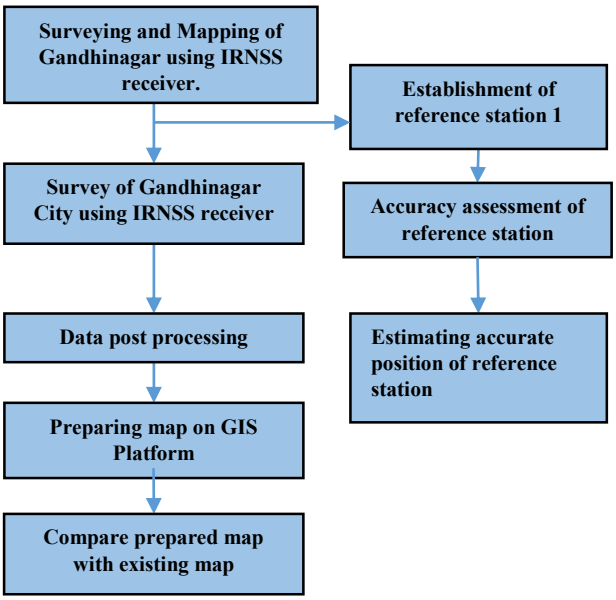

Figure 2: Methodology

3. Experimental setup

A reference station was established at Nirma university campus at B Block building, Institute of Technology. Positional data is being collected regularly for reference station from 21/07/2017. IRNSS Antenna is capable to receive signals of IRNSS L5 and S1 bands and GPS L1 band signals. It has TNC female connector, which Further takes received signals to IRNSS receiver (Figures 3 and 4).

IRNSS receiver is capable of working in three different modes IRNSS, GPS and Hybrid. LED display on receiver provides visual information. The computer system is connected with receiver Via Ethernet cable for data transfer/storage.

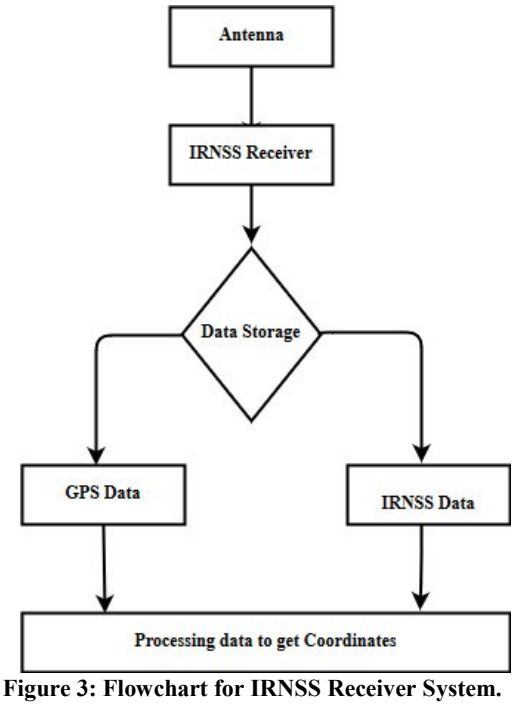

Figure 3: Flowchart for IRNSS Receiver System.

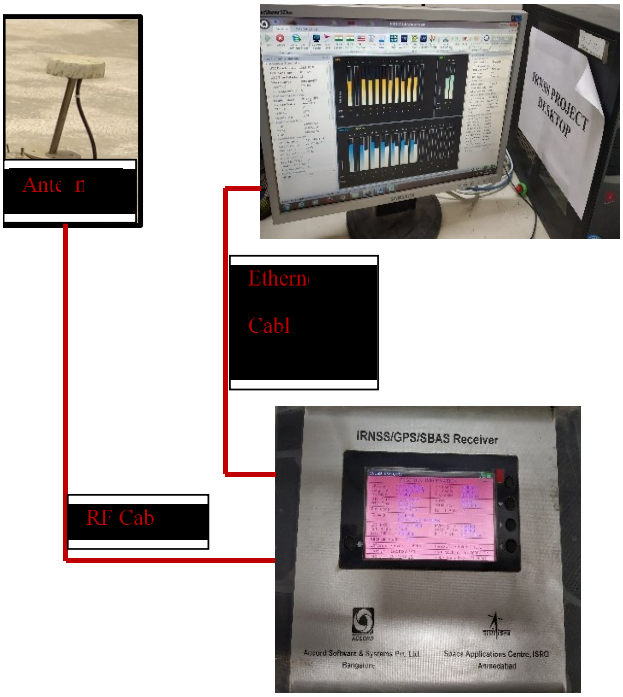

Figure 4: Experimental setup for the IRNSS receiver system

3.1 Estimating accurate position of the reference station

The reference station is continuously collecting positional data for a longer period, data were extracted using IRNSS_UR software. Data output supports two different formats .csv and.rinex. We have used .csv format to extract positional and other required information form the received data. IRNNS and GPS signals are used here to extract positional information. Radio waves get affected by the presence of electrons in the ionosphere, the total electron content (TEC) is the total number of electrons present along with a path between a radio signals transmitter and receiver. Few research studies suggest that the average standard deviations (STDs) of the satellite Differential Code Bias estimated during daytime data are higher than that with night-time data (Li et al. 2015). Therefore, we have used data collected between times 03.00 to 06.00 for better accuracy. Further positional information is extracted from POSB file, it consists of information such as TOWC (Time of week count), Week number, System Status, Block count, Mean sea level Correction and Latitude, Longitude and Altitude (X, Y, Z) of a given point. Average mean of extracted positional information is calculated for 3 hours (03.00 to 06.00) of each day. Position information is retrieved every second so for every three hours, we get 10,800 positional values for reference station. Minimum value, the maximum value and standard deviation of retrieved positional data is calculated for each day. Following are the graphs showing the Mean and standard deviation of Latitude, Longitude and altitude of reference station for the month from July to September (Figures 5-7).

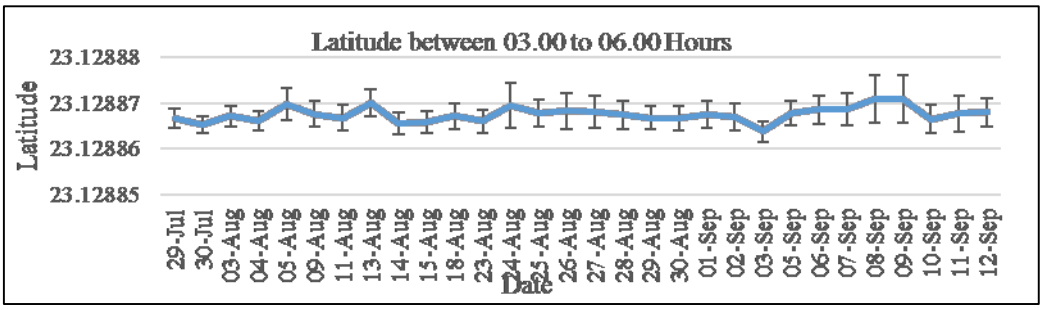

Figure 5: Latitude of the reference station from 29 July to 12 September

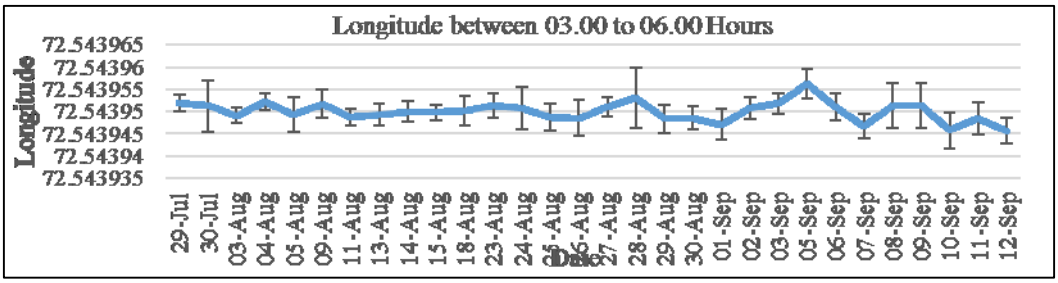

Figure 6: Longitude of the reference station from 29 July to 12 September

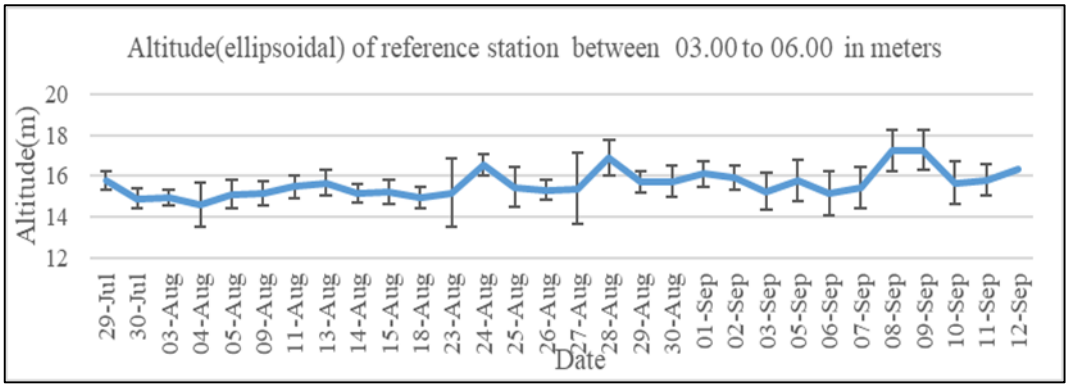

Figure 7: Altitude of the reference station from 29 July to 12 September

3.2 Accuracy assessment of reference stations

In order to check the horizontal stability of received positional data for reference station. The temporal station was established at B Block building, Nirma University campus. It was established 5.40 Meters distance from the reference station (Towards North direction from reference station) (Figure 8). Data had been collected of the temporal station for almost same time-period as of reference station. The longer average mean is calculated of received position data for both reference station and temporal station, so that single most accurate X, Y and Z position value can be estimated. The physically measured distance between temporal and reference station was 5.40 Meters which is termed as the true value and the distance Measured between both stations by calculated longer average mean was 5.22 Meters which is termed as Observed value. Absolute error in the distance was 12 Centimetre and percentage error was 3.34%.

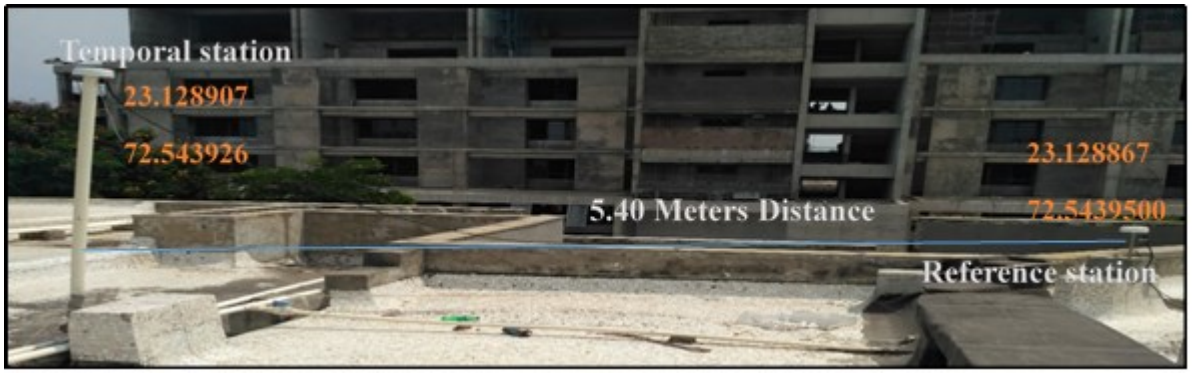

Figure 8: True value and observed value of the distance between the temporal station and reference station.

The temporal station was established for temporary time period i.e. July-2017 to September-2017 and reference station is still in use and data is been collected on regular basis. Following are the graphs showing Month Wise Longer average mean of positional data collected of reference station (Figures 9-11).

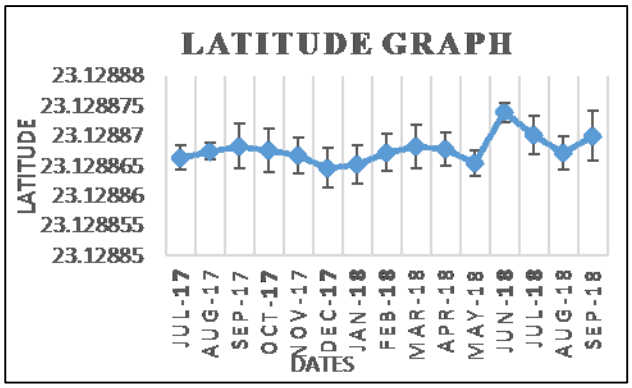

Figure 9: Month-wise graph of Longitude for reference station9

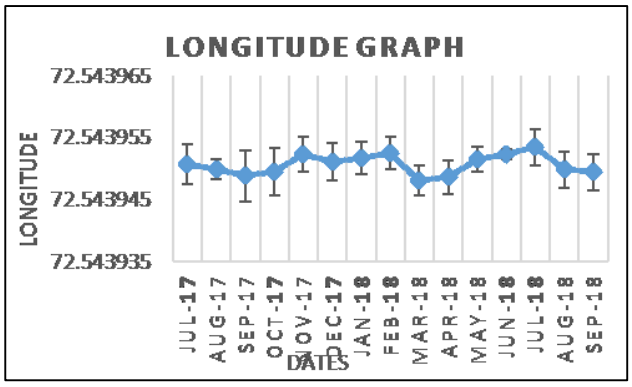

Figure 10: Month-wise graph of latitude for reference station

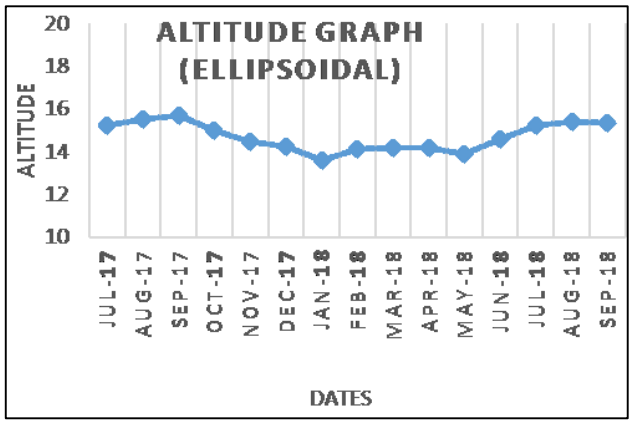

Figure 11: Altitude graph in ellipsoidal for reference station

Table 1 shows the positional data of the reference station and temporal station. Minimum, maximum, mean, standard deviation and RMSE error are been calculated for reference station and temporal station by using positional data collected by NAVIC/IRNSS receiver. It is being observed that IRNSS/NAVIC receiver provides higher horizontal accuracy compared to vertical accuracy. A value in decimal degrees to 5 decimal places is precise to 1.02 meters at the 23°N/S from Equator. Reference station and temporal station are compared; temporal station was having high RMSE Error than Reference station. The reason for less RMSE error in reference station is due to high amount of availability of positional data. Minimum, maximum, mean, standard deviation and RMSE of reference station are been calculated by using 15-month data (July-2017 to September 2018). It is observed that RMSE error was least, which makes reference station point more accurate.

Table 1: Positional data of reference station and temporal station with the minimum, maximum and mean values with standard deviation and RMSE error

	Minimum	Maximum	Mean	Standard deviation	RMSE
Reference Station	July 2017 to August 2017				
Latitude	23.128853	23.128889	23.128867	9.42753E-07	5.93E-13
Longitude	72.543936	72.543974	72.543950	9.63944E-07	6.19E-13
Altitude	12.427117	25.061950	15.472907	0.252438998	0.063725448
Temporal station	July 2017 to August 2017				
Latitude	23.128155	23.128867	23.128630	0.000411053	1.12643E-07
Longitude	72.541713	72.543951	72.543204	0.001292	1.11E-06
Altitude	15.206269	15.504228	15.351452	0.149124	0.014825
Reference Station	July 2017 to September 2018				
Latitude	23.12885273	23.12888946	23.1288677	2.30006E-06	4.93757E-12
Longitude	72.54394	72.54398	72.54395	1.62E-06	2.45E-12
Altitude	14.71194	11.13281	31.4992	0.66312	0.410413

4. Surveying and Mapping with IRNSS receiver

IRNSS dual-frequency receiver was Carried infield along with the different instruments and laptop for data surveying Purpose. The first experimental field trial was conducted at S.P Ring Road, Ahmedabad. Road network was surveyed from Vaishno Devi circle to Slilaj Circle, Ahmedabad. Positional data collected was plotted on Google earth Platform. Collected data was reasonably accurate and shows good results. Data collected has the least amount of Errors as there were no obstacles in a received signal. So we now wanted to conduct a survey at Moderate/High dense Environment. So the survey was initiated at Nirma University campus, where trees are planted along the road of both sides and there are buildings nearby each other. The results of the survey at ring road and Nirma Campus indicated that Signals are healthy and providing good results at places where there was less/no obstacle and at moderate dense/high dense areas, where signals were poor has a high amount of position error. Heavy dense part of the campus cannot be mapped due to receiver's signals were not able to penetrate at few places with dense vegetation. From this field trials, we have studied the behaviour of IRNSS receivers Signals and based on it we have initiated survey of our study area (Figures 12 and 13).

Figure 12: Road Survey for S.P Ring road.

Figure 13: Survey of Nirma University

4.1 Surveying and mapping of Gandhinagar

Surveying work of Gandhinagar city was initiated from sector-4, East of KH Road. Field data has been collected for a total of six sectors (vertically from sector 4 to sector 27). The whole survey was carried on a motorbike or by walking. IRNSS receiver, antenna and laptop were carried together for field data collection. The battery was also used in order to provide power supply to the receiver. IRNSS_UR software has been used for data extraction and storage. Extracted data consist of many different files having various information. Required positional information from the surveyed data was extracted to a new file. ArcGIS platform has been further used to import surveyed positional data. Now the data can be overlapped on Google Base map or other Geo-Reference Layers/maps. Path or shapes of points can be interpreted easily and Map can be prepared from these superimposed points, multi-point features. Figure 14 shows the field surveyed point data, overlapped on Google Maps platform. WGS 194 projection was assigned to Surveyed data so that data layer at ArcMap and imported point data both have the same projection

Figure 14: Surveyed data Superimposed on Google Maps

4.2 Digitization, classification and comparison on ArcMap Platform

Field data which were collected using IRNSS/NavIC receiver can now be digitized on ArcMap platform. Land Use map has been generated by digitizing different features. In attribution table, each feature has been had been assigned unique ID number (OBJECTID) and name. Figure 15 shows digitized of field data. On ArcMap platform, digitized data can further be classified. Using Symbology tool, different features have been classified based on its type. Here roads are classified as Highway, Primary roads, Secondary road, tertiary road and internal roads. Different colour coding has been assigned in order to identify each feature uniquely. Administrative boundaries of Sectors and sub-sectors have also been digitized. Attribute table has also been generated, which can be further be used as a database. The prepared map on

ArcMap platform for sector 4 was compared with Freely available open streets maps (Figures 15-18).

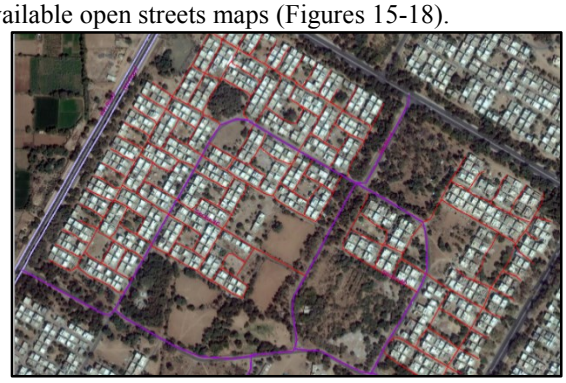

Figure 15: Digitization of Surveyed data.

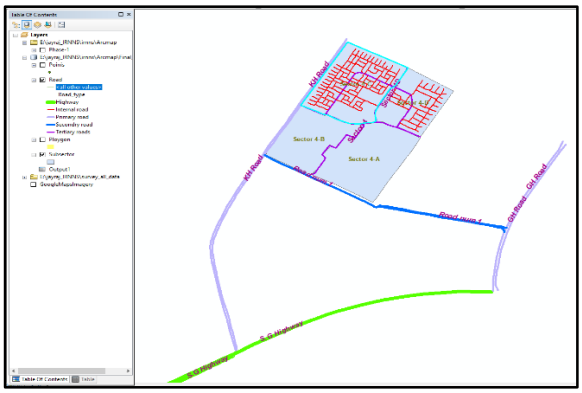

Figure 16: Sector 4 Map of Gandhinagar.

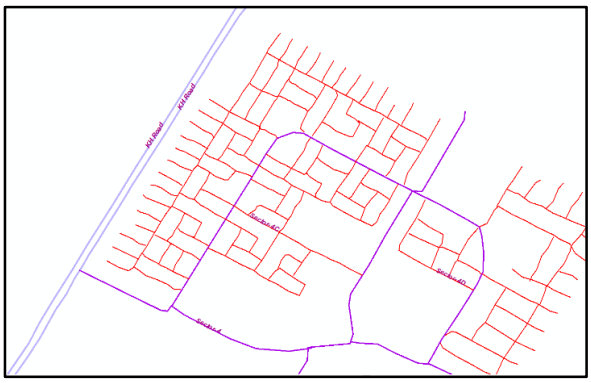

Figure 17: Sector 4 map on openstreetmaps

Figure 18: Prepared map for Sector 4 using IRNSS.

5. Conclusion

Firstly, the reference station was established at the terrace of B Block building, Nirma University and its position data were retrieved regularly. An analysis was carried out for received Positional data. The resulted accuracy provided by IRNSS/NavIC receiver was quite reasonable. So with confidence, we had initiated field trial, which was SP Ring Road. The survey was carried on a motorbike, during survey receiver and other instruments were carried in a bag. The result of the field trial was superimposed on Google earth and results were quite impressive, when it was superimposed and compared with google earth, it was providing good accuracy for collected position data. There was less/no obstruction for received signals during a survey at S.P ring road and due to that, there were less Positional errors. Survey at Nirma University Campus was conducted to check positional errors in the Moderate dense environment. There were positional errors at few places due to an obstacle in IRNSS received signals. For Phase 1 we started a survey of Gandhinagar city for a total of 6 sectors 4,5,13,15, 24 and 26 was surveyed. Land use Featured surveyed was road network and administrative boundaries. Data collected was post-processed. ArcMap platform was used to digitize the different features, further different Tools of ArcMap platform have been used for attribution and classification of digitized data. The accuracy of surveyed data was estimated by superimposing it on google map imaginary. Using the IRNSS system map generated by Sector 4, Gandhinagar was compared with OpenStreetMap. The results show that there were not many errors when it has been compared with Google Maps Imaginary and OpenStreetMap. From the results, we conclude that the data collected from the IRNSS/NavIC receiver has reasonable accuracy and can be used for various applications.

References

Ganesh, L.G.S. (2014). Performance evaluation of standard positioning service GPS receiver with LS and LQ estimators over the southern region of the Indian subcontinent. ICSEMR-2014.

ISRO-IRNSS-ICD. (2017). Indian Regional Navigation Satellite System Signal In Space ICD for Standard Positioning Service. Version 1.1, ISRO-IRNSS-ICD-SPS-1.1.

Li, L. X., D.H. Zhang, S.R. Zhang, A.J. Coster, Y.Q. Hao and Z. Xiao. (2015). Influences of the day-night differences of ionospheric variability on the estimation of GPS differential code bias. Radio Science an AGU Journal, 50(4), 339-353.

Ravi, S S. (2016). Indian Regional Navigation Satellite System. International Journal Of Research In Science & Engineering, 690-698.

Satellite Geodesy. (1994). In G. Seeber, Satellite Geodesy. Artech House Publishers, New York (USA).

Journal of Geomatics Vol. 13, No. 2, October 2019

Development of Oceansat-2 OCM Data Cube over Indian Subcontinent

Tushar Shukla*, Sampa Roy and Debajyoti Dhar
Space Applications Centre, Ahmedabad
*Email: tushar@sac.isro.gov.in

(Received: Jan 18, 2019; in final form: Nov 18, 2019)

Abstract: The number of Earth observation(EO) data users and developers are growing and a number of challenges need to be solved to fill the gap of acquisition and use of ever-increasing satellite data acquired by ISRO. The majority of EO data still remains underutilized mainly because of the challenges of big data namely, volume, velocity, veracity and variety. However, the full information potential of EO data can be utilized by directly providing Analysis-Ready-Data(ARD) to the user community. The ARD has all pre-applied corrections for radiometry and geometry. EO Data Cube (DC) is a new paradigm aiming to realize the full potential of satellite data by eliminating the barriers caused by these big data challenges and providing access to large Spatio-temporal data in a user and developer-friendly environment, thereby fulfilling both visualization and analysis needs. Systematic and regular provision of Oceansat-2 OCM Analysis Ready Data (ARD) will significantly reduce the post-processing burden on ISRO's Oceansat series data users and application scientists. Nevertheless, ARD is not commonly produced as a part of standard data processing chain of Oceansat-2 mission (operational at IMGEOS/NRSC, Hyderbad) and therefore getting uniform and consistent ARD remains a challenging task. This paper presents an approach to enable rapid data access and pre-processing to generate ARD using interoperable services chains. The approach has been tested and validated by generating OCM-2 ARD while building the Oceansat-2 OCM Data Cube.

Keywords: DataCube, Oceansat-2, Ocean Color Monitor(OCM), ARD, Pre-processing, ISRO.

1. Introduction

Due to pressures from climate change, demographic, and economic growth, natural resource consumption and exploitation are more than ever (Rockstrom, et al., 2009). To better preserve the quality of the environment and improve the management of natural resources and land planning, it is useful to monitor these changes through time (Wulder et al. 2008). One of the main characteristics of remote sensing is the ability to provide a synoptic view of a given spatial extent. With the archives from ISRO's Ocean colour monitoring satellite sensors, the evolution of this coverage can be monitored all the way back to 1999 (with the launch of IRS-P4). Now with the introduction of new satellite sensors (e.g. Oceansat-2 and upcoming Oceansat-3) facilitate inter-decade comparison and analysis of EO data. Remotely sensed Earth Observations (EO) data are increasingly available from a number of freely and openly accessible repositories. These data are highly valuable because of their unique and globally consistent information that they include (Lewis, et al., 2016). Indeed, global observations together with scientific expertise and appropriate tools provide substantial benefit supporting economic development, decision-making, and policy implementation for all countries. However, the full information potential of EO data has not been yet realized. They remain still underutilized and stored in electronic silos of data. This is due to several reasons:

(1) increasing volumes of data generated by EO satellites;
(2) lack of expertise, infrastructure, or internet bandwidth to efficiently and effectively access, process, and utilize EO data;
(3) the particular type of highly structured data that EO data represent introducing challenges when trying to integrate or analyze them;
(4) and the substantial effort and cost required to store and process data limits the efficient use of these data.

The EO data can be considered as Big Data, data that are too large, fast-lived, heterogeneous, or complex to get understood and exploited (Baumann, et al., 2016a). Consequently, we need new approaches to fully benefit from EO data and support decision-makers with the knowledge they require by systematically analyzing all available observations and convert them into meaningful geophysical variables. To address these Big Data challenges, it is necessary to move away from traditional local processing (e.g. desktop computer) and data distribution methods (e.g. scene-based file download) and lower the barriers caused by data size and related complexities in data preparation, handling, storage and analysis. This paradigm shift is currently represented by EO Data Cubes (Baumann, et al., 2016b), an approach that is receiving increasing attention as a new solution to store, organize, manage, and analyze EO data in a way that was not possible before. Data Cubes (DC) are aiming to realize the full potential of EO data repositories by addressing Volume, Velocity, and Variety challenges, providing access to large Spatio-temporal data in an analysis-ready form.

2. Related Research and Operation

Currently, there are various operational DC like the Australian Geoscience Data Cube (AGDC). These different initiatives are covering different spatial scales (e.g. AGDC, EODC (Earth observation Data cube by ESA [European Space Agency]); storing different data (e.g. only Landsat 8 for the EODC while the AGDC stores Landsat 5, 7, 8, MODIS, and Sentinel 2 data; only processed products for the ESDC); using different infrastructure (e.g. high performance computer for the AGDC, and cloud used by many others); using different

software implementations (e.g. Open Data Cube for the AGDC; RasDaMan by ESA). Figure 1 illustrates a spatial Hadoop framework for storing and serving the petabytes of EO data. Rasdaman used by ESA follows a similar framework for storing their datacube. The diversity of approaches asks also for a clear definition of an EO Data Cube. A recent publication of The Datacube Manifesto by CEOS defines a Data Cube as a massive multi-dimensional array, also called raster data or gridded data; massive entails that we talk about sizes significantly beyond the main memory resources of the server hardware. Data values, all of the same data type, sit at grid points as defined by the d axes of the d-dimensional datacube. Coordinates along these axes allow addressing data values unambiguously. A d-dimensional grid is characterized by the fact that each inner grid point has exactly two neighbours along each direction; border grid points have just one. The main objective of this initiative is to provide a data architecture solution to lower the technical barriers for users to exploit EO data to its full potential and consequently solving the problem of accessibility and use while increasing the impact of EO data. The primary problems for users are data access, data preparation, and efficient analyses to support user applications. The two first issues are essential challenges to tackle while building a DC. Indeed, these steps concern the generation of Analysis Ready Data (ARD). CEOS defines ARD as satellite data that have been processed to a minimum set of requirements and organized into a form that allows immediate analysis without additional user effort. Figure 2 shows the ARD production steps from RAW satellite data. It is envisioned that systematic and regular provision of ARD will significantly reduce the burden on EO data users. To be considered as ARD, data should satisfy the following requirements:

(1) metadata description; (2) radiometric calibration; (3) geometric calibration. ARD data from various ISRO missions such as Oceansat series and Resources at series can be ordered by placing a request at UOPS (User online processing system) maintained by NRSC, Hyderabad. However, getting uniform and consistent ARD remains a challenging task due to various environmental challenges and acquisition-related problems. As such, data ordering and delivery can take long time (e.g. several hours or days); and the full process from ordering to getting the data has not been automated yet. This clearly limits the accessibility and ingestion processes while building and updating a DC and consequently ask to find alternative ways to generate ARD products. Recognizing these issues, the aim of this paper is to present an approach to enable rapid data access and pre-processing to generate Analysis Ready Data. The approach has been tested and validated by significantly facilitating the generation of ARD using Oceansat-2 OCM medium-resolution imagery allowing to build the first version of the OCM-2 Data Cube.

3. Building OCM-2 Datacube: Techniques and Infrastructure Implementation

The Data Cube is a system designed to:
1) Catalogue large amounts of Earth Observation data
2) Provide a Python-based API for high-performance querying and data access
3) Give scientists and other users easy ability to perform Exploratory Data Analysis
4) Allow scalable continent-scale processing of the stored data
5) Track the provenance of all the contained data to allow for quality control and updates.

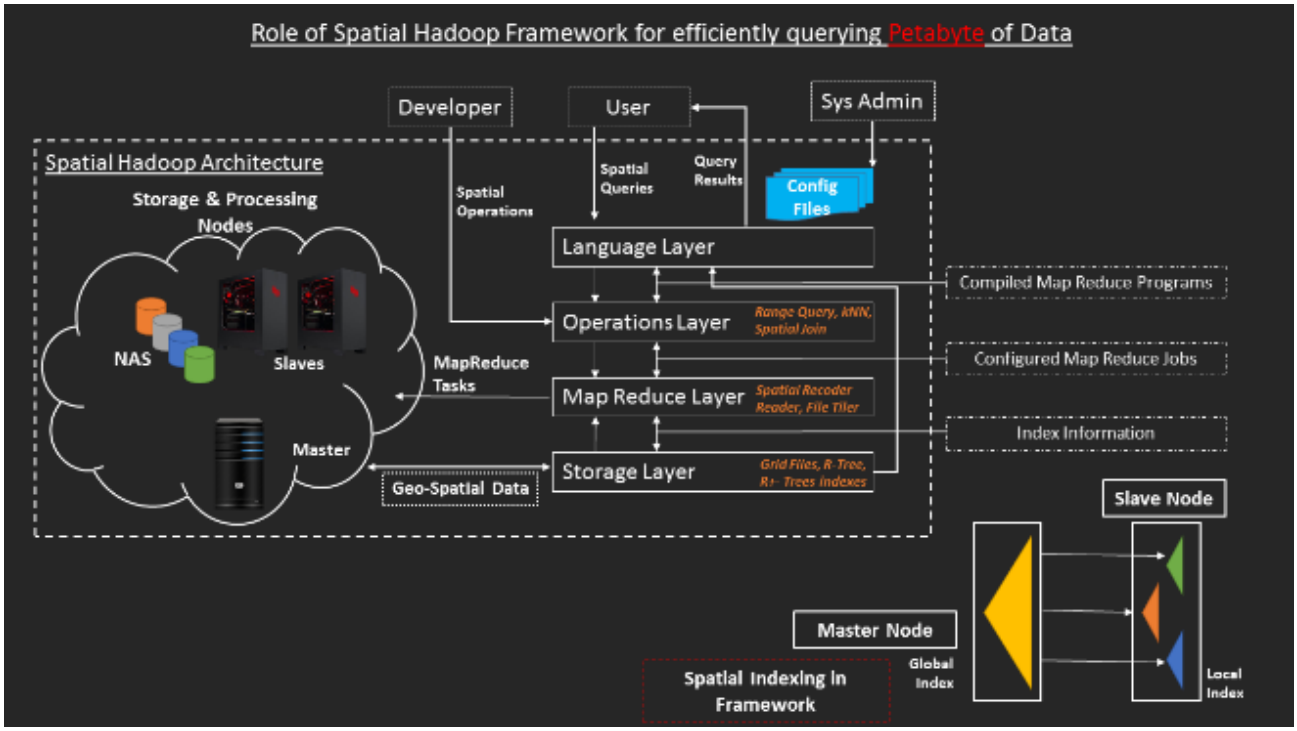

Figure 1: Spatial Hadoop Architecture for DataCube Infrastructure

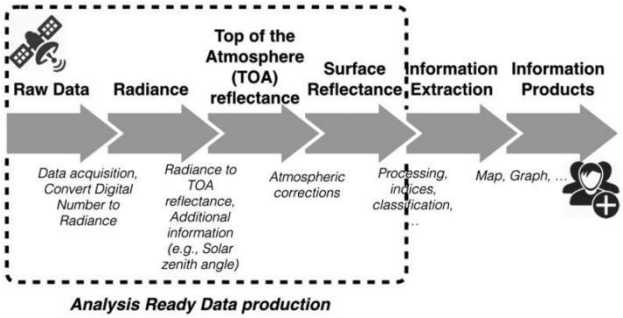

Figure 2: ARD production steps

A fundamental aspect while building a DC is having ARD products ingested, stored in the database, and readily available. Considering that ARD products are not commonly generated by data providers and the fact that current delivery mechanisms are not efficient, this requires finding a procedure to routinely generate ARD ensuring that all observations stored in a Data Cube are consistent and comparable. Ideally, this procedure must be automated as much as possible (e.g. discover, download, and pre-processing), should be able to discover and access data from different repositories, should handle different sensors (e.g. Oceansat-2 OCM, Resources at-2 LISS-3, LISS-4 and AWIFS), and should be interoperable (e.g. to enhance reusability).

To satisfy these requirements, the ARD Product Generation and Ingestion (APGI) framework has been developed and used. Figure 3 illustrates this automatic processing workflow for directly preparing the raw product for ingestion into datacube. APGI is a framework that helps to automate EO data discovery and (pre-)processing using interoperable service chains for transforming observations into information products suitable for monitoring environmental changes (Giuliani, et al., 2017). This framework is developed using a combination of large storage capacities, high-performance computers, and interoperable standards to develop a scalable, consistent, flexible, and efficient analysis system that can be used on various domains through decades of data for monitoring purposes. APGI take the discovers the RAW product and Generated ARD and finally Ingests specified data to Datacube. While building the DC, the APGI framework has helped to automatically generate ARD products by overcoming the obstacles presented manual product generation and ingestion. Figure 4 highlights the key components of OCM-2 datacube framework for accessing ingested data via API and OGC compliant services.

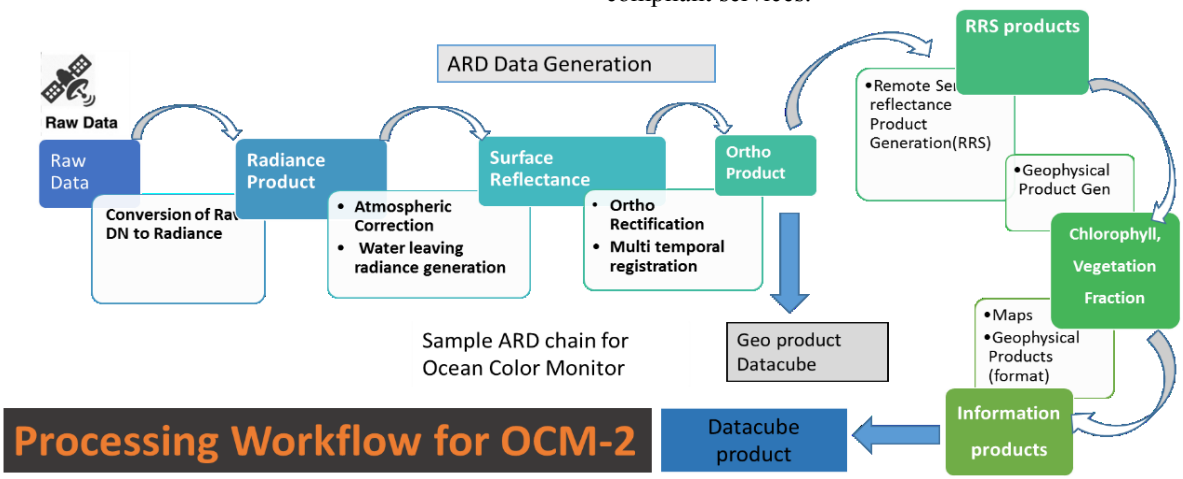

Figure 3: Processing workflow for OCM-2 RAW to ARD to Datacube Chain

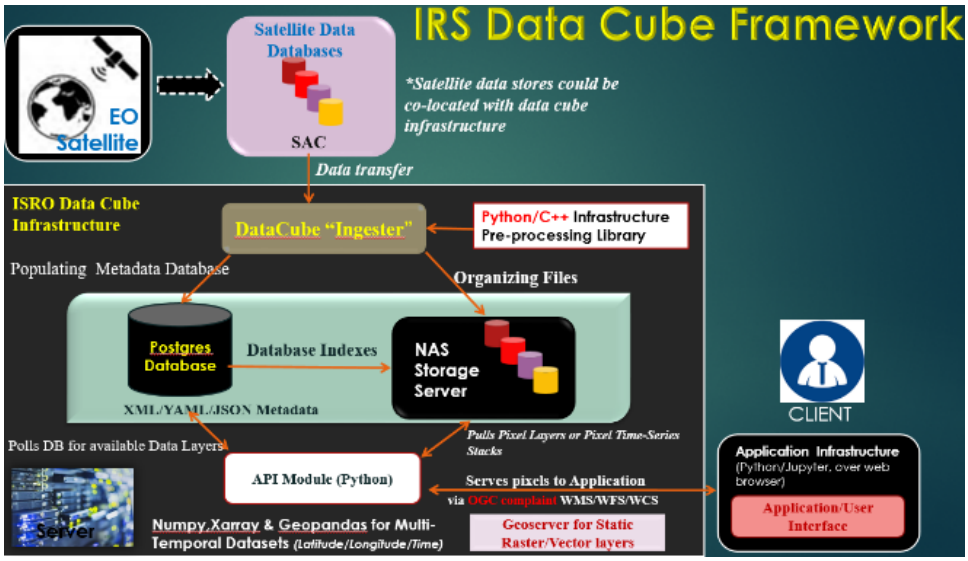

Figure 4: IRS Data cube framework for OCM2

2.1 Indexing Data

When you load data into the Data Cube, all you are doing is recording the existence of and detailed metadata about the data into the index. None of the data itself is copied, moved or transformed. This is, therefore, a relatively safe and fast process. There are a few pre-requisites for Indexing data:

1) A working Data Cube setup.
2) Some Analysis Ready Data to load.
3) A Product definition added to your Data Cube for each type of dataset.
4) Dataset metadata documents for each individual dataset.

2.2 Oceansat OCM-2 data volume, coverage and Computing performance

The available OCM-2 data had the total cumulative size of more than 30 TeraBytes (TB) (2-day repetivity and total year duration of 2011-2018) and as such high computing performance became one the major requirement of generating the datacube structure. Figure 5 illustrates the coverage of OCM-2 Path 9 and 10 coverage over India, Srilanka and parts of Tibet and Pakistan. High computing and processing performance was achieved by developing efficient software written in python and c++ for geophysical parameter generation, multi-temporal image registration, indexing and ingestion; to efficiently utilize multi-processing environment. Both data and task-level parallelism techniques were employed to process data within a meaningful time duration. The entire activity was divided into smaller goals for building this huge Datacube: development of scripts for

(a) large data handling and reducing redundancy;
(b) efficient storage and categorization of radiance,
(c) reflectance and geophysical data for rapid access;
(d) reference generation and multi-temporal image registration; and finally
(e) development of geo-spatial web user interface.

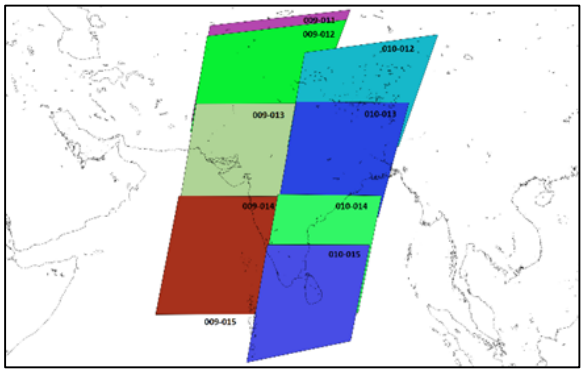

Figure 5: OCM-2 Path Row coverage over India

3.2.1 Working behind Data loading

Types of Data Loading

There are two major use-cases for loading data from the Datacube Ad hoc access, and Large scale processing. These are described below.

1. Ad hoc access
   - A small spatial region and time segment are chosen by the user.
   - Data is expected to fit into RAM.
2. Large scale processing (GridWorkflow)
   - Continental-scale processing
   - Used to compute new products or to perform statistics on existing data
   - Often unconstrained spatially
   - Often unconstrained along the time dimension
   - Data is accessed using a regular grid in small enough chunks

The specific access pattern is algorithm/compute environment-dependent and is supplied by the user and requires manual tuning.

For large scale processing, we turn to Dask (Dask Development Team, 2016) library which offers lazy load processing, this is explained in the following section.

3.2.2 Lazy load with Dask

In computer science, context lazy means roughly not computed until needed. Rather then loading all the data immediately load_data() function can instead construct a array (Hoyer, et al., 2016). The dataset that the user can use in the same way as a fully loaded data set, except that pixel data will be fetched from disk/network on-demand as needed. The on-demand loading functionality is provided by third-party libraries xarray and dask (used internally by array). Datacube code constructs a process for loading data on demand, this process is executed as needed by xarray + dask library when real data is required to be loaded for the first time.

3.2.3 Internal interfaces

The primary internal interface for loading data from storage is BandDataSource class, unfortunately, this rather generic name is taken by the specific implementation based on the raster library. BandDataSource is responsible for describing data stored for a given band, one can query:

- The Shape (in pixels) and data type
- Geospatial information: CRS + Affine transform

and also provides access to pixel data via 2 methods

1. **read**(): access a section of source data in native projection but possibly in different resolution
2. **reproject**(): access a section of source data, re-projecting to an arbitrary projection/resolution

This interface follows very closely the interface provided by the raster library. Conflating the reading and transformation of pixel data into one function is motivated by the need for efficient data access. Some file formats support multi-resolution storage for example, so it is more efficient to read data at the appropriate scale rather than reading highest resolution version followed by downsampling. Similarly, re-projection can be more memory efficient if source data is loaded in smaller chunks interleaved with raster warping execution compared to a conceptually simpler but less efficient load all then warp all approach.

3.3 Improved SIFT-based data product registration

Achieving sub-pixel accuracy is a must for valid time-series data and composite data product generation. An improved Scale Invariant Feature Transformation technique was developed to solve this challenge. For all the years 2011-2018, seasonal references are generated and geometrically registered for within the year image

registration. Further to handle the huge amount of associated data processing, extensively parallel C++ software were written for the utilizing full potential of multi-processor environment using OpenMP, SSE, and AVX (Shukla et. al, 2018).

3.4 Geo-Spatial Web-Interface

Developing a multi-temporal data analysis portal which will help users in the visualization and analysis of pre-processed data. It utilizes the strength of the underlying On-Line Processing of ARD temporal data-stacks for same geospatial regions.

The platform provides freedom to develop and integrate pluggable applications for various algorithms which in turn can help users to process data online and get results instead of downloading input data and setting up environment for applications to run for the same this, in turn, saves lot of user's time. The developed Web User interface uses Geoserver for serving Static layers such the pre-computed monthly composite layers to quickly serve data using WMS, and Datacube API calls for accessing multi-temporal ARD. Some major highlights of Web Interface are:

- Online available Analysis Ready Data (includes Multi-Temporal Registration correction)
- On-the-fly post-processing of ARD data (ingested in datacube framework) to generate custom mosaic for different Bio-geophysical products such as
    - Vegetation fraction
    - Land Surface Water,
    - Chlorophyll-a concentration
    - Aerosol Optical Depth
    - Remote sensing reflectance (6 bands)
- Online Application for Change Detection between selected dates (includes PCA, SSIM etc.)
- Tool for ROI based on-the-fly pixel drilling query over available geophysical products. (Figure 6)
- Online Time-series Trend analysis algorithms such ARIMA.

Figure 7 illustrates the web interface for data cube system allowing easy access to multi-temporal data and time series of geophysical products.

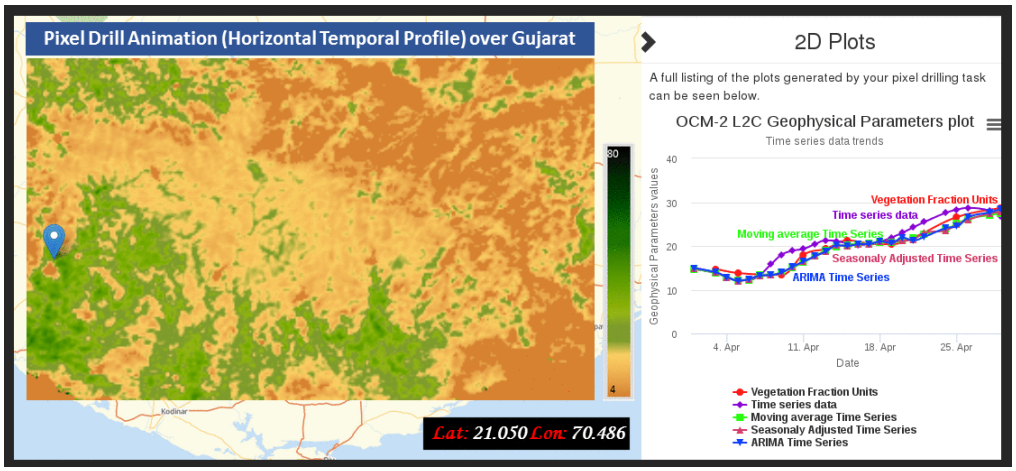

Figure 6: Pixel drilling and Trend Analysis Application Integrated with Web User Interface

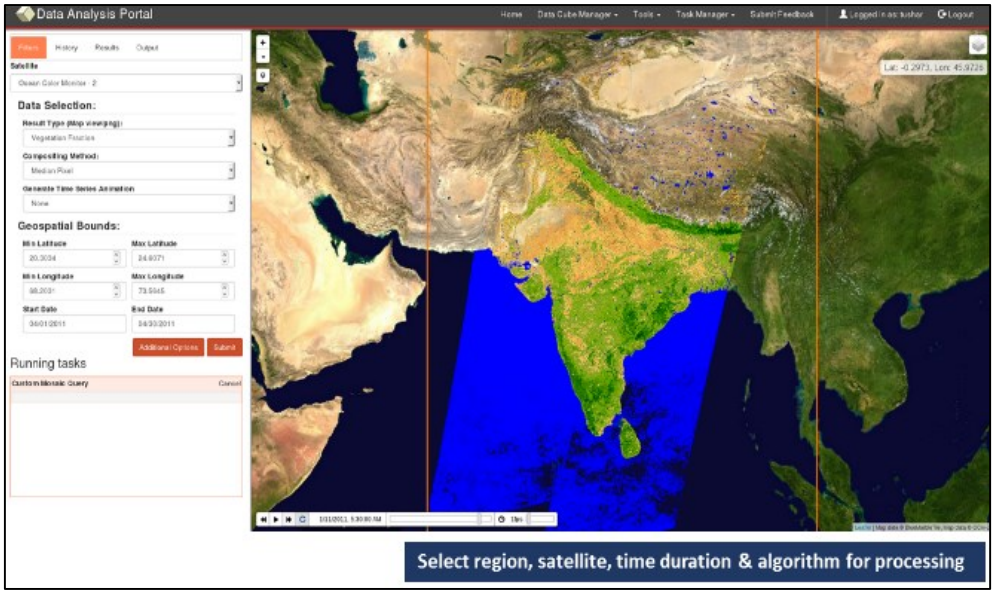

Figure 7: Web User Interface with a static monthly composite layer of Vegetation fraction and Land surface water product

4. Conclusions

Data Cubes are revolutionizing the way users can work with EO data. It is a disruptive technology that is significantly transforming the way that users interact with EO Data. It has the potential to routinely transform Earth Observations into useful and actionable information for users. To reduce the processing burden on users, generating Analysis Ready Data is a fundamental requirement. ARD products minimize the time and scientific knowledge required to access and prepare satellite data having consistent and spatially aligned calibrated surface reflectance observations. The proposed approach makes use of the APGI framework to build interoperable data processing chains for generating ARD products. This methodology has been tested in building the OCM-2 Data Cube, a country scale DC for monitoring the environment in space and time, and has allowed to efficiently download, pre-process, and ingest thousands of Oceansat scenes in a couple of days. The Datacube infrastructure allows for the integration of EO data from multiple satellites and as such, our future work focusses primarily on addition and assimilation of more and more data to the cube. Currently, the Resources at-2 LISS-3 ARD is being generated and invested in the existing infrastructure.

References

Baumann, P., A.P. Rossi, O. Clements, A. Dumitru, B. Evans, P. Hogan, … J. Wagemann (2016a). Fostering cross-disciplinary earth science through datacube analytics (p. 32).

Baumann, P., P. Mazzetti, J. Ungar, R. Barbera, D. Barboni, A. Beccati, … S. Wagner (2016b). Big data analytics for earth sciences: The earth server approach. International Journal of Digital Earth, 9(1), 3–29.

Dask Development Team (2016). Library for dynamic task scheduling. URL https://dask.org

Giuliani, G., H. Dao, A. De Bono, B. Chatenoux, K. Allenbach, P. De Laborie and P. Peduzzi (2017). Live monitoring of earth surface (LiMES): A framework for monitoring environmental changes from earth observations. Remote Sensing of Environment.

Hoyer, S. and J. Hamman (2016), Journal of Open Res. Software, xarray: {N-D} labelled arrays and datasets in Python.

Lewis, A., L. Lymburner, M.B.J. Purss, B. Brooke, B. Evans and S. Oliver (2016). Rapid, highresolution detection of environmental change over continental scales from satellite data – The Earth Observation Data Cube. International Journal of Digital Earth, 9(1), 106–111.

Rockstrom, J., W. Steffen, K. Noone, A. Persson, F.S. Chapin, E. Lambin and J. Foley (2009). Planetary boundaries: Exploring the safe operating space for humanity. Ecology and Society, 14(2).

Shukla, T., S. Roy and D. Dhar (2018), Improved SIFT-based Geometric Accuracy Improvement of Oceansat-2 OCM Imagery for Time-series Datacube, ICRIEECE – 2018.

Wulder, M. A., J.C. White, S.N. Goward, J.G. Masek, J.R. Irons, M. Herold, … C.E. Woodcock (2008). Landsat continuity: Issues and opportunities for land cover monitoring. Remote Sensing of Environment, 112(3), 955–969.

Journal of Geomatics Vol. 13, No. 2, October 2019

Lichenology and geomatics for monitoring air pollution and climate change impacts

Rajesh Bajpai[1], C. P. Singh[2], T. S. Rana[1], D. K. Upreti[1]
[1]Lichenology laboratory, Plant Diversity Systematics and Herbarium Division
CSIR-National Botanical Research Institute, Lucknow
[2]AED/BPSG/EPSA, Space Applications Centre, ISRO, Satellite Road, Ahmedabad, Gujarat, India
Email: bajpaienviro@gmail.com

(Received: Dec 20, 2018; in final form: Nov 19, 2019)

Abstract: Lichen monitoring has become a widely used standard to evaluate air quality and is an effective early-warning system to evaluate the rate of retreat of glaciers, accumulation of metals, metalloids, polycyclic aromatic hydrocarbons and radioactivity in terrestrial ecosystems. The lack of vascular system, absence of root system and dependence to absorb water and nutrients passively from their environment make it sensitive against environmental perturbation. Lichens have long life and without organ shedding; they are able to accumulate air pollutants for many years. The sensitivity of lichen epiphytes to environmental change has resulted in their wide use as indicator for pollution monitoring and to identify forest habitat for biodiversity protection. The understanding of lichens for the microclimatic changes may be used to estimate the ecological continuity of forest and to establish network for monitoring and climate change. Lichens have numerous functional roles in forests including nutrient cycling (especially nitrogen fixation in moist forest and as component of food webs). In India, a total of nineteen lichen communities are described that may be used to indicate the status of the habitat condition, age structure of forest, type of substrates and predict the surrounding air quality. An attempt was made to utilize lichen properties to monitor air pollution and climate change impact and geomatics tools to expedite the quality of work as robust, timely, reliable and cost-effective.

Keywords: lichens, air pollution, climate change, herbarium, mapping, GPS, geomatics

1. Introduction

Lichens are a group of non-vascular plants composed of mycobiont (fungi) and Photobiont (algae) species growing in a symbiotic relationship. The fungi develop structural support to the organism, and the algae produce nutrition through photosynthesis. Lichens are an extremely diverse plant group, occupying ecological niches on varied physical and biological substrates such as soil, rocks, branches and bark of trees as well as on man-made artefacts. Lichens lack an epidermis, stomata and a waxy cutin, and consequently lack the control over gas exchange as vascular plants do. Due to its unique features, lichens are widely used in air pollution monitoring. Lichens were first recognized as organisms' sensitive to high concentrations of gaseous pollutants such as sulphur dioxide (Rose and Hawksworth, 1981).

The lichen air pollution monitors being widespread, permit a higher sampling density. In this context, lichens are recognized as the best indicator of air pollution and can be utilized as a 'tool' for monitoring different atmospheric pollutants (Haffner et al., 2001). The use of lichens in estimating the quality of the air, from different parts of the world are available since more than four decades and from that time more than 2000 published accounts on the lichen and environmental studies are available in different reputed and dedicated air quality journals worldwide (Shukla et al., 2014). Lichens being natural sampler provide good data on the environmental status of the place. Integrated monitoring programmes are clearly essential in conjunction with physiochemical measurements and geomatics techniques, where lichenologists can investigate lichen diversity as an indicator of atmospheric levels of SO_2, NO_X and O_3 parallel to the measurement of trace metals. It is recognized that a wide range of other substances like ammonia, arsenic, fluorine, alkaline dust (pesticides, fertilizers), heavy metals and radionuclides, chlorinated hydrocarbon and acid rain may also be detected and monitored using lichens. Various heavy metals such as Pb, Cd, Ni, Hg, Cu and Cr are considered to be toxic for many other living organisms, may be accumulated simultaneously in one lichen specimen which may appear to be unharmed in many cases.

The wide geographical distribution of lichens enables one to adopt sampling strategies with a relatively high density of sampling points which considering the nature of air pollution phenomenon greatly enhance the data quality. The distribution map, lichen zone mapping, indices of atmospheric purity and transplantation technique are the most common techniques categorized under active as well as passive methods to monitor environmental pollution at various part of the country. The main aim of the work is to provide some basic methods to assess air pollution and climate change studies with the aid of geomatics techniques.

2. Methodologies

2.1 Field methods

2.1.1 Floristic survey

Floristics may be defined as a compilation of species present in an area and the distribution information for those species. A complete and accurate species list is an ideal basis for understanding the flora of the area studied which provides ecological information about the unit and information necessary for determining appropriate species for biomonitoring as well as information concerning the resources of the unit. The collection and identification of lichens involve recognizing habitats, substrates and specimens in the field, and using the appropriate collection, curation, and identification procedures. Quality assurance (QA) and quality control (QC) standards must

be met, and prior to the fieldwork, literature review on lichens of the study area should be done. The surveyed species needs to be geotagged using a handheld global positioning system (GPS) receiver. The statistically significant number of records spread over a wide geographic area can be used for niche modelling using bioclimatic indices and machine learning algorithms (Singh et al., 2016).

2.1.1.1 Sample collection

The collections of lichens are valuable for comparing lichen floras, community structure, and elemental concentrations with herbarium samples collected in pre pollution eras. It is important to obtain adequate amounts of tissue for analysis. The GPS should be used to record the latitude and longitude of the sample location, so that its habitat can be compared at genus or species level, moreover, an interpolated map of the pollutant concentration can be developed using geomatics techniques. Similarly, the records of lichen specimens collected in the past from a particular area and its comparison with the present diversity (revisit of the sites) can provide an assessment of important changes on plant community and ecological parameters which can be correlated with climate change.

Changes in lichens at the community or population level are used as sensitive indicators of the biological effect of pollutants. Presence/absence or dominance of a species or a group of species may provide valuable information about the alterations in the air quality of an area due to air pollution or due to microclimatic changes (Bajpai et al., 2016a). The historical data of the species also provide valuable information in the selection of indicator species for long term monitoring of an area. Common indicator lichens found growing in different areas of India is given in table 1.

2.1.1.2 Identification

Lichen identification is the most important factor in terms of environmental pollution monitoring and climate change studies. The identification of specimens starts at the time of the collection itself. During collection, we need to find out their substratum i.e. lichens growing over bark/twigs (corticolous), rock (saxicolous), mosses (mossicolous), on cloth (fabricolous), lignin (lignicolous), vehicles (vehicolous) on other lichens (lichenicolous) (refer Figure 1).

The morphological and anatomical identification of the specimen collection can be done in the laboratory using microscopes. The chemistry of lichens also plays an important role in identification of taxa. The spot test, thin layer chromatography and microcrystallography are common methods for initial identification.

Figure 1: Lichens growing over different substratum a. Natural b. man-made

Table 1: Common indicator lichens found growing in different areas of India (after Shukla et al. 2014)

Climatic zones	Bioindicator species
Tropical areas	*Dirinaria consimilis* (Stirton) Awasthi; *Rinodina sophodes; Pyxine cocoes* (Sw.) Nyl.; *Lepraria lobificans* Nyl.; *Cryptothecia sp.*
Subtropical areas	*Phaeophyscia hispidula* (Ach.) Essl.; *Pyxine subcinerea* Stirton; *Parmotrema praesorediosum* (Nyl.) Hale; *Parmelinella wallichiana* (Taylor) Elix & Hale
Temperate areas	*Cladonia praetermissa*. A. W. Archer; *Heterodermia diademata* (Tayl.) Awasthi; *Candelaria concolor* (Dicks.) Arnold; *Dermatocarpon vellereum* Zschacke, *Usnea sp.*
Alpine areas	*Rhizocarpon geographicum* (L.) DC*, Aspicilia* sp.*, Xanthoria elegans* (Link) Th. Fr*, X. fallax* Arnold*, Lecanora muralis* (Schreb.) Rabenh.
Mangrove area	Species of lichen genera *Dirina, Dirinaria, Arthonia, Lecanora, Opegrapha, Rocella*
Arid area	*Phaeophyscia hispidula* (Ach.) Essl.; *Parmotrema praesorediosum* (Nyl.) Hale, *Caloplaca* sp., *Graphis* sp. *Phylliscum* sp. *Endocarpon* sp.

2.1.2 Zone mapping

The zone maps of common and sensitive lichen species are a relatively simple and inexpensive method of air quality monitoring. The method distinguishes areas with varying degrees of pollution. The studies can be in relation to point emission sources such as power plants and smelters, a general source area such as an urban area or industrial complex, automobile exhaust or as a means of producing baseline data of a previously unsurveyed site or in pre-development appraisals. The occurrence of each species can be GPS tagged and plotted on a map to provide an idea about the overall picture of the lichen distribution in the area. Such distribution map helps to determine the distribution of a species that has changed in the area, in the course of time. A sufficient number of reliable distribution data collected in the past help to assess the changes more easily.

Lichen zonation is a method used to indicate the severity of pollution with reference to distance from sources reflected by the number of species present or absent. The detailed physical investigation of epiphytic vegetation of cities or of larger areas around factories can be used to segregate the area into three, four or more major lichens zones (Herzig et al., 1989) (Figure 2).

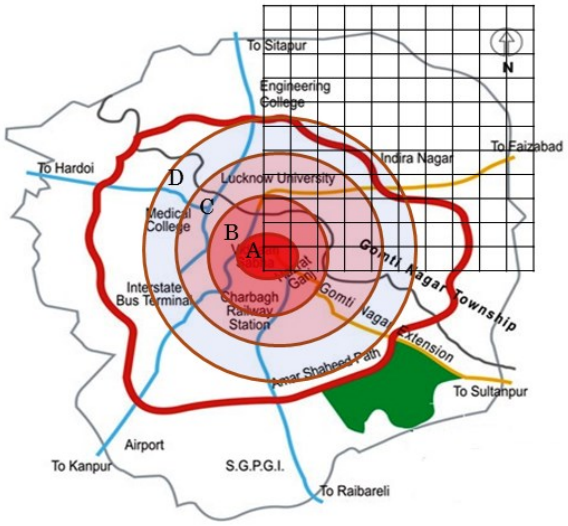

Figure 2: Lichen zone map of Lucknow city and zones categorised as a. no lichens (lichen deserts) b. presence of some calcicolous lichens (Inner struggle zone) c. Scare growth of few crustose & foliose lichens (Outer struggle zone or Transition zone) d. The luxuriant growth of Foliose, Crustose, Folicolous lichens (normal zone)

2.1.3 Quadrate

Quadrate sampling is a basic tool to study population ecology, particularly biodiversity. The passive quadrate sampling can be done in a habitat of interest and the species within those quadrates are identified and recorded. Abundances of organisms found at the study site can be calculated using the number found per quadrate and the size of the quadrate area. The quadrate is a square area of varying size marked off in the studied community for the purpose of detailed study. The quadrate may be List Quadrate (only listing the names of different species growing in the quadrat); List-Court Quadrate (records the number of individuals of each species represented in each quadrate); Chart Quadrate (record the position and areas covered by twigs, mats or tufts of grasses, mosses on the graph paper, these graphs help to compare any change in structure of community in future); Clip Quadrate (record the biomass or weight of each species, all individuals are collected (but when the weight of a particular organ, e.g., twigs or leaf are to be determined only the concerned organ is clipped and its fresh or dry weight is recorded); Nested quadrates (a series of quadrats, laid one over the other with gradually increasing size). The size of quadrates to be used in a given community is determined by constructing a species-area curve.

2.1.4 Community composition

The purpose of quantitative sampling of lichen communities for air quality and climate change assessment is the accurate and sensitive detection of changes in lichen communities through time. The composition of lichen communities is highly sensitive to climate and are strongly correlated to the climatic factors of the area. The community composition provides distinct evidence of the climate-driven effect on species diversity. According to Insarov and Schroeter (2002) the large scale monitoring systems are parts of complex systems usually aimed to study the combined effect of air pollution and climate change on forest ecosystem. The small scale monitoring involves altitude or distances from seashore aims to ascertain the relationship between climatic factors and lichen biodiversity (species diversity and community composition). Because of their sensitive physiology, changes in temperature or water availability lead to shifting in the lichen communities therefore, repeated monitoring of the lichen community indicators provides an early warning of response to climate change. Lichen community composition combined with type of forest vegetation and environmental data suggest causes for variation in the communities. The richness and abundance of species can be correlated with the climate value of the area. Biotic indexes can be developed based on lichen community data along with climate and air pollution gradients.

The lichen communities are also sensitive to landscape structure and land use context and to forest management. The forest lichen communities respond to primary climate variables such as precipitation and temperature and to geographical gradients such as elevation and latitude that integrate climate factors. Some of the lichen bioindicator communities are listed below

Some of the field procedure recommended by McCune (1992) with modification are as follows:

- The area to be sampled (i.e. lichen plot) is a circular area 36.6 m (120 ft) radius or quadrate size 1x1 m or depend upon your study objectives.
- Take a reconnaissance walk through the lichen plot, locating lichen epiphytes on woody plants, and collecting voucher samples and estimating abundances as you go.

- Collect lichen species with fruticose and foliose growth forms (i.e. macrolichens).
- Inspect all trees and shrubs 0.5 m tall within the lichen plot for lichens. Also inspect branches collected for the destructive samples (the same trees used for foliar nutrient analyses, branch and foliage visible symptoms, and tree cores) for lichens.
- Be careful to inspect the full diversity of substrates present: trunks and branches, fallen branches, hardwoods and conifers, large shrubs.
- Be careful to inspect the full range of microhabitats present: shaded and exposed, upper branches and lower branches, and trees in particular topographic positions (for example, in a draw, on an otherwise uniform slope, so long as the draw occurs within the lichen plot)
- Record relative abundances within the lichen plot. Relative abundance for each species is estimated using the following abundance code: Rare (3 individuals in area); uncommon (4-10 individuals in area); common (10 individuals in area but less than half of the boles and branches has that species present); Abundant (more than half of boles or branches have the subject species present
- How to grip doubts during fieldwork, when field worker, not full expert in lichenology for on spot identification of an organism during collections. Some procedures for the field worker are designed to put the responsibility for identification who is not properly trained members. First of all, when you in doubt, assume it is a lichen; when the growth form is in doubt, assume it is a macrolichen; when in doubt, assume that two different forms are different species. The purpose of these doubts is to encourage the field workers to make as many distinctions in the field as possible.
- The overall assessment can be summarized under 3M that is measuring (of pollutants/diversity); monitoring (periodical observations); modelling (to develop indices or models).

2.1.5 Multi-summit approach (MSA) for long term ecological monitoring

Long term ecological studies not only enhance our understanding of the relationship between vegetation and environment but are a necessity for documenting responses of global climate change. Such continued studies help to distinguish between pathways, causes and mechanisms of vegetation change (Pickett et al., 1987). MSA for permanent monitoring indicate different stages of succession and also generate hypotheses on its pace and causes. The MSA has become an essential tool for monitoring vegetation and presently, there is a renewed emphasis on establishing long term monitoring changes in mountain vegetation that are early indicators of climate change.

Mountain ranges play a significant role in influencing the regional and global climate. Further, being governed by low temperature, high-altitude regions of the world are more responsive to the changing climatic conditions and hence better indicators of the same (Grabher et al., 1994; Grace et al., 2002; Bajpai et al., 2018). The researches prove that the growth and reproduction of plant communities in mountain ranges are mainly controlled by the temperature that gives rise to steep ecological gradients and narrow ecotones and any minor change in temperature may lead to change in tree line and nival zones (Singh et al., 2018). At high altitude regions the lichens and bryophytes are abundantly growing over boulders, shrubs and some time on soil and living without any interruptions. In recent year MSAs, in Indian Himalayan states such as Jammu & Kashmir, Himachal Pradesh, Uttarkhand, Sikkim and Arunachal Pradesh was established with support of Space Applications Centre (ISRO), Ahmedabad for long term climate change assessment under Himalayan Alpine Dynamics Research Initiative (HIMADRI) programme (Singh, 2015). In this programme, permanent plots were established throughout alpine regions and lichen diversity was analyzed (Figure 3). The plot protocol determines the way in which current or future samples are taken. The permanent plots in which no destructive sampling takes place must be distinguished from temporary plots from which material is collected. Designation of sampling areas within temporary plots may be desirable so that the location of disturbance is known. Methods for marking and mapping plots must be identified with current options for establishing coordinates for study sites include topographic maps and global positioning systems.

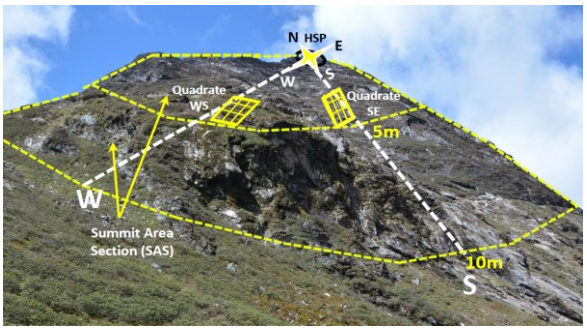

Figure. 3: Long term monitoring setup at Arunachal Pradesh under HIMADRI programme (Source: Bajpai *et al.*, 2016c)

2.1.6 Remote sensing

Remote sensing technologies can be used for long term monitoring due to its nature of revisit in the study area (Melesse et al., 2007). Several types of remotely sensed data are available, which can be used for the assessment of lichen diversity for climate change purpose. The airborne, hyperspectral, and space-borne multispectral remote sensing datasets can be employed to map their distribution patterns at various scales. Remote sensing practices help to map spatial distribution, identifying spatiotemporal changes in the distribution and analyzing the disturbance patterns among the major lichen community (Nordberg and Allard 2002).

The use of Digital Elevation Models (DEMs) and GIS (Geographic Information Systems) technologies help in analyzing the spatial patterns of lichens. The field information collected through the field plots can be visualized and correlated for a better understanding of the relationship of lichens along with its surrounding environment. Predictive modelling provides potentially suitable habitats for the major lichen community and also can be used with various climate datasets to predict the distribution pattern due to climate change. Assessment on

large scale patterns of responses with broad species representation like air pollution data, diversity and distribution and community composition towards understanding current and future importance of climate change on species performance and diversity can be done. In the Indian context, few studies are available on use of geographic information systems and lichens to map air pollution (Bajpai et al 2014, Singh et al 2016). Waser et al., (2007) developed several models to predict lichen species richness on soil, rocks and trees in Swiss Pre-Alps following a gradient of land-use intensity combining remote sensing data and regression models. Though the remote sensing techniques cannot replace lichen survey altogether, however, these methods provide information that is remotely similar to field samples and which would allow to considerably reduce extensive field surveys (Cousins and Ihse, 1998).

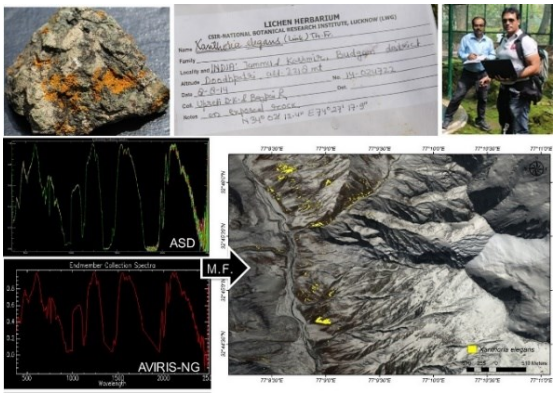

Figure 4: Match filtering technique based classification of Xanthoria elegans lichen using endmember spectra collected from the herbarium records of CSIR-NBRI, Lucknow and AVIRIS-NG data over Lahaul Taluka, Himachal Pradesh (DOA: 18/02/2016)

There is a need to develop a field method to spectrally analyze lichen species and communities that will be able to quantify species composition and cover. The comparison of community structure changes over time, and the correlation of spectral signatures with physiology or toxic element uptake in lichens are the supportive elements for the study. Because of the good development of lichen dominated communities in the Alpine region of Indian Himalaya the potential of mapping their distribution directly by matching image (narrowband) pixel spectra with the reference (hyperspectral) spectra of lichens using a matched filtering algorithm can be used (Figure 4). This is a more appropriate technique, as partial unmixing can detect the presence of a given material (in our case lichens) at a sub-pixel scale. Such techniques have been widely used in mineralogical and lithological studies and recently been applied for the mapping of lichens (Casanovas et al., 2015). Moreover, the concept of spectral species can be explored further, using hyperspectral imageries at high spatial resolution.

2.1.7 Lichenometry

Quantitative estimation of paleoclimate is fundamental for the reconstruction of past environmental and biotic change and that provides a baseline for predicting the effects of future regional and global climate change. Glaciers are recognized as one of the most sensitive indicators of climate change, advancing substantially during climate cooling and retreating during climate warming. Lichenometric technique has been proved useful in dating moraine ridges on recent glacier forelands in alpine regions. Since once attached to the substratum, the position of lichen thallus during the entire life span does not change; therefore, the age of lichen is an alternate for the minimum exposure time of a substrate to the abiotic factors.

The method of lichenometry was originally developed and used by Beschel (1973), and since then it has been widely applied in dating recently exposed rocky substrates in the world (Armstrong, 2005). In the Indian context, Joshi and Upreti (2010); Bajpai et al., (2016b) recently studied lichenometry, to study the glacier retreat in some major Indian Himalayan Glaciers (Figure 5). Based on the methods applied, lichenonometry may be direct and indirect. The direct lichenometry deals with observations on individual lichens at repeated intervals overtime where, indirect lichenometry is a correlation established between the size of the thallus and the surface age, based on lichens growth measurements from surface of known age e.g: Graves's stones, stone wall/ manmade artefacts etc.

Figure 5: Lichenometry with lichen a. *Xanthoria elegans* b. *Rhizocarpon geographicum*

The percentage of lichen cover is also used as a growth index. Innes (1988), provided a list of micro-and macrolichens that can be used in lichenometric studies. Mainly the species having more or less typical centrifugal pattern of growth are recommended for dating purpose. The most often used species in lichenometric studies is *Rhizocarpon geographicum*, because of its bright colour easy to recognized in field, circular growth and worldwide distribution in alpine areas. In alpine environments, *R. geographicum* attains slow growth rates of 0.2 mm/year (Hansen, 2008) and lives up to a considerable age. Morphologically, this lichen comprises discrete areolae that contain algal cells of *Trebouxia*, located on a fungal medulla, which is attached to the substratum and extends into a black algal-free marginal zone around the thallus called hypothallus. Primary areolae near the edge of the hypothallus may develop from free-living algal cells on the substratum that are trapped by the hypothallus whereas secondary areoles may develop from zoospores produced within the thallus, thus ultimately resulting in the radial growth of *Rhizocarpon*.

Due to their slow growth rate and uniform growth size, lichens help in dating the exposure time of the sequences of the rock-forming glacier moraines due to retreat of the glacier thus providing the approximate time of glacier retreat. The lichenometry appears to be superior to many other techniques; it attempts to date glacial deposits in the most accurate way. The technique is easy, cheap and can

be applicable to date surfaces less than 500-years-old where radiocarbon dating is least efficient.

2.1.8 Lichen biological soil crust (BSC) assessment

The biological soil crusts are a complex community of primaeval organisms that flourish worldwide in harsh, arid, semi-arid and cold desert regions. The bare ground is not an abiotic ground, truly, the soil surface in areas free of higher vegetation is often covered by a casing made up of a community of cryptogams, like lichens, bryophytes cyanobacteria and algae forming a complex structure known as biological soil crusts (BSCs). They are also the first colonizers of disturbed soils and have major influences on the soil properties through stabilization, erosion limitation, and facilitation of colonization by higher plants. The BSCs plays a crucial role in stabilizing bare soil, stemming erosion from wind and rain, trapping moisture, fixing carbon and nitrogen in the soil, and providing shelter for the seeds of vascular plants (Lehnert et al. 2018).

The spectral characteristics of BSCs or their species components were investigated by a certain research study (review Ager et. al. 1987, Chongfeng et al. 2013). Chen et. al. (2005) recognized that mapping BSCs by relying on remote sensing images was feasible, and they effectively-identified lichen crust in the Namibia desert using Landsat Thematic Mapper 3 data (TM bands 4, 5,and 7) and compared both true colour air-photos and hyperspectral imagery at around 10 m spatial resolution to identify BSCs, and successfully assimilated BSCs patterns. Further to detect cyanolichens BSCs, the crust index (CI) was established by Karnieli and Tsoar (1995) using aerial photograph and Landsat TM data. After CI the biological soil crust index (BSCI) was proposed to identify lichen-dominated BSCs which allowed more accurate separation of BSCs from the background (Chen et al. (2005). The composition and stage of BSCs significantly affect its spectrum and found that BSC index can serve as a good indicator during the early years after a disturbance when relatively few microphytes are established in the soil surface (Zaady et al. 2007). However, despite the important information attained from mapping indices and reflectance spectroscopy, specifically, the ability to spectrally monitor BSCs functional response to climatic change is increasingly important, as these organisms will experience significant shifts in both function and composition, resulting in large scale changes to soil stability, soil fertility, and biogeochemical cycling in future climate. Further to understand the roles of BSCs in carbon and nitrogen fixation and monitor their distribution patterns in the region by remote sensing technology, and to evaluate the roles of carbon and nitrogen fixation in the whole ecological system may definitely open a new path for further researches in the country.

2.2 Active methods

2.2.1 Transplantation

The lichen transplants are used to assess air quality in an area where lichens are absent or sparse. Richardson (1992) reviews the use of transplants to assess air quality in the urban environment and to monitor contaminants in air and water. The healthy lichens are transferred from an area where they occur naturally to test area. The changes in physiology, morphology and element accumulation provide data that can be correlated with extend and impact of pollution in an area. Most of the transplantation experiments have been performed with corticolous lichen and particularly with foliose lichen because they are generally more tolerant of gaseous or airborne pollutants. The twigs having lichens or lichen bearing bark are fixed in 20x20 cm cardboard with any fixative (Araldite), are placed or hanged on trees and if trees are absent, the electric pole or other objects are used for hanging the board. The observations on morphological, anatomical changes and the health status of lichens together with physiological changes provide important data related to the degree of pollution prevailing in the area.

2.2.2 Open top chambers (OTC)

Open-top chambers used in the field duplicate the ambient environment as closely as possible while allowing control of pollutant concentration within the chambers. Appropriate experimental designs for using open-top chamber systems include pollutant-free and ambient chambers as well as non-chambered control plots to estimate any chamber effects. The open-top chambers are the best currently available experimental technique for developing functional relationships useful for predictive purposes (Shriner et al., 1990).

Figure 6: Open Top Chamber (OTC)

The OTCs are made-up of polyvinyl chloride (PVC) plastic film enclosed by hexagonal frame constructed by aluminium (Figure 6). The OTC approach for long-term climate change monitoring with lichens in Indian Himalayan region is also initiated recently. Due to the unhurried growing rate and sensitive nature of lichens can be utilized as an indicator of climatic changes, on which they are growing as well as kept in OTC for continuous observations. Other parameters like lichen diameter, qualitative and quantitative estimation of secondary metabolites in high altitude lichens may perform in OTC and their comparison with control may also lead to correlate with rising temperature as well as against high UV radiations.

2.2.3 Dust load

Dust may also be secondary stress like drought, insects and pathogens. Effects of dust on natural communities may alter the competitive balance between species in a community. The dust interception and its accumulation in different plant species not only depends upon the sources and amount of pollutants in the environment but also depends on morphological characters of plants too. The most extensive evidence for the effects of dust on plant

communities has come from studies on epiphytic lichens. Gilbert (1976) studied the effect of dust on lichens and described the effects of limestone on epiphytic lichen communities form distinctive zones around sources of sulphur dioxide pollution. He found zones surrounding a lime dust source and resulted that heavily dusted trees had few lichens, but this was followed by a zone containing lichens that are normally saxicolous i.e. *Caloplaca decipiens*, *Catillaria chalybeia*, *Lecanora Calcarea*, *L. campestris, Lecidella scabra* and some species of *Bacidia* and *Micarea*. In 1980 Kaupii stated that fertilizer factories dust also affect lichens and showed the application of fertilizer dust to *Hypogymnia physodes* and *Cladonia Stellaris* caused a temporary increase in net photosynthesis and an increase in the number of algal cells in the thalli. The measurement of dust is an important parameter to observe the qualitative as well as quantitative particulate matter in the area.

2.2.4 Accumulation assessment

The various heavy metals, metalloids, pesticides, persistent organic pollutants (POPs, radionucliotides are widely accumulated in lichens through active as well as passive methods. These pollutants accumulated in lichen thallus through absorption as well as adsorption beyond their physiological needs. In Indian context the metal accumulation data on different lichens species growing in and around major Indian cities such as Pune, Bengaluru, Lucknow, Mahabaleshwar, Darjeeling, Dehradun, Pauri and Srinagar are available (Shukla et al., 2014).

Apart from metals, metalloids (inorganic) and organic pollutants lichens have an ability to accumulate the radioactive substances like Cesium, Thorium, Cobalt, Plutonium, Radium, Radon, Uranium and Strontium in their thalli in huge amount. The analysis of these radionuclides in the lichen thallus can be done following the procedure of US EPA (1986) and modified by Kircher and Daillant (2002). The radionuclides in lichen samples can be analyzed through gamma-spectrometrically using a large volume reversed electrode high purity germanium detector (Canberra, 55% relative efficiency). Unlike conventional coaxial detectors, this detector has a usable energy range which extends down to 5keV and thus enables to determine ^{210}Pb by measuring its 46.5 keV gamma line.

3. Conclusion

It is assumed that apart from a number of complex and costly techniques available for monitoring air pollution and climate change, the present methods help to familiarize some easy and low cost, practices which would not only reduce considerably the wide-field survey but also help to obtain simple data for developing pollution and climate change models using Geomatics techniques. The methods described in the present communication are ample contribution to the ongoing discussion of global as well as regional pollution and, climate change methodologies assessment in the near future.

Acknowledgements

Authors are thankful to Director, CSIR-National Botanical Research Institute, Lucknow, for allowing to use of facilities and for continuing support and encouragement during the course of study. One of the authors RB would like to thank the Council of Scientific and Industrial Research, New Delhi for award of Scientist Pool fellowship (8909-A). Authors are also thankful to Director, SAC/ISRO and DD, EPSA/SAC for their support in conducting research over lichens under SHRESTI program of ISRO.

References

Ager, C. M. and N. M., Milton (1987) Spectral Reflectance of Lichens and their Effects on the Reflectance of Rock Substrates. Geophysics 52, 898

Armstrong, R.A. (2005). Radial growth of *Rhizocarpon* section *Rhizaocarpon* lichen thalli over six years at Snoqualmie Pass in the Cascade Range, Washington State. Arctic, Antarctic and Alpine Research, 37 (4), 411-415.

Bajpai, R., C. P. Singh, P. Shukla and D. K. Upreti (2016b). Preliminary lichenometric studies in Eastern and North-Western Himalaya. Journal of Geological Society of India 57, 535-538.

Bajpai, R., S. Mishra, S. Dwivedi and D. K. Upreti (2016a). Change in an atmospheric deposition during last half-century and its impact on lichen community structure in Eastern Himalaya. Scientific Report 6, 30838 (doi: 10.1038/srep30838)

Bajpai, R., V. Shukla, C. P. Singh, O. P. Tripathi, S. Nayaka and D. K. Upreti (2018). Lichen community composition in Tawang district of Arunachal Pradesh, a tool for long-term climate change monitoring. Proceedings of the National Academy of Sciences, India Section B: Biological Sciences, 88 (3), 915-922

Bajpai, R., V. Shukla, C.P. Singh, O.P. Tripathi, S. Nayaka and D.K. Upreti (2016c). Lichen Community Composition in Tawang District of Arunachal Pradesh, Tool for Long-Term Climate Change Monitoring, Proc. Natl. Acad. Sci., India, Sect. B Biol. Sci. (PNASI), DOI 10.1007/s40011-016-0830-z,.

Bajpai, R., V. Shukla, D. K. Upreti and M. Semwal (2014). Selection of suitable lichen bioindicator species for monitoring climate change variability in the Himalaya. Environmental Science and Pollution Research, 21, 11380-11394.

Beschel, R. (1973). Lichens as a measure of the age of recent moraines. Arctic and Alpine Research, 5, 303–309.

Casanovas, P., M. Black, P. Fretwell and P. Convey (2015). Mapping lichen distribution on the Antarctic Peninsula using remote sensing, lichen spectra and photographic documentation by citizen scientists, Polar Research 34(1), 25633 (DOI: 10.3402/polar.v34.25633).

Chen, J., Y.Z., Ming, L.m Wang, H., Shimazaki and M. Tamura (2005) A new index for mapping lichen-

dominated biological soil crusts in desert areas. Remote Sens. Environ., 96, 165–175.

Chonyfeng B., W. Shufang, X. Yungsheng and Z. Xingchang (2013) The study of Biological soil crust: Hotspot & prospects. Clean- soil, air-water, 41(9), 889-906.

Cousins, S. A. O. and M. Ihse (1998). A methodological study for biotype and landscape mapping based on CIR aerial photographs. Landscape and Urban planning, 41, 183-192.

Gilbert, O. L. (1976). An alkaline dust effect on epiphytic lichens. Lichen., 8, 173-8.

Grace, J., F. Berninger and L. Nagy (2002). Impacts of climate change on the tree line. Ann. Botany, 90, 537–544.

Haffner, E., B. Lomsky, V. Hynek, J. E. Hallgren, F. Batic and H. Pfanz (2001). Air pollution and lichen physiology. Physiological responses of different lichens in a transplant experiment following an SO_2 gradient. Water air and soil pollution, 131 (1-4), 185-201.

Hansen, E.S. (2008). The application of lichenometry in dating glacier deposits. Geogr. Tidsskr. Dan. J. Geography, 108, 143–151.

Herzig, R., L. Liebendorfer, M. Urech, K. Ammann, M. Cuecheva and W. Landolt (1989). Passive biomonitoring with lichens as a part of an integrated biological measuring system for monitoring air pollution in Switzerland. International Journal of Environmental and Analytical Chemistry, 35, 43-48.

Innes, J. L. (1988). The use of lichens in dating. In: Galun M (ed.) Handbook of lichenology vol III, CRC Press, Boca Raton, Florida, 75-91.

Insarov, G. E and B. Schroeter (2002). Lichen monitoring and climate change. In: Nimis PL, et al. (eds.) Monitoring with Lichens–Monitoring Lichens. NATO Science Series, IV, vol. 7. Kluwer, Dordrecht, 183-201.

Joshi, S and D. K. Upreti (2010). Lichenometric studies in the vicinity of Pindari Glacier in the Bageshwar district of Uttarakhand, India, Current Science, 99 (2), 231-235.

Karnieli, A., and H. Tsoar (1995) Spectral reflectance of biogenic crust developed on desert dune sand along the Israel-Egypt border. International Journal of Remote Sensing 16, 369-374.

Lehnert, L.W., P. Jung, W.A. Obermeier, B. Burkhand and J. Bendix (2018) Estimating net photosynthesis of biological soil crust in the Atacama using Hyperspectral Remote Sensing. Remote Sensing, 10, 891.

McCune, B (1992). Lichen Communities. Forest Health Monitoring, Field Methods Guide. Section 14. USDA Forest Service, Southeast Forest Experiment Station, Research Triangle Park, NC 27709, 1-6.

Melesse A. M., Q. Weng, P. S. Thenkabil, G. D. Senay (2007). Remote sensors and application in Environmental resource mapping and modelling. Sensors (Basel), 7 (12), 3209-3241.

Nordberg, M.L., A. Allard (2002). A remote sensing methodology for monitoring lichen cover. Canadian Journal of Remote Sensing, 28(2), 262-274.

Pickett, S. T. A., S. L. Collins and J. J. Armesto (1987). A hierarchical consideration of causes and mechanisms of succession. Vegetatio, 69, 109–114.

Richardson, D. H. S. (1992). Pollution Monitoring with Lichens, Richmond Publishing Co. Ltd., Slough, UK, pp 76-80.

Rose, C.I. and D.L. Hawksworth (1981). Lichen recolonization in London's cleaner air. Nature 289, 289-292

Shriner, D. S., W. W. Heck, S. B. McLaughlin, and D. W. Johnson. (1990). The response of Vegetation to Atmospheric Deposition and Air Pollution NAPAP SOS/T Report 18, In Acidic Deposition: State of Science and Technology, Volume III, National Acid Precipitation Assessment Program, 722 Jackson Place NW, Washington DC. 20503.

Shukla, V., D. K. Upreti and R. Bajpai (2014). Lichens to biomonitor the environment, Springer, Heidelberg New York Dordrecht London.

Singh, C. P., R. Bajpai, R. P. Singh, D. K. Upreti (2016). Improving bioclimatic develop modelling for lichens through remote sensing-based substratum corrections: A study over Indian Himalaya. Cryptogamic Biodiversity Assessment, 1(2), 1-19.

Singh, C.P., (2015). Long-term monitoring of alpines of the Himalaya, ENVIS Newsletter on Himalayan Ecology, 12 (2).

Singh, C.P., J. Mohapatra, H.A. Pandya, B. Gajmer, N. Sharma, D.G. Shrestha (2018). Evaluating changes in treeline position and land surface phenology in Sikkim Himalaya, Geocarto International, (DOI:10.1080/10106049.2018.1524513).

US Environmental Protection Agency (1986). Guidelines for Carcinogen and Risk Assessment. EPA/630/R-00/004, Sep 1986. http://www.epa.gov/ cancerguidelines/guidelines-carcinogen-risk-assessment-1986.htm, 23-06

Waser, L.T., M. Kuechler, M. Schwarz, E. Ivits, D. Stofer and C. Scheidegger (2007). Prediction of lichen diversity in a UNESCO biosphere reserve-correlation of high-resolution remote sensing data with field samples. Environmental Monitoring Assessment, 12, 315-328.

Zaady, E., A. Karnieli and M., Shachak (2007) Applying a field spectroscopy technique for assessing successional trends of biological soil crusts in a semi-arid environment. Journal of Arid Environments, 70, 463-47

Reviewers for Journal of Geomatics, Volume 13 No. 1 and 2

Editorial Board places on record its sincere gratitude to the following peers for sparing their valuable time to review papers of the Journal of Geomatics, Volume 13.

Dr. A.S. Rajawat
Chief Editor

Mrs. Shweta Mishra	Mrs. Shivani M. Shah	Dr. Sujay Dutta
Dr. S.P. Vyas	Dr. Rahul Nigam	Dr. K.M. Sreejith
Shri Naveen Tripathy	Dr. Sanjib Deb	Dr. Sandip Oza
Dr. Abhisek Chakraborty	Dr. Sameer Saran	Dr. C.P. Singh
Dr. Kasturi Chakraborty	Dr. Mehul pandya	Dr. Anjana Vyas
Dr. Chetan R. Patel	Dr. Abha Chabra	Shri. K.S. Pandya
Dr. Aloke Mathur	Ms. Kriti Rastogi	Shri. Jaya Prasad
Dr. Nikhil Lele	Shri. T V R Murthy	Dr. A.S. Arya
Shri. Amitabh	Dr. Ranendu Ghosh	Dr. IM Bahuguna
Dr. Praveen Gupta	Dr. P K Thapliyal	Dr. N R Patel
Dr. V N Sridhar	Dr. Anup Das	Shri Ritesh Agrawal
Dr. Sasmita Chaurasia	Dr. Manoj Mishra	Shri Ramdayal Singh
Shri C. Patnaik	Dr. Kiran chand	Dr. Amit Kumar Dubey
Dr. Ashish Shukla	Shri Ashwin Gujarati	Dr. Rashmi Sharma
Ms. Preeti Rajput	Dr. Shard Chander	Dr. Bimal Bhattacharya
Dr. Markand P Oza	Dr. Nitant Dube	Shri Vibhuti Jha
Dr. Shiv Mohan	Shri. Utkarsh	Shri D.K Patel
Dr. Sushil.Kumar Singh	Dr. R.M. Gairola	Dr. Arvind Sahay
Dr. K.N. Babu	Dr. Smitha Ratheesh	Shri Anurag Gupta
Dr. Neeraj Agarwal	Mr. Hrishikesh Kumar	Dr. Phani Rajasekhar
Dr. Mulemwa Akombe	Dr. Gaurav Jain	Mr. Ashutosh Gupta
Dr. Kaushik Gopalan	Dr. Salil Goel	Dr. Anupam Singh
Shri Manish Parmar	Dr. Pabitra Kumar Mani	Shri R.J. Bhanderi
Prof. Darshana Rawal	Shri J.G. Patel	Dr. S.A. Sharma
Shri Rajendra Gaikwad	Dr. Atul Varma	Dr. Bipasha Shukla
Dr. V. Sathyamoorthy	Mr. T.P. Srinivasan	Dr. Manthira Moorthy
Neeta Bhagia	Dr. Arvind Kumar Singh	Dr. Siva Kumar
Dr. R. Jaishanker	Dr. C P Johnson	Dr. R. Anbalagan
Dr. K. V. Suryabhagavan	Prof. B.S. Mipun	Dr. Sandeep Maithani
Dr. Ashutosh Bhardwaj	Prof. Sunil Kumar Wanchoo	Dr. S. Muralikrishnan
Dr. Anil Kumar	Dr. Chandan Goswami	Dr. P.L.N. Raju
Dr. Siva Kumar	Dr. B. Kartikeyan	Ms. Sunanda Trivedi
Dr. Hitendra Padaliya	Prof K.S. Jayappa	Dr. Nandini Ray Chaudhury

Journal of Geomatics Author index (Vol. 13)

INDIAN SOCIETY OF GEOMATICS: AWARDS

National Geomatics Award for Excellence

This award has been instituted to recognize outstanding and conspicuously important contribution in promoting geomatics technology and applications at the country level. The contributions should have made major impact on the use of this technology for national development.
Areas of contribution considered for the award are:

1. Geographical Information System
2. Global Positioning System
3. Photogrammetry
4. Digital Cartography
5. Applications of Geomatics

The award shall consist of Rs. 50,000/- in cash, a medal and citation.

Eligibility

Any citizen of India, engaged in activities related to geomatics technology and its applications is eligible for this award. The prize is awarded on the basis of work primarily done in India.

The age limit for awardees is 45 years or above as on June 30 of the year of award.

Selection

A duly constituted Award Committee will evaluate all nominations received. The committee shall consist of eminent experts in the field of geo-spatial technology, to be identified by the Executive Council, ISG. The committee shall forward selected name/s to ISG – EC for approval and announcement. Apart from those persons, whose nominations have been received, the Committee may consider any person or persons who, in their opinion, have made outstanding contributions to development of geo-spatial technology and applications.

The award can be withheld in any year if, in the opinion of the committee, no candidate is found suitable in that particular year.

Presentation of the Award

The award shall be presented during the Annual Convention of ISG. Local Hospitality shall be taken care by ISG & Air fare (low cost) may be reimbursed if awardees request for it.

How to make Nomination

The nominations can be proposed by Head of a major research institute/ centre; Vice-Chancellor of a university; Secretary of Government Scientific Departments; President of a National Academy, President, Indian Society of Geomatics / Indian Society of Remote Sensing / Indian National Cartographic Association / ISG fellow or two life members of the society with more than 10 year old membership.

A candidate once nominated would be considered for a total period of two years. Nomination should be sent in the prescribed format to Secretary, ISG.

The last date for receiving nominations shall be September 30 or otherwise extended.

Format for nomination of Geomatics Award for Excellence

1. Name of the Nominee
2. Postal Address
3. Academic Background (Bachelor degree onwards)
4. Field of Specialisation
5. Important positions held (in chronological order)
6. Professional Experience including foreign assignments.
7. Important Awards / Honours
8. Important Publications/Patents: (A set of ten most important publications to be enclosed with this form)
9. Contributions of Nominee based on which the nomination is sent (in 1000 words, also provide a statement in 50 words which may be used for citation.):
10. Other Relevant Information:

Proposer:

Signature
Name
Address
Phone/ Fax
E-mail
Life Membership No. (in case of ISG Member):

Place & Date

Endorsed by (in case nomination is by 2 ISG Life members)

Signature
Name
Address
Phone/ Fax
E-mail
Life Membership No. (in case of ISG Member):

Place & Date
(The proposer should give a brief citation of the nominee's work)

National Geomatics Award

National Geomatics Award to be given each year: a) for original and significant contribution in Geomatics technology, b) for innovative applications in the field of Geomatics. Each award comprises a medal, a citation and a sum of Rs 25,000/- The guidelines for these awards are available on ISG website.

ISG Chapter Award for Best Performance

The best chapter award will be given to an active chapter of Indian Society of Geomatics, which has made significant contribution to further the mandate and goal of the society. The award consists of a citation and medal

President's Appreciation Medal for Contribution to the ISG

This award will be given to a member of the society, who has made noteworthy contribution to the growth of the ISG (its main body or any chapter). The Award consists of a Medal and a Citation.

Prof. Kakani Nageswara Rao Endowment Young Achiever Award

Indian Society of Geomatics instituted a new award from year 2013 named "Prof. Kakani Nageswara Rao Endowment Young Achiever Award", to encourage young researchers/scientists/academicians pursuing research in the field of geospatial technology/applications. The award carries a cash prize of Rs. 10,000/- along with a citation.

NATIONAL GEOMATICS AWARD

Indian Society of Geomatics has instituted two National Geomatics Awards to be given each year for (a) Original and significant contribution in Geomatics technology, (b) Innovative application(s) in the field of Geomatics. Each award comprises a medal, a citation and a sum of Rs. 25,000/-.

The guidelines for the award are as under

Areas of contribution considered for the award (both technology and applications)

1. Geographical Information System
2. Global Positioning System
3. Photogrammetry
4. Digital Cartography
5. Remote Sensing

Eligibility

Any citizen of India engaged in scientific work in any of the above-mentioned areas of research is eligible for the award.

The awards are to be given for the work largely carried out in India.

- First award will be given for original contribution in the field of Geomatics technology supported by publications in a refereed journal of repute.
- Second award will be given for carrying out innovative application(s). Supported by publications in rear reviewed Journals of repute.
- The contribution for the first award should have been accepted by peers through citation of the work.
- Work based on the applications of existing technologies will not be considered for the first award.
- The work should have made impact on the overall development of Geomatics.

How to Send Nomination

Nominations should be sent in the prescribed format, completed in all aspects to the Secretary, Indian Society of Geomatics, Space Applications Centre Campus, Ahmedabad 380 015 by August 31, 2017.

Selection Process

An expert committee, consisting of at least three members, constituted by the Executive Council of the Indian Society of Geomatics, will scrutinize the nominations and recommend the awardees' names to the Executive Council. The Council will decide on the award based on the recommendations.

FORMAT FOR AWARD NOMINATION

1. Name of the Candidate:
2. Present Position:
3. Positions held earlier (chronological order):
4. Academic qualifications (Bachelor's degree onwards):
5. Names of at least three Indian Scientists/Technologist in the area as possible referees *:
6. Brief write up on the work (500 words) for which award is claimed:
7. Publication(s) on the above work (reprint(s) to be enclosed):
8. List of other publications of the candidate:
9. Citation of the work for which award is claimed:
10. Impact of the work (for which award is claimed) on the development in the field of Geomatics (500 words):
11. Whether the work has already won any award? If so, give details:

The Applications in the above format (five copies) should be submitted (by Registered Post or Speed Post) to

The Secretary, Indian Society of Geomatics,
Space Applications Centre Campus,
Ahmedabad-380015

so as to reach by September 30, 2018

*ISG is, however, not bound to accept these names and can refer the nomination to other experts/peers

INDIAN SOCIETY OF GEOMATICS: FELLOWS

Shri Pramod P. Kale, Pune
Dr George Joseph, Ahmedabad
Dr A.K.S. Gopalan, Hyderabad
Dr Prithvish Nag, Varanasi
Dr Baldev Sahai, Ahmedabad
Shri A.R. Dasgupta, Ahmedabad
Dr R.R. Navalgund, Bengaluru
Shri Rajesh Mathur, New Delhi
Dr Ajai, Ahmedabad
Prof P. Venkatachalam, Mumbai
Dr Shailesh Nayak
Prof I.V. Murli Krishna
Prof SM Ramasamy, Tiruchirapalli
Dr Ashok Kaushal, Pune
Shri A.S. Kiran Kumar, Bengaluru
Prof. P.K. Verma, Bhopal
Maj. Gen. Siva Kumar, Hyderabad

INDIAN SOCIETY OF GEOMATICS: PATRON MEMBERS

P-1 Director, Space Applications Centre (ISRO), Jodhpur Tekra Satellite Road, Ahmedabad - 380 015
P-2 Settlement Commissioner, The Settlement Commissioner & Director of Land Records-Gujarat, Block No. 13, Floor 2, Old Sachivalay, Sector-10, Gandhinagar – 382 010
P-3 Commissioner, Mumbai Metropolitan Region Development Authority, Bandra-Kurla Complex, Bandra East, Mumbai - 400 051
P-4 Commissioner, land Records & Settlements Office, MP, Gwalior - 474 007
P-5 Director General, Centre for Development of Advanced Computing (C-DAC), Pune University Campus, Ganesh Khind, Pune - 411 007
P-6 Chairman, Indian Space Research Organization (ISRO), ISRO H.Q., Antariksha Bhavan, New BEL Road,Bengaluru 560 231
P-7 Director General, Forest Survey of India, Kaulagarh Road, P.O. I.P.E., Dehra Dun – 248 195
P-8 Commissioner, Vadodara Municipal Corporation, M.S. University, Vadodara - 390 002
P-9 Director, Centre for Environmental Planning and Technology (CEPT), Navarangpura, Ahmedabad - 380 009
P-10 Managing Director, ESRI INDIA, NIIT GIS Ltd., 8, Balaji Estate, Sudarshan Munjal Marg, Kalkaji, New Delhi - 110 019
P-11 Director, Gujarat Water Supply and Sewerage Board (GWSSB), Jalseva Bhavan, Sector – 10A, Gandhinagar - 382 010
P-12 Director, National Atlas & Thematic Mapping Organization (NATMO), Salt Lake, Kolkata - 700 064
P-13 Director of Operations, GIS Services, Genesys International Corporation Ltd., 73-A, SDF-III, SEEPZ, Andheri (E), Mumbai - 400 096
P-14 Managing Director, Speck Systems Limited, B-49, Electronics Complex, Kushiaguda, Hyderabad - 500 062
P-15 Director, Institute of Remote Sensing (IRS), Anna University, Sardar Patel Road, Chennai - 600 025
P-16 Managing Director, Tri-Geo Image Systems Ltd., 813 Nagarjuna Hills, PunjaGutta, Hyderabad - 500 082
P-17 Managing Director, Scanpoint Graphics Ltd., B/h Town Hall, Ashram Road, Ahmedabad - 380 006
P-18 Secretary General, Institute for Sustainable Development Research Studies (ISDRS), 7, Manav Ashram Colony, Goplapura Mod, Tonk Road, Jaipur - 302 018
P-19 Commandant, Defense institute for GeoSpatial Information & Training (DIGIT), Nr. Army HQs Camp, Rao Tula Ram Marg, Cantt., New Delhi - 110 010
P-20 Vice President, New Rolta India Ltd., Rolta Bhavan, 22nd Street, MIDC-Marol, Andheri East, Mumbai - 400 093
P-21 Director, National Remote Sensing Centre (NRSC), Deptt. of Space, Govt. of India, Balanagar, Hyderabad - 500 037
P-22 Managing Director, ERDAS India Ltd., Plot No. 7, Type-I, IE Kukatpalli, Hyderabad - 500 072
P-23 Senior Manager, Larsen & Toubro Limited, Library and Documentation Centre ECC Constr. Gp., P.B. No. 979, Mount Poonamallee Road, Manapakkam, Chennai - 600 089.
P-24 Director, North Eastern Space Applications Centre (NE-SAC), Department of Space, Umiam, Meghalaya 793 103
P-25 Progamme Coordinator, GSDG, Centre for Development of Advanced Computing (C-DAC), Pune University Campus, Pune – 411 007
P-26 Chief Executive, Jishnu Ocean Technologies, PL-6A, Bldg. No. 6/15, Sector – 1, Khanda Colony, New Panvel (W), Navi Mumbai – 410 206
P-27 Director General, A.P. State Remote Sensing Applications Centre (APSRAC), 8th Floor, "B" Block, Swarnajayanthi Complex, Ameerpet, Hyderabad- 500 038
P-28 Director, Advanced Data Processing Res. Institute (ADRIN), 203, Akbar Road, Tarbund, Manovikas Nagar P.O., Secunderabad –500 009
P-29 Managing Director, LEICA Geosystems Geospatial Imaging Pvt. (I) Ltd., 3, Enkay Square, 448a Udyog Vihar, Phase-5, Gurgoan- 122 016
P-30 Director, Defense Terrain Research Limited (DTRL), Ministry of Defense, Govt. of India, Defense Research & Development Organisation, Metacafe House, New Delhi – 110 054
P-31 Chairman, OGC India Forum, E/701, Gokul Residency, Thakur Village, Kandivali (E), Mumbai – 400 101
P-32 Managing Director, ML Infomap Pvt. Ltd., 124-A, Katwaria Sarai, New Delhi – 110 016
P-33 Director, Rolta India Limited, Rolta Tower, "A", Rolta Technology Park, MIDC, Andheri (E), Mumbai – 400 093
P-34 Director, State Remote Sensing Applications Centre, Aizawl – 796 012, Mizoram

Journal of Geomatics Vol 13, No. 2, October 2019

Instructions for Authors

The journal covers all aspects of Geomatics – geodata acquisition, pre-processing, processing, analysis and publishing. Broadly this implies inclusion of areas like GIS, GPS, Photogrammetry, Cartography, Remote Sensing, Surveying, Spatial Data Infrastructure and Technology including hardware, software, algorithm, model and applications. It endeavors to provide an international forum for rapid publication of developments in the field – both in technology and applications.

A manuscript for publication must be based on original research work done by the author(s). It should not have been published in part or full in any type of publication nor should it be under consideration for publication in any periodical. Unsolicited review papers will not be published.

The Editorial Board or the Indian Society of Geomatics is not responsible for the opinions expressed by the authors.

Language

The language of the Journal will be English (Indian). However, manuscripts in English (US) and English (British) are also acceptable from authors from countries located outside India.

Manuscript Format

Each paper should have a title, name(s) of author(s), and affiliation of each of the authors with complete mailing address, e-mail address, an abstract, four to six keywords, and the text. The text should include introduction/background, research method, results, discussion, followed by acknowledgements and references. The main text should be divided in sections. Section headings should be concise and numbered in sequence, using a decimal system for subsections. Figures, images and their captions should be inserted at appropriate points of the text. Figures, images and tables should fit in two column format of the journal. If absolutely necessary, figures, images and tables can spread across the two columns. Figures and images, however, should not exceed half a page in height. A title should be provided for each Table, Image and Figure. All figures and images should be in 600 dpi resolution and sized as per column/margin width. Authors must ensure that diagrams/figures should not lose easy readability upon reduction to column size. The SI (metric) units and international quantities should be used throughout the paper. In case measurements are given in any other system, equivalent measurements in SI (metric) units should be indicated in brackets.

Use MS Word with English (UK/US) or English (Indian) dictionary. The page size should be A4 paper, with 2 cm margin on all sides. Title, authors and affiliation should be centred. Abstract should be justified across margins. The manuscript text should be in two columns of 8.2 cm each with a gutter of 6mm between them. Use only Times New Roman fonts. Title should be 12 points bold. Authors and affiliation should be 9 points. All other text including headings should be 10 points. Heading numbering scheme should be decimal e.g. 1, 1.1, 1.2.3, etc. Headings should be in bold.

Normally length of a published paper should be about 6-10 pages in A4 size including figures. Use of illustrations in colour should be restricted and resorted to only where it is absolutely necessary and not for enhancing the look of the paper. If the number of colour illustrations exceeds five, authors' institution may be asked to reimburse the extra cost involved, which at current rates is about Rs. 2500 per coloured figure/diagram/plate/illustration.

Submission of Manuscript

Submissions should be in electronic form via email. The manuscript may be sent by email to drajai1953@gmail.com. In exceptional cases hard copy submission in camera ready form may be allowed with the prior permission of the Chief Editor. Submission in any other form will be returned to the author. To speed up the review process, authors are advised to provide a list of three probable reviewers with their institutional address and e-mail IDs.

Guidelines for Citing References

Names of all cited publications should be given in full. No abbreviations should be used. Following procedure is to be adopted.

Journal Publications

Bahuguna, I.M. and A.V. Kulkarni (2005). Application of digital elevation model and orthoimages derived from IRS-1C Pan stereo data in monitoring variations in glacial dimensions, Journal of the Indian Society of Remote Sensing, 33(1), 107- 112. (to be referred to in the text as Bahuguna and Kulkarni (2005) or if more than two sets of authors are to be referred to, as (Bahuguna and Kulkarni, 2005; Jain et al., 1994)) When more than two authors are to be referred to, use Jain et al. (1994). However, in References, all authors are to be mentioned.

Publication in a Book

Misra, V.N. (1984). Climate, a factor in the rise and fall of the Indus Civilization – Evidence from Rajasthan and Beyond in Frontiers of the Indus Civilization (B.B. Lal and S.P. Gupta: Chief Editors) Books and Books, New Delhi, pp. 461-489

Papers Published in Seminar/ Symposium Proceedings

Jain, A., A.R. Shirish, M. Das, K. Das, M.C. Porwal, and P.S. Roy (1994). Remote Sensing and Geographic Information System – An approach for the assessment of biotic interference in the forest ecosystem. Proceedings. 15th Asian Conference on Remote Sensing, Bangalore, November 17-23, 1994, pp. 65-72.

Books

Possehl, Gregory L. (1999). Indus Age: The beginnings. Oxford and IBH Publishing Corporation, New Delhi.

Reviewing

Each paper will be reviewed by three peers. Papers forwarded by members of the Editorial or Advisory Boards along with their comments would get processed faster and may be reviewed by two referees only.

Sample format for Authors is available in downloadable form at ISG website: www.isgindia.org/JOG/Sample_format.doc

Copyright

The copyright of the paper selected for publication will rest with the Indian Society of Geomatics. Corresponding author shall be required to sign a copyright assignment form, on behalf of all authors, once the paper is selected for publication. Authors are, however, at liberty to use this material elsewhere after obtaining permission from the Indian Society of Geomatics.

If the authors have used any copyright material in their manuscript, it is understood that they have obtained permission from the owner of the copyright material and they should convey the same along with the manuscript to the Chief Editor.

Certificate of Original Work

The authors will also provide a certificate that the paper is an original work, not published or being considered for publication elsewhere.

In the event the certificate turns out to be false, the Journal shall ban the author(s) from publishing in the Journal for a period of five years and inform the same to all other related publications.

Reprints

Authors will be allowed to download the (PDF) of their paper from ISG Website www.isgindia.org, No hard copy reprints will be provided.

Journal of Geomatics

Advertisement Rates

	1 Issue	4 Issues
Back Cover Page in colour	**Rs. 25,000**	**Rs. 80,000**
Inside Cover Page in colour	**Rs. 20,000**	**Rs. 64,000**
Full Page inside in colour	**Rs. 15,000**	**Rs. 48,000**
Full Page inside in B/W	**Rs. 10,000**	**Rs. 32,000**

Advertisement Details

Mechanical Details
Double Spread/Center Spread (42 x 29.7) cm
Full page bleed (21 x 29.7) cm
Full page non-bleed (19 x 27.7) cm

Art Requirements

Negatives: Art must be right reading, emulsion, down. Film must be supplied in one piece per color, each identified by color. Camera-ready art is accepted for black & White adds; however, film is preferred. Electronic Files are also accepted.

Electronic File Requirements: All material must be received before ad close dates.

Software: Adobe illustrator 9.0 (saved as EPS). Adobe Photoshop CS (saved as EPS or TIFF). Please convert higher versions down. If you can only supply an IBM format, the file must be in viewable EPS or TIFF format with fonts embedded as that format.

Colour Ads: Colour separations must be provided, right reading, emulsion down. Please note that files using RGB or Pantone colours (PMS) must be converted to CMYK before we receive files.

ISG

To,
The Secretary, Indian Society of Geomatics
6202, Space Applications Centre (ISRO)
AHMEDABAD – 380 015. INDIA

Sir,

I want to become a Member/ Life Member/ Sustaining Member/ Patron Member/ Foreign Member/ Student Member of the Indian Society of Geomatics, Ahmedabad for the year _____. Membership fee of Rs. _____ /- is being sent to you by Cash/ DD/ Cheque. (In case of DD/ Cheque No._____dated_____drawn on Bank
_____ . I **agree to abide by the Constitution of the Society.**

Date:

Place: **Signature**

- Name: Mr/Ms/Mrs/Dr_____
- Address: _____

_____PIN: _____

Phone: _____ Fax: _____Email:

_____ • Date of Birth

_____

•Qualifications_____

- Specialisation: _____
- Designation: _____ Organisation. _____
- Membership in other Societies: _____
- Mailing Address: _____

_____PIN: _____

Proposed by:
(Member's Name and No)
Signature of Proposer

For Office Use: A/P/L Member No.		Receipt No.		Date:	

Indian Society of Geomatics (ISG), Room No. 6202 Space Applications Centre (ISRO), Ahmedabad-380015, Gujarat. Url: www.isgindia.org Phone: +91-79 26916202
Email: secretary@isgindia.org or sasharma@sac.isro.gov.in Fax +91-79-26916287

MEMBERSHIP FEES

Sr. No.	Membership	Life/Patron Membership fees		Annual Subscription
	Category	₹ Indian	US $ Foreign	₹ Indian
1.	Annual Member	10	---	300
2.	Life Member a) Admitted below 45 years of age	2500	250	
	b) Admitted after 45 years of age	2000	200	
3.	Sustaining Member	---	---	2000
4.	Patron Member	50000	3000	---
5.	Student Member	10	---	100

MEMBERSHIP GUIDELINES

- Subscription for Life Membership is also accepted in two equal instalments payable within duration of three months, if so desired by the applicant. In such a case, please specify that payment will be in instalments and also the probable date for the second instalment (within three months of the first instalment).
- A Member of the Society should countersign application of membership as proposer.
- Subscription in DD or Cheque should be made out in the name of **'Indian Society of Geomatics'** and payable at Ahmedabad.
- Direct deposit in ISG A/Cs must include bank fee RS. 25/- for cash payment.
- Financial year of the Society is from April 1 to March 31.
- For further details, contact Secretary, Indian Society of Geomatics at the address given above.
- ISG has chapters already established at the following places. Ahmedabad, Ajmer, Bhagalpur, Bhopal, Chennai, Dehradun, Delhi, Hissar, Hyderabad, Jaipur, Ludhiana, Mangalore, Mumbai, Mysore, Pune, Shillong, Trichi, Srinagar, Vadodara, Vallabh Vidya Nagar, Visakhapatnam and Trivandrum. Applicants for membership have the option to contact Secretary/Chairman of the local chapter for enrolment. Details can be found at the website of the Society: www.isgindia.org.
- Journal of the Society will be sent to Life Members by softcopy only.

Indian Society of Geomatics (ISG), Room No. 6202 Space Applications Centre (ISRO), Ahmedabad-380015, Gujarat. Url: www.isgindia.org Phone: +91-79 26916202
Email: secretary@isgindia.org or sasharma@sac.isro.gov.in Fax +91-79-26916287

Geomatics Revealed

IGiS

Integrated GIS & IP Software

VERSION 2.0

MAKE IN INDIA

National Awards on Technology
By The Former President of India,
Dr. A. P. J. Abdul Kalam

Launch of IGiS Version 2.0
By Padam Shri AS Kiran Kumar, Chairman, ISRO and
Shri Tapan Mishra, DIRECTOR, SAC, ISRO.

What's new in IGiS

IGiS Version 2.0 is full of enhancements which you'll appreciate every day. New advanced GIS/IP and SAR modules are vital now a days. New COM Based Architecture makes you even more productive. The more you do with IGiS Version 2.0, the more you'll wonder how you ever did without it.

Enhancements in IGiS Version 2.0

- Advanced GIS / Image Processing
- Microwave SAR Analysis
- Meteorological Analysis
- COM Based Scalable Architecture
- New Ribbon Bar GUI
- Python Customization
- OGC Standards

Product Development Partner

इसरो isro
Government of India | Department of Space
Indian Space Research Organisation - (ISRO)

SGL Scanpoint Geomatics Ltd.
www.scanpointgeomatics.com

Scanpoint Geomatics Ltd.
Corporate Office : 12, Abhishree Corporate Park, Iskcon - Ambli Road, Ahmedabad - 380 058. Gujrat (India)
[P] +91 2717 297096-98 [F] +91 2717 297039 [E] info@scanpointgeomatics.com [W] www.scanpointgeomatics.com

INDIAN SPACE RESEARCH ORGANISATION
GOVERNMENT OF INDIA

A Smart Destination For Geospatial Solutions

National Remote Sensing Centre
Hyderabad, India
www.nrsc.gov.in
www.bhuvan.nrsc.gov.in
data@nrsc.gov.in

nrsc

इसरो isro

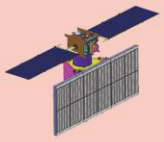

Only Organization in the Country to Acquire & Supply Satellite Data to Users

Aerial Acquisition for Specific User Demands & Disaster Management Support

Open Data & Value Added Products Dissemination Through Bhuvan

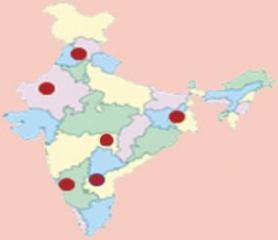

Region Specific Solutions

Capacity Building in Remote Sensing Applications